INTEGRATED PLANT AND CONTROL DESIGN FOR VEHICLE – ENVIRONMENT INTERACTION

BY

YANGMIN XIE

DISSERTATION

Submitted in partial fulfillment of the requirements
for the degree of Doctor of Philosophy in Mechanical Engineering
in the Graduate College of the
University of Illinois at Urbana-Champaign, 2013

Urbana, Illinois

Doctoral Committee:

Professor Andrew Alleyne, Chair
Professor Alexander Vakakis
Associate Professor Srinivasa Salapaka
Assistant Professor Timothy Bretl
Professor Brian Steward, Iowa State University

Abstract

Vehicle-environment interaction (VEI) systems are a specific class of systems whereby a vehicle, or some component of the vehicle, is required to interact with its environment above and beyond simple locomotion tasks. This dissertation examines the automation of the VEI system where the positioning of a particular vehicle subsystem or end effector with respect to the environment is accomplished in a controlled manner. The interaction between the vehicle and its environment or terrain acts as a disturbance to the controller attempting to position the subsystem. To obtain accurate and highly productive operation, the VEI system under control is required to have a sufficiently high bandwidth so as to achieve the desired task. Unfortunately, this is often not achievable due to fundamental limitations arising from the physical system design. This dissertation studies the fundamental limitations that stem from these physical systems and develops a systematic solution to alleviate the limitations. The results developed are made specific to a VEI system of interest: a combine harvester with automated header height control (HHC).

By modeling and system analysis of the system, the under-actuation and non-collocation sensor/actuator properties of the mechanical system are presented. These properties cause lightly damped low frequency zeros and poles in the open loop transfer functions of interest, thereby preventing effective feedback control beyond a given

frequency. In addition, the actuation system, which is electro-hydraulic in the system of interest in this work, introduces a considerable delay and places another bandwidth limitation. To mediate the limitations caused by the mechanical system dynamics, an integrated design and control method is proposed to synergistically optimize parameters in both the physical system and the controller to minimize a novel type of control-oriented objective function. As a result, the redesigned open loop plant obtains more desirable zeros and poles compared to the original product thereby leading to higher performance in the closed loop behavior. To compensate for the delay cause by the hydraulic actuator, this dissertation proposes a two DOF control, adding a feedforward channel to the optimally designed feedback control loop. Both model uncertainty and signal uncertainties are considered in the two DOF controller design to guarantee robust stability and performance. The methods mentioned above are applied and validated with both simulation and experimental results for the combine harvester system of interest. The generality of the approaches presented indicate the research can be applied on other VEI systems with possibly slight modifications due to the nature of the specific system.

To my parents and my husband

Acknowledgements

I would like to express my deepest appreciation to my advisor, Prof. Andrew Alleyne, for his dedicated mentorship through the five years of my Ph. D. study. From him, I learned much more than doing research work and writing papers; his encouragements and supports are the reasons of many successes of mine in graduate school, and I can expect to continue benefiting from his advices in the future of my life. I feel grateful that I have the opportunity studying in Alleyne Research Group. Prof. Alleyne makes it a friendly and professional environment, which is very important for each member, especially for an international student like me. I also want to thank my committee members, Prof. Alexander Vakakis, Prof. Srinivasa Salapaka, Prof. Timothy Bretl, and Prof. Brian Steward. Thank you for your efforts in improving the quality of my research work. Your feedback and suggestions have been very helpful in completing this dissertation.

I also own many thanks to my peers in Alleyne Research Group. They play many roles in every aspect of my life for this past five years: colleagues, friends, mentors, listeners and family. Kira, David and Sandipan, thank you for your selfless advices as senior members; you helped me pass down times as a fresh. Neera, Vikas, Tim, Bin, Nanjun, and Erick, we spent the longest time together and the trust and friendship we have built are the

treasures of my life. Joey, Megan, Justin, Sarah, Rich, and Matt, thank you all for your friendship, and the fun time we spent together is a beautiful memory for me.

I also want to thank Dustin, Pathik, Ashley, Jim and Dan from Deere&Com for their help on establishing the experimental system and providing illustrative suggestions on improving the research work from more practical perspective.

Finally, I want to thank my parents for their love and supports throughout my life. You are the one of the motivations for me to keep proceeding. And to my husband, Hang, thank you for your patience, support, and partnership in our life and work.

Table of Contents

List of Tables

List of Figures

Nomenclature

A	area	m^2
$C(s)$	controller	--
c	leakage coefficient	dimensionless
d	disturbance	--
E_β	fluid bulk modulus	dimensionless
F	force	N
G(s)	transfer function	--
GM	gain margin	dB
J	objective function	--
k	spring constant	N/m
$L(s)$	loop transfer function	--
l	length	m
$M(s)$	Non-minimum transfer function	--
m	mass	kg
n	noise	--
$P(s)$	plant	--
PM	phase margin	degree
p	pole	--
$Q(s)$	filter	--
Q	flow rate	m^3/s
q	degree of freedom	--

r	reference	--
S	sensitivity function	--
$T(s)$	Complementary sensitivity function	--
T	delay	s
t	time	s
u	control input	--
V	volume	m^3
v	velocity	$m \cdot s^{-1}$
W(s)	weight function	--
y	output	--
z	zero	--
ω	bandwidth/achievable bandwidth	Hz
ξ	damping ratio	--
Δ	uncertainty	--

Chapter 1

Introduction

This dissertation investigates the integrated system design and control problem for a class of vehicle-environment interaction (VEI) systems. In particular, a header height control (HHC) problem for combine harvesters is utilized as a case study to illustrate some common existing system properties in VEI systems, and to validate the approaches proposed in this dissertation. Broadly speaking, the limitations from the physical system behavior can result in performance barriers when designing a controlled system. This dissertation first seeks to understand two aspects to the fundamental limitations in VEI systems: mechanical system dynamics and actuator delay. Subsequently, this dissertation proposes design and control solutions in order to extend the achievable system bandwidth by mediating such limitations.

Section 1.1 provides a general overview of the class of VEI systems discussed in this dissertation, and Section 1.2 describes the specific research objectives within the dissertation scope. In addition to the objectives associated with specific limitations, Section 1.2 indicates solution paths to achieve each the individual objectives. These solutions will eventually be combined into a systematic procedure for addressing the VEI-induced limitations. The framework for introducing the organizations of the chapters is present in Section 1.3.

1.1 Vehicle-Environment Interaction Systems

Figure 1.1 Systems with vehicle-environment interaction

Vehicle-environment interactions often occur for mechanical vehicle systems when some apparatus is attached on the vehicle body for a specific task or purpose. Figure 1.1 illustrates several examples of vehicles that interact with an environment. The vehicle functions as a moving carrier, and the apparatus is controlled by actuators to interact with the environment for the purpose of precisely accomplishing a certain task. Whilst the vehicle is manipulating the particular apparatus, the dynamics of the vehicle are influenced by the environment as it is proceeding over the surface of the ground or water.

For example, a mine-clearing vehicle has an extended detector ahead of the vehicle to discover any hidden ordinance. To be most effective, the detector must maintain a specific height with respect to the ground; at the same time, it needs to avoid contact with the ground to prevent the detonation of a mine. In this case, it is important for the detector to follow the shape of the terrain while the vehicle is in motion, but the irregular surface of the ground will

induce vibrations in the vehicle, thereby affecting the ability of the detector to maintain its prescribed stand-off height. Similar mechanical structures and phenomena can be found in many other classes of working vehicles such as: construction vehicles, agricultural vehicles, and crane ships. The vehicle-environment interaction during the working process in these systems have a significant influence on the working efficiency of the vehicle system by introducing an unknown reference (the terrain profile) or disturbances (the terrain profile disturbing the vehicle dynamics) to the systems. In addition, a potential challenge for precisely-controlled operation results from the vehicle dynamics, which, in many cases, are with undesirable properties such as delay and non-minimum phase or lightly damped zeros.

Such factors can induce difficulties in the design of feedback control systems when faster speed, higher productivity, or greater operational precision is required. When the vehicle/apparatus system is required to tracking an unknown environmental reference, or to reject any environmental disturbances, the VEI may cause limitations on the corresponding reference tracking or disturbance rejecting bandwidth.

The combine harvester shown in Figure 1.2, abbreviated as “combine” below, is one of the examples of a VEI system, and this system is the specific focus of this dissertation. Figure 1.2 provides both a photograph and a simplified schematic of a combine in the vertical plane. The combine is a key component in the agricultural process, and it is used to extract and collect crops from the field. It has been estimated that approximately 75% of the crop losses occur at the header [1], and a significant portion of the header loss is caused by improper positioning of the header [2]. Therefore, the header height control (HHC) problem under study is motivated by the interest in improving the efficiency and productivity of the harvesting process; specifically, to decrease the total time required for the harvest and

increase the yield of the harvest. The header height is defined as the distance between the header tip and ground, and the height error is defined as the deviation between the current header height and the desired set point for the header height. By raising or lowering the header with an actuator, which is usually hydraulic, the header height can be adjusted. If the header height is too high, the harvest's yield will be considerably reduced since much of the viable crops will be left un-harvested. Conversely, if the header height is maintained too low, equipment damage or operator fatigue will result.

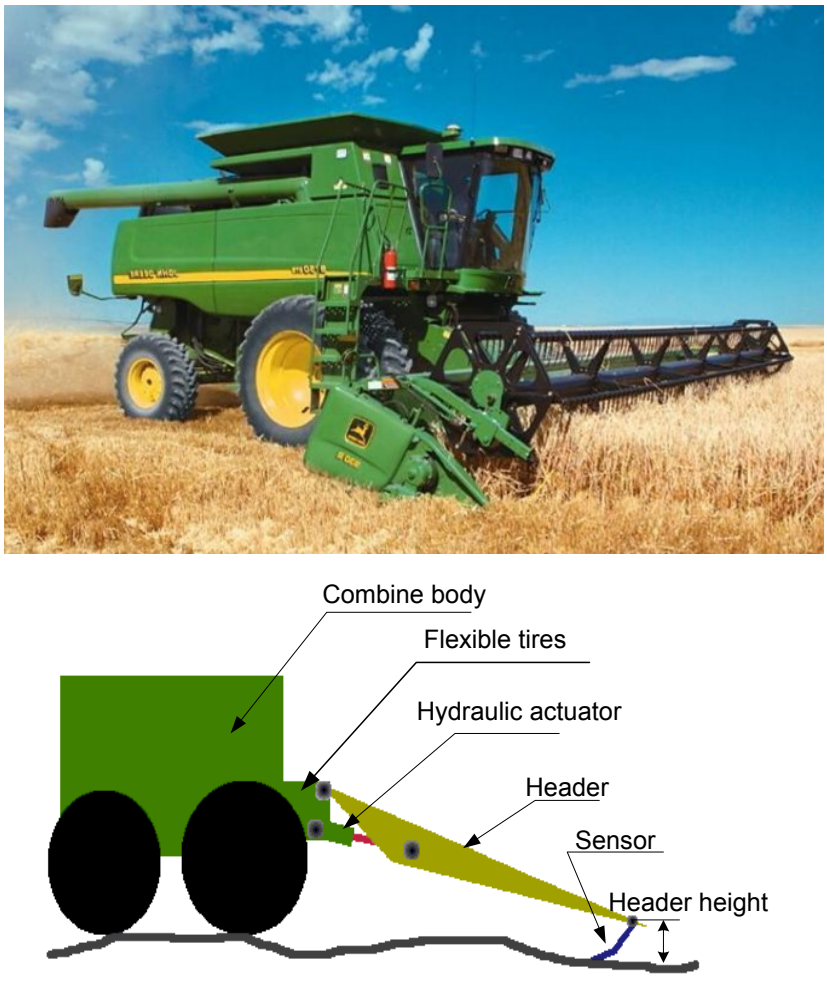

Figure 1.2 Combine system

The combine was widely adopted in U.S. as powerful harvesting tool since 1930s[3], and the autonomous header height control has gained research interest since 1960s [4]. The combine, with its header suspended in front of the main vehicle body, is a typical example of the VEI system mentioned above. In the current agricultural industry, one way to improve the productivity of the harvesting operation is to increase the size of the system, which means to geometrically enlarge the scale of the system proportionally. This results in wider and heavier headers suspended on larger and more powerful combine bodies. Another direction is to pursue higher working speed of the combine through the field. Both ways require higher working efficiency of the processing parts. However, increasing the combine speed by 2X would have the same effect on the harvesting process as doubling the size of the combine. Given the HHC is the bottleneck for increasing combine forward velocity, effective HHC design becomes a cost effective solution as will introduced below to achieve productivity enhancement. Although this benefit is highly appreciated, in agricultural practice, however, difficulties have been encountered for decades in efforts to break this obstacle.

The HHC system is required to track the reference and reject the disturbance from the ground profile; therefore, the bandwidth requirement for HHC is determined by two factors: the surface shape of the ground and the forward velocity of the combine. The current product is able to maintain a 3mph speed in relatively flat field, where the period of the ground is around 100m with peak-to-peak amplitude as 3m if it is approximated as a sinusoid shape. Assuming the sensitivity function has a slope as 20dB/decade, which will be shown in the control design result of Chapter 6, the bandwidth required to maintain a height error with 20cm is approximately 1.13 rad/sec. To double the speed, the required bandwidth has to be above 2.26 rad/sec, i.e. 0.36Hz. Without detailed discussion on physical system properties,

many efforts have been devoted to achieve such HHC performance using software and controller design unfortunately without much success in the implementation on the real combine system[5, 6].

As will be detailed in later chapters, the inherent reason is the fundamental limitations derived from the legacy design of the combine system. The original design of the combine system utilized manual control. Automatic control for HHC was introduced into a plant that was not well suited for feedback control. As a result, there exist performance limits that cannot be circumvented solely by control design; although good design can maximize the use of available performance. This dissertation aims to reveal the inherent causes for the performance barrier and provide validated solutions.

Although the methods introduced are based specifically on the HHC problem of combine harvesters, the approaches and procedures can be readily applied to many other VEI systems such as those illustrated in Figure 1.1.

1.2 Research Objectives

The primary objective of this research, as mentioned in the previous section is to provide a systematic approach to achieve satisfactory control performance for a class of VEI systems. It includes analysis of control limitations, physical system design and the development of control solutions. The specific research objectives pursued in this dissertation are described below.

1.2.1 Analysis of the fundamental limitations of control

The performance of a controlled system is determined by two entities: the physical system dynamics and the control algorithm. From a control engineering perspective, the controller design is usually based on fixed system dynamics. Parameters in a controller are tuned to obtain desired performance. In modern control theory, some objective function is usually chosen to be minimized for optimal control design, where the controller contains the design variables and system dynamics works as an invariant dynamical function. However, this often conceals the role of the physical dynamics in the closed loop system performance. It is not a problem when the system performance under control can achieve the design requirement specifications. However, when this does not happen, the fundamental causes as well as the best solutions can be difficult to determine. The possible reasons for unmet specifications can be ill-tuned controller parameters, inappropriate choice of the objective functions, or the specs may be unachievable due to the inherent limitations from the physical system.

If the control limitations are inherent in the plant's dynamical structure, the analysis usually involves two steps. Firstly, Studies must be conducted to determine the most influential factors from the physical system. This usually requires to establish a model for the system, i.e., to describe the system dynamics mathematically with proper approximations. Secondly, the control limitations induced by these highlighted features need to be analyzed. For example, when time delays exist in a system, the feedback control bandwidth has an upper bound. Independent of the feedback controller design, the closed loop performance cannot surpass this upper bound. Understanding how various features in the physical

system's dynamics can influence achievable bandwidth would isolate the causes for limitations in control performance.

Knowing which features from the physical system limit the controlled system's performance and determining the relative magnitudes of these limitations are useful during the control design process. The limitation analysis provides an estimate of the 'best' performance that any controller could achieve. Therefore, the designer can determine whether the current control objective or specification can be met. When the desired performance cannot be met, alternative solutions can be introduced; these include redesigning the physical system to eliminate the corresponding limitations or introducing additional sensors and/or actuators. When the objective is achievable, the upper bound of the performance can serve as a reference to specify realistic objective functions for optimal control. Once the control performance is obtained, either by simulation or experiments, the performance limits can be used to evaluation the controller design by comparing the achieved performance with the maximum value possible.

Taking the HHC problem as a specific example, the difficulty in improving the performance stems from the physical dynamics of the plant, which are undesirable zeros and poles. These are combined with a considerable actuator delay in the system to reduce the achievable system bandwidth. The bandwidth limitation limits the combine's ability to track high frequency signals, which induces a slow driving speed and lower than desired working efficiency.

With the understanding of the inherent problems caused by the physical system design, two corresponding solutions are proposed in this dissertation as research objectives. The effects of the mechanical system characteristics on the controlled system can be

improved by finding a feasible redesign of the current system; this will be elaborated on in Section 1.2.2. The redesign can change the relationships among the rigid body components in the mechanical systems, and improve the dynamical features of the open loop system. For the actuator delay, feedback control is very limited in its ability to compensate for the induced loss of phase. As a result, feedforward control with pre-view knowledge can be used in an anticipatory fashion. This increases the overall system responsiveness, and will be introduced further in Section 1.2.3.

1.2.2 Integrated design and control

One approach to improving the effect of the plant system behavior on the control performance is to redesign the physical system such that it is easier to control. In this dissertation, an integrated design and control method is used for the purpose of improving physical system properties and calculating a desirable control algorithm. The integrated design and control approach uses control performance as a design criterion. As a result, both the system dynamics and controller can be improved together during this process to achieve improved control performance. What follows is a brief review of previous attempts at integrating control and plant design.

For mechatronic systems, the integration of controller design and mechatronic system design was proposed in [7]. Since it is often the case that the mechatronic systems exist when the controller design phase is begun, many restrictions are inadvertently placed on the controller design. Therefore, the integrated design and control is recognized ‘a necessary step in mechatronics’ [8] to fully achieve the benefits of integrating mechanical and electronic (i.e. mechatronic) systems.

Some work has been done to preserve physical insight and provide guidance in the selection of the proper physical architecture for control. For example, Bond graph approaches were used to formalize the concept of 'design in physical domain', which is to preserve the physical structure when modeling and designing the system with control oriented approaches [9]. In another research direction, the integrated design goals and requirements are formulated as a nonlinear programming problem. This nonlinear programming approach is the design method used in this dissertation. Design variables in both the controller and system are chosen, subject to structural and control constraints, to optimize an objective function whose construction captures the essence of the integrated design problem. The control design must also provide satisfactory closed-loop stability and robustness properties. For example, the objective function can be the steady-state error due to white-noise disturbance at the inputs [10], the sum of the time constants of the closed-loop eigenvalues [11], the largest possible safety margin [12], etc. Sometimes, the system is assumed to be perturbed by some stochastic disturbances and the constraints are formulated in terms of allowable means square responses and control energy [13].

For VEI systems, the physical plant design involves the change of key parameters in the vehicle-apparatus system. In such integrated design and control work, it is important to determine: (a) what the influential parameters are in the system, (b) what the suitable control performance functions are in the design criterion, and (c) what numerical method can be used to calculate the optimal system design and the corresponding controller. In this dissertation, the HHC problem will be used as an example to be redesigned for the purpose of getting better dynamical characteristics in order to improve the control performance.

1.2.3 Robust two degree-of-freedom (DOF) controller design

As stated in Section 1.2.1, when a delay appears in the feedback control loop, the feedback controller is not capable of eliminating the delay from its closed loop response. Therefore, feedforward control can be considered as a solution for improving the bandwidth of a time-delayed system. Usually, a feedback controller is still needed to maintain robust closed loop stability and a feedforward controller is added on to the feedback loop to obtain better performance. The designs for both the feedback and feedforward controller forms a two degree-of-freedom (DOF) control problem.

The difficulty in designing a feedback controller for time-delayed system stems from the delay term which is irrational in continuous time. This makes the system dynamics infinite-dimensional and causes problems using classical robust control synthesis. Therefore, this dissertation introduces a way to find a robust controller design method for a delayed system.

In addition to improving feedback design, the work in this dissertation also explores the feasibility of using feedforward controller to compensate for the delay in the system. Two main uncertainties that undermine the feedforward performance are signal measurement uncertainty and model uncertainty. When there is error between the actual and estimated signals, the compensating action from the designed feedforward channel can be less effective. Similarly, when the assumed model deviates from the true system dynamics, the effect of the feedforward input signal on the output is not accurate, and this also induces additional tracking error. Therefore, this dissertation also proposes a method to design a feedforward controller that takes both model and signal uncertainties into consideration during design. When both feedback and feedforward controllers are designed with respect to

uncertain conditions, the robust stability and performance of the delayed system can be guaranteed.

1.3 Organization of the Dissertation

Figure 1.3 shows the framework of the research work in this dissertation. The relationship among the three main objectives proposed in Section 1.2 is clearly outlined. With an understanding of the fundamental limitations in the VEI systems, particularly for the HHC problem, we propose two solutions corresponding to the primary control limitations. Integrated design and control aims to improve the dynamical properties of the physical system, and the robust two DOF control design aims to compensate the delay and obtain a high bandwidth controlled system response under the influence of system model and signal uncertainties.

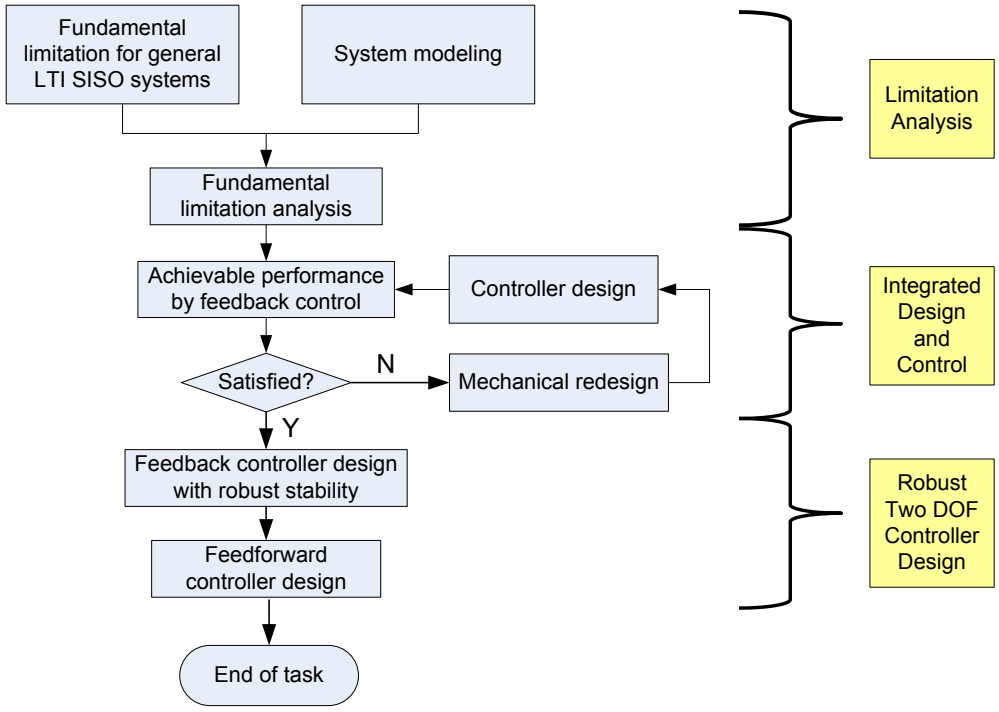

Figure 1.3 Research framework

The remainder of this dissertation is organized as follows. Chapter 2 introduces the commonly seen control limitations for the physical system and studies how the bandwidth limitation is induced by these factors. Chapter 3 provides a physical description of the HHC problem, which is used as an example of a VEI system to be studied in this dissertation. Chapter 3 also presents the mathematical modeling of the actuator and mechanical system. In addition, the two major limitations in the HHC control problem are illustrated with quantitative results of the bandwidth limitation analysis using the conclusions from Chapter 2. The details of the integrated design and control method aimed at improving the mechanical system dynamics is developed in Chapter 4. Chapters 5 and 6 present the design of a robust feedback controller and a feedforward controller for delayed system, respectively. Lastly, the conclusions and research contributions from this work are summarized in Chapter 7.

Chapter 2
Fundamental Limitation in Control of SISO LTI Systems

With the development of control theory, various optimal control algorithms have been proposed to achieve the 'best' control performance with certain specifications of the control objectives and system characteristics. Examples of these algorithms include robust control [14, 15], adaptive control [16, 17], model predictive control [18, 19], and iterative learning control [20, 21]. The variations and implementations of these control methods have been widely discussed. However, less attention has been paid to the more fundamental question: what characteristic in the system would inherently limit the performance of these controllers and induce upper bounds on achievable performance? The understanding of such limitations can help in exploring the design and control approaches in the preliminary assessment stage, understanding the bottlenecks of system performance, and providing an estimate of the ultimate performance. This chapter will discuss the research work on fundamental limitations for Single-Input-Single-Output (SISO) control systems with consideration of factors such as system dynamics, delays, signal uncertainties, and modeling uncertainties. First, the basic structures of feedback, feedforward, and combined two DOF control are introduced. Then the common factors that have an impact on control performance are listed; this is followed by

discussions on the limitations of feedback and feedforward control. Finally, two limitations that are commonly found in VEI systems are specifically studied and serve as the motivation for the integrated design and control work in the following chapters of this dissertation.

2. 1 Basic Architectures for Control Strategies

2.1.1 Feedback control

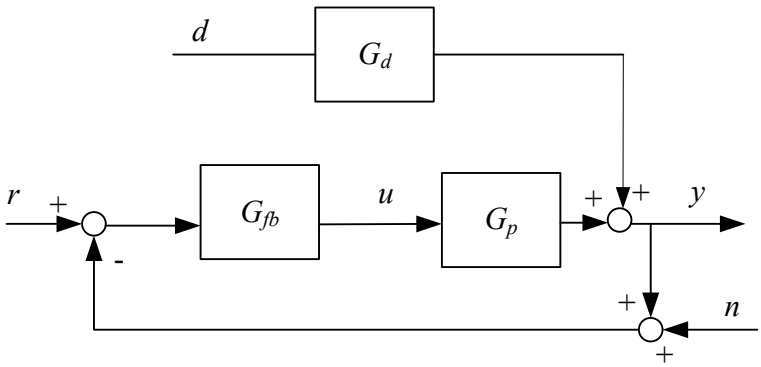

Figure 2.1 Block diagram of feedback system

Feedback control is the most common and powerful control strategy that has been studied in the control community and applied in industry. A block diagram for a basic feedback loop is shown in Figure 2.1, where r is the reference signal for the output signal y to follow. When r is a constant signal, or in other words, a set point, the feedback control problem is called a regulation problem. When r is a time-varying signal, the feedback control problem is called a tracking problem. The former problem is a special case of the latter. G_p describes the dynamics of the plant where n is the noise corrupting the measurement of y and d is an exogenous disturbance which is shown as affecting the output y. G_d represents the disturbance dynamics describing the influence of disturbance d on the output y; $G_d = 1$

indicates d is an output disturbance whereas $G_d = G_p$ indicates d is an input disturbance. G_{fb} is the feedback controller which generates a control signal u to control the plant behavior by utilizing the reference r and measured feedback information consisting of the output y and measurement noise n. The feedback control uses the feedback information to stabilize the system and improve the performance of reference tracking whilst rejecting disturbances.

The system model uncertainty is assumed to be additive as shown in Eqs. (2.1) and (2.2). G_{p0} and G_{d0} represent the plant dynamics model and disturbance dynamics model, respectively, while G_p and G_d are the true plant dynamics and disturbance dynamics.

$$G_p(s) = G_{p0}(s) + \Delta_p(s) \Rightarrow \Delta_p(s) = G_p(s) - G_{p0}(s) \tag{2.1}$$

$$G_d(s) = G_{d0}(s) + \Delta_d(s) \Rightarrow \Delta_d(s) = G_d(s) - G_{d0}(s) \tag{2.2}$$

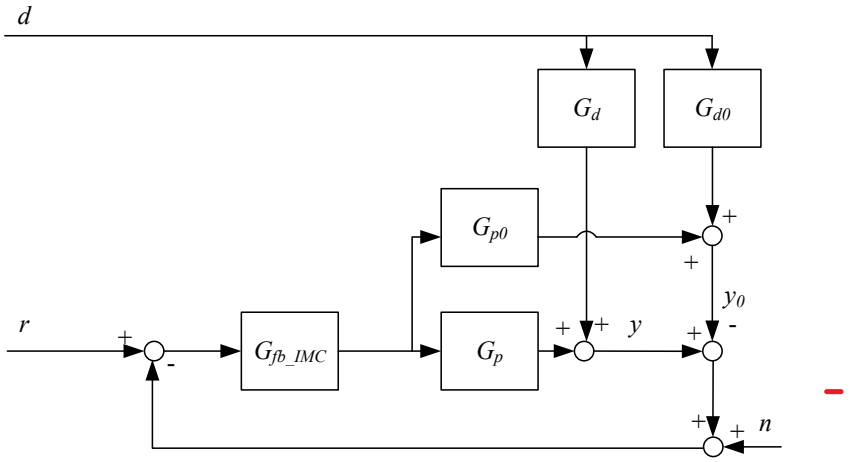

Figure 2.2 Block diagram of transformed feedback structure using IMC framework

For the purpose of later analysis, a transformation on the feedback system of Figure 2.1 is introduced in Figure 2.2 using an internal model control (IMC) schematic which employs the difference between the measured output and estimated output as a feedback

signal [22]. Here the additive plant and disturbances models are explicitly incorporated into the particular feedback structure.

The feedback controller element in Figure 2.2 is related to the feedback element in Figure 2.1 by a simple transform shown in Eq. (2.3).

$$G_{fb} = \frac{G_{fb\_IMC}}{1 - G_{p0} G_{fb\_IMC}} \tag{2.3}$$

Note that $G_{fb\_IMC} = G_{p0}^{-1}$ is equivalent to setting $\left|G_{fb}\right| \to \infty$, which would achieve perfect tracking for the original system of Figure 2.1 via a very high gain feedback controller. The benefit of the transformed system in Figure 2.2 is that it can be further simplified, as shown in Figure 2.3, to consider solely the uncertainty dynamics, $\Delta_p(s)$ & $\Delta_d(s)$, when analyzing the feedback loop properties. This will aid the frequency domain analysis for maximum achievable bandwidth in later sections; the results obtained for Figure 2.3 can be readily applied to Figure 2.1. This property is also further used in the two DOF control design that will be discussed in Section 2.1.3.

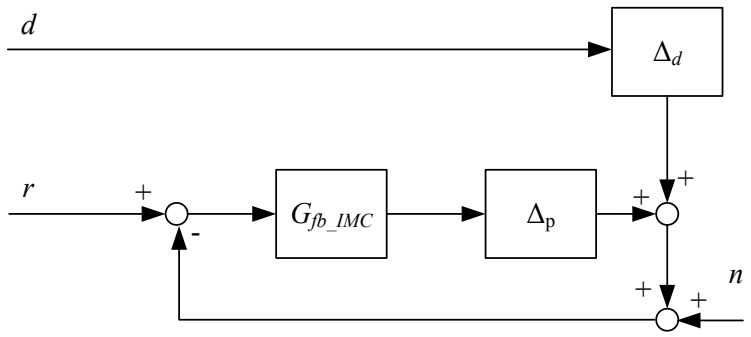

Figure 2.3 Block diagram of simplified feedback system

2.1.2 Feedforward control

Feedforward control utilizes knowledge of exogenous signals (including references and disturbances) to predict and compensate the system outputs before they are affected by the exogenous signals. Usually feedforward is used in series or in parallel with feedback controllers to achieve better tracking and/or disturbance rejection performance.

When using feedforward approaches, the exogenous signals need to be ascertained by the controller. If the exogenous signals can be represented analytically, such as for periodic signals [23], methods such as an adaptive feedforward controller (AFC) or an adaptive feedforward disturbance cancellation (AFDC) can be used to 'learn' their patterns [24, 25], and the effect of the signals can be attenuated accordingly. Another kind of control approach, iterative learning control (ILC), learns the repetitive effect of the exogenous signals on the system outputs by repeating the process and adjusting the control signal to improve the performance [21]. A third type of feedforward control approach, which is the focus here, addresses exogenous signals that are pre-known or measured. This is the most general feedforward approach since the exogenous signals are not assumed to have an analytical form and are not the result of a repetitive process.

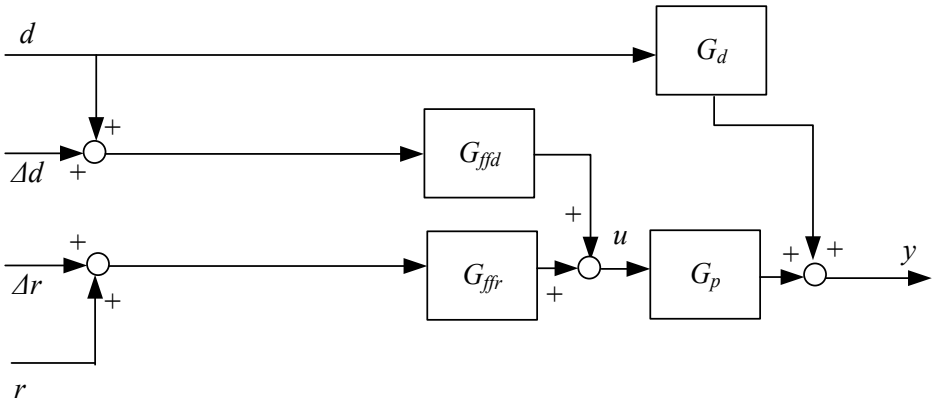

Figure 2.4 Block diagram of feedforward system

As shown in Figure 2.4, the feedforward controller uses the estimation or measurement of the exogenous signals r and d to generate the control input u. The estimations/measurements deviate from the true exogenous signals r and d by Δr and Δd, respectively. Therefore, Δr and Δd represent the feedforward signal uncertainties. G_{ffr} and G_{ffd} are, respectively, the feedforward controllers designed for r and d. Compared with feedback control, feedforward control can use the known information for r and d to construct non-casual control. This anticipatory action improves the system response, particularly for sudden changes in the exogenous signals. However, feedforward control is sensitive to the system model uncertainty and any signal uncertainties. Anticipating a slightly wrong action can cause significant errors at the output y and is why feedforward is usually combined with feedback to create a two DOF controller.

2.1.3 Two degree-of-freedom (DOF) control

As mentioned above, when the feedback and feedforward controllers are combined to track references and reject disturbances, they become a two DOF controller. For the two DOF scheme, the commonly used structures of the controller are shown in Figure 2.5.

Figure 2.5(a) shows the architecture of a classic two DOF controller, where G_{fb_a} is the feedback controller; G_{ffr_a} and G_{ffd_a} are the feedforward controllers to address the reference and disturbance signals, respectively. G_p represents the plant dynamics and G_d describes the disturbance dynamics. Due to the estimation/measurement uncertainty, the signals that the feedforward controller uses deviate from the true reference r and disturbance d by Δr and Δd, respectively.

Many variations of this control structure have been used in the literature for the convenience of performance analysis and controller derivation [26]. For example, Figure 2.5(b) and Figure 2.5(c) change the relationship between the reference feedforward block and the feedback controller, where Figure 2.5(b) separates the reference from the feedback loop and Figure 2.5(c) changes the feedforward controller to a pre-filter for the reference under the assumption that the reference is pre-known and accurate. Figure 2.5(d) and Figure2.5(e) change the feedback signal in the feedback loop: (d) is called the internal model control (IMC) feedback-feedforward structure [27], which is basically an extension of Figure 2.2 to two DOF control; Figure 2.5 (e) is a further revision of Figure 2.5 (d) which separates the disturbance feedforward controller design with the feedback loop under the nominal condition, (i.e., $G_p = G_{p0}$, $G_d = G_{d0}$) [28]. The feedback signals of the last two structures are closely related to the model uncertainty in the system; therefore, they are used to design the feedforward controller and analyze control performance for uncertain systems.

The general relationship between the output y and the exogenous signals is shown in Eq. (2.4), from which there are a total of five exogenous signals that impact the output. For the variations listed above, the corresponding transfer functions from the exogenous signals to the output signal are listed in Appendix A. Although different structures are adopted for the purpose of controller design and analysis, they are inherently consistent with one another and can be transformed under certain assumptions with the conversions shown in Appendix A.

$$y = T_r r + T_{\Delta r}\Delta r + T_d d + T_{\Delta d}\Delta d + T_n n \tag{2.4}$$

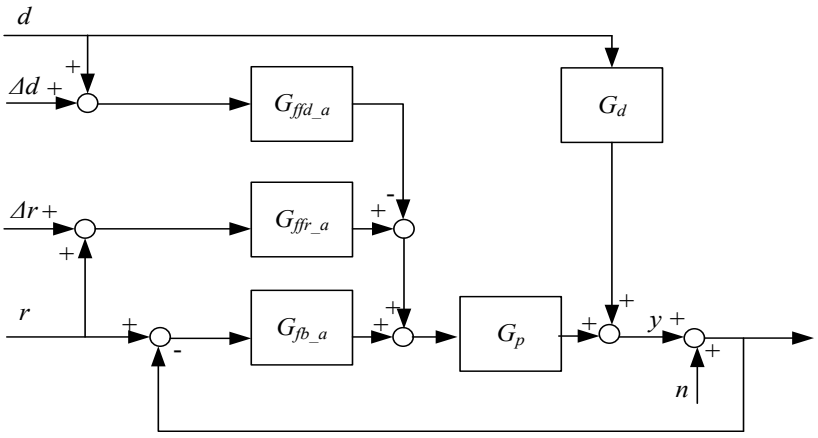

(a) Classical Structure

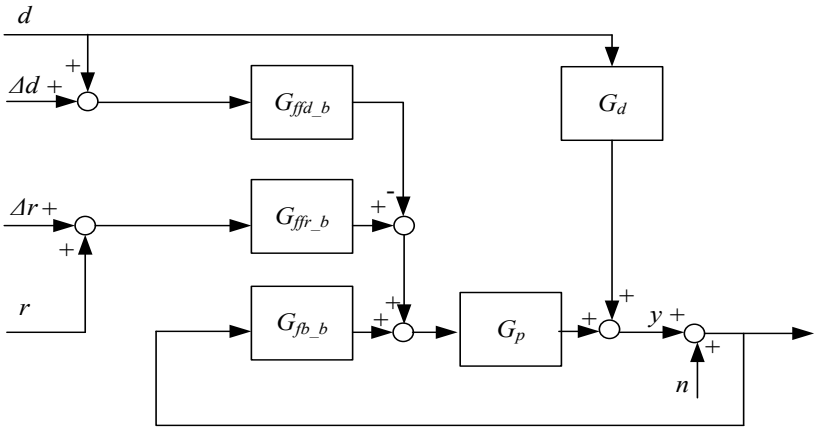

(b) Separated Reference from Feedback Loop

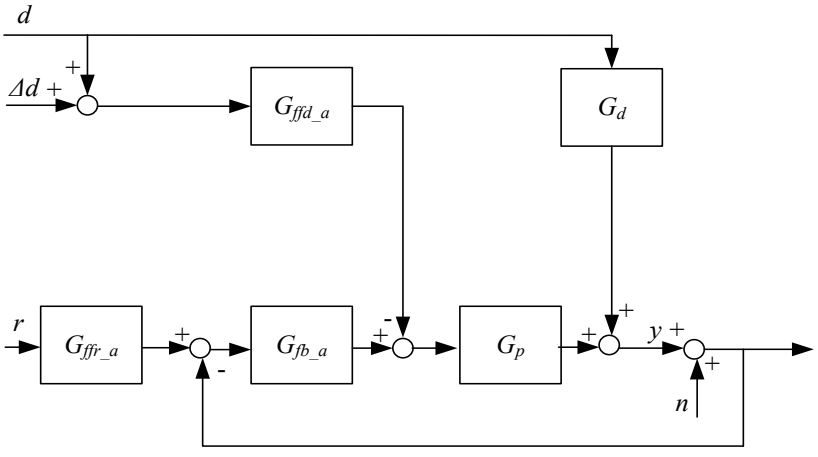

(c) Pre-filtered Reference for Feedback Loop

Figure 2.5 Structures of two DOF control

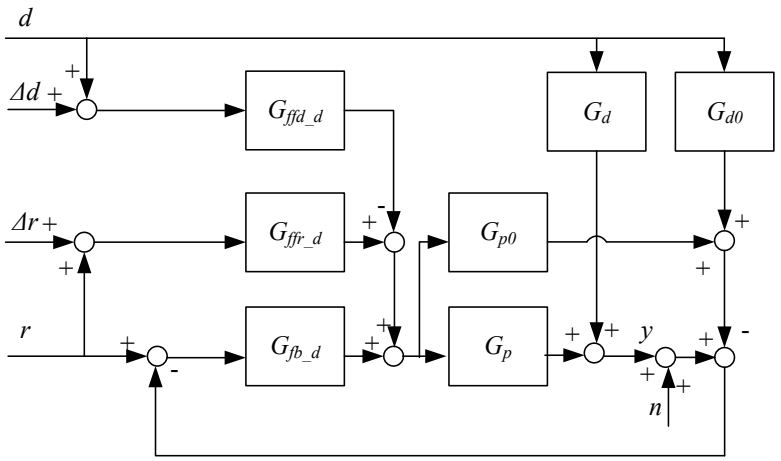

(d) Internal Model Control Feedforward-Feedback control

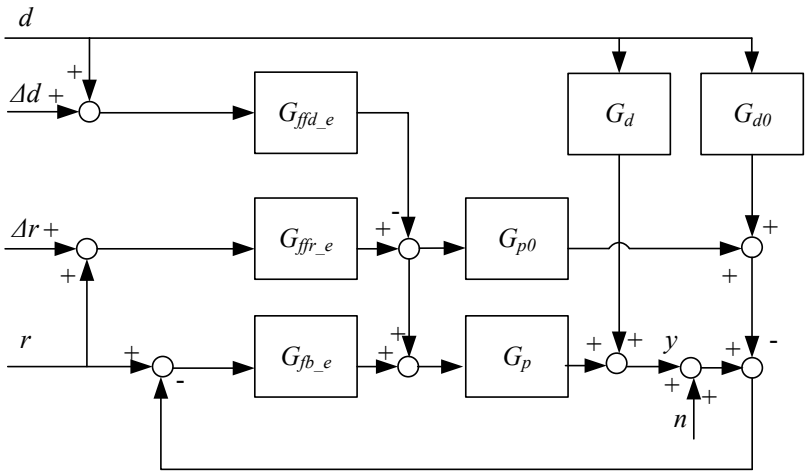

(e) Internal Model Feedforward Control

Figure 2.5 (cont.)

2.2 Limitations on Control Performance

2.2.1 Limitations on control schematics

Factors in the physical system can create performance limitations when algorithms are implemented within the control architecture discussed in Section 2.1. The most common linear limitations, discussed in the following Section, are listed below.

a) Non-minimum phase systems

A non-minimum phase system (NMP) refers to a system that has an unstable inverse. For a linear system, an NMP system indicates that the system contains zeros on the right half plane (RHP). An NMP system has a larger phase drop than the minimum phase (MP) system with the equivalent magnitude properties. Therefore, these undesirable phase properties can cause difficulties in feedback control.

b) Time delay

The presence of loop delays typically imposes strict limitations on achievable feedback performance. The delay introduces phase lag into the loop transfer function; as a result, feedback control is not able to respond in time to changes of exogenous signals, which reduces the control efficiency. The delay compromises the stability of the system and thus enforces conservative control.

c) Model uncertainty

For many model-based controller designs, the fidelity of the model directly determines how well the controller can achieve its desired performance. For feedback control, there is a balance between achieving high nominal performance with maintaining closed loop stability when the true physical system dynamics deviates from the nominal model. The larger the model uncertainty is, the more conservative the feedback controller has to be to ensure robust stability. For feedforward control, on the other hand, model uncertainty is an even bigger concern. Feedforward control requires accurate knowledge of the system to make corresponding compensations in the output for exogenous signals. Therefore, the accuracy of the model directly impacts how much the compensating signal deviates from its desired value, and how much error such deviation causes in the output.

d) Signal uncertainty

Signal uncertainty in this dissertation particularly refers to the error in signals used for feedforward control, which is defined as $\Delta r, \Delta d$ in Section 2.1.3, compared to the true reference and disturbance signals. Similar to model uncertainty, it can cause the deviation of the compensating feedforward signals and hence introduce additional error in the output.

e) Measurement noise

Measurement noise refers to the noise signal that introduces inaccurate information in the output measurement. For feedback control, it is usually difficult to distinguish the noise from the true output signal, which constrains the ability of the feedback controller to react to the real output signal. As a result, the noise might be amplified in the feedback loop and cause unexpected error.

2.2.2 Error analysis for two DOF control

The analysis of the performance limitations from the factors described above usually can be divided into two categories: (1) the limitation for all possible controller designs with tools such as the Bode integral theorem [29, 30] and (2) the "best" achievable performance under certain control criteria or system specifications [27, 31-33]. In this dissertation, we mainly discuss the former, which serves to provide a deeper understanding for the constraints from the physical system on control performance independent of the particular controller applied.

To analyze these commonly existing limitations, the sensitivity functions are the main objects to study. As stated earlier, since configuration of a two DOF controller, shown in Figure 2.5(d), has the advantage when dealing with model uncertainty, we adopt this structure to analyze the sensitivity functions from the exogenous signals to the error signal, as shown in Eqs. (2.5) and (2.6). The effect of the five factors that cause control limitations

on the output are shown in Eq. (2.5): non-minimum phase and time delay, if they exist, can appear in G_{p0}; Δ_p and Δ_d are the model uncertainties, Δr and Δd are the signal uncertainties, and n is feedback measurement noise. Together, these factors influence the tracking error e of the system, and their combined effect usually can induce even stricter constraints on performance. However, to make the analysis clear and structured, these two factors will be discussed separately for both feedback control and feedforward control.

$$e_{\_d} = S_{r\_d} r + S_{\Delta r\_d} \Delta r + S_{d\_d} d + S_{\Delta d\_d} \Delta d + S_{n\_d} n \tag{2.5}$$

$$\begin{aligned}
S_{r_d} &= \frac{1 - G_{fb_d} G_{p0} - G_{ffr_d}\left(G_{p0} + \Delta_p\right)}{1 + \Delta_p G_{fb_d}} \\
S_{\Delta r_d} &= \frac{G_{ffr_d}\left(G_{p0} + \Delta_p\right)}{1 + \Delta_p G_{fb_d}} \\
S_{d_d} &= \frac{\left(G_{d0} + \Delta_d\right) - \left(G_{p0} + \Delta_p\right) G_{ffd_d} + (\Delta_p G_{d0} - \Delta_d G_{p0}) G_{fb_d}}{1 + \Delta_p G_{fb_d}} \\
S_{\Delta d_d} &= \frac{-G_{ffd_d}\left(G_{p0} + \Delta_p\right)}{1 + \Delta_p G_{fb_d}} \\
S_{n_d} &= -\frac{G_{fb_d}\left(G_{p0} + \Delta_p\right)}{1 + \Delta_p G_{fb_d}}
\end{aligned} \tag{2.6}$$

To ensure that the analysis is consistent, the performance criterion is chosen to be bandwidth, which in this dissertation is defined as where the magnitude of sensitivity functions from exogenous signals to the error signal increases over 0dB the first time, denoted as ω_0. This bandwidth indicates that no controller can make the error to signal ratio smaller than when the frequency is above ω_0. This provides an upper bound for describing how fast the system can respond to exogenous signals with limited error.

2.3 Performance Limitations for Feedback Control

2.3.1 Non-minimum phase zeros

A. Introduction to RHP zeros

When there are RHP zeros, the system is a non-minimum phase system. In this case, extra phase lag is introduced to the loop transfer function by the RHP zeros. As a result, undesirable characteristics can be induced for feedback control.

One well-known phenomenon of a feedback system with non-minimum zeros is the 'undershoot' of its step response. When the system has an odd number of real RHP zeros, the output response goes first to the wrong direction. The number of times that the output crosses over the zero value is determined by the number of real RHP zeros [34] . This undershoot not only slows down system response to the step change in the reference signal but also restricts the application of feedback control for some physical systems where movement in the wrong direction is not desirable.

Non-minimum zeros also limit the aggressiveness of the feedback controller. As is well known in root locus theory, the closed loop poles move from the open loop pole locations to the open loop zero locations when the feedback gain increases. Therefore, a large feedback gain will inevitably induce system instability, and hence, high gain control is not permissible for a system with RHP zeros.

To enable the derivation of the bandwidth limitation caused by RHP zeros, the system is formulized below. The loop transfer function can be expressed as Eq. (2.7) with $M(s)$ representing the non-minimum part of the plant dynamics and $G_m(s)$ representing the rational minimal phase part of the loop transfer function. $M(s)$ is an all-pass function with

its magnitude equaling 1 at all frequencies. As shown in Eq. (2.8) a_i at $i = 1, 2.., m$ are the m RHP zeros in the system. $G_m(s)$ includes feedback controller $G_{fb\_d}(s)$ and the minimal phase part of the plant dynamics $G_{p\_m}(s)$, as shown in Eq. (2.9).

$$G_L(s) = M(s) G_m(s) \tag{2.7}$$

$$M(s) = \prod_{i=1}^{m} \frac{s - a_i}{s + a_i} \tag{2.8}$$

$$G_m(s) = G_{fb\_d}(s) G_{p\_m}(s) \tag{2.9}$$

When only the non-minimal plant dynamics are taken into consideration, Eq. (2.5) can be reduced to Eq. (2.10), and the two sensitivity functions from the reference and disturbance to error are shown in Eqs. (2.11) and (2.12) , respectively.

$$e_{\_d} = S_{r\_d}(s) r + S_{d\_d}(s) d \tag{2.10}$$

$$S_{r\_d}(s) = 1 - M(s) G_{fb\_d}(s) G_{p\_m}(s) \tag{2.11}$$

$$S_{d\_d}(s) = G_d(s) - M(s) G_{p\_m}(s) G_{ffd\_d}(s) \tag{2.12}$$

The perfect control would make the two sensitivity functions zero at all frequencies, which requires $G_{fb\_d}(s)$ and $G_{ffd\_d}(s)$ to satisfy Eqs. (2.13) and (2.14). However, note that $M^{-1}(s)$ is unstable; hence, the 'perfect' controller design does not apply in the real physical system. In other words, the 'ideal' control cannot be found and performance is limited due to $M(s)$.

$$G_{fb\_d}(s) = M^{-1}(s) G^{-1}{}_{p\_m}(s) \tag{2.13}$$

$$G_{ffd\_d}(s) = G_d(s) M^{-1}(s) G_{p\_m}^{-1}(s) \tag{2.14}$$

B. Bandwidth limitation

Since the sensitivity functions for r and d have similar properties, in the following discussion, we use S_{r_d} to analyze the tracking performance limitation due to the factor introduced in Section 2.2.1. Similar procedures and results can be applied to the disturbance rejection performance for S_{d_d}.

Although Eq. (2.13) does not apply due to the instability of $M^{-1}(s)$, the feedback controller can still be constructed as Eq. (2.15) to cancel $G_{p\_m}(s)$, the minimal phase part of the plant dynamics. $N(s)$ is a transfer function left to be designed to achieve desired system behavior based on the distribution of the non-minimum phase zeros in $M(s)$. As a result, the loop transfer function can be reformed as Eq. (2.16) , and the performance limitation is simplified to be only related to the all-pass non-minimal phase term $M(s)$.

$$G_{fb\_d}(s) = N(s)G^{-1}{}_{p\_m}(s) \tag{2.15}$$

$$G_L(s) = M(s)N(s) \tag{2.16}$$

Researchers have studied the bandwidth limitation for feedback control with specifications on desired phase margin (PM) or gain margin (GM). One way to define the relationships among RHP zero a, the crossover frequency of the loop transfer function ω_{co}, PM, and GM, is to approximate the Bode diagram of the loop transfer function around ω_{co} [35][36]. The relationship for the variables mentioned above can be graphically found and shown in Eqs. (2.17) and (2.18), where α is a design parameter to define the approximate slope of the minimal phase part of the loop transfer function above ω_{co}.

$$\omega_{co} = a\tan\left((1-\alpha)\frac{\pi}{2} - \frac{PM}{2}\right) \tag{2.17}$$

$$GM = \left(\frac{\tan\frac{\alpha\pi + PM}{2}}{\tan\frac{\alpha\pi}{2}}\right)^{2\alpha} \tag{2.18}$$

Another way to estimate the achievable bandwidth is to calculate the optimal cheap controller with certain reference specifications, such as the step reference $r = u(t)$ [37, 38]. In this case, the bandwidth approximation is summarized in [30] as Eqs. (2.19) and (2.20). Further related research using similar techniques on a multiple input multiple output (MIMO) system can be found in [39].

$$\omega_0 \approx \frac{a}{2} \quad \text{for real } a \tag{2.19}$$

$$\omega_0 \approx \begin{cases} |a|/4 & \mathrm{Re}(a) > \mathrm{Im}(a) \\ |a|/2.8 & \mathrm{Re}(a) = \mathrm{Im}(a) \\ |a| & \mathrm{Re}(a) < \mathrm{Im}(a) \end{cases} \quad \text{for complex } a \tag{2.20}$$

Although perfect control is not achievable due to the presence of RHP zeros, there are some methods to design the controller using modified model inversion control, such as non-minimum phase zero ignore methods: zero-phase-error tracking controller (ZPETC) [40] and zero-magnitude-error tracking controller (ZMETC) [41]. Their performances are compared in [42].

2.3.2 Time delay

One significant influence from time delay on loop dynamics is the dramatic decrease of phase which increases proportionally with the frequency. Assuming a delay of T seconds,

the loop transfer function can be obtained as Eq. (2.21), where $G_{fb}(s)$ is the feedback controller, $G_{p\_r}(s)$ is the rational part of the transfer function, and e^{-sT} represents the phase lag effect from the delay. The corresponding sensitivity function is shown in Eq. (2.22). Since the feedback controller $G_{fb}(s)$ is causal, it is not able to compensate the delay which then induces the best achievable sensitivity function as Eq. (2.23). The Bode diagram of the sensitivity function is shown in Figure 2.6, where the achievable bandwidth ω_0 is at the first point where its magnitude curve crosses over 0dB.

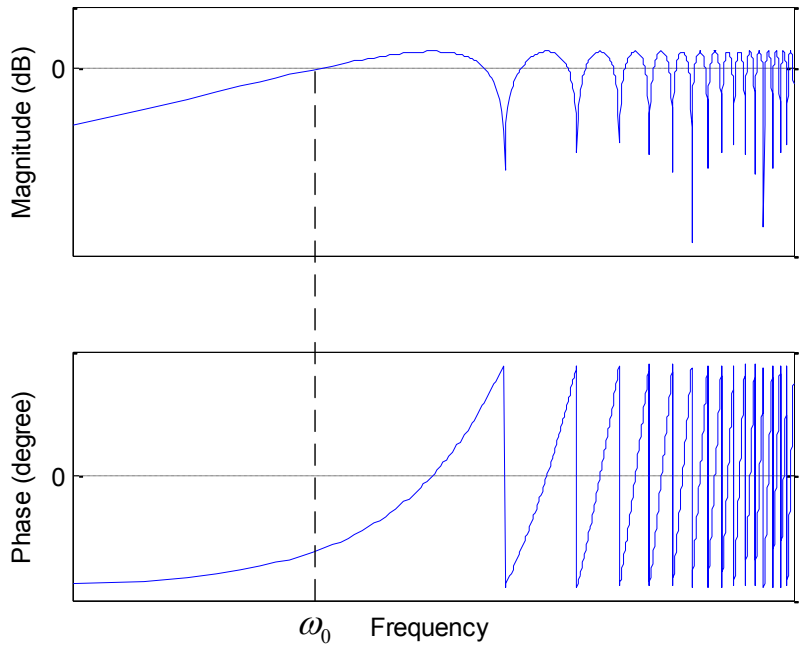

Figure 2.6 Bode Diagram of ideal sensitivity function of delayed system

The achievable bandwidth ω_0 is approximated as $1/T$ in [30] using Taylor series expansion. More precisely, by solving Eq. (2.24), one can calculate Eq. (2.25), which means

that for systems with delays as large as T, no feedback control can achieve a bandwidth higher than $\frac{\pi}{3T}$.

$$G_L = G_{fb}(s)G_{p\_r}(s)e^{-sT} \tag{2.21}$$

$$S_{r\_d} = 1 - G_{fb}(s)G_{p\_r}(s)e^{-sT} \tag{2.22}$$

$$S_{r\_d\_opt} = 1 - e^{-sT} \tag{2.23}$$

$$\left|S_{r\_d\_opt}(j\omega)\right| = \left|1 - e^{-j\omega T}\right| = 1 \tag{2.24}$$

$$\omega_T = \frac{\pi}{3T} \tag{2.25}$$

2.3.3 Model uncertainty

When discussing achievable performance for systems with modal uncertainty, there are two aspects to consider: robust stability and robust performance. The former is a necessary requirement to make the closed loop system stable under certain tolerance of modal uncertainty, and the latter is to discuss the best performance to achieve when robust stability is guaranteed.

Using the IMC structure in Figure 2.5(d), the internal stability of the system is equivalent to letting $G_{fb\_d}(s)$ stabilize $\Delta_p(s)$ with a unity feedback loop as shown in Figure 2.3. In the following analysis, $\Delta_p(s)$ is assumed to be stable which is usually true for a large class of physical systems. If we draw the loop transfer function in a complex plane, according to the Nyquist stability criterion, the stability condition for the feedback loop in Figure 2.3 is that $G_{fb\_d}(j\omega)\Delta_p(j\omega)$ cannot be smaller than $(-1,0)$ for all ω as shown in

Figure 2.7. The red curve represents the transfer function $G_{fb\_d}(j\omega)$ that is to be designed. With the uncertainty $\Delta_p(s)$ bounded by $\bar{\Delta}_p(s)$ for some ω, $G_{fb\_d}(j\omega)\Delta_p(j\omega)$ will always lie in the uncertain disk with the center at the original point and radius equal to $\bar{\Delta}_p(\omega)\left|G_{fb\_d}(j\omega)\right|$. To ensure robust stability of the system, the disk cannot cover the point $(-1,0)$ for any ω. In other words, the inequality of Eq. (2.26) must be satisfied.

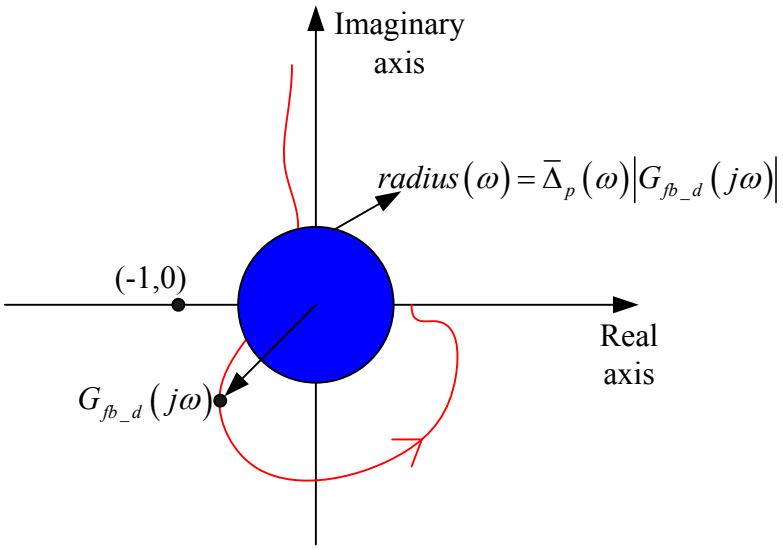

Figure 2.7 Uncertain disk for feedback control

$$\left|G_{fb\_d}(j\omega)\right| < \frac{1}{\bar{\Delta}_p(\omega)} \tag{2.26}$$

To analyze the achievable robust performance when model uncertainty exists, the sensitivity function can be expressed as Eq. (2.27). The candidate feedback controller, $G_{fb\_d}(s)$, to minimize $S(s)$ must satisfy the constraint in Eq. (2.26). ω_{co_Δ} is defined as the frequency where $\bar{\Delta}_p(\omega)$ intersects the magnitude of $G_{p0}(s)$, as shown in Figure 2.8.

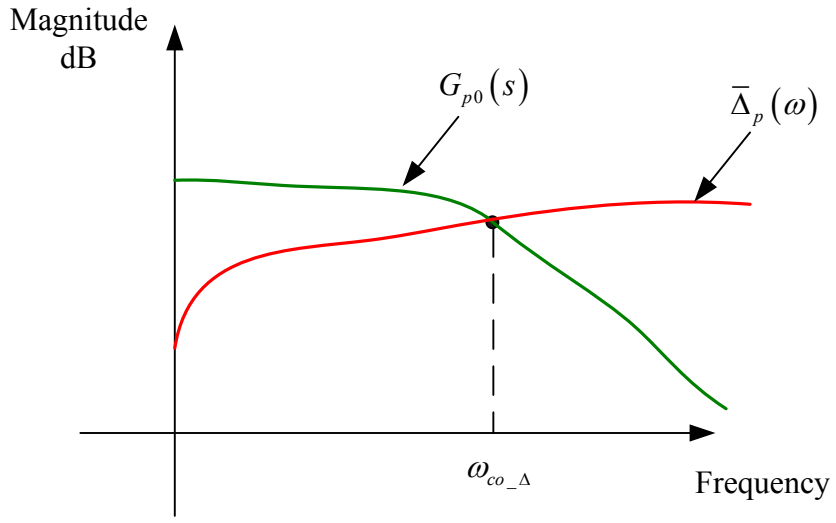

Figure 2.8 Uncertainty crossover frequency

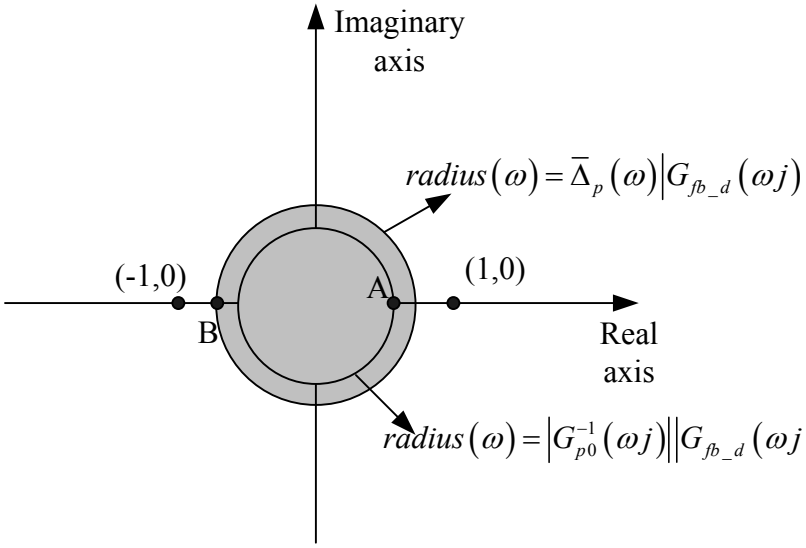

Figure 2.9 Optimal Design for $G_{fb\_d}(s)$

$G_{fb\_d}(s)$ must be carefully designed to minimize the magnitude of the sensitivity function $|S(j\omega)|$. Figure 2.9 shows the relationship between the magnitudes of the transfer functions in Eq. (2.27).

$$S(s)=\frac{1-G_{p0}(s)G_{fb\_d}(s)}{1+\Delta_p(s)G_{fb\_d}(s)} \tag{2.27}$$

To minimize $|S(\omega j)|$, $G_{fb\_d}(j\omega)$ needs to minimize the magnitude of the numerator in Eq. (2.27). The magnitude of the numerator $|1-G_{p0}(j\omega)G_{fb\_d}(j\omega)|$ can be viewed as the distance between $G_{p0}(j\omega)G_{fb\_d}(j\omega)$ and the point $(1,0)$ in the complex plane. Therefore, the smallest magnitude $|1-G_{p0}(j\omega)G_{fb\_d}(j\omega)|$ can be found by choosing $G_{p0}(j\omega)$ to place $G_{p0}(j\omega)G_{fb\_d}(j\omega)$ at point A on the real axis in Figure 2.9. This adds one constraint to $G_{fb\_d}(j\omega)$ by making $\angle(G_{fb\_d}(j\omega))=-\angle(G_{p0}(j\omega))$.

On the other hand, the magnitude of the denominator $|1+\Delta_p(j\omega)G_{fb\_d}(j\omega)|$ can be viewed as the distance between $\Delta_p(j\omega)G_{fb\_d}(j\omega)$ and $(-1,0)$ in the complex plane. The worst case uncertainty $\Delta_p(s)$ will induce a value of $\Delta_p(j\omega)G_{fb\_d}(j\omega)$ located at point B on the real axis in Figure 2.9 with the minimum magnitude of the denominator.

The above analysis gives the relationship between the magnitude of $|G_{fb\_d}(\omega j)|$ and the resulting sensitivity function magnitude denoted as $|S(\omega j)|_{ach}$ shown in Eq. (2.28) under the uncertainty $\Delta_p(s)$. The optimal $|G_{fb\_d}(\omega j)|$ is to minimize $|S(\omega j)|_{ach}$, as shown in Eq. (2.29).

It is possible to find some $G_{fb\_d}(s)$ such that $\left|G_{fb\_d}(j\omega)\right| = \frac{1}{\left|G_{p0}(j\omega)\right|}$ and $\angle G_{p0}(j\omega) = -\angle\left(G_{p0}(j\omega)\right)$ (or equivalently $G_{fb\_d}(s) = G_{p0}^{-1}(s)$), which makes $\left|S(\omega j)\right|_{ach} = 0$.

$$\left|S(\omega j)\right|_{ach} = \frac{1-\left|G_{p0}(\omega j)\right|\left|G_{fb\_d}(\omega j)\right|}{1-\bar{\Delta}_p(\omega)\left|G_{fb\_d}(\omega j)\right|} \tag{2.28}$$

$$\left|G_{fb\_d}(\omega j)\right|_{opt} = \min_{\left|G_{fb\_d}(\omega j)\right|}\left\{\left|S(\omega j)\right|_{ach}\left|\left|G_{fb\_d}(\omega j)\right| < \frac{1}{\bar{\Delta}_p(\omega)}\right\} \tag{2.29}$$

For $\omega \in \left[\omega_{co\_\Delta}, \infty\right)$, the two magnitude inequalities become $\left|G_{p0}(\omega j)\right| < \bar{\Delta}_p(\omega)$ and $\left|G_{fb\_d}(j\omega)\right| < \frac{1}{\bar{\Delta}_p(\omega)}$. Accordingly, $\left|G_{fb\_d}(j\omega)\right| = \frac{1}{\left|G_{p0}(j\omega)\right|}$ is not feasible anymore. In this case, the relationship between $\left|G_{fb\_d}(j\omega)\right|$ and $\left|S(\omega j)\right|_{ach}$ is illustrated in Figure 2.10, which indicates that any non-trivial feedback will cause the magnitude of the sensitivity function to be larger than 1 at frequencies above ω_{co_Δ}. Therefore, ω_{co_Δ} becomes the bandwidth limitation for the feedback controller as a result of model uncertainty $\Delta_p(s)$. Increasing $\left|G_{fb\_d}(j\omega)\right|$ will deteriorate the control performance so a high gain controller is not desirable where $\omega > \omega_{co\_\Delta}$.

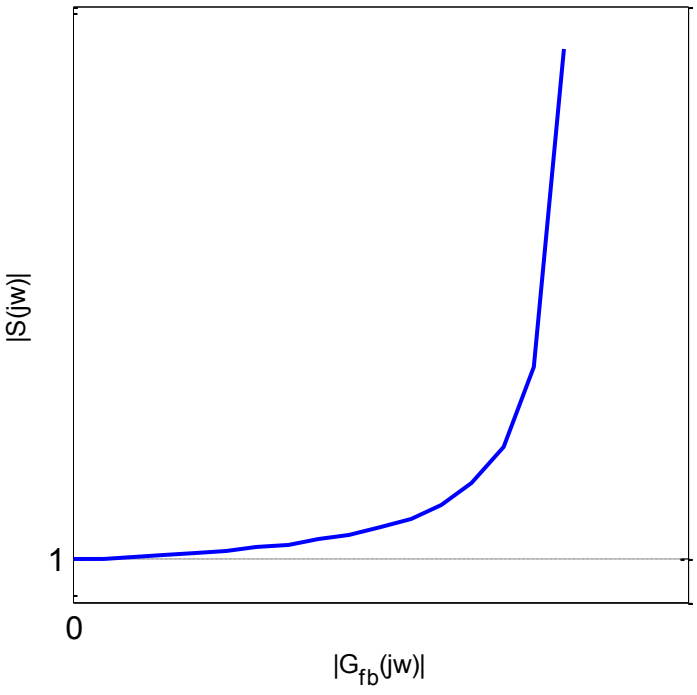

Figure 2.10 Relationship between $\left|G_{fb\_d}(j\omega)\right|$ and $\left|S(\omega j)\right|_{ach}$ for $\omega \in \left[\omega_{co\_\Delta}, \infty\right)$

It is worth mentioning that this result has the same implication as the concept 'available bandwidth' Ω_a in[33], which is defined as the frequency range over which the unstructured multiplicative perturbations are substantially less than unity (equivalent to $0 \le \omega \le \omega_{co}$). The Bode Integral for such uncertain systems is reduced to be Eq. (2.30), which implies that for a given feedback design, the sensitivity improvements as well as the sensitivity deteriorations, must occur within $0 < \omega < \Omega_a$; therefore Ω_a, which is ω_{co_Δ} in the analysis above, is the bandwidth limitation.

$$\int_0^{\Omega_a} \ln\left|S(\omega j)\right| d\omega = -\frac{\pi}{2}\lim_{s\to\infty} sL(s) + \delta \text{ where } \delta \text{ is small value} \qquad (2.30)$$

2.3.4 Noise

In order to respond to fast-changing exogenous signals, the feedback controller must have large gain by intuition. However, this inevitably amplifies the noise in the feedback signal at the same time, which potentially limits the closed loop performance.

The influence of noise on information transmission has been thoroughly explored in the field of information theory which mainly studies the transmissibility of information channels when noise is present. In recent decades, the impact of noise on feedback control has been studied by using tools from both information science and control theory. The relevant research focuses mainly on how the feedback control stability and bandwidth are limited in two ways: 1) the transmitting capacity of the channel, or in other words the upper bound of the transmitting rate [43, 44] and 2) the signal-to-noise ratio (SNR) [45, 46].

The topic described above is beyond the focus of this dissertation; therefore, only the simple case where neither limitations on the capacity nor SNR appears is discussed. In this case, the limitation caused by the noise is due to the relationship of the two sensitivity functions: the sensitivity function in Eq. (2.31) and the complementary sensitivity function in Eq. (2.32). To achieve perfect tracking, $S_{r\_d}(s)$ should be 0; to achieve perfect noise attenuation, $T_{r\_d}(s)$ should be 0. However, due to the relationship $S_{r\_d}(s)+T_{r\_d}(s)=1$, these two objectives can never be achieved at the same time. Instead, they work as trade-offs in designing $G_{fb\_d}(s)$. At a certain frequency ω, the closed loop error can be expressed as Eq. (2.33).

$$S_{r\_d}=\frac{1-G_{fb\_d}G_{p0}}{1+\Delta_p G_{fb\_d}} \tag{2.31}$$

$$T_{r\_d} = -S_{n\_d} = \frac{G_{fb\_d}\left(G_{p0} + \Delta_p\right)}{1 + \Delta_p G_{fb\_d}} \tag{2.32}$$

$$e(\omega) = S_{r\_d}(\omega) r(\omega) + (1 - S_{r\_d}(\omega)) n(\omega) \tag{2.33}$$

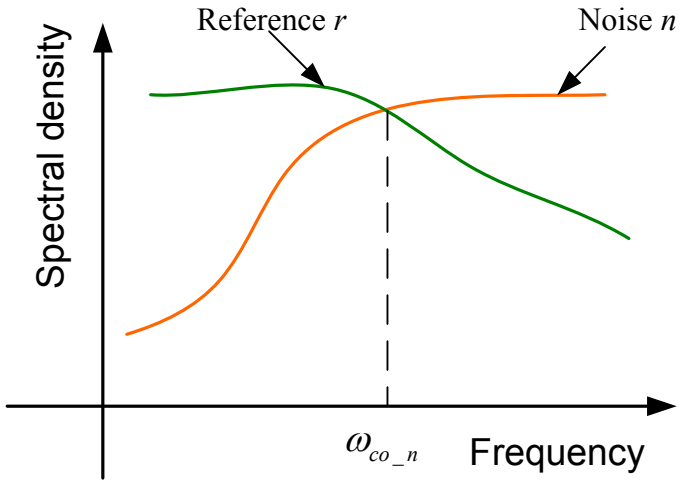

Figure 2.11 Spectral density for reference and noise

To make $e(\omega) < r(\omega)$, the inequality $n(\omega) < r(\omega)$ has to be satisfied. If we draw the power density function of r and n as in Figure 2.11, the frequency where the power density of noise crosses over the reference signal is denoted as ω_{co_n}. For a frequency beyond ω_{co_n}, it is not possible to get the error signal smaller than the reference itself. Therefore, ω_{co_n} works as the bandwidth limitation for feedback control.

2.3.5 Combined effect from model Uncertainty and delay

The advantage of feedforward control compared to feedback control is the ability to generate a non-causal input using pre-known exogenous signal information. The causal feedforward limitation, in terms of performance, is equivalent to feedback control given its lack of ability to act proactively. This conclusion has been drawn for Iterative Learning

Control (ILC) in [47], and we will discuss this equivalence briefly using the schematics in Figure 2.5(d).

With both delay and model uncertainty considered, the sensitivity function $S_{r\_d}(s)$ from the reference to the tracking error in Figure 2.5(d) can be expressed in Eq. (2.34).

$$S_{r\_d}(s)=\frac{1-e^{-Ts}G_{p0}(s)G_{fb\_d}(s)}{1+\Delta_p(s)G_{fb\_d}(s)} \tag{2.34}$$

$$\left|S_{r\_d}(\omega j)\right|_{ach}=\frac{1-\left|G_{p0}(\omega j)\right|\left|G_{fb\_d}(\omega j)\right|}{1-\bar{\Delta}_p(\omega)\left|G_{fb\_d}(\omega j)\right|} \text{ with } \left|G_{fb\_d}(\omega j)\right|<\frac{1}{\bar{\Delta}_p(\omega)} \tag{2.35}$$

For $\omega\in\left[\omega_{co\_\Delta},\infty\right)$, $\left|G_{fb\_d}(\omega j)\right|$ needs to be carefully chosen to minimize the magnitude of the sensitivity function. For a fixed controller magnitude $\left|G_{fb\_d}(\omega j)\right|$ at ω, the smallest magnitude of the numerator in Eq. (2.34) can be achieved by placing $e^{-T\omega j}G_{p0}(\omega j)G_{fb\_d}(\omega j)$ at point A in Figure 2.12 by making $\angle G_{fb\_d}(\omega j)=-\angle\left(e^{-T\omega j}G_{p0}(\omega j)\right)$. On the other hand, the worst case uncertainty $\Delta_p(s)$ will induce a $\Delta_p(\omega j)G_{fb\_d}(\omega j)$ located at point B with the minimum magnitude of the denominator. This gives the relationship between the magnitude of $\left|G_{fb\_d}(\omega j)\right|$ and the minimum of the sensitivity function magnitude denoted as $\left|S_{r\_d}(\omega j)\right|_{ach}$, under the uncertainty $\Delta_p(s)$ as shown in Eq. (2.35). Since $\left|G_{p0}(\omega j)\right|<\bar{\Delta}_p(\omega)$, any non-trivial feedback will cause the magnitude of the sensitivity function to be larger than 1 at frequencies above ω_{co_Δ}. Therefore, ω_{co_Δ} becomes a bandwidth limitation for the feedback

controller as a result of model uncertainty. Increasing the feedback gain $\left|G_{fb\_d}(\omega j)\right|$ will deteriorate the control performance so a high gain controller is not desirable when $\omega > \omega_{co\_\Delta}$.

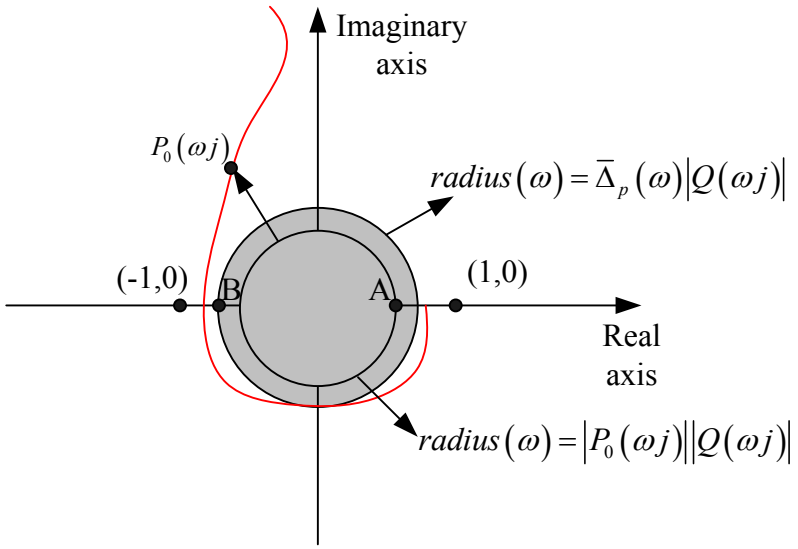

Figure 2.12 Optimal design for $G_{fb\_d}(s)$

Upon further examination of the range $\omega \in [0, \omega_{co}]$, the combined effect of the delay T and model uncertainty Δ_p provide a more restrictive bandwidth limitation. Choosing $G_{fb\_d}(s) = G_{p0}^{-1}(s)$, the upper bound of the sensitivity function magnitude is shown in Eq. (2.36); therefore, the closed loop bandwidth is limited by ω_{T_Δ} defined in Eq. (2.37), which synthesizes the combined effect of the delay and model uncertainty on the overall achievable performance. By comparing ω_{T_Δ} with ω_T and ω_{co_Δ}, it satisfies $\omega_{T\_\Delta} < \omega_T$ and $\omega_{T\_\Delta} < \omega_{co\_\Delta}$. Therefore, as previously mentioned, the combined limitation is more restrictive on the achievable performance than either individual limitation.

$$\bar{S}_1(\omega) = \frac{\left|1 - e^{-T\omega j}\right|}{1 - \bar{\Delta}_p(\omega)\left|G_{p0}^{-1}(\omega j)\right|} \tag{2.36}$$

$$\omega_{T\_\Delta} = \max\left(\omega \; s.t. \; \bar{\Delta}_p(\omega) \le \left(1 - \left|1 - e^{-T\omega j}\right|\right)\left|G_{p0}(\omega j)\right|\right) \tag{2.37}$$

The analysis above can be summarized as follows. For feedback control, the bandwidth limitation from the delay is ω_T and the bandwidth limitation from plant uncertainty is ω_{co_Δ}. These are combined to result in an overall limitation ω_{T_Δ} which is lower than either ω_T or ω_{co_Δ}.

2.4 Performance Limitations for Feedforward Control

2.4.1 Causal feedforward control

The advantage of feedforward control compared to feedback control is the ability to generate a non-causal input using pre-known exogenous signal information. The causal feedforward, in terms of performance limitation, is equivalent to feedback control for it is lack of the ability to act proactively. This conclusion has been drawn for Iterative Learning Control (ILC) in [47], and we will discuss this equivalence briefly using the schematics in Figure 2.5(d).

When there is no model uncertainty, the sensitivity function from the reference to the output in Eq. (2.6) can be simplified as in Eq. (2.38), which shows that the feedforward controller $G_{fb\_d}(s)$ plays the exactly same role with the feedback controller $G_{ffr\_d}(s)$ for the system in Figure2.5(d). Therefore, achievable performance for feedback control and feedforward control are the same for systems with no model uncertainty. This means if there

are non-minimum phase zeros or a delay in $G_{p0}(s)$, the causal feedforward control has the exact same performance limitation as the feedback control, which is shown in Section 2.3.1 and Section 2.3.2.

$$S_{r\_d} = 1 - \left(G_{ffr\_d} + G_{fb\_d}\right) G_{p0} \tag{2.38}$$

$$S_{r\_d} = \frac{1 - G_{fb\_d} G_{p0} - G_{ffr\_d}\left(G_{p0} + \Delta_p\right)}{1 + \Delta_p G_{fb\_d}} \tag{2.39}$$

$$G_{ffr\_d}(s) = G_{p0}^{-1}(s) - G_{fb\_d}(s) \tag{2.40}$$

When there is model uncertainty, the sensitivity function becomes Eq. (2.39). The feedback controller $G_{fb\_d}(s)$ ensures robust stability based on the analysis described in Section 2.3.3. The feedforward controller, on the other hand, is designed to achieve the best nominal performance.

For a MP system, the feedforward controller can be designed using the model inversion shown in Eq. (2.40) to achieve perfect nominal performance. In the presence of model uncertainty $\Delta(s)$, however, the sensitivity function becomes Eq. (2.41) instead of 0. Similar to the work discussed in Section 2.2, the transfer function relationship is drawn in Figure 2.13 to analyze the best achievable sensitivity function magnitude.

$$S_{r\_d} = \frac{\Delta_p\left(G_{p0}^{-1} - G_{fb\_d}\right)}{1 + \Delta_p G_{fb\_d}} \tag{2.41}$$

$$\left|S(\omega j)\right|_{ach} = \frac{\bar{\Delta}_p(\omega)\left(\left|G_{p0}{}^{-1}(\omega j)\right| - \left|G_{fb\_d}(\omega j)\right|\right)}{1 - \bar{\Delta}_p(\omega)\left|G_{fb\_d}(\omega j)\right|} \tag{2.42}$$

$$\left|G_{fb\_d}(\omega j)\right|_{opt} = \min_{\left|G_{fb\_d}(\omega j)\right|}\left\{\left|S(\omega j)\right|_{ach} \left| \left|G_{fb\_d}(\omega j)\right| < \frac{1}{\bar{\Delta}_p(\omega)}\right.\right\} \tag{2.43}$$

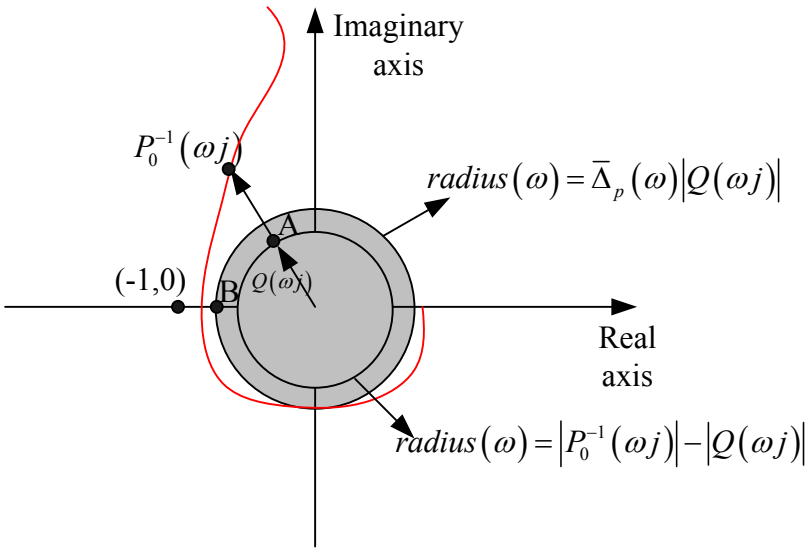

Figure 2.13 Robust performance analysis for MP plant system with causal feedforward

To minimize $|S(\omega j)|$, $G_{fb\_d}(j\omega)$ must minimize the magnitude of the numerator in Eq. (2.41). The magnitude of the numerator $|G_{p0}^{-1}(j\omega) - G_{fb\_d}(j\omega)|$ can be viewed as the distance between $G_{fb\_d}(j\omega)$ and $G_{p0}(j\omega)$ in the complex plane. Therefore, the smallest magnitude $|G_{p0}^{-1}(j\omega) - G_{fb\_d}(j\omega)|$ can be found by designing $G_{p0}(j\omega)$ to be at point A in Figure 2.13. This adds one constraint on $G_{p0}(j\omega)$ by making the following equality true: $\angle(G_{fb\_d}(j\omega)) = -\angle(G_{p0}(j\omega))$.

On the other hand, the magnitude of the denominator $|1 + \Delta_p(j\omega)G_{fb\_d}(j\omega)|$ is the same as what is shown in Section 2.3.3; the worst-case uncertainty $\Delta_p(s)$ will induce a value of $\Delta_p(j\omega)G_{fb\_d}(j\omega)$ located at point B on the real axis in Figure 2.13 with the minimum magnitude of the denominator.

The above analysis gives the relationship between the magnitude of $\left|G_{fb\_d}(\omega j)\right|$ and the minimum of the sensitivity function magnitude denoted as $\left|S(\omega j)\right|_{ach}$ and shown in Eq. (2.42) under the uncertainty $\Delta_p(s)$. The optimal $\left|G_{fb\_d}(\omega j)\right|$ can be obtained by minimizing $\left|S(\omega j)\right|_{ach}$ as shown in Eq. (2.43).

For $\omega \in \left[0, \omega_{co\_\Delta}\right)$, the situation is similar to feedback control. Since $\left|G_{p0}(\omega j)\right| > \bar{\Delta}_p(\omega)$ and $\left|G_{fb\_d}(j\omega)\right| < \frac{1}{\bar{\Delta}_p(\omega)}$, some $G_{fb\_d}(s)$ exists such that $G_{fb\_d}(s) = G_{p0}^{-1}(s)$, which makes $\left|S(\omega j)\right|_{ach} = 0$.

For $\omega \in \left[\omega_{co\_\Delta}, \infty\right)$, since the inequalities $\left|G_{p0}(\omega j)\right| < \bar{\Delta}_p(\omega)$ and $\left|G_{fb\_d}(j\omega)\right| < \frac{1}{\bar{\Delta}_p(\omega)}$ are true, $\left|G_{fb\_d}(j\omega)\right| = \frac{1}{\left|G_{p0}(j\omega)\right|}$ is no longer feasible. In this case, the relationship between $\left|G_{fb\_d}(j\omega)\right|$ and $\left|S(\omega j)\right|_{ach}$ is drawn in Figure 2.14, which indicates that any non-trivial feedback will cause the magnitude of the sensitivity function to be larger than 1 at frequencies above ω_{co_Δ}. Therefore, ω_{co_Δ} is also the bandwidth limitation for the feedforward control as a result of model uncertainty $\Delta_p(s)$.

From the analysis above, the causal model inversion feedforward control cannot improve the achievable bandwidth compared to pure feedback control neither for the nominal performance nor the robust performance. A similar conclusion can be found in [48]. After analyzing the two norms of the error expression by the optimal H_2 controller, no benefit was found from adding a feedforward controller for a MP system.

$$\left|S(\omega j)\right|_{ach} = \frac{1-\left|G_{p0}(\omega j)\right|\left|G_{fb\_d}(\omega j)\right|}{1-\bar{\Delta}_p(\omega)\left|G_{fb\_d}(\omega j)\right|} \tag{2.44}$$

$$\left|G_{fb\_d}(\omega j)\right|_{opt} = \min_{|G_{fb\_d}(\omega j)|}\left\{\left|S(\omega j)\right|_{ach}\left|G_{fb\_d}(\omega j)\right| < \frac{1}{\bar{\Delta}_p(\omega)}\right\} \tag{2.45}$$

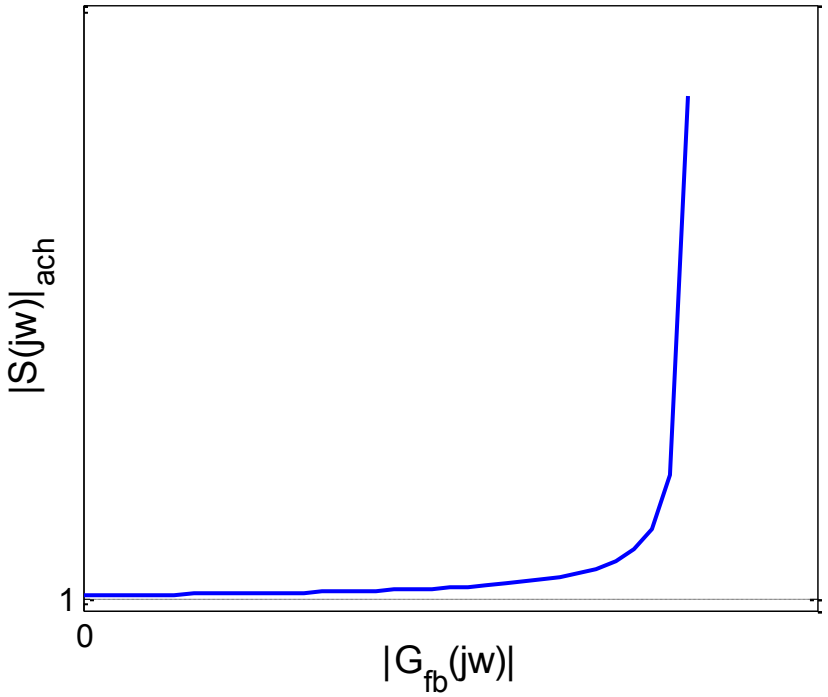

Figure 2.14 Relationship between $\left|G_{fb\_d}(j\omega)\right|$ and $\left|S(\omega j)\right|_{ach}$ when $\omega \in \left[\omega_{co\_\Delta}, \infty\right)$ for causal feedforward control for MP system

2.4.2 Non-causal feedforward with modal uncertainty

If there is neither model uncertainty nor signal uncertainty, the non-causal feedforward controller can eliminate the limitation caused by the non-minimum phase system and delay for feedback control [48]. However, when there are uncertainties, such ideal control performance cannot be achieved. Instead, extra error is introduced. To answer the question of when a non-causal feedforward controller can improve the performance under

model uncertainty, Devasia compared the corresponding error sensitivity functions for both controlled systems [49]. The feedforward control is designed to achieve perfect performance for a normal system, as discussed in Section 2.4.1. The conclusion is intuitively correct and shown in Eq. (2.46); for small model uncertainties, the feedforward controller can decrease the tracking error. When the uncertainties are larger than certain conditions, the extra error induced by model uncertainty from the feedforward loop will actually increase the error.

$$\begin{cases} \left\|\Delta(j\omega)\right\|_2 \le \dfrac{\left\|G_{p0}(j\omega)\right\|_2}{\kappa G_{p0}(j\omega)} & e_{(ff+fb,\Delta)}(j\omega) \le e_{(fb,\Delta)}(j\omega) \\ \left\|\Delta(j\omega)\right\|_2 > \left\|G_{p0}(j\omega)\right\|_2 & e_{(ff+fb,\Delta)}(j\omega) > e_{(fb,\Delta)}(j\omega) \end{cases} \tag{2.46}$$

$\kappa G_{p0}(j\omega) := \left\|G_{p0}(j\omega)\right\|_2 \left\|G_{p0}^{-1}(j\omega)\right\|_2$ is the condition number of the matrix $G_{p0}(j\omega)$ based on the induced two-norm with the model uncertainty defined as $\Delta = G_{p0} - G_p$.

Almost all of the analyses for robust performance of feedforward control are more or less similar to the methods discussed above which usually needs to minimize a certain norm of the sensitivity function of the two DOF control system under the influence of model uncertainties. In detail, there is some difference in how such a robust feedforward controller is designed. One way is to directly use model inversion-based control such as Fannes and Skogestad's work in [50]. They also discussed how different classes of uncertainties, such as static gain uncertainty, delay uncertainty, time constant uncertainty, pole uncertainty, and more general uncertainty by frequency domain representation, affect the error. Another way is to add a modifying term/filter to the model inversion feedforward controller. The parameters in the filter, such as time constant, can be tuned to obtain the minimum value for the sensitivity functions [51]. In [52], one can assume that the magnitude and phase values of

the model uncertainty in all frequency ranges are known, and the filter can be calculated correspondingly. The trade-off by adding a filter is discussed in [28]; it will deteriorate the nominal performance and reduce performance degradation due to uncertainty. The third method is to use robust control synthesis for improving reference tracking [26]. The feedforward controller is designed either with a pre-existing feedback controller or optimized simultaneously with the feedback controller to minimize sensitivity functions from reference and the uncertainty output to the error. The resulting controller usually obtains higher order controllers than the other two methods.

The non-causal feedforward controller works no different than the causal feedforward controller for the MP system (Eq. (2.40) is valid for both). From the work in [27] , the feedforward controller (even a non-causal one) works no better than pure feedback for MP system when the H_2 norm of the error is examined for a step reference. In the following discussion, we mainly focus on the influence of the non-causal feedforward control on the NMP system.

For the time delay term in the plant dynamics, non-causal feedforward control can obviously improve performance by using a time-forward term e^{sT}. For example, if we let $G_{fb\_d}(s)=0$ and $G_{ffr\_d}(s)=e^{sT}$ (the rational part of the plant is ignored here to simplify the discussion), then we can obtain perfect nominal tracking performance which is not achievable by pure feedback control or causal feedforward control. When there is model uncertainty, however, the sensitivity function becomes Eq. (2.47). The sensitivity function magnitude equals $\left|\Delta_p\right|$ since the delay does not contribute to magnitude at all frequencies; the achievable bandwidth is where $\bar{\Delta}_p(\omega)$ crosses over 0dB, which is denoted as $\omega_{\Delta 0}$.

$$S(s) = \Delta_p(s) e^{sT} \tag{2.47}$$

For a RHP zero, the design of the non-causal controller is much more complicated. The inversion of the model will be unstable; therefore, it is difficult to find a non-causal controller for perfect nominal tracking performance that can be represented by the transfer function. For this reason, the research on non-causal feedforward control focuses more on generation of the input signal with the specification of a reference (or disturbance) signal. For example, when the input signal is a unit step, the control signal that generates perfect tracking for $M(s) = \frac{(-s+z)}{s+z}$ is shown in Eq. (2.48) [53], the Laplace transform of which does not exist. In reality, it is not possible to use the information in an infinite horizon; therefore, for non-causal feedforward control (or preview control), the controller usually uses a finite predicted horizon; model predictive control (MPC) is one such example. Theoretically, the more distant and more accurate the controller can predict, the better the performance will be. An interesting result is shown in [54] stating that the achievable minimum value of the H_∞ norm of a preview controller is approximately proportional to $e^{-\min(\mathrm{Re}(z_i))T_{pre}}$, where T_{pre} is the prediction horizon. However, when designing the controller, it is also important to consider the trade-off between the preview time length and practical control constraints (e.g., signal accuracy, computational complexity).

$$u(t) = \begin{cases} 2e^{zt} & t < 0 \\ 1 & t \geq 0 \end{cases} \tag{2.48}$$

2.4.3 Non-causal feedforward with signal uncertainty

While there has been significant effort towards understanding model uncertainty effects, the influence from signal uncertainty has received less research attention in designing feedforward controllers. This may be because the feedforward terms are assumed to be generated by reference commands and not by measureable exogenous signals with their associated uncertainties. However, in some applications, such as path-following tasks, the reference is unknown. This implies that when using non-causal feedforward control, the signal fed to the controller ahead of time can deviate from the true value for a certain amount of time. This deviation, herein called signal uncertainty, can induce large errors by feedforward control. Such a phenomenon is more common when the feedforward controller is used to cancel pre-measured disturbances or noises.

When there is no model uncertainty, the sensitivity function from the reference signal and signal uncertainty to the error signal for the feedforward controller is shown in Eq. (2.49); to make S_{r_d} equal to 0, $G_{ffr\_d} = G_{p0}^{-1}$. If we want to decrease the error caused by model uncertainty, G_{ffr_d} should be small. These two objectives compete with each other and cannot be satisfied simultaneously.

The error e can be expressed as shown in Eq. (2.50). To make $e(\omega) < r(\omega)$, the inequality $\Delta r(\omega) < r(\omega)$ must be satisfied. Therefore, the frequency at which the power density of Δr increases over r, denoted as $\omega_{co\_\Delta rvsr}$, becomes a bandwidth limitation for the feedforward control.

$$\begin{aligned} S_{r\_d} &= 1 - G_{ffr\_d} G_{p0} \\ S_{\Delta r\_d} &= G_{ffr\_d} G_{p0} \end{aligned} \tag{2.49}$$

$$e = \left(1 - G_{ffr\_d} G_{p0}\right) r + G_{ffr\_d} G_{p0} \Delta r \tag{2.50}$$

$$e = \left(1 - G_{ffr\_d} G_{p0}\right) r + G_{ffr\_d} G_{p0} \Delta r < r \tag{2.51}$$

2.5 Conclusions

This chapter discusses the achievable performance using different control architectures under various constraints from physical system properties. Limitations are caused by undesirable system dynamics and inaccurate knowledge of the system dynamics and exogenous signals. The factors discussed include non-minimum phase zeros, delays, model uncertainty, signal uncertainty, and noise. The induced control limitations cannot be overcome solely by control algorithm design. Though understanding for the existing limitation cannot explicitly provide a specific control solution, it can contribute in exploring the system design and control approaches in the preliminary stage, understanding the bottleneck of the system performance, and providing estimation on the ultimate performance before significant calculation and simulation.

The main results are listed in Table 2.1 which describes the upper bound of the achievable bandwidth independent of what design criterion or method is used to obtain the controller. Two illustrative conclusions are drawn from the results shown in the table: 1) the causal feedforward controller does not help to improve achievable performance compared to the feedback controller; 2) for the MP plant, the feedback controller has the same performance limitation as the feedforward controller (including the non-causal feedforward controller). Non-causal feedforward control can eliminate the bandwidth limitation imposed by delays or RHP zeros in feedback control. However, it does not help to improve the

performance when there is model uncertainty; in addition, extra error can be induced by signal uncertainty.

When there are several factors existing at the same time, which is usually the case for real systems, the combined effect can induce even lower bandwidth limitations. This topic has been studied in some research articles [55-57] but is still an open research area.

Chapter 3 will give a comprehensive modeling and analysis for the HHC problem, which is used as an example of a VEI system in this dissertation. The separate and combined bandwidth limitations from the combine system are provided according to the results in Table 2.1.

Table 2.1 Bandwidth limitations from physical system

	Model Uncertainty	RHO zeros	Delay	Signal Uncertainty	Feedback Noise
Feedback	ω_{co_Δ}	$\frac{a}{n}$	$\frac{\pi}{3T}$	N/A	ω_{co_n}
Casual Feedforward	ω_{co_Δ}	$\frac{a}{n}$	$\frac{\pi}{3T}$	$\omega_{co\_\Delta rvsr}$	N/A
Non-Casual Feedforward	ω_{co_Δ}	∞	∞	$\omega_{co\_\Delta rvsr}$	N/A

Chapter 3
Control Challenges for Vehicle-Environment Interaction (VEI) Systems

In this chapter, commonly existing characteristics of VEI systems that cause performance limitations for feedback control are discussed. In particular, a header height control (HHC) problem for combine harvesters is used as an example to study. Under-actuation and non-collocation are two important features of the vehicle header mechanical system which contribute to these performance limitations. Another influential factor is the significant impact of the hydraulic actuator delay on feedback bandwidth. In combination, the two problems mentioned above each reinforce the effect of the other, thereby exacerbating the overall system limitation of the closed loop bandwidth.

The HHC system is firstly modeled to reveal the existence of the two characteristics mentioned above. Theoretical analysis for achievable bandwidth in Chapter 2 is used to get a quantitative estimation for the bandwidth limitations that stem from specific system features. The model and corresponding limitations analysis are validated by both simulation and experimental results. The problems discussed in this chapter then serve to motivate the work in the following content of this dissertation.

3.1 Physical features of VEI systems

3.1.1 Under-actuated and non-collocated systems

Under-actuated systems are those that possess fewer numbers of actuators than the number of degrees of freedom (DOFs). This is commonly seen in the area of robotics such as the Pendubot [58], Acrobot [59], and Brachivation robot [60]. For rigid body systems, under-actuation means the system is non-holonomic, which creates control problems such as feedforward nonlinearity and non-minimum phase dynamics [61].

Assume an under-actuated manipulator has *n* independent DOFs, *m* of which are actuated; the remaining *l*=*n*-*m* DOFs are termed passive. As illustrated in [62], the corresponding *n* generalized coordinates can be written as $q^T = \left(q_1^T, q_2^T\right)$, where $q_1 \in R^l$ and $q_2 \in R^m$ correspond to the passive DOFs and active DOFs, respectively. The dynamic equations of the *n* DOF system can be written as follows [63]:

$$m_{11}\ddot{} \qquad \ddot{} \qquad \phi_1 = 0 \tag{3.1}$$

$$m_{21}\ddot{} \qquad \ddot{} \qquad \phi_2 = \tau \tag{3.2}$$

where the vector functions $h_1\left(q,\dot{}\right.$ and $h_2\left(q,\dot{}\right.$ contain Coriolis and centrifugal terms (likely small in the current application), the vector function $\phi_1\left(q\right) \in R^l$ and $\phi_2\left(q\right) \in R^m$ contain gravitational terms, and $\tau \in R^m$ represents the input generalized force.

The combine system discussed as an example in this dissertation is a typical under-actuated system. Figure 3.1 shows a schematic of a combine harvester system operating in the vertical plane. As it is stated in Chapter 1, the HHC objective is to maintain a constant header height with respect to the ground surface. The hydraulic actuator, which is installed

between the header and the vehicle body, is used to adjust the header height under a current command sent by the controller.

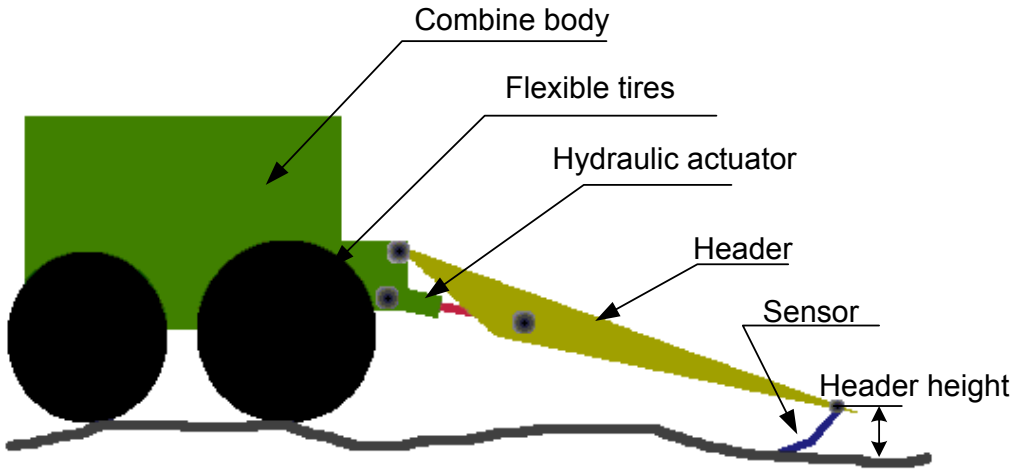

Figure 3.1 Structure of a combine harvester

The combine system can be simplified as the planar multi-body system shown in Figure 3.2 and Figure 3.3. Thus, it contains two rigid bodies: the vehicle body and the header. There are three DOFs with one actuator mounted between the header and the vehicle body. The active DOF is the header rotation around the attachment point A with respect to the vehicle body, and the corresponding generalized coordinate is γ. The two passive DOFs are the vehicle body rotation and vertical translation relative to its center of gravity, and the corresponding generalized coordinates are θ and υ, respectively. The output sensor is installed on the header tip to measure the header height with respect to the ground. Therefore, the sensor is non-collocated with the actuator yet its measurement is influenced by all three DOFs. The mathematical model for this under-actuated and non-collocated mechanical system is established in Section 3.2.

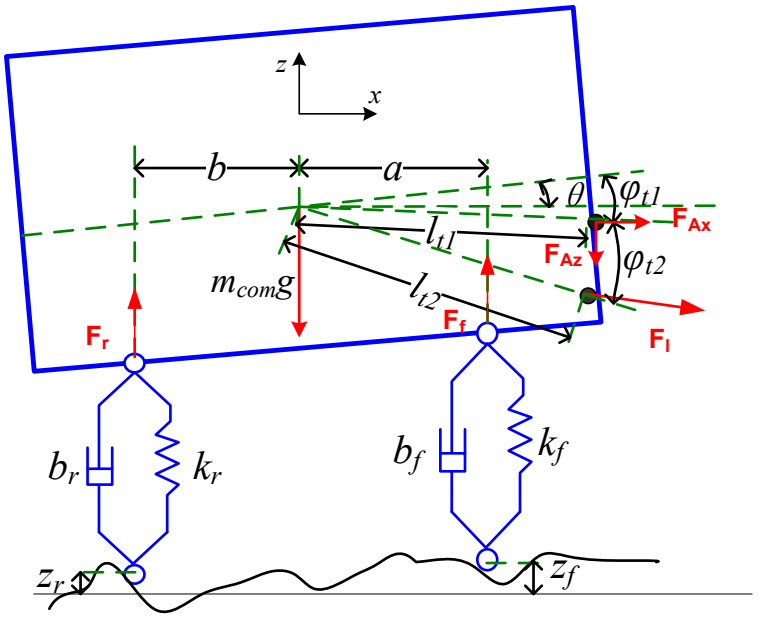

Figure 3.2 Schematic of a combine harvester

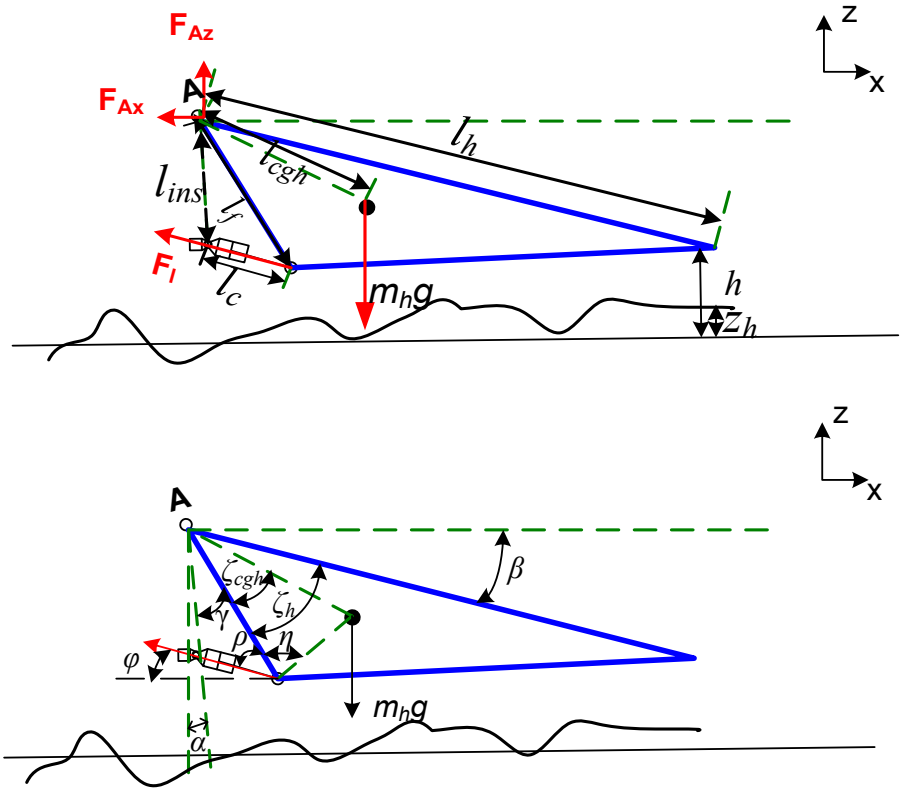

Figure 3.3 Force analysis for a combine harvester

3.1.2 Actuator properties

Hydraulic systems are widely used for heavy load tasks in industry. Although the hydraulic actuator is highly appreciated for its advantages in accomplishing efficient and consistent work, easy maintenance, high power density, and adaption to various work environments, it also introduces undesirable features to the system from a control point of view [64]. Strong nonlinearities such as the pressure-flow rate relationship in different hydraulic components, dead zone of control valves, friction, and internal dynamic delays are commonly seen in hydraulic systems. Each of these undesirable features can create challenges for traditional linear control approaches.

The dominant feature varies for different hydraulic systems; however, in the following analysis we specifically focus on the common existing problem: time delay. It is shown in [65] that magnetic hysteresis and the mechanical motion of the spool valve can cause significant delays in the hydraulic system, and sometimes the delay can exceed the dominant dynamics of the mechanical system. Therefore, it often becomes a non-negligible factor in controller design [66]. In Section 3.3, we will mainly focus on modeling for the specific hydraulic system used in combine harvester header height control and show how the delay is generated in the actuation process.

3.2 Control Challenges Caused by Plant Dynamics

3.2.1 Mechanical subsystem modeling

The internally generated forces (F_{Ax}, F_{Az}, F_l) for the vehicle body and header are shown in Figure 3.2 and Figure 3.3. In this combine system, flow control valves are used to lift and lower the header. Assuming the flow compressibility and the cylinder leakage are

relatively small, the control input to the mechanical system can reasonably be assumed to be the velocity of the hydraulic cylinder $\dot{\ell}$. Eqs. (3.3) - (3.12) present geometric relationships between the system variables defined in Figure 3.2 and Figure 3.3. Eqs. (3.13) - (3.15) represent force balances by which the three primary dynamic equations can be represented. Eqs. (3.16) - (3.19) represent relationships among forces, motions of rigid bodies, and external disturbances caused by vertical displacement of the ground. Appendix B provides the nomenclature for the symbols presented in Eqs. (3.3) - (3.19) along with values representative of an actual combine. Exact manufacturer values were not available, but the values in Appendix B are sufficiently accurate to make subsequent analysis valid as shown in Section 3.4.

$$l_c^2 = l_{ins}^2 + l_f^2 - 2l_{ins}l_f \cos\gamma \tag{3.3}$$

$$l_{ins}^2 = l_c^2 + l_f^2 - 2l_c l_f \cos\rho \tag{3.4}$$

$$\alpha + \gamma + \zeta_h + \beta = \pi/2 \tag{3.5}$$

$$\zeta_h + \beta - \rho = \varphi \tag{3.6}$$

$$x_A = l_{t1}\cos\left(\varphi_{t1} - \theta\right) \tag{3.7}$$

$$z_A = v - l_{t1}\sin\left(\varphi_{t1} - \theta\right) \tag{3.8}$$

$$x_{cgh} = x_A + l_{cgh}\cos\left(\beta + \zeta_h - \zeta_{cgh}\right) \tag{3.9}$$

$$z_{cgh} = z_A - l_{cgh}\sin\left(\beta + \zeta_h - \zeta_{cgh}\right) \tag{3.10}$$

$$\alpha + \theta = \alpha_0 \tag{3.11}$$

$$h = -l_h \sin\beta + z_A + h_0 \tag{3.12}$$

$$I_h \ddot{} \quad {}_{cgh}\cos\left(\beta+\zeta_h-\zeta_{cgh}\right)-F_l l_f \sin\left(\rho\right) \tag{3.13}$$

$$m_{com} \ddot{} \quad {}_z+F_l \sin\varphi - m_{com} g + F_f + F_r \tag{3.14}$$

$$I_{com} \ddot{} \quad -F_r b - F_l l_{t2} \sin\left(-\varphi+\varphi_{t2}-\theta\right)+F_{Ax} l_{t1} \sin\left(\varphi_{t1}-\theta\right)-F_{Az} l_{t1} \cos\left(\varphi_{t1}-\theta\right) \tag{3.15}$$

$$F_{Ax} = -m_h \ddot{} \quad \cos\varphi \tag{3.16}$$

$$F_{Az} = m_h \ddot{} \quad \sin\varphi + m_h g \tag{3.17}$$

$$F_f = -k_f\left(a\theta - z_f + v\right) - b_f\left(a\dot{} \right. \tag{3.18}$$

$$F_r = -k_r\left(-b\theta - z_r + v\right) - b_r\left(-b\dot{} \right. \tag{3.19}$$

Table 3.1 Variable value at the equilibrium point

Symbol	Value	Symbol	Value	Symbol	Value
a_{ss}	0.124rad	ρ_{ss}	0.489rad	γ_{ss}	1.124rad
φ_{ss}	-0.167rad	$l_{c,ss}$	1.535m	β_{ss}	0.0227rad
θ_{ss}	-0.011rad	v_{ss}	-0.0596m	$x_{A,ss}$	2.76m
$z_{A,ss}$	-0.948m	$F_{Ax,ss}$	113277N	$F_{Az,ss}$	29881N
$F_{l,ss}$	114878N	$F_{f,ss}$	137267N	$F_{r,ss}$	58733N
$x_{cgh,ss}$	4.711m	$z_{cgh,ss}$	-1.39m		

To maintain a desired header height, the absolute header height h in Eq. (3.12) should track the time-varying ground profile z_h by controlling the cylinder velocity $\dot{}$. To obtain the open-loop transfer function from z_h (the tracking reference) to h (absolute header height), Eqs. (3.3) - (3.19) are linearized around an equilibrium point using Eq. (3.20). The

kinematic relationships in Eqs. (3.3) - (3.12) are linearized using small angle approximations where appropriate. The equilibrium point considered is a header height of 0.15m with the vehicle on level ground with corresponding values given in.

$$\frac{\partial f(\quad}{\partial \quad}\Big|_{ss} \tag{3.20}$$

where $\quad \theta \ \upsilon \ \rho \ \varphi \ \gamma \ F_l \ F_{Ax} \ F_{Az} \ F_f \ F_r \ x_A \ z_A \ x_{cgh} \ z_{cgh}\big)$, $f(\quad$ represents Eqs. (3.3) – (3.19). $\quad_{ss}$ is the steady state value of $\quad$ at the equilibrium point, and $\Delta\quad$ is the deviation of $\quad$ from the equilibrium point.

With the data from Appendix B and Table 3.1, we can obtain 17 linear equations. Since the system is a 3 DOF system, choose the variables $(\Delta\theta \ \ \Delta\upsilon \ \ \Delta\gamma)$ as the independent variables, and others in $\Delta\quad$ as dependent variables. The resulting dynamics can be represented by Eqs. (3.21) and (3.22), where $q_1 = (\Delta\theta \ \ \Delta\upsilon)^T$ corresponds to the displacements of the two passive DOFs discussed above, and $q_2 = \Delta\gamma$ corresponds to the displacement of the active DOF. The coefficient matrices are also given based on the linearized system. The deviation of header height output can be expressed as a linear combination of the displacements of the three DOFs, as in Eq. (3.23).

$$M_1 \quad \quad = 0 \tag{3.21}$$

$$M_2 \quad \quad = \tau \tag{3.22}$$

$$y = \begin{bmatrix} C_1 & C_2 \end{bmatrix} \begin{pmatrix} q_1 \\ q_2 \end{pmatrix} \tag{3.23}$$

where $M_1 = \begin{bmatrix} M_{11} & M_{12} \end{bmatrix}, M_{11} = m_{11} = \begin{bmatrix} 1 & 0 \\ 0 & 1 \end{bmatrix}, M_{12} = m_{12} = \begin{bmatrix} 0.22314 \\ 0.12265 \end{bmatrix}, H_1 = \begin{bmatrix} H_{11} & H_{12} \end{bmatrix},$

$H_{11} = \begin{bmatrix} 1.2764 & -0.23168 \\ -1.5577 & 2.814 \end{bmatrix}, H_{12} = \begin{bmatrix} 0 \\ 0 \end{bmatrix}, \Phi_1 = \begin{bmatrix} \Phi_{11} & \Phi_{12} \end{bmatrix}, \Phi_{11} = \begin{bmatrix} 77.762 & -4.0543 \\ -33.721 & 155.5 \end{bmatrix},$

$\Phi_{12} = \begin{bmatrix} -1.0936 \\ 12.539 \end{bmatrix}, M_2 = \begin{bmatrix} M_{21} & M_{22} \end{bmatrix}, M_{21} = m_{21} = 0, M_{22} = m_{22} = 1, H_2 = \begin{bmatrix} H_{21} & H_{22} \end{bmatrix},$

$H_{21} = 0, H_{22} = 0, \Phi_2 = \begin{bmatrix} \Phi_{21} & \Phi_{22} \end{bmatrix}, \Phi_{21} = 0, \Phi_{22} = 0, \tau = k_\tau \ddot{\quad}, C_1 = \begin{bmatrix} 7.3596 & 1 \end{bmatrix},$

$C_2 = 4.5989.$

3.2.2 Zero and pole position constraints

In the following analysis, we will show how the characteristics of the under-actuation and non-collocation influence the position of the open loop zeros and poles for the linearized system. First, the mechanical subsystem is examined to illustrate how zero dynamics, or open loop zeros, result from plant dynamics. To make the analysis relevant to the case of the header height problem, only a single-input-single-output (SISO) system is considered. Defining the coordinate transform matrix $T_{trans} = \begin{bmatrix} I_m & 0 \\ C_1 & C_2 \end{bmatrix}$, the coordinates can be transformed as $\bar{q} = T_{trans} q$, where $\bar{q}^T = \left(q_1^T, \bar{q}_2^T \right)$. Since $|C_2| \neq 0$, the transformed matrix T_{trans} is nonsingular, and this coordinate transformation is valid. The inverse of the matrix T_{trans} can be calculated as $T_{trans}^{-1} = \begin{bmatrix} I_m & 0 \\ \bar{C}_1 & \bar{C}_2 \end{bmatrix}$, where $\bar{C}_1 = -\frac{1}{C_2} C_1, \bar{C}_2 = \frac{1}{C_2}$. Applying the coordinate transformation above to the system in Eqs. (3.21) and (3.22) and substituting generalized force τ with $\tau = k_\tau i$ (u is the output of hydraulic cylinder velocity $\dot{\ }$), the new system can

be expressed as Eqs. (3.24) - (3.26). In the new coordinate system, the output y is not correlated to the passive DOFs q_1 anymore.

$$\bar{M}_{1} \ddot{} \quad \cdot \quad : 0 \tag{3.24}$$

$$\bar{M}_{2} \ddot{} \quad \cdot \quad \cdot \tag{3.25}$$

$$y = \bar{q}_2 \tag{3.26}$$

where $\bar{M}_1 = M_1 T^{-1}, \bar{H}_1 = H_1 T^{-1}, \bar{\Phi}_1 = \Phi_1 T^{-1}, \bar{M}_2 = M_2 T^{-1}, \bar{H}_2 = H_2 T^{-1}, \bar{\Phi}_2 = \Phi_2 T^{-1}$. Define a feedback controller as

$$\bar{u} = \tilde{\Lambda} \quad \cdot \tag{3.27}$$

where $\tilde{\Lambda}$ $-\bar{M}_{21}\bar{M}_{11}^{-1}\bar{M}_{12}, \tilde{I}$ $\bar{M}_{21}\bar{M}_{11}^{-1}\bar{H}_1, \tilde{\zeta}$ $\bar{M}_{21}\bar{M}_{11}^{-1}\bar{\Phi}_1$.

Substituting Eq. (3.27) into Eqs. (3.24) and (3.25) results in the system given in Eq. (3.28) - Eq. (3.29). By inspection, the zero dynamics of the system are represented by Eq. (3.30) since the dynamics of q_1 do not affect the output y. Note that $\bar{M}_{11}$, $\bar{H}_{11}$, and $\bar{\Phi}_{11}$ deviate from the original coefficient matrices of the passive DOFs (M_{11}, H_{11}, Φ_{11}) with terms ($\bar{C}_1 M_{12}$, $\bar{C}_1 H_{12}$, $\bar{C}_1 \Phi_{12}$).

$$\bar{M}_{11} \ddot{} \quad \cdot \quad = \bar{M}_{12} \ddot{} \quad \cdot \tag{3.28}$$

$$\ddot{} \tag{3.29}$$

where $\bar{M}_{11} = M_{11} + \bar{C}_1 M_{12}, \bar{H}_{11} = H_{11} + \bar{C}_1 H_{12}, \bar{\Phi}_{11} = \Phi_{11} + \bar{C}_1 \Phi_{12}, \bar{M}_{12} = M_{12}\bar{C}_2, \bar{H}_{12} = H_{12}\bar{C}_2,$ $\bar{\Phi}_{12} = \Phi_{12}\bar{C}_2$.

The zero dynamics then can be further represented as Eq. (3.30). For the under-actuated and non-collocated system expressed as Eqs. (3.21) and (3.22), the zeros of the system are the eigenvalues of the matrix N_z.

$$\begin{pmatrix} \ddot{} & \cdot \\ \dot{} & q_1 \end{pmatrix}$$
$$N_z = \begin{bmatrix} -\bar{M}_{11}^{-1}\bar{H}_{11} & -\bar{M}_{11}^{-1}\bar{\Phi}_{11} \\ I & 0 \end{bmatrix} \tag{3.30}$$

The open loop poles also have a close and explicit relationship with the dynamics of the DOFs. For an under-actuated system, the dynamics of the active DOFs q_2 is directly determined by the input u without coupling to the passive DOFs q_1. These coefficient matrices $M_{21}, H_{21}, \Phi_{21}$ are always null. Applying a Laplace transformation on Eq. (3.22) gives the transfer function from u to q_2 , as in Eq. (3.31).

$$q_2(s) = \left(M_{22}s^2 + H_{22}s + \Phi_{22}\right)^{-1} k_\tau s u(s) \tag{3.31}$$

Additionally, the response of the passive DOFs q_1 is determined by the behavior of active DOF q_2. Then Eq. (3.28) can be re-written as Eq. (3.32).

$$M_{11}\ddot{} \quad \cdot \quad \ddot{} \quad \cdot \tag{3.32}$$

The transfer function from q_2 to q_1 can be obtained by again using Laplace transformations.

$$q_1(s) = \left(M_{11}s^2 + H_{11}s + \Phi_{11}\right)^{-1} \left(-M_{12}s^2 - H_{12}s - \Phi_{12}\right) q_2(s) \tag{3.33}$$

Substituting Eq. (3.33) and Eq. (3.31) into Eq. (3.23), the transfer function from input u to output y can be expressed as Eq. (3.34).

$$y(s)=\frac{C_1\left(-M_{12}s^2-H_{12}s-\Phi_{12}\right)+C_2\left(M_{11}s^2+H_{11}s+\Phi_{11}\right)}{\left(M_{11}s^2+H_{11}s+\Phi_{11}\right)}\times\frac{k_\tau s}{\left(M_{22}s^2+H_{22}s+\Phi_{22}\right)}u(s) \quad (3.34)$$

Eq. (3.34) clearly illustrates how the open loop zeros for the under-actuated and non-collocated system depend on the passive DOFs and the poles are determined by both the active and passive DOFs. Particularly in this combine system, the matrices of the active DOF dynamics H_{22} and Φ_{22} are null, so all the non-trivial poles are determined by the passive DOFs, which can be calculated by the eigenvalues of the matrix N_p in Eq. (3.35). Additionally, the derivative of the numerator cancels one integrator and induces a 5th order system instead of a 6th.

$$\begin{pmatrix} \ddot{} & \dot{} \\ \dot{} & q_1 \end{pmatrix}$$
$$N_p=\begin{bmatrix} -M_{11}^{-1}H_{11} & -M_{11}^{-1}\Phi_{11} \\ I & 0 \end{bmatrix} \quad (3.35)$$

Using the linearized system values from Table 2, the analysis from above gives:

$$P_{com}(s)=L\begin{Bmatrix} v \\ \vdots \end{Bmatrix} \quad \frac{4.822\left(s+1.49\pm12.2i\right)\left(s+0.88\pm11.3i\right)}{\left(s+1.48\pm12.4i\right)\left(s+0.57\pm8.7i\right)} \quad (3.36)$$

The four non-trivial poles have undamped natural frequencies of 2.1 Hz and 1.4 Hz with corresponding damping ratios of 0.104 and 0.069, respectively. The undamped natural frequencies of the zeros are 2.07 Hz and 1.87 Hz with the damping ratios as 0.114 and 0.0894. Figure 3.4 shows the open loop poles and zeros for the system demonstrating an interlacing of poles and zeros close to the $j\omega$ axis. This type of phenomenon is also present and well recognized in other under-actuated control systems such as flexible structures [67].

It is well known that input/output pairs with low frequency and lightly damped zeros and poles can limit the effectiveness of any feedback control approach [30, 68]. Due to the proximity between open loop poles and zeros, as shown in Figure 3.4, there is difficulty in moving closed loop poles far from their open loop location. Clearly, this is a fundamental limitation regardless of any feedback controller $C(s)$.

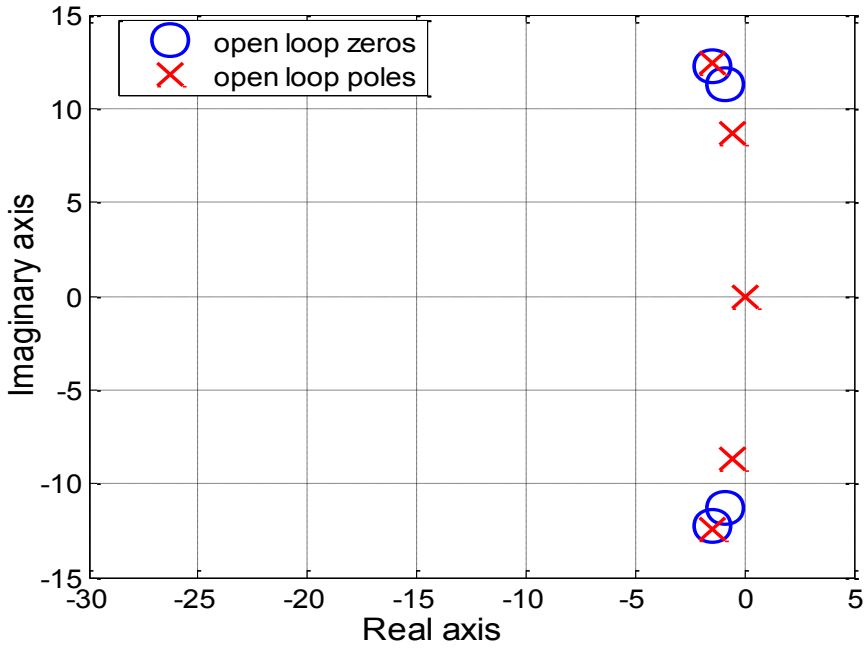

Figure 3.4 Zero and pole distribution for a combine harvester

3.2.3 Performance limitation by mechanical dynamics

In the following, a frequency domain analysis is given to show how the undesirable zeros and poles would induce limitations on feedback control. Figure 3.5 illustrates the closed loop sensitivity function associated with the system of Eq. (3.36) using a proportional feedback gain tuned by experience to be 0.3. It clearly shows the effects on the magnitude and phase plots caused by the zeros and poles. From Figure 3.5, the closed loop bandwidth is limited to below approximately 1.43Hz.

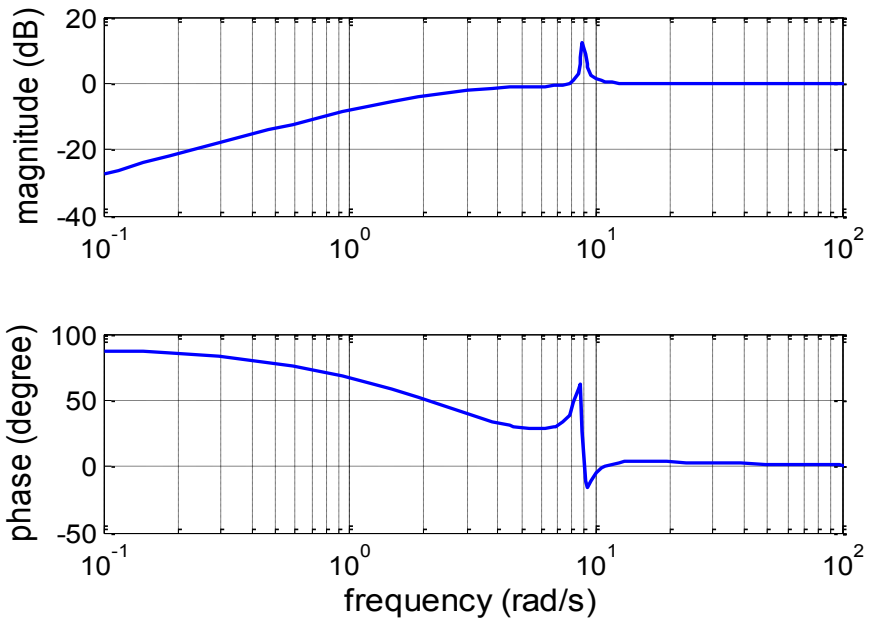

Figure 3.5 Bode plot for a combine harvester

To obtain a higher closed loop bandwidth, a more sophisticated controller $C(s)$ could be introduced to decrease the sensitivity function over a broader range of low frequencies. However, according to the Bode Sensitivity Integral (Eq. (3.37)), any reduction in the sensitivity function at lower frequencies would result in an increase in higher frequencies [69].

$$\int_0^\infty \ln\left|s(j\omega)\right| d\omega = -\frac{\pi}{2}\lim_{s\to\infty} sC(s)P(s) \tag{3.37}$$

The effort of this $C(s)$ to improve the sensitivity function in frequency under 1.43Hz will cause a 'piling up' of the sensitivity function at and above 1.43Hz, This will make the system lose robustness at these higher frequencies possibly leading to instability. In Section 2.3.3, this limitation is described as the achievable bandwidth ω_{co_Δ}, defined as the frequency where the magnitude of uncertainty intersects the magnitude of plant model. In HHC

problem, the uncertainty can be resulted from both delay variation and mechanical model mismatch. Consequently, the zeros and poles in the model can deviate from their true locations, which induce considerable model uncertainty at the frequencies nearby. This situation is further deteriorated due to the nature of lightly damped and closely distributed zeros and poles, in which case small difference in the position of zeros and poles would cause large system uncertainty. In the following Section 3.2.4, experimental results are used to provide a stricter estimation of ω_{co_Δ} in the HHC system.

3.2.4 Uncertainty analysis

The knowledge of system uncertainty is very useful to assist the designer for the purpose of system performance analysis. To compare the difference between real system response and the model simulation, HHC system is investigated in closed loop with a simple proportional controller. Experimental data is obtained by using sine waves of various frequencies as the header height position reference, when the combine is at rest on level ground. Therefore, the effect of ground disturbances on the vehicle body is not present. Comparison of the amplitude and phase characteristics of the plant input and output results an experimental frequency response curve as shown in Figure 3.6. The Bode plot of the model fits the experimental curve well, which indicates that the model captures the major dynamics in the system. However, there is still some model error particularly in the neighborhood of ~1.5Hz (10 rad/s) as what is expected in the analysis of Section 3.2.3.

The model uncertainty between open loop dynamics $e^{-sT}G_{p\_r}(s)$ and its experimental counterpart is calculated and shown in Figure 3.7. The frequency ω_{co_Δ} where the additive

model uncertainty magnitude is larger than the plant magnitude, is observed to be 0.64Hz (4rad/s) in Figure 3.7, which is lower than the preliminary analysis in Section 3.2.3.

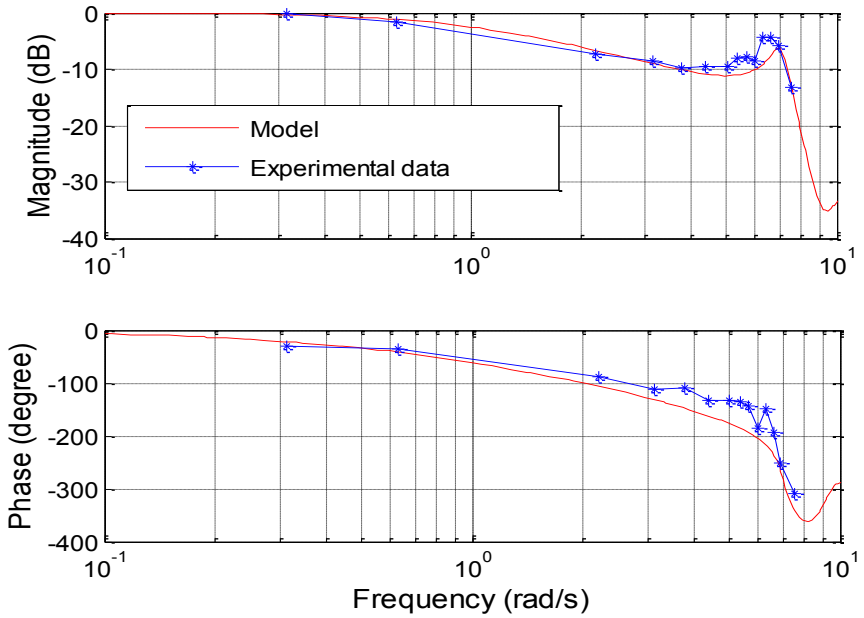

Figure 3.6 Closed-loop frequency response comparison between experimental results and simulation

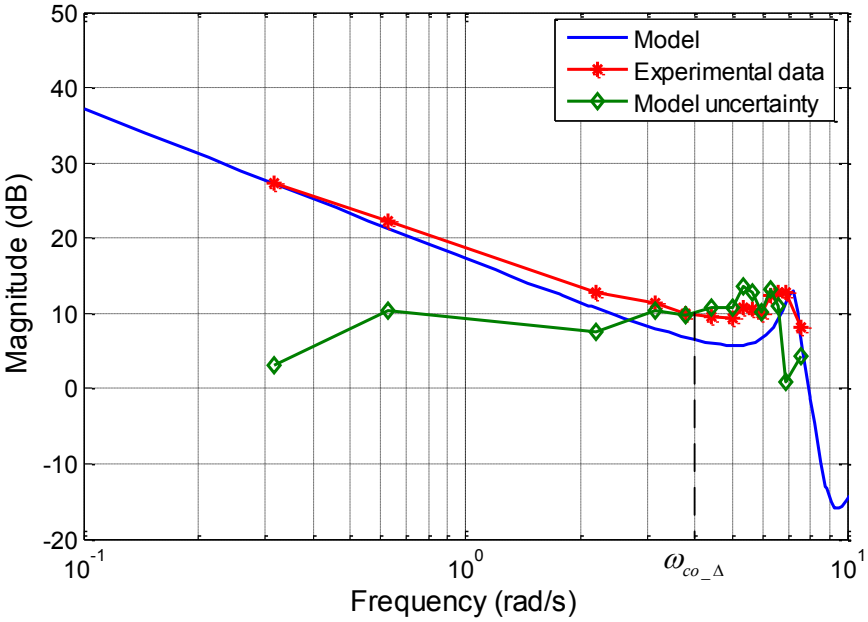

Figure 3.7 Performance limitation by model uncertainty

With the analysis above, the performance is fundamentally limited by the positions of open loop zeros and poles, which is due to the non-collocated and under-actuated nature of this system as shown above.

This systems-level behavior is not unique to the header height control system on a combine. Any under-actuated system with non-collocated sensing and actuation and light damped, low natural frequency passive DOFs will introduce similar pole and zero pairs (or even worse, unstable zeros) in the open loop transfer function, thereby fundamentally limiting the bandwidth achievable by any controller [70, 71]. Below, in Section 3.3, we illustrate that the situation is even more challenging with the delays from the actuation sub-system.

3.3 Control Challenges Caused by the Actuation System

3.3.1 Hydraulic system modeling

An electro-hydraulic actuator is used to control the angle between the header and vehicle body in the specific experimental combine harvester shown in Figure 3.8. It is a flow control system, meaning that the pressure compensator is used for the lifting flow valve to maintain a constant working load for the valve. The following content shows a detailed nonlinear model for this system, with the simplified model shown in Section 3.3.2.

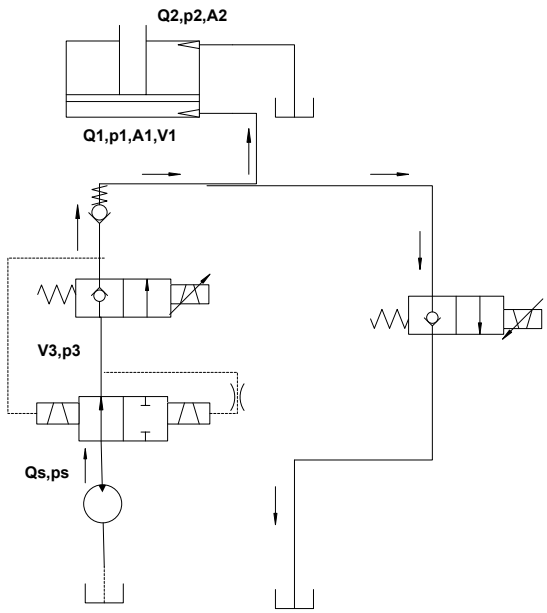

Figure 3.8 Schematic for the hydraulic system

i. For the chamber V_1 (cap-end of cylinder):

$$Q_1 - 2A_1 \dot{} \qquad - p_2) - 2c_e p_1 = \frac{V_1}{E_\beta} \dot{} \tag{3.38}$$

ii. For the chamber V_2 (rod-end of cylinder):

$$2A_2 \dot{} \qquad c_i(p_1 - p_2) - 2c_e p_2 = \frac{V_2}{E_\beta} \dot{} \tag{3.39}$$

where:

$c_i = 1\text{e-}14$ is the inner leakage coefficient of the cylinder,

$c_e = 1\text{e-}14$ is the external leakage coefficient of the cylinder, and

$E_\beta = 7 \times 10^8$ is the fluid bulk modulus.

$$V_1 = V_{10} + 2A_1(l_c - l_{c\min}) \tag{3.40}$$

$$V_2 = V_{20} - 2A_2(l_c - l_{c\min}) \tag{3.41}$$

V_{10}, V_{20} are the initial volume of chamber V_1 and V_2, respectively.

A_1 is the cap-end area,

A_2 is the rod-end area,

$l_{c\min} = 0.943\text{m}$ is the minimum length of l_c when the rod is totally retreated, and p_2 is the oil pressure of the tank, which can set at 0 here.

iii. For the flow of the valve SP16-20: (manufacturer data is given in Figure 3.9)

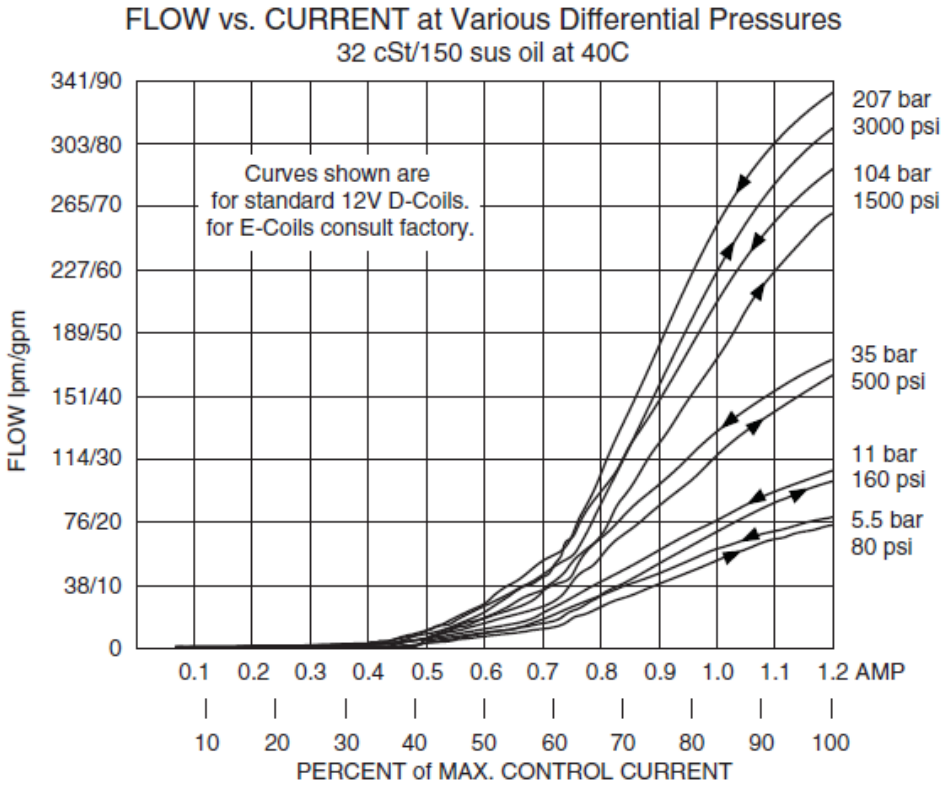

Figure 3.9 Current and flow rate relationship of the control valves

$$Q_{1static} = K_1 \sqrt{\Delta p}\left(I_{in} - I_{start}\right) \tag{3.42}$$

where

K_1 is the valve gain, which can be calculated from the performance curve Figure 3.9.

Δp is the pressure drop stabilized by EC16-32-150, which makes it a constant $\Delta p = 150\,psi$ with corresponding $K_1 = 2.02\times10^{-6}$.

The dynamic flow is simply the static flow modified by a 2nd order transfer function dynamics:

$$Q_1 = \frac{Q_{1static}}{\frac{s^2}{\omega_V^2} + \frac{2\varsigma_V}{\omega_V}s + 1} \tag{3.43}$$

iv. For the flow of valve SP12-20:

$$Q_{1static} = K_2\sqrt{p_1}\left(I_{in} - I_{start}\right) \tag{3.44}$$

where $K_2 = 0.7e-6$ is the valve gain with a curve similar to SP16-20.

v. The dynamic equation for the load is given as:

$$2m_{ZB}\ddot{} \qquad \dot{} \qquad {}_f = 2p_1A_1 - 2p_2A_2 \tag{3.45}$$

where

m_{ZB} is the total mass of the piston and rod and the equivalent mass of oil,

b_p is the viscous drag coefficient of the cylinder,

F_l is the load of the cylinder applied by the cutter,

$F_f = f_0\,\mathrm{sgn}(\dot{}$ is the friction force of the cylinder, and

f_0 is the static friction of the cylinder.

We assume the mass of the piston is far smaller than the mass of the feeder house and header, i.e. $m_{ZB} \approx 0$. Hence:

$$F_l = 2p_1A_1 - 2p_2A_2 - 2b_p\dot{} \tag{3.46}$$

3.3.2 A Simplified model for the hydraulic system

Though seemingly complicated, the model in Section 3.3.1 can be effectively simplified using some reasonable assumptions. Assuming the fluid is incompressible and ignoring the leakage of the fluid, we find that the steady state valve flow to be proportional to the current command I_{in} as given in Eq. (3.47). The flow dynamics are thereby dominated by the second order characteristics between the current command and the actual valve displacement given in Eq. (3.48).

$$Q_{1,static} = K\sqrt{\Delta p}(I_{in}) \tag{3.47}$$

$$Q_{1,dynamic} = \frac{Q_{static}}{s^2 + 2\zeta_v \omega_v s + \omega_v^2} \tag{3.48}$$

where K is a flow coefficient, Δp is the pressure difference across the valve, and ζ_v and ω_v are the damping ratio and natural frequency of the valve, respectively. For the experimental system, the valve bandwidth was validated as 10Hz.

If one assumes that the pressure difference upstream and downstream of the flow control valve is constant, which is reasonable due to the pressure compensator, and the valve dynamics have sufficiently high bandwidth, the electro-hydraulic system can be further simplified to a cylinder velocity $\dot{}$ proportional to the current command I_{in} with a time delay. The delay incorporates frictional effects [72] in the cylinder seals and linkage bearings. When the system is operating at different header positions, the time delay varies due to the kinematic dependency of the nonlinear friction characteristics in the mechanical system. However, for clarity of exposition, the delay is assumed here to be constant. The

hydraulic system dynamics can then be considered as given in Eq.(3.49), where k_{hydr} is the corresponding coefficient (Appendix B).

$$\dot{} \quad {}_{r}I_{in}\left(t-T\right) \tag{3.49}$$

3.3.3 Performance limitation by actuator delay

The actuator delay present in the combine header height system is up to 0.3 seconds, as will be illustrated in the validation Section 3.4.1. This time is large relative to the desired closed loop system bandwidth of 3Hz. The delay can vary somewhat with the hardware configuration but will exist in some form for all header height actuations systems due to cost and manufacturing constraints of these agricultural systems. The delay can't be eliminated by means of feedback. According to Chapter 2, the bandwidth limitation caused by a time delay can be expressed by Eq. (3.50). Therefore, in the present combine system, the time delay from the actuator will limit the closed loop bandwidth to below 0.5Hz.

$$\omega_T < \frac{\pi}{3T} \tag{3.50}$$

where ω_T is the achievable bandwidth and T is the delay.

This limitation deteriorates the already low bandwidth induced by the mechanical structure characteristics discussed in Section 3.2.3. Figure 3.10 shows a sensitivity function of the closed loop system, including a delay of 0.3 seconds. Clearly, the situation has been deteriorated by the extra phase decrease, thereby putting the available bandwidth further below the desired target.

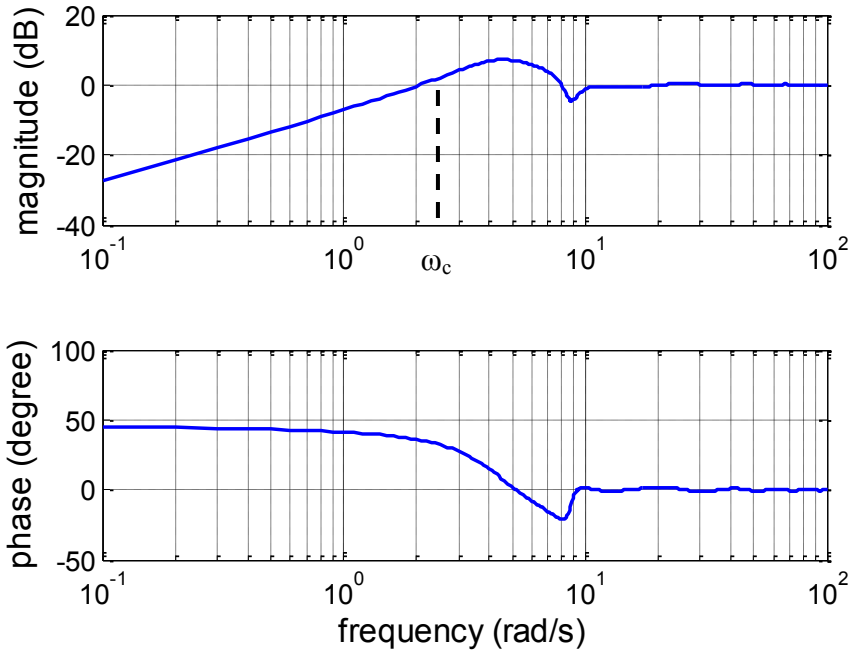

Figure 3.10 Closed loop sensitivity plot of linearized combine system with actuator delay

3.3.4 Effect by combining delay and mechanical system

With both the delay and mechanical uncertainty exist, the combined effect of the delay T and model uncertainty Δ_p provides a more restrictive limitation on the robust performance. In Section 2.3.5, the robust performance bandwidth is estimated.

The delay T in the system is about 0.3s, which induces a bandwidth limitation of 0.53Hz (3.6rad/s) as shown in Section 3.3.3. The model uncertainty induces a bandwidth limitation as 0.64Hz as shown in Section 3.2.4 for the robust performance analysis. Their combined effect, according to Eq. (2.37), is where the upper bound of model uncertainty crosses over the magnitude curve of $\left(1-\left|1-e^{-T\omega j}\right|\right)\left|G_{p0}(\omega j)\right|$. Their relationship is shown in

Figure 3.11, which illustrates the bandwidth ω_{T_Δ} caused by the combination of the two aspects as 0.25Hz.

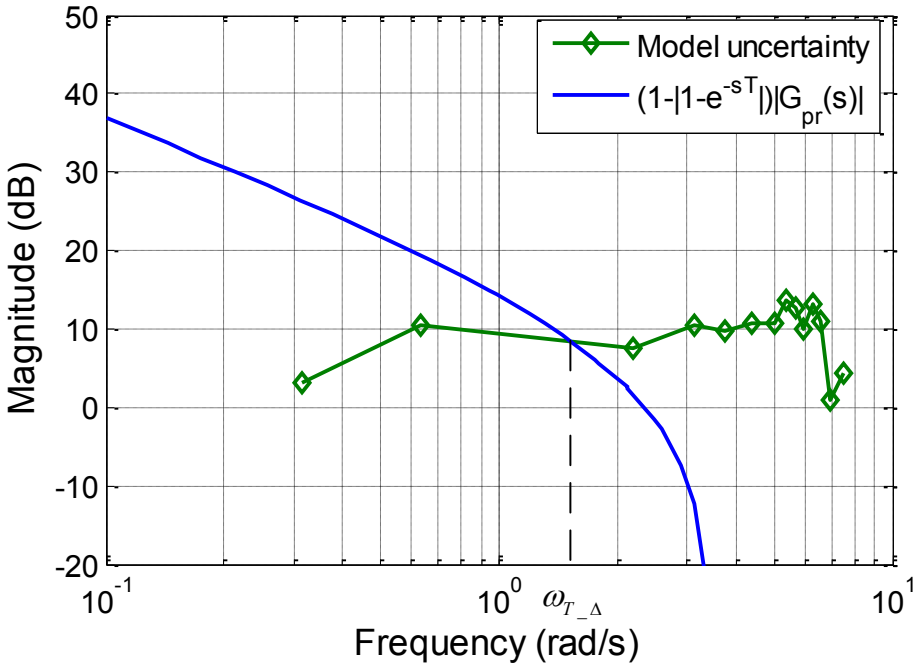

Figure 3.11 Performance limitation by combined effect of delay and uncertainty

3.4 Validation and Analysis

The modeling and analysis of Sections 3.2 and 3.3 posit the existence of fundamental limitations to feedback control for the header height control problem in combines. This Section describes the experimental procedures and results of the models created in Sections 3.2 and 3.3 to validate the analysis on a real-world system. First the hydraulic system model given in Section 3.3.2 is validated in the time domain. Subsequently, the mechanical system model is validated in the frequency and time domains. The results of this Section indicate the validity of the plant models used in the analysis above.

3.4.1 Hydraulic sub-system model validation

To validate the simplified electro-hydraulic system from Section 3.2.3, the hydraulic actuation had to be separated from the combine. Figure 3.12 illustrates a test stand designed to perform this task. The foundation pile acts as a reaction wall for the actuator to push on with no pitch or heave dynamics as would be found on the actual combine. A header is also attached to provide a realistic inertial load for the actuator to move. The valve and pump systems are replicated from a production combine system and a height sensor is installed on the header tip to measure the header height. Additionally, several pressure sensors are installed throughout the hydraulic system for diagnostic purposes.

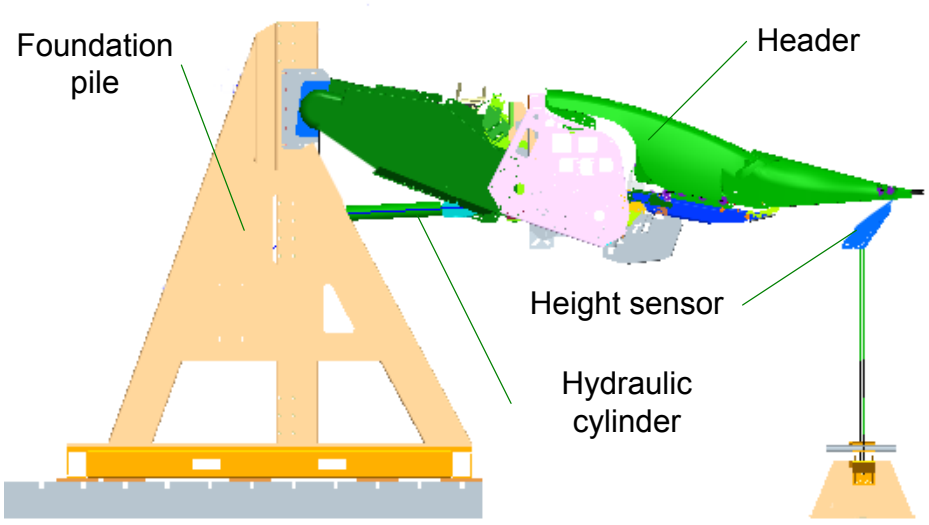

Figure 3.12 Hydraulic system test bed

To measure the time domain response of the hydraulic system, a step command was applied to the control valve and the available signals were monitored as shown in Figure 3.13. The sampling rate for the sensors was 20Hz. There is a combination of responses which included the times to open the valves (t1), stroke the load sensing pump (t2), build up

pressure of the pump output (t3), and overcome system friction (t4). Summing these effects resulted in a total time delay $T = 0.3s$. This delay constant can vary with different combines and different operation positions. However, for this particular investigation, it is treated as constant for clarity of exposition.

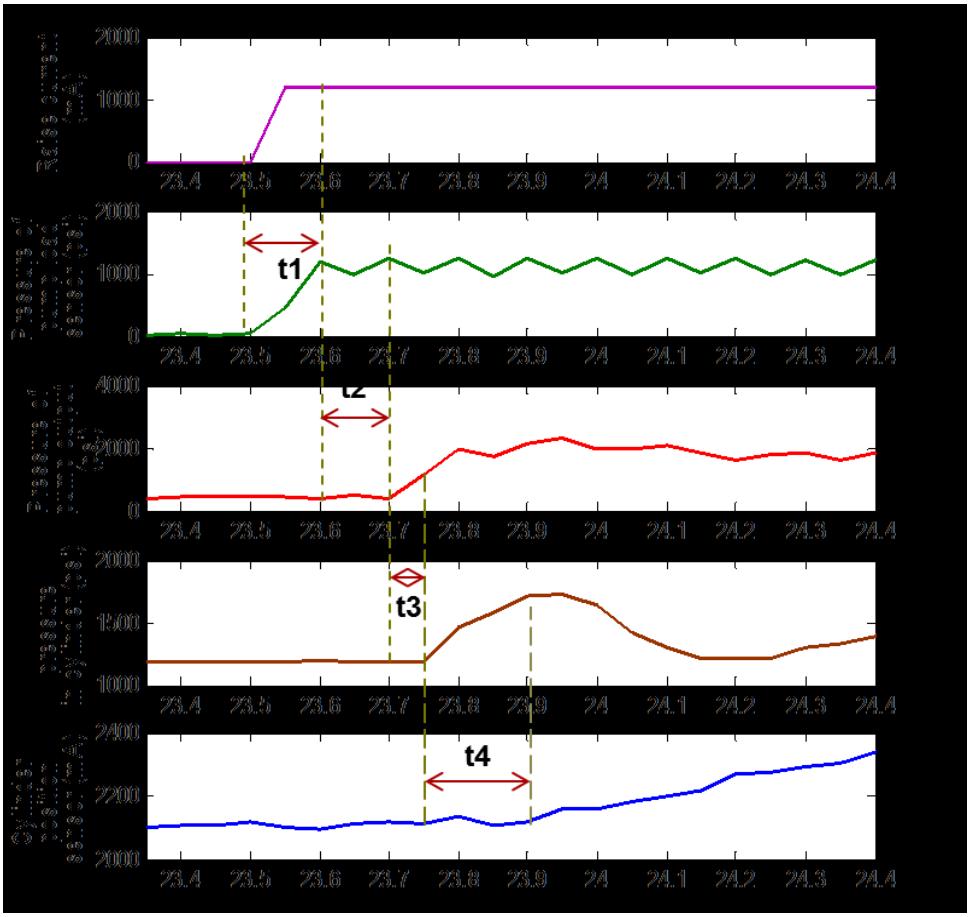

Figure 3.13 Open loop step response of hydraulic system for input current

To verify that a pure time delay (Eq. (3.49)) represents the major characteristic of the hydraulic system, the closed loop step responses from simulation and experiment are compared in Figure 3.14. A proportional controller is used to make the header follow a step reference. The results of Figure 3.14 indicate that the simulation results match the response of the actual system sufficiently well so as to have confidence in the simplified model in

Section 3.3.2. The large dead zone in the figure was setup by manufacturer's embedded proportional controller in the lab and therefore it is adopted in the simulation to guarantee consistency between the experiments and simulations.

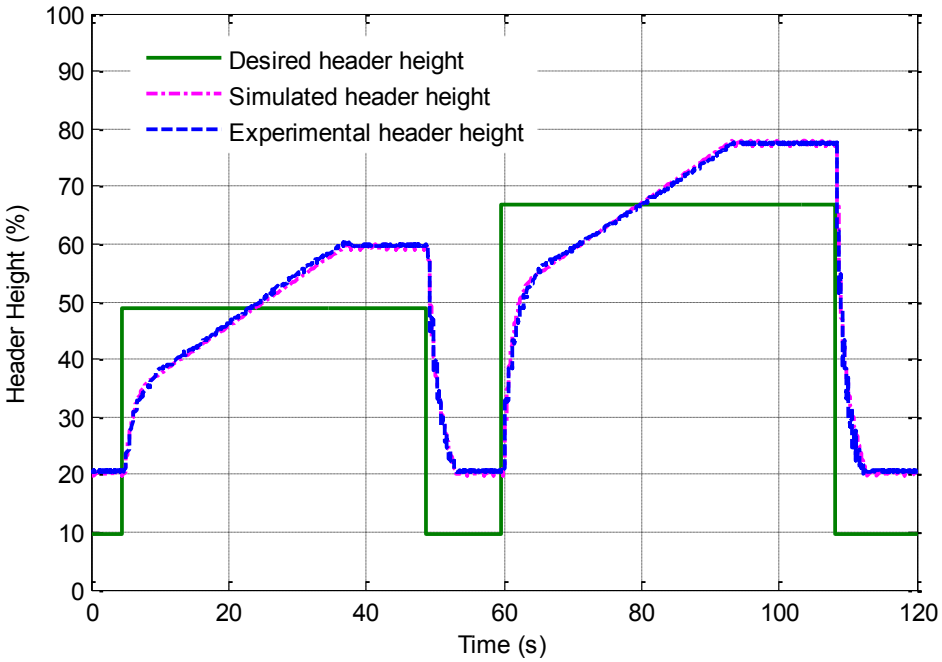

Figure 3.14 Closed loop step response of the test system

3.4.2 Mechanical sub-system model validation

Figure 3.15 Experimental combine used for field test results

The mechanical sub-system experiments were performed on an experimental John Deere combine + header system, shown in Figure 3.15. For this validation, it was not possible to introduce a perfect actuator and thereby separate the electro-hydraulic sub-system from the mechanical sub-system. However, given the validity of the electro-hydraulic sub-system demonstrated in Section 3.4.1, the effect of actuation model error influencing the validation of the mechanical sub-system model is minimized. The mechanical sub-system model from Section 3.2.1 was validated by both frequency domain and time domain responses. Since the open loop system in Eq. (3.23) is type 1, a sine sweep frequency response must be performed in a closed loop manner. For the frequency domain responses, a simple controller was used to generate a closed-loop transfer function both in simulation and experimentally.

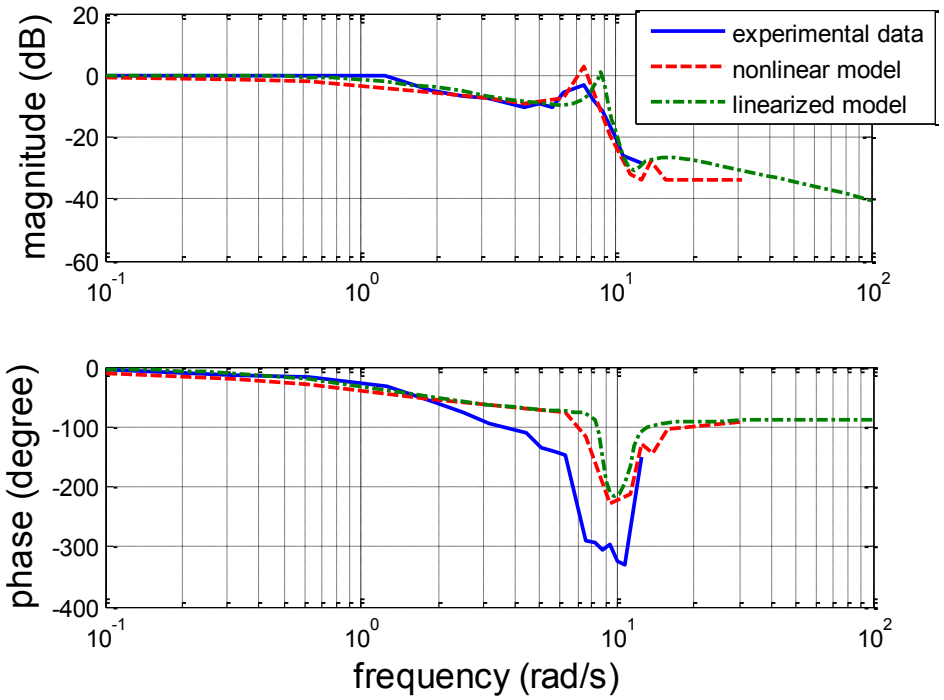

Figure 3.16 Closed-loop frequency response comparisons between experimental results and simulation results

A series of sinusoidal height references, constant amplitude with varying frequency, were fed to both simulated and experimental closed loop systems for a stationary combine on level ground. The output heights from the header height sensor were collected and compared to the reference signals. Performing a frequency-by-frequency analysis of magnitude and phase differences allowed for the construction of a frequency response plot in Figure 3.16. The result from the experiment is compared with the simulation for the nonlinear system given by Eqs. (3.3) - (3.12). The nonlinear model fits the physical system well in the magnitude plot. The phase plots have some differences, primarily due to the assumption of a constant friction level, and hence a constant delay, in the hydraulic sub-system. In the experimental system, the friction varies with a change in relative orientation between the combine and header, which is the primary cause of the phase differences. While the nonlinearity of the system would lead to amplitude-dependent responses, the nature of Figure 3.16 clearly illustrates the matching of the major dynamic modes. By comparing the linearized system with the nonlinear system, the linearization preserves the main model information and can describe the system behavior accurately enough.

3.4.3 Tracking performance validation

The overall results in Section 3.4 are representative of the entire class of agricultural combines performing active header height control. The parameters may vary with combine and header sizes and more or less expensive electro-hydraulics resulting in quantitative variation from the results presented here. However, the qualitative nature will remain. The mechanical sub-system is subject to under-actuation and non-collocation of sensing and actuation; the electro-hydraulic subsystem incurs a time delay in the input-output response.

These are both combined in the overall system to severely limit achievable terrain disturbance rejection/tracking. This will now be demonstrated by examining performance tests for the experimental vehicle.

A header tracking test was set up as shown in Figure 3.17. These tests were performed at a proving ground provided by an industrial partner. The combine is driven on level flat ground (concrete) between the test blocks and its wheels do not encounter the blocks. The header attempts to track the profile of the trapezoidal blocks as the combine proceeds. Since the vehicle body does not incur the ground disturbances from the blocks, the test isolates the performance of the header height closed loop tracking performance and does not confound it with a ground disturbance rejection test. Figure 3.18 clearly shows that the phenomena described in Sections 3.2 and 3.3 are present and account for the level of performance achievable, and the responses in the black circle demonstrates that the performance of the system to track the test ground profile is unacceptable.

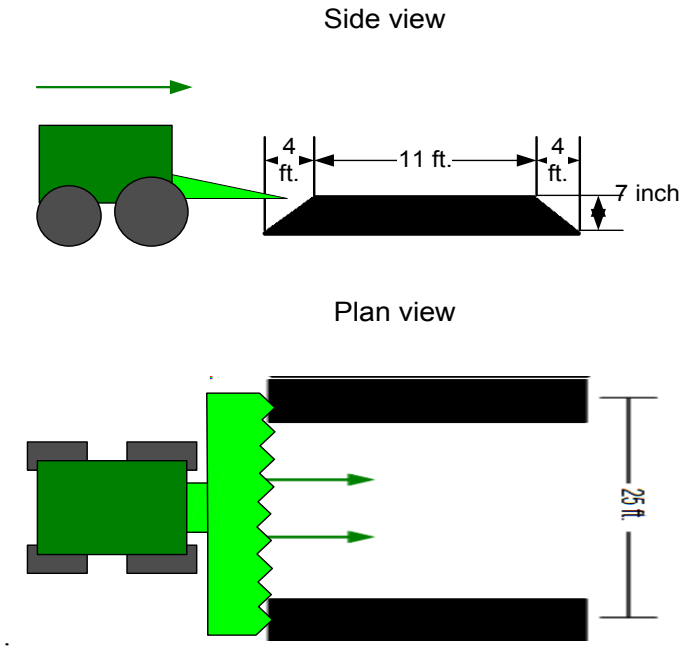

Figure 3.17 Ramp test setup

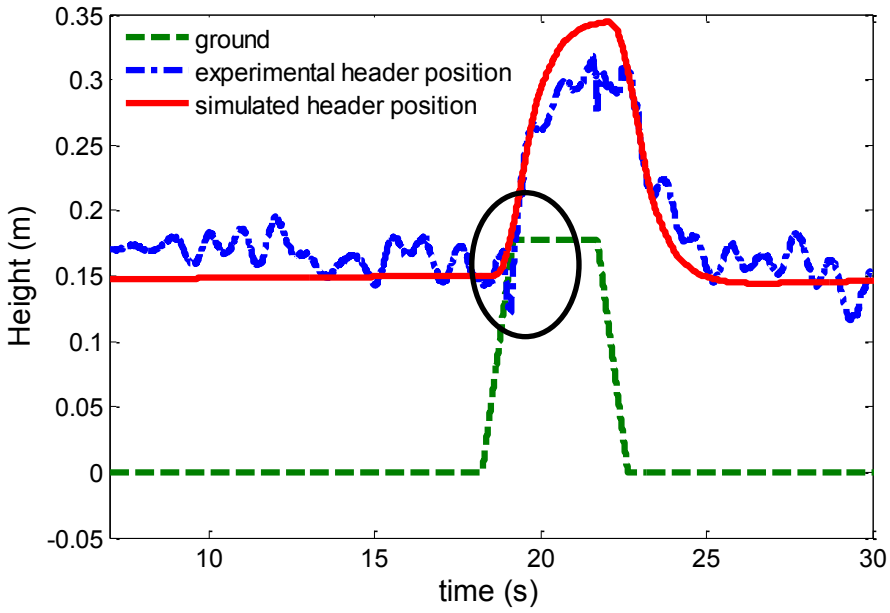

Figure 3.18 Experiment verification for existence of limitations

To specifically investigate the separate influences of the limitations described in Sections 3.2 and 3.3, we utilized the validated system and sub-system models in a simulated test environment. We used the same test shown in Figure 3.18 and compared three cases: (1) the header is mounted on the test bed from Figure 3.14 and travels between the test blocks with no actuator time delay (i.e., no combine dynamics), (2) the combine+header system tracks the test block profiles with no actuator time delay, and (3) the combine+header system tracks the test block profiles with actuator delay. These three cases represent the system without any limitations, with only mechanical sub-system limitations, and with both mechanical and hydraulic limitations. In cases 1 and 2, the coefficients from Eq. (3.51) are used to maximize the performance, while in case 3, the coefficients in Eq. (3.52) are used to ensure stability. Obviously, in case 1, without the limitations, a much more aggressive controller than the simple PI controller could be designed and implemented. However, we

chose to maintain consistency here to quantitatively demonstrate the effects of the limitations.

$$k_{p2} = 0.1482 \quad k_{i2} = 1 \tag{3.51}$$

$$k_{p1} = 0.1482 \quad k_{i1} = 0.018 \tag{3.52}$$

Figure 3.19 illustrates the results of the 3 cases. When there are no limitations to the closed loop system (case 1), the header height can change rapidly to track the terrain shape. This would correspond to enabling high speed travel through the field and increased productivity. Unfortunately, when the mechanical sub-system limitation is introduced (case 2), the response of the system is reduced corresponding to the results of Section 3.2.3 and Section 3.3.3. When both limitations are present (case 3), which is the case for the experimental combine system, the performance is even further deteriorated.

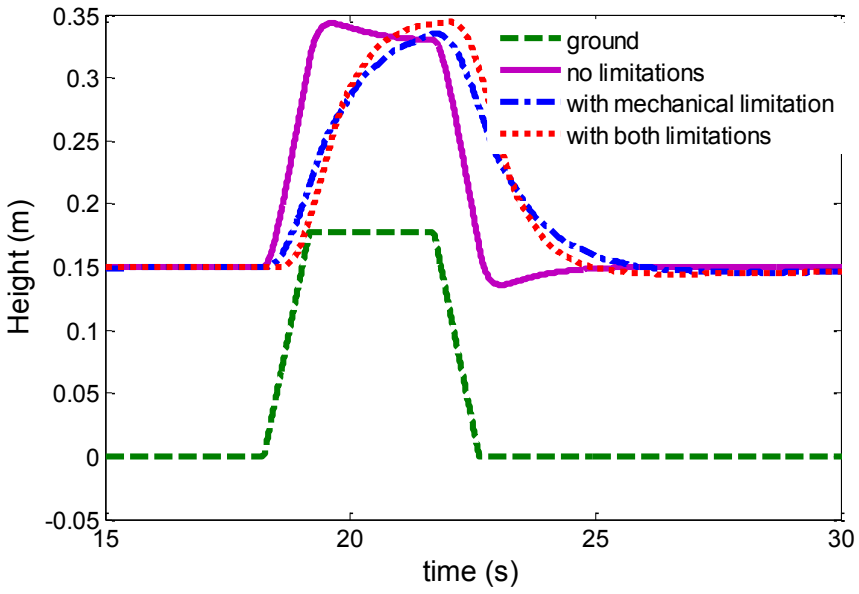

Figure 3.19 Simulations for header ramp tracking that illustrate individual limitations

3.5 Conclusion

Using system dynamics and common analytical tools, we gained insights into the fundamental limits for VEI systems. The modeling and analysis of Sections 3.2 and 3.3 clearly demonstrate the challenges present in a combine harvester HHC problem and the reasons for the relative bottleneck in increasing working productivity. The under-actuation and non-collocation properties of the mechanical system determine the position of the open-loop poles and zeros, which results in a system bandwidth upper limit at 0.64Hz. A time-delay from the hydraulic actuator further deteriorates the bandwidth limitation to be 0.25Hz when the robust performance is considered.

Clearly, a drastic improvement in the overall system performance cannot be achieved solely by feedback control design. To eliminate or decrease the undesirable mechanical characteristics, the mechanical system needs to be redesigned. One method is to redesign the mechanical structure and eliminate the non-collocation characteristic. For example, by replacing the tires with tracks, the DOFs for the system reduce to 1 and the system becomes fully actuated. Alternatively, active suspensions can be added between the tires and vehicle body to increase the number of actuators and therefore eliminate the under-actuation in the system. Another possible way to redesign the system is to change the value of key parameters in the system, such as suspension elements, to improve the low natural frequency and lightly damped characteristics of the passive DOFs. The latter method induces fewer changes to current products and decreases the costs of implementation; therefore, it is studied in Chapter 4.

As for the actuator delay problem arising from the electrohydraulic system, it may be possible to reduce or eliminate the delay with very high performance servo hydraulics. As

with the mechanical redesign, these types of system changes would have to be performed under realistic cost and design constraints. High-performance servo-actuators may not be appropriate for an all-weather all-terrain agricultural vehicle and may not meet market price points. Therefore, in Chapters 5 and 6, a robust two DOF controller is proposed and experimentally validated to compensate the delay and break the corresponding performance limitations.

Chapter 4
Integrated Plant Design and Control

Limitations from physical system are difficult to break solely by control algorithm design. For the HHC problem studied, the control limitation from mechanical system is caused by the undesirable zeros and poles, especially the lightly damped low frequency zeros. Zero dynamics is an important feature for a single-input-signal-output (SISO) system and it cannot be influenced by control compensation. The results in Chapter 3 show that such zero and pole pairs, which are determined by the under-actuation and non-collocation features of the vehicle-header system, place a bandwidth limitation of 0.64 Hz on the robust feedback control performance.

To avoid or mediate the control limitations from mechanical systems, the system properties should be analyzed and tuned during the design phase. When the achievable performance cannot satisfy design requirements, integrating design and control is a necessary approach to be considered. The integrated design and control method uses both physical system and controller as design variables. Therefore, it targets improving plant dynamic features with the simultaneous optimization of controller parameters. During the design procedure, control performance is used as design criteria; therefore, the design decision is

finally made to minimize certain control performance functions, which reduces the control limitations automatically.

In this chapter, a general review for the integrated design and control is firstly introduced in Section 4.1. It serves as the background to propose the design method described in Section 4.2, where the HHC system is taken as an example to be studied. Key parameters in the physical system are optimized to obtain better performance with the consideration for both robust stability and performance. Numerical results are provided in Section 4.3 as demonstrations for the design effectiveness with the application of the proposed integrated design and control approach.

4.1 Review for Integrated Design and Control

4.1.1 Introduction

Integrated design and control refers to designing the system/process and the controller simultaneously. The idea of simultaneous design is not new. Its first appearance was mentioned by Ziegler and Nichols in [73]. In this reference, the authors pointed out that the performance of a feedback controller depends not only on the tuning parameters but also very strongly on the structure of the loop and the inherent dynamics of the process.

The integration of process design and control has been well developed in chemical process control since the 1960s [74]. Researchers originally emphasized the steady-state economics when designing chemical processes. However, many chemical engineering examples showed the inherent conflict between steady-state economics and dynamic performance. Therefore, the control engineers were urged to become involved in all stages of process development, particularly at the conceptual and detailed design stages. The general

method is to test multiple process designs using different control criteria [75]. By comparison, the most economically efficient design, which also should guarantees product quality, is determined.

In mechatronic systems, the integration of controller design and mechatronic system design was proposed by Andre Sharon, Neville Hogan, and David E. Hardt [7]. They were motivated by the problem of flexible robot manipulators. Because it is commonly assumed that the mechatronic systems exist when the controller design phase is begun, many restrictions are inadvertently placed on the controller design. Therefore, some characteristics that are considered beneficial from a mechanical design point of view may actually be detrimental from a control point of view. They used the concept of controller design in the physical domain as a method to unify control systems design with mechanical systems design by preserving physical insight and providing guidance in the selection of the proper physical architecture for control. Peter J. Gawthrop further formalized this using the bond graph approach [76]. He pointed out that by using generic techniques (Bode and Nichols diagram designs, root-locus designs, observer/state-feedback designs, polynomial designs), specific physical details are lost. For example, both the parameters and the states of such representations may not easily be related back to the original physical properties of the system. To preserve physical information, the bond-graph-based method was used to describe both the dynamics of the system and the controller, as well as to design a controller on this basis.

Kamal Youcef-Toumi [8] further emphasized the importance of modeling, design, and control integration, and called it a necessary step in mechatronics. He did not only designed the controller in the physical domain, but also provided techniques for modifying

system configurations, leading to proper system topologies for control benefits. He stated that it is necessary to predict the system behavior with and without a control system during the system design phase.

Compared to such work on design system structures, in the aero-astro community, researchers proposed to integrate parameters optimization for both space structures and controller with a fixed structural configuration [77]. Assuming the configuration is pre-designed, the shape or parameters of the elements are left to be decided along with the controller. Therefore, compared to pure controller optimization, control performance can be further improved by modifying the mechanical parameters simultaneously [78]. Though all those efforts have been made, this general theory of integrated control and design for a large class of systems is still not mature. There is no systematic way to provide a complete solution for integrated design and control. Specific study needs to be done for particular systems to categorize the problems in physical system from a control perspective, to analyze the achievable control performance, and to determine the proper design for both mechanical system and controller.

4.1.2 Configuration design and parametric design

Mechatronic system design can be divided into four steps: conceptual design, configuration design, parametric design, and embodiment design [79]. Conceptual design is the early stage of the design process wherein physical concepts are synthesized to generate a prototypical device that can satisfy the design specifications. Configuration design addresses the spatial organization of components that are assembled to generate a new device. Parametric and embodiment design further refine the concept design with the use of

analytical models to choose the different design parameters and finalize the design for production. Conceptual design is a creation process which is very difficult to formalize. However, configuration and parametric design are likely to be set up by certain algorithms and, therefore, can be solved by the sequence of steps. Thus, integrated design and control mainly focus on these two design steps to optimize plant dynamics and controller parameters as stated in Section 4.1.1.

For configuration design, analytical and graphical descriptions for modeling physical dynamic systems are necessary. If multiple design choices are provided, the control performance limitations from the system structure need to be analyzed and compared, and this requires synthesis in the physical domain. Therefore, the modeling method should be able to represent the information of physical structure and reveal the inherent limitations of the configuration. Bond graph, for example, is a well-developed tool for this purpose. Once the criteria for performance estimation are established, the relevant information needs to be qualitatively or quantitatively abstracted and analyzed directly from the Bond graph. In this way, the different mechanical topologies and placements of actuators and sensors can be compared and evaluated, and corresponding adjustments can be made to avoid or relax the limitations from the physical system structure. This completes the configuration design.

In the parametric design step, on the other hand, a control algorithm can be selected and simultaneously optimized together with the parameters in the plant. This optimization achieves the best control performance with the pre-determined physical system and controller structure. Compared to the conventional control design methods, which involve optimizing control parameters for a fixed plant, this method can further improve the control performance by considering the interactions and trade-offs between the mechanical design and controller

design. Parametric design mostly do not change the topology of the plant, but rather are used to design objects such as the shape and mass distribution, parameters in the plant (truss member sizes, material properties, and spacecraft dimensions), and controller parameters [80-82].

Both of the steps described above can influence the system dynamics. The configurations design can help to eliminate control limitations caused by mechanical structure, and the parametric design usually requires fewer changes to the prototype and is thereby more suitable to be applied to existing products for upgrading purpose. It is pointed out in Chapter 3 that one of the HHC performance limitations is inherently caused by the under-actuated and non-collocated mechanical system structure. Theoretically, to eliminate such limitation the configuration redesign might be more effective; for example, the undesirable under-actuation or non-collocation properties can be removed by adding extra actuators or sensors. However, configuration redesign usually involves large changes in mechanical system, which is difficult for mature products that have been in the market such as the combine harvester. Therefore, the parametric design might be a more realistic way to adopt in the HHC case.

4.1.3 A brief review for parametric design method

Fundamentally, the parametric design are formulated as a nonlinear programming problem, wherein design variables in mechanical system and the controller are chosen subject to structural and performance constraints, to optimize an objective function whose construction captures the essence of the integrated design problem. The integrated design must provide satisfactory closed-loop stability and robustness properties by specifying

particular design requirements in the objective function. For example, the objective function can be chosen as the steady-state error due to white-noise disturbance at the inputs [10], the sum of the time constants of the closed-loop eigenvalues [11], or the largest possible safety margin that does not exceed the weight budgeted for the structure [12]. Sometimes, the system is assumed to be disturbed by stochastic disturbances, and the constraints are formulated in terms of allowable means square responses and control energies [13]. To achieve a realistic design, constraints can be placed on the control power, the structural mass, or other structural design variables to address buckling and stress failures as well as manufacturing limitations.

The choice of controller configuration is also critical to the integrated optimization. The output feedback controller and the filtered output feedback controller (including PID/PD/PI) were considered in some of the literature [13]. These controllers do not necessarily guarantee that the controllers will actually result in a stable closed-loop system, since neither is inherently robust to system modeling errors or neglected dynamics. Although the gain matrices and filter parameters found by solving the respective problems may indeed be "optimal" with respect to the constraints, serious unexpected problems may arise when they are applied to the real physical system. Another choice to make is the model-based controller, which generally consists of a state estimator (a Kalman-Bucy filter or an observer) followed by a linear quadratic regulator. The state estimator uses the knowledge of the design model (consisting of the rotational rigid body modes and a few elastic modes) in its prediction part [83]. Using multi-variable frequency-domain design methods, they can be made robust to un-modeled structural dynamics. The integrated design can also be done in the time domain. The plant and controller are expressed in state space, and linear algebra is

used to develop the relationship between the cost function and the covariance matrix, as well as the feedback gain matrix [84]. However, such controllers generally tend to be very sensitive to uncertainties in the design model, in particular, to uncertainty in the structural mode frequencies. Dissipative controllers, which use collocated and compatible actuators and sensors, employ special passivity-type input/output properties of the plant and offer robust stability in the presence of both nonparametric and parametric uncertainties [85]. The main characteristic of all dissipative controllers is that they do not rely on the knowledge of the design model to ensure stability, although they use it to obtain the best possible performance. However, the collocation of the actuator and sensor is a rigorous constraint to the applicable systems. Another controller to guarantee stability is called positive real control. If nonlinearity or uncertainty can be characterized by a positive real system, then the classic results in stability theory can be used to guarantee robust stability provided an appropriate closed-loop system is strictly positive real [86]. A positive real output filter feedback control then is proposed to preserve stability in the presence of modeling errors [12]. For the HHC problem discussed in this dissertation, both robust stability and performance are taken as the design objectives. Therefore, as will be shown in Section 4.2.2, the controller is chosen to be a H_∞ controller that to form mixed sensitivity problem for the integrated design.

With controller structure and design parameter specified, the design problem is formulized as an optimization problem to be numerically solved. When the optimization problem is formed as a linear structure (generally for simple conditions), the convex methods can be used to obtain the optimal solution. However, in the general problem formulation presented, the constraint functions are highly nonlinear implicit functions of the design variables mainly due to the nonlinear relationship between physical parameters and plant

dynamics. The direct application of nonlinear programming techniques, that is, using the exact functional expressions for the constraints, would computationally expensive. This is a broadly applied mathematics topic and not the focus of this dissertation. In this dissertation, the adopted numerical optimization methods only involve mature mathematical tools to get a local optimal solution for the design problem. The relevant details will be further discussed in Section 4.3.4.

4.2 Design Methodology

4.2.1 Design process

The integrated design and control process can be divided into two kinds of design: iterative and combined. Iterative design refers to designing the plant and the controller in separate steps within one iteration and repeating this process until the design requirement is satisfied. Combined design refers to optimizing the plant and controller in one step.

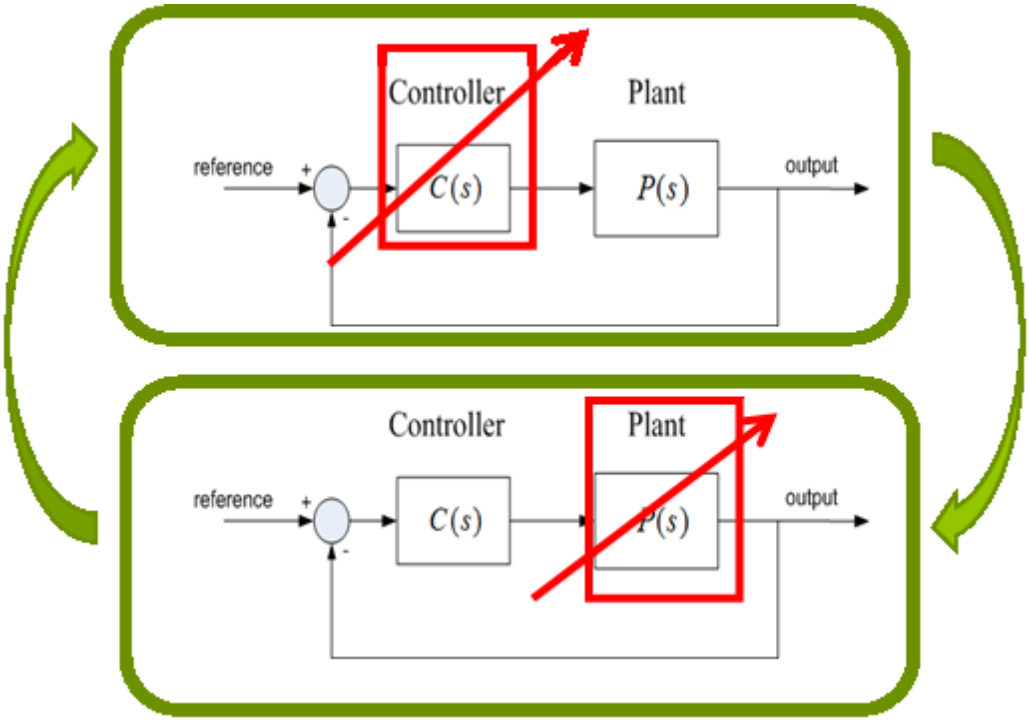

Figure 4.1 Iterative Design Process

The process of iterative design can be seen in Figure 4.1. In the step for controller design, the optimization problem is formed as Eq. (4.1). $P_{i-1}(s)$ is the plant designed in the $i-1^{\text{th}}$ iteration and can be considered fixed in this step. $C(s)$ is the feedback controller to be designed. J_{ci} is the design objective function specified for certain design purpose. With feedback control transfer function $C(s)$ as the design variable, this is a frequency domain optimization problem.

In the step of plant design, the optimization problem is formed as Eq. (4.2). $C_i(s)$ is the controller designed in the i^{th} iteration and can be considered fixed in this step. ξ is the design parameters in the mechanical system to be optimized with the constraints specified by S. $J_{\xi i}$ is the design objective function that can take the same form as J_{ci}. In this case, the relationship between the variable ξ and plant $P_i(s)$ is nonlinear, which results a nonlinear optimization problem.

$$C_i(s) = \min_{C(s)} J_{ci}\left(C(s), P_{i-1}(s, \xi_{i-1})\right) \quad C(s) \in L_2 \tag{4.1}$$

$$\xi_i = \min_{\xi} J_{pi}\left(P_i(s, \xi), C_i(s)\right) \quad \xi \in S \tag{4.2}$$

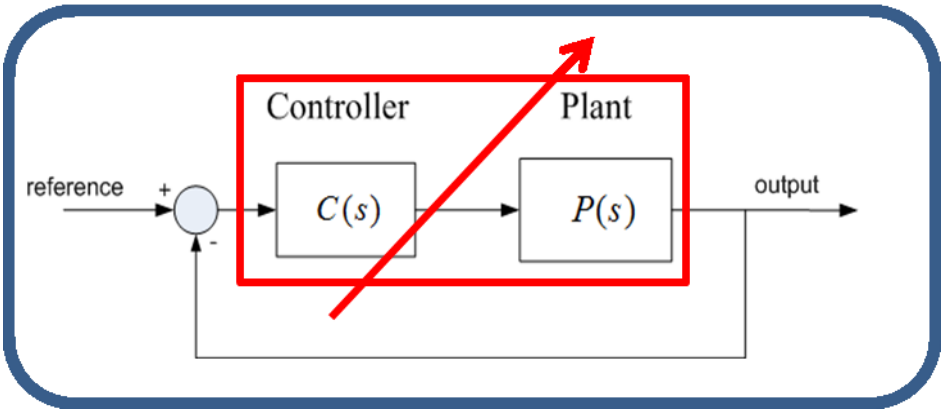

Figure 4.2 Combined Design Process

The process of combined design is shown in Figure 4.2. The optimization result can be achieved in one step. Similar to iterative design, J is the objective function to be specified. In most cases, this is also a nonlinear optimization problem due to the nonlinear function $P(s,\xi)$. Therefore, it is worth mentioning that neither iterative design nor combined design can guarantee a global minimum for the design results. The final result depends on the numerical optimization algorithm and initial point, which will be discussed in Section 4.3.

$$\left(C(s),\xi\right)=\min_{C(s),\xi} J\left(C(s),P(s,\xi)\right) \quad C(s)\in L_2,\xi\in S \tag{4.3}$$

To complete the design task for both iterative design and combined design, there are two aspects that need to be considered: 1) specification of the objective function J and 2) the choice of parameters to be designed in the mechanical system.

4.2.2 Control objective function

The objective function J is chosen based on the designer's expectation for closed loop control performance. The plant dynamics are included in the objective function and designed to optimize performance functions. In this case, the design does not aim to improve the open loop dynamic properties of the system such as modes and natural frequencies, but instead to pursue the 'best' achievable performance when the control action is effective. Therefore, the optimization algorithm to minimize the objective function can automatically find the more desirable physical design of the mechanical system when the controlled performance is taken into consideration.

Compared to open loop plant design, this integrated design and control approach can use more specific performance requirements as the design criteria. The general aspects that can be included in the objective function are the tracking and disturbance rejection performance, the robustness to model uncertainties and signal noise. Also, the objective function can be specified in both the time domain [87] and the frequency domain as discussed below, to satisfy requirements for various systems and tasks.

In this dissertation, the objective function is constructed as a multi-sensitivity H_∞ norm in Eq. (4.4). For the HHC problem, H_∞ norm can help to examine the worst case scenario when the ground height has absurd changes, which is the major concern in field operation. The mixed sensitivity problem helps to capture multiple aspects of the closed loop properties of concern. $W_P(s)$, $W_u(s)$, and $W_I(s)$ are, respectively, the weighting functions on the sensitivity function, input sensitivity function, and complementary sensitivity function. They are used to specify the design requirements for performance, robustness to multiplicative and additive uncertainties, and minimizing control input usage. Such choice of objective function has several advantages: 1) it is consistent with general robust control design criteria and has well-studied properties for each term in the objective function, 2) the emphasis on the different aspects of performance can be easily customized by designing the weight functions, and 3) in some steps of the optimization, mature synthesis tools can be used to obtain the optimal controller, as shown in Section 4.3. This objective function is constructed in frequency domain; therefore, it is convenient for the designer to specify the expected performance in terms of bandwidth, such as tracking bandwidth, disturbance, or noise rejection bandwidth. It would be even more effective if the frequency properties of the

system and external signals could be estimated ahead of design. For example, if the available bandwidth mentioned in Section 2.3 is pre-known, it can be used to specify $W_u(s)$ and place proper constraints on the robustness requirement.

$$J(C(s),\xi)=\left\| \begin{matrix} W_P(s)S(C(s),\xi) \\ W_u(s)C(s)S(C(s),\xi) \\ W_I T(C(s),\xi) \end{matrix} \right\|_\infty \tag{4.4}$$

4.2.3 Design parameter choice

There are two main principles for choosing the design parameters denoted as vector ξ: (1) they should have considerable influence on plant dynamics, (2) the corresponding physical change in the parameters in the current product should be achievable.

As discussed in Chapter 3, the passive DOF dynamics are the most influential factors to both the positions of zeros and poles in the HHC problem. Therefore, we need to look for the physical parameters that affect the passive dynamics, which are the pitch and vertical movement of the combine system. By examination, the dynamics of the combine body are closely related to the wheel distance (d_w), damping ratio (ζ_t), and rigidity (k_{spr_t}) of the tires. The header mass m_h affects the mass ratio between the header and the combine body, which also influences the interactive dynamics between the two bodies. In addition, for different tasks, a combine harvester can carry different headers. Therefore, the header's weight and inertia change in practice. It can be helpful to examine how such change can influence the control performance by including m_h in the design parameters.

From the analysis above, several parameters are chosen as candidates for design: the wheel distance (d_w), damping (ζ_t), and rigidity (k_{spr_t}) of the tires and the head mass m_h. Now the second principle for choosing parameters needs to be examined to decide whether the candidate parameters can be physically adjusted with relatively "minor changes." One can tune the damping and spring rigidity of the combine body dynamics by adding an extra suspension or shock absorber system between the combine body and tires. Also, the header mass naturally changes when different headers are installed. However, the wheel distance d_w is not easy to change for new products. It requires a series of geometric redesigns of many mechanical parts in the combine body system, so it does not satisfy the second principle mentioned at the beginning of this subsection. To conclude, the final parameters that are chosen for design are the header mass m_h, damping ratio of the front and rear tires denoted by ζ_{t_f} and ζ_{t_r}, and the spring constant of the front and rear tires denoted by $k_{spr\_t\_f}$ and $k_{spr\_t\_r}$. Table 4.1 shows the damping ratio and natural frequency of the zeros and poles for the original system. One can see that both the zeros and poles are lightly dampened with low natural frequencies, as analyzed in Chapter 3. As a result, the HHC performance is limited.

Table 4.1 Zeros and poles properties for original HHC system

Zeros/Poles	Undamped natural frequency(Hz)	Damping ratio
$z_1, \bar{z}_1$	1.9634	0.1213
$z_2, \bar{z}_2$	1.7839	0.0776
$p_1, \bar{p}_1$	1.9938	0.1181
$p_2, \bar{p}_2$	1.3734	0.0641

To further validate that the choice of redesigned parameters does influence the system dynamics, simulations are done below to show the relationship between parameter variations with zero and pole positions of the system. The parameter variation ranges are shown in Table 4.2. The parameters are set to vary by ±50% of the ranges in the simulation, and the corresponding variation of the zero and pole locations are shown in Figures 4.3 - 4.12. From the simulation results, all the parameters to be designed have significant impact on the position of zeros and poles within their varying ranges shown in Table 4.2. The combined effects of the parameter changes would impact the plant dynamics more than individual factors shown in Figures 4.3 - 4.12; therefore, the variable space of the design optimization problem should be sufficient for getting desirable plant dynamics for the redesigned system.

Table 4.2 Parameters to be designed in HHC system

Parameters	Lower bound	Upper bound	Initial value
m_h (kg)	4000	10000	5000
ζ_{t_f}, ζ_{t_r}	0.05	1	0.1
$k_{spr\_t\_f}, k_{spr\_t\_r}$ (N/m)	0.1	20	1

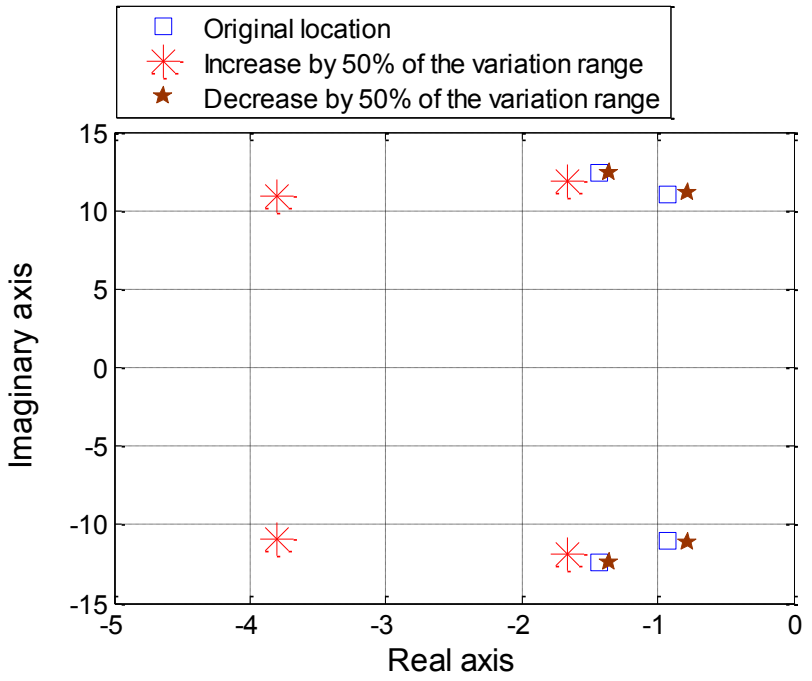

Figure 4.3 Zero position variation caused by changing ζ_{t_f}

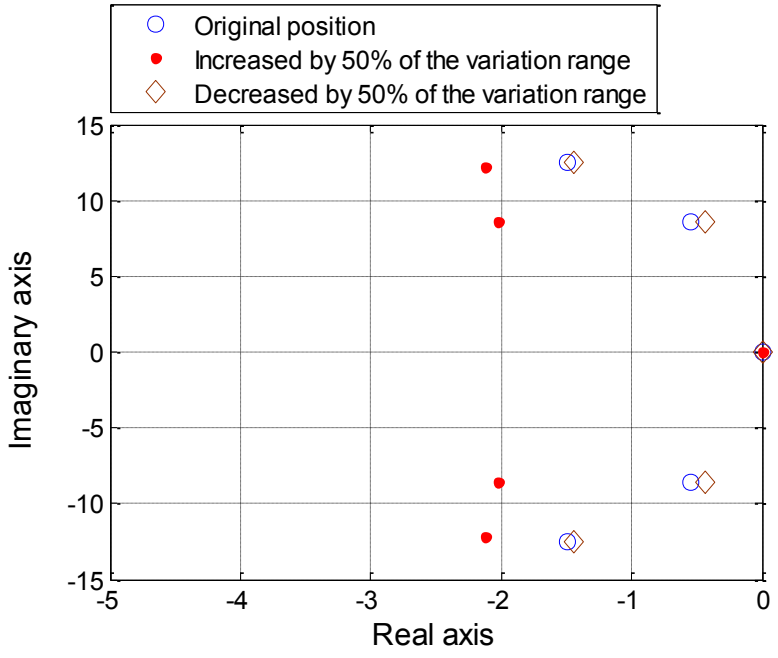

Figure 4.4 Pole position variation caused by changing ζ_{t_f}

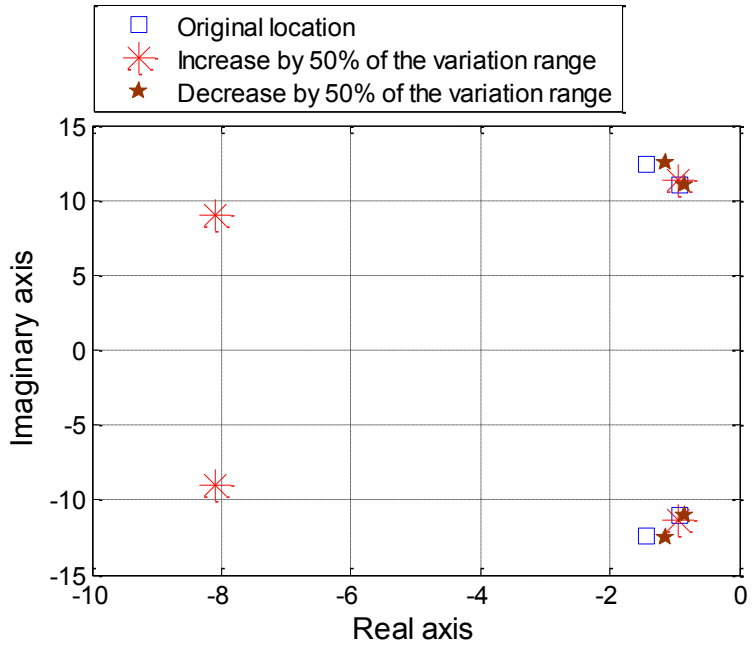

Figure 4.5 Zero position variation caused by changing ζ_{t_r}

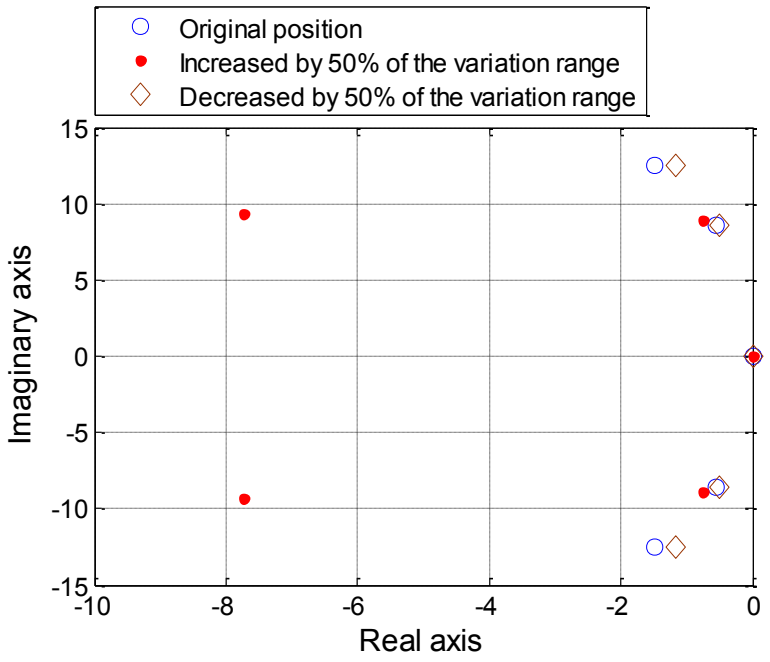

Figure 4.6 Pole position variation caused by changing ζ_{t_r}

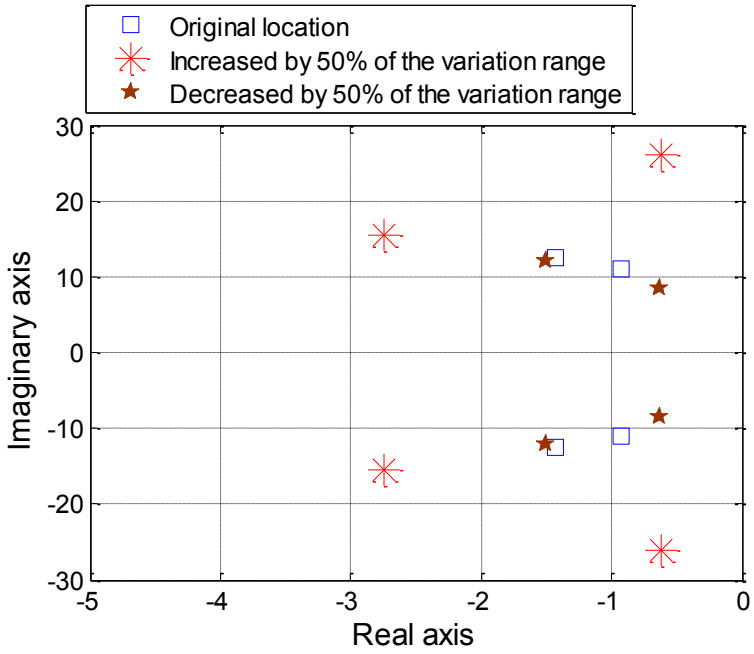

Figure 4.7 Zero position variation caused by changing $k_{spr\_t\_f}$

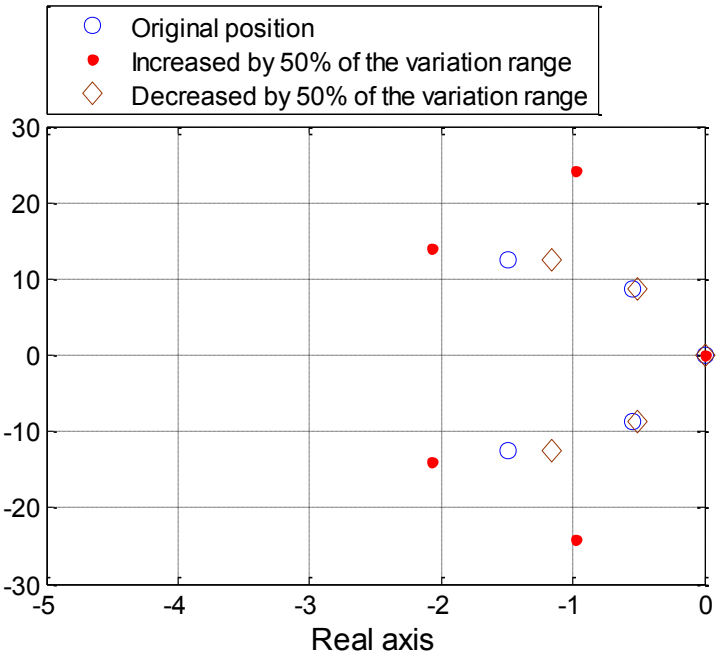

Figure 4.8 Pole position variation caused by changing $k_{spr\_t\_f}$

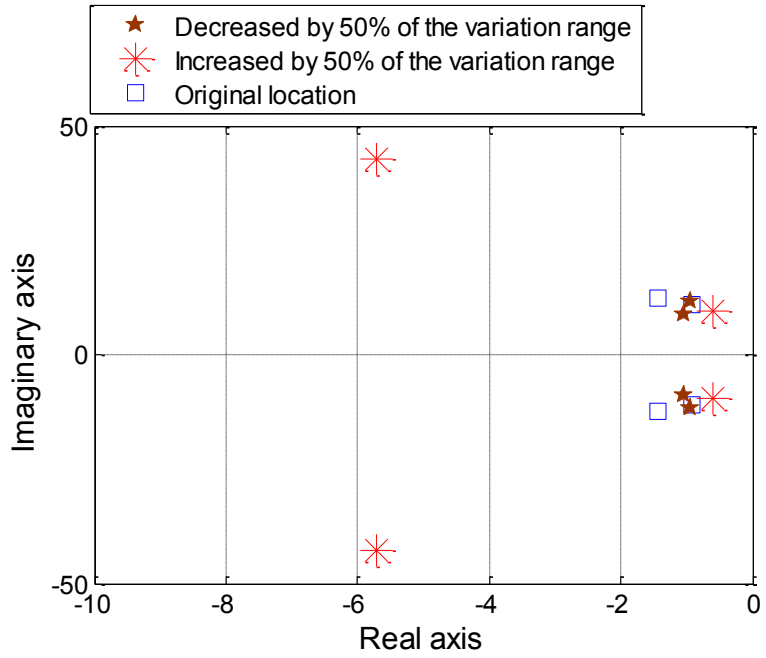

Figure 4.9 Zero position variation caused by changing $k_{spr\_t\_r}$

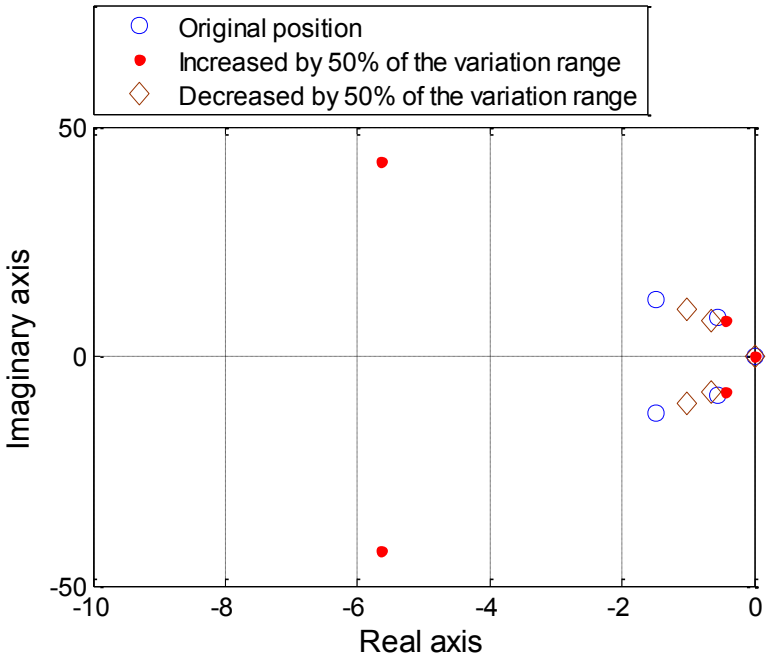

Figure 4.10 Pole position variation caused by changing $k_{spr\_t\_r}$

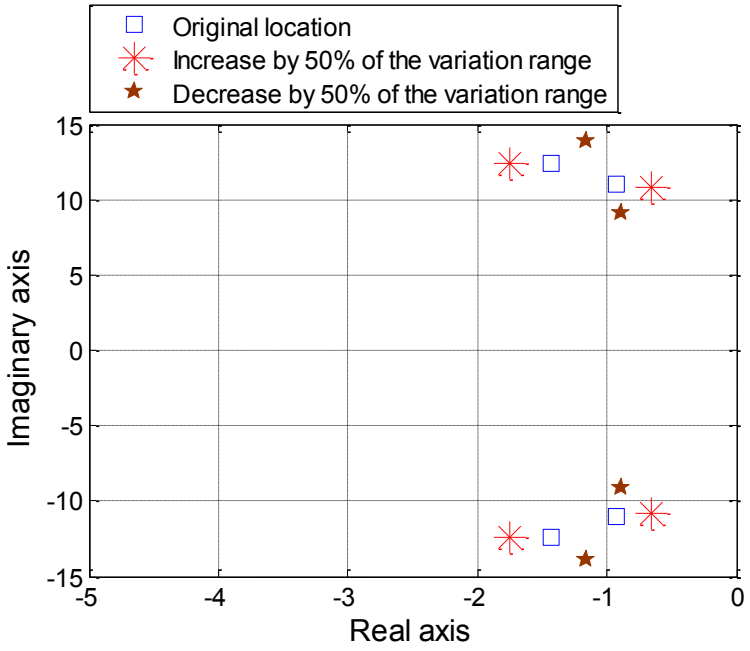

Figure 4.11 Zero position variation caused by changing m_h

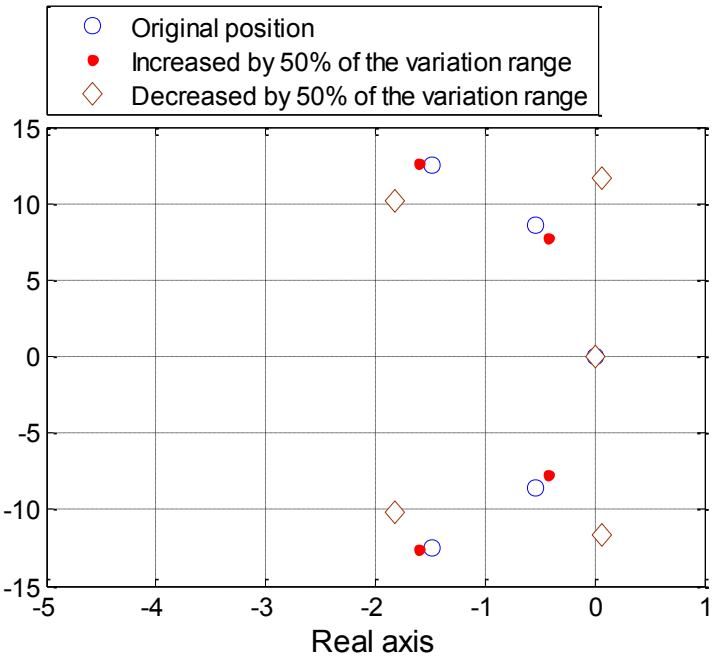

Figure 4.12 Pole position variation caused by changing m_h

4.3 Numerical Design Result

4.3.1 System specification

The HHC problem for combine harvesters is taken as an example in this section to obtain numerical validation of the methodology stated in Section 4.2. As far as the combine HHC problem is concerned, the undesirable locations of the zeros and poles are inherently caused by the mechanical structural features. The solution involving mechanical structure redesign may be more capable of eliminating the performance limitation. However, this may not be possible with the legacy designs of current products. Another solution involving parameter optimization causes a smaller change to the current product and thus may be sufficiently cost-effective as to be feasible in practice. If by this way the achievable bandwidth can satisfy the task requirement, parameter redesign is a relatively economical way to solve the problem, which is pursued as the solution path in this dissertation.

The detailed analysis for how the mechanical system induces undesirable plant dynamics and how such dynamics places restrictions on achievable bandwidth is elaborated in Chapter 3. It is well known that input/output pairs with low frequency and lightly damped zeros and poles can limit the effectiveness of any feedback control approach [30, 68]. Due to the proximity between open loop poles and zeros in HHC problem, as shown in Figure 3.4, there is difficulty in moving closed loop poles far from their open loop location. Clearly, this is a fundamental limitation regardless of any feedback controller $C(s)$. For HHC problem, the resulting robust performance bandwidth limitation is 0.64Hz as shown in Section 3.2.4.

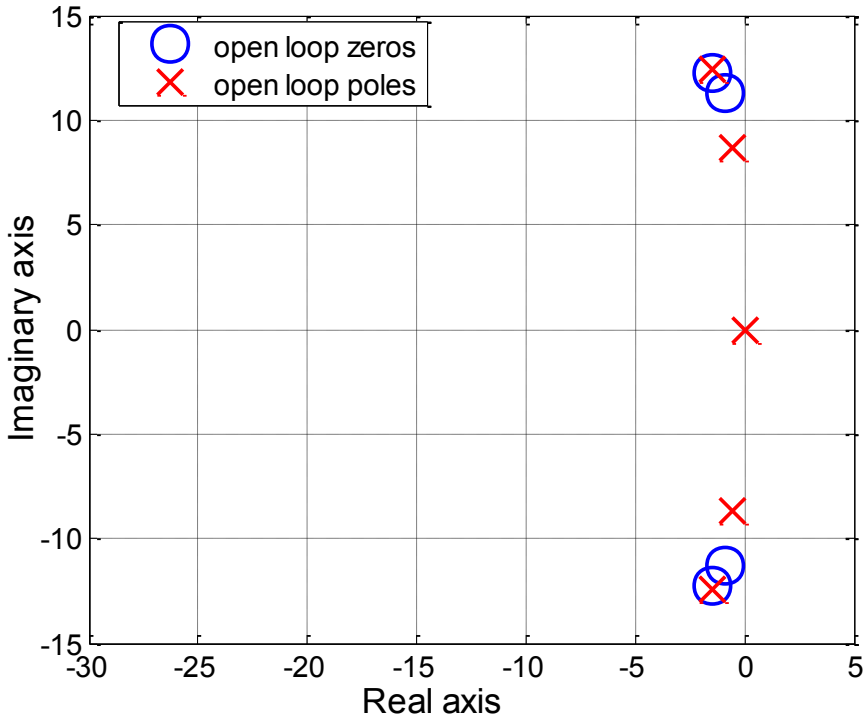

Figure 4.13 Position relationship between zeros and poles

With the choice of parameter in Section 4.2.3, the design methods in Section 4.2.1 can be applied with the objective functions specified in Section 4.2.2. $W_P(s)$, $W_u(s)$ and $W_I(s)$ are the weighting functions on the sensitivity function, input sensitivity function, and complementary sensitivity function respectively. According to the design objectives, they are specified as Eqs. (4.5) - (4.7). The inversion of these weight functions forms the upper bound of the sensitivity function's magnitude when the parameters and controller are designed, and the objective closed loop bandwidth is specified to be around 3Hz.

$$W_P(s) = \frac{s+10}{1.5s+2.4} \tag{4.5}$$

$$W_I(s) = \frac{0.02s+1}{0.01s+0.95} \tag{4.6}$$

$$W_U(s) = 0.5 \tag{4.7}$$

4.3.2 Iterative design method results

The controller and plant design are processed iteratively as shown in Figure 4.1. With the control objective function in Eq. (4.4), plant and controller parameters are optimized in separate steps to finally achieve satisfactory closed loop performance.

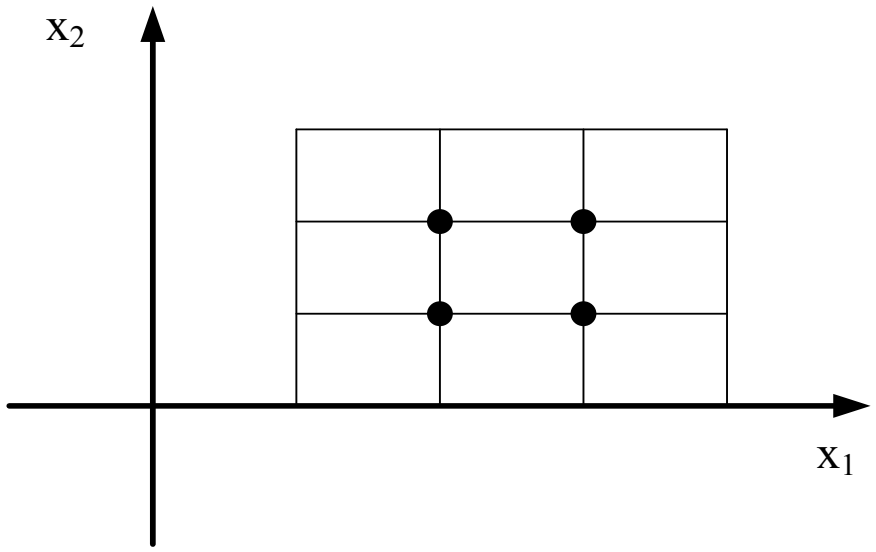

Figure 4.14 Gridding in parameter space for initial points

By choosing suitable weighting functions shown in Section 4.3.1, both the controller and plant are optimized to obtain the balance between performance, robustness, and input gain constraint. As stated in Section 4.2.2, this is a nonlinear optimization process where a global minimum point is not guaranteed. Therefore, the design result is influenced by the numerical optimization method and initial point. We used the 'fmincon' function in Matlab to find the local minimums, in which the interior point method is used for the optimization [88]. To cover most of the variable space, the initial points were chosen at various positions. Take the two-variable optimization problem in Figure 4.14 as an example; the initial points,

shown as black dots, are chosen to lie on the cross points of the 3*3 grid of the two variables. For the HHC problem, we chose five parameters to be designed at the same time, which gives a 3^5 grid and results in 2^5 initial points. Therefore, we have 32 optimization results with the optimized objective function values shown in Figure 4.15. From Figure 4.15, the variations of the optimized objective function values among different optimizations are small.

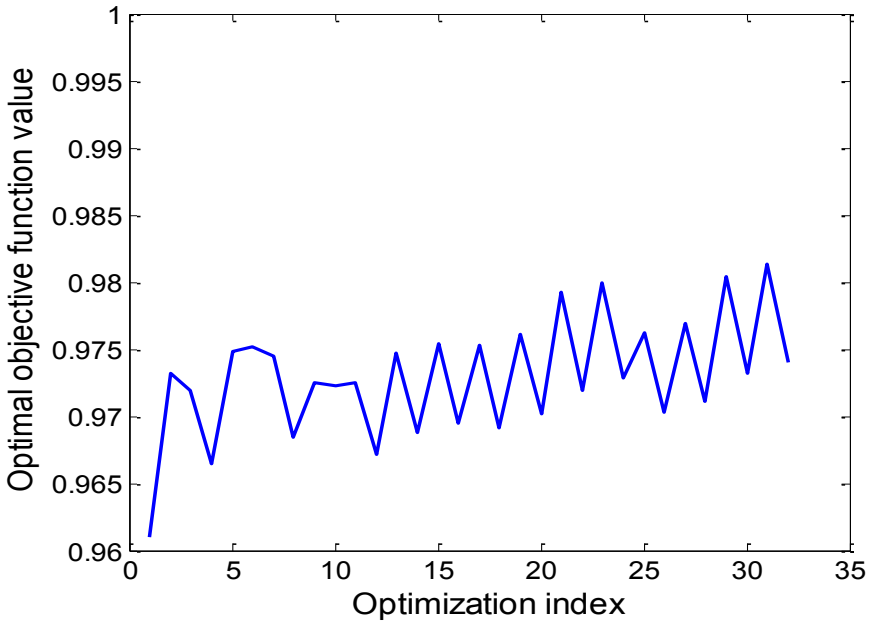

Figure 4.15 Optimal objective function value for 32 initial points

Figure 4.16 through 4.20 show the optimal parameter values of the optimizations with the 32 different initial conditions. Optimizations starting at different initial conditions tend to converge to several same final values. For example, in Figure 4.16, the optimal m_h are obtained at two values from optimization #14 - #32. Similar situations happen to the other four design parameters as shown in Figure 4.17 - 4.20. Therefore, the design variables calculated by different initial conditions fall into several local minimums.

Another useful conclusion illustrated in Figure 4.16 is that heavier header mass does not necessarily lead to worse performance. With proper redesign of the other four parameters, it is not necessary to decrease the mass of the header for better HHC performance. In other words, a larger, heavier header, which implies higher harvesting productivity, is valid for use in the next generation of product.

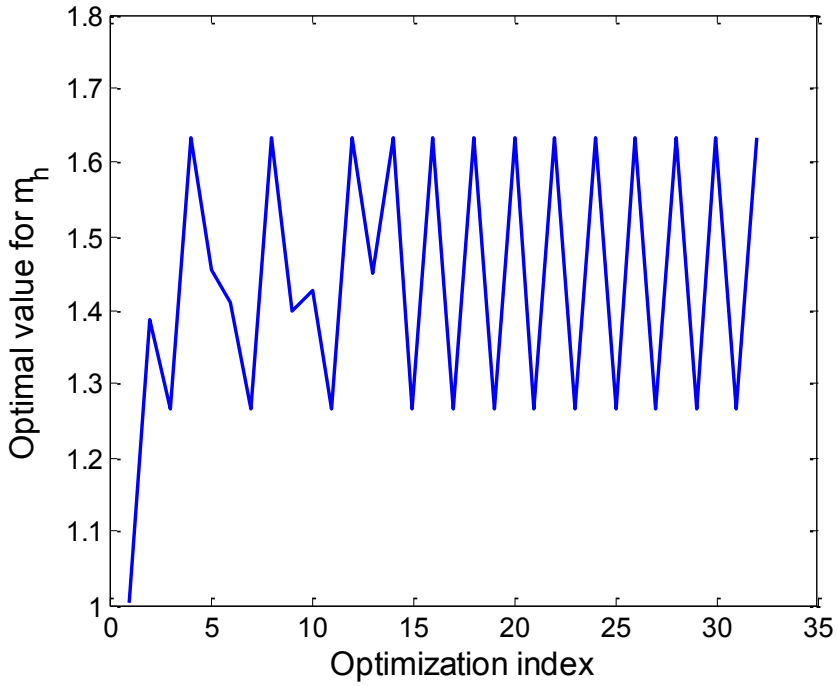

Figure 4.16 Optimal m_h for 32 initial points

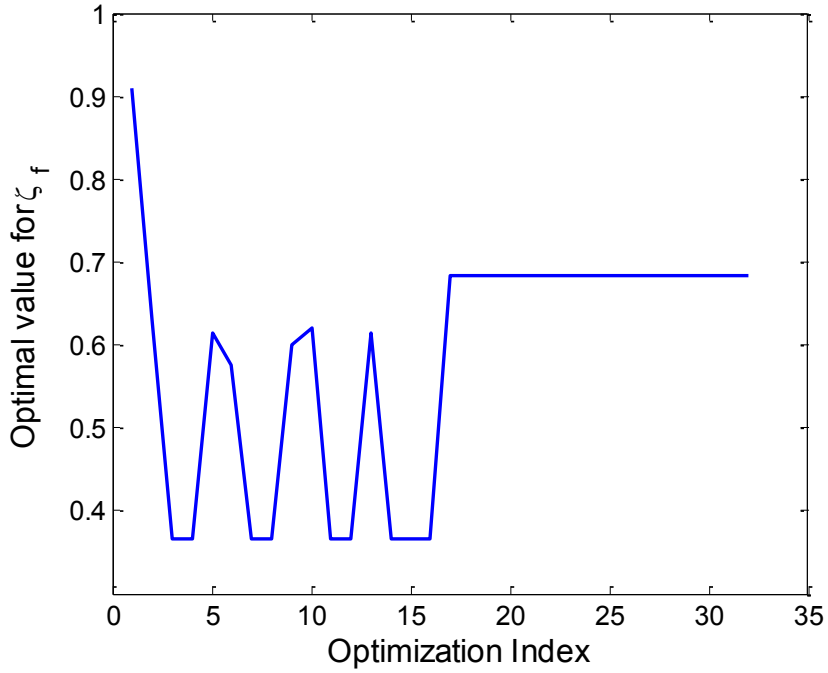

Figure 4.17 Optimal ζ_{t_f} for 32 initial points

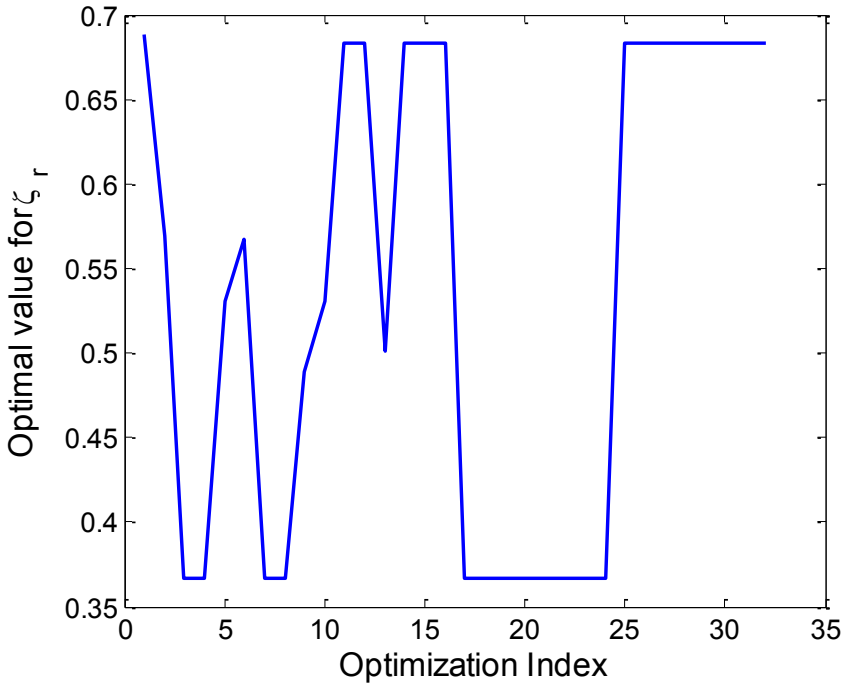

Figure 4.18 Optimal ζ_{t_r} for 32 initial points

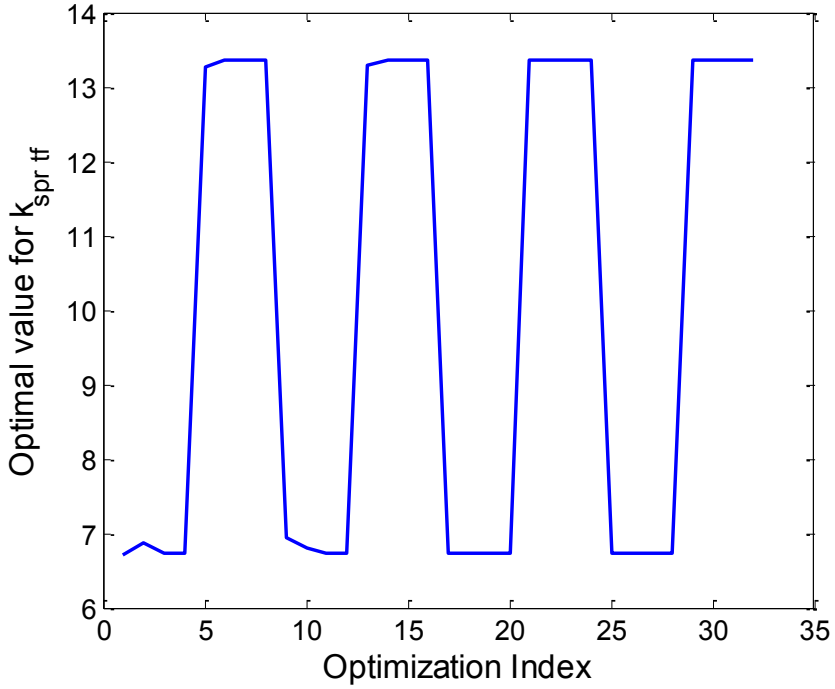

Figure 4.19 Optimal $k_{spr\_t\_f}$ for 32 initial points

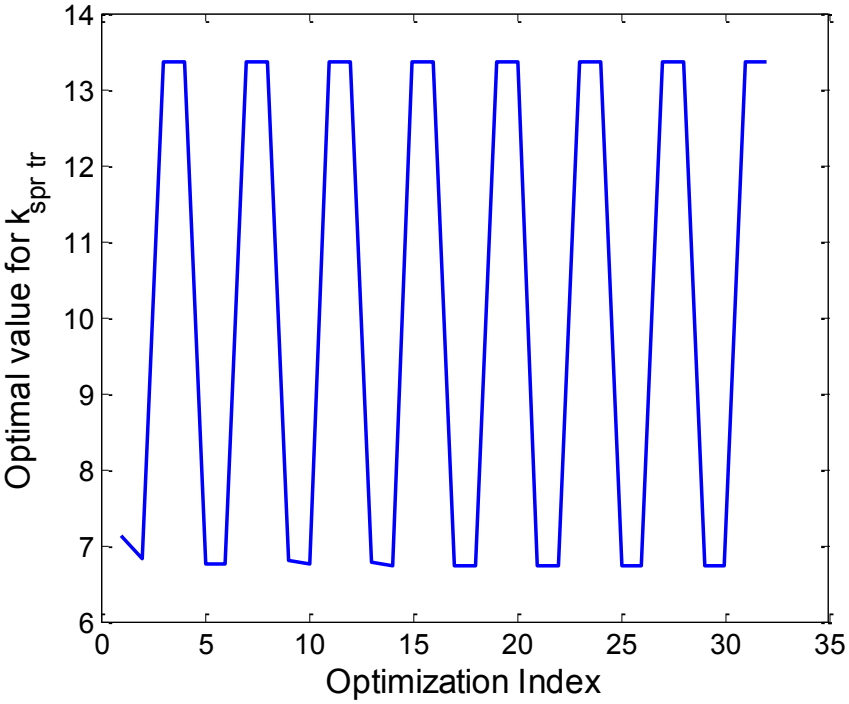

Figure 4.20 Optimal $k_{spr\_t\_r}$ for 32 initial points

The value of the optimized parameter vector ξ^* for the smallest objective function value is shown in Table 4.3, and the corresponding zeros and poles for the optimal plant transfer function $P^*(s)$ are compared to their original positions in Figure 4.21. Table 4.4 shows how such change influences the natural frequency and damping ratio of the plant dynamics, which have increased significantly for the redesigned system, and the design purpose is achieved.

Table 4.3 Parameters design result using iterative method

Parameters	Lower bound	Upper bound	Original value	Designed value	Variation (%)
m_h (kg)	4000	10000	5000	5001.8	0.36
ζ_{t_f}	0.05	1	0.1	0.9096	809.6
ζ_{t_r}	0.05	1	0.1	0.6888	688.8
$k_{spr\_t\_f}$ (N/m)	0.1	20	1	6.72	572
$k_{spr\_t\_r}$ (N/m)	0.1	20	1	7.18	618

Table 4.4 Zero and pole properties for redesigned system using iterative method

Zeros/Poles	Undamped natural frequency(Hz)	Damping ratio
$z_1, \bar{z}_1$	5.2699	0.8517
$z_2, \bar{z}_2$	4.5958	0.6868
$p_1, \bar{p}_1$	5.2878	0.8533
$p_2, \bar{p}_2$	3.5720	0.5347

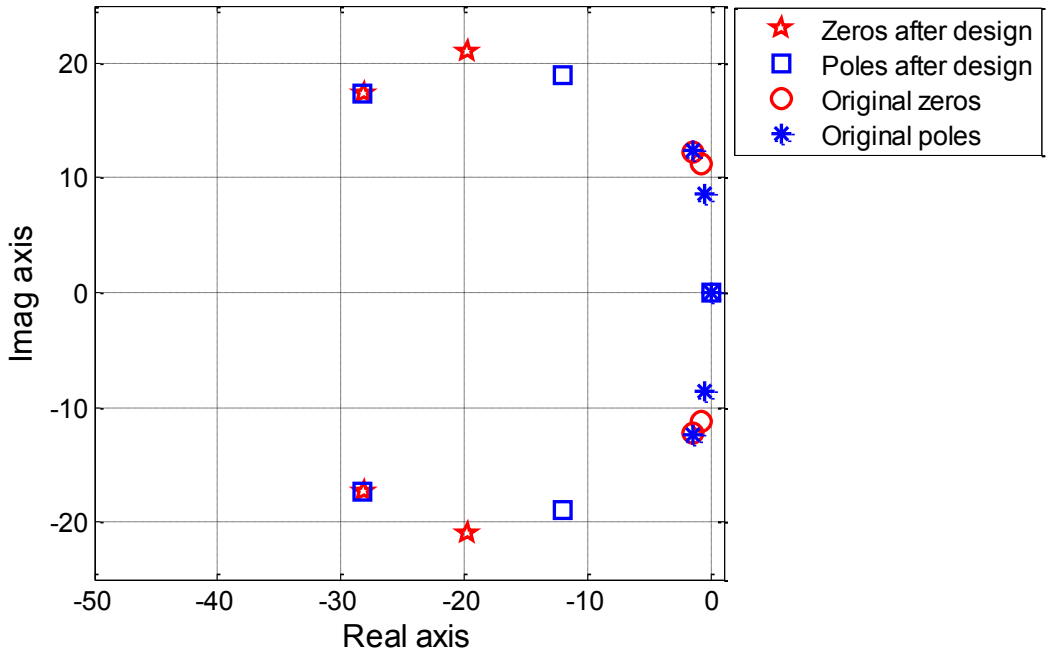

Figure 4.21 Pole and zero position comparison between original and designed systems

Inspecting the change of parameters, the damping ratio and spring constant of the tires increased considerably. This is consistent with our intuition: Increase of the damping ratio and spring constant can decrease the flexibility of the passive DOFs and thus mediate the system's under-actuation problem.

4.3.3 Combined design results

For the combined design method, the controller and plant design are processed together in one step, as shown in Figure 4.2. With the control objective function in Eq. (4.4), plant and controller parameters are optimized. The controller is chosen to be 6^{th} order transfer function, which is consistent with the order of the plant dynamics and ensures that the stable closed loop system can be found in the design space. This gives a nonlinear optimization problem with more variables and increases the nonlinearity of the objective function with respect to the design variables.

Such conclusion can be drawn from Figures 4.22 - 4.27. The optimal points starting from different initial conditions no longer fall into the same area in the variable space. The value of the optimized parameter vector ξ^* for the smallest objective function value is shown in Table 4.5, and the corresponding zeros and poles for the optimal plant transfer function $P^*(s)$ are shown compared to their original positions in Figure 4.28. The result is similar to the one obtained by iterative design. Both the damping ratios and natural frequencies have increased significantly for the redesigned system as shown in Table 4.6.

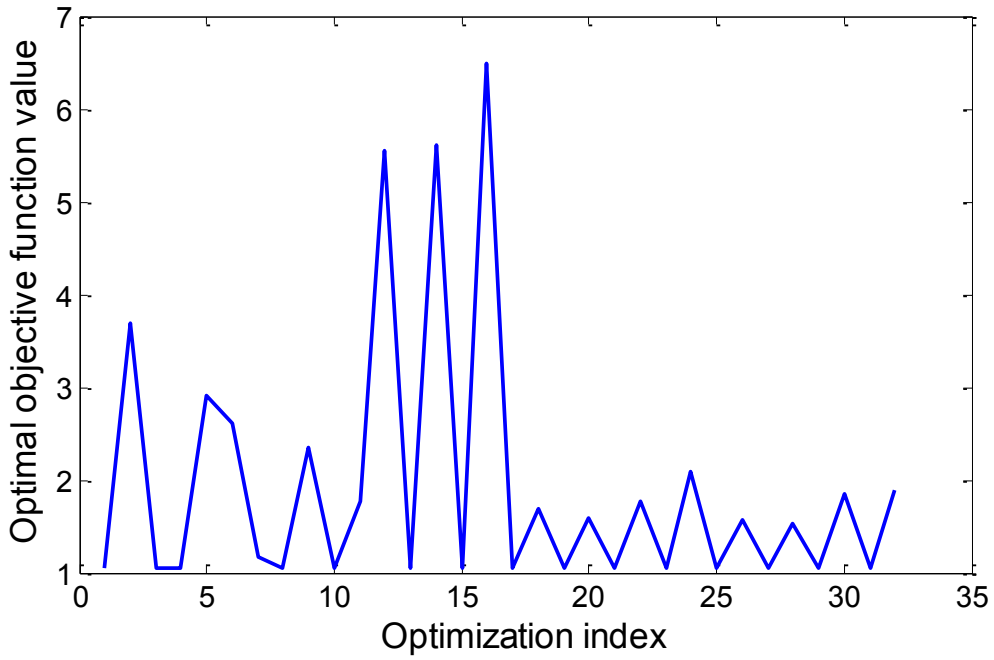

Figure 4.22 Optimal objective function value for 32 initial points by combined method

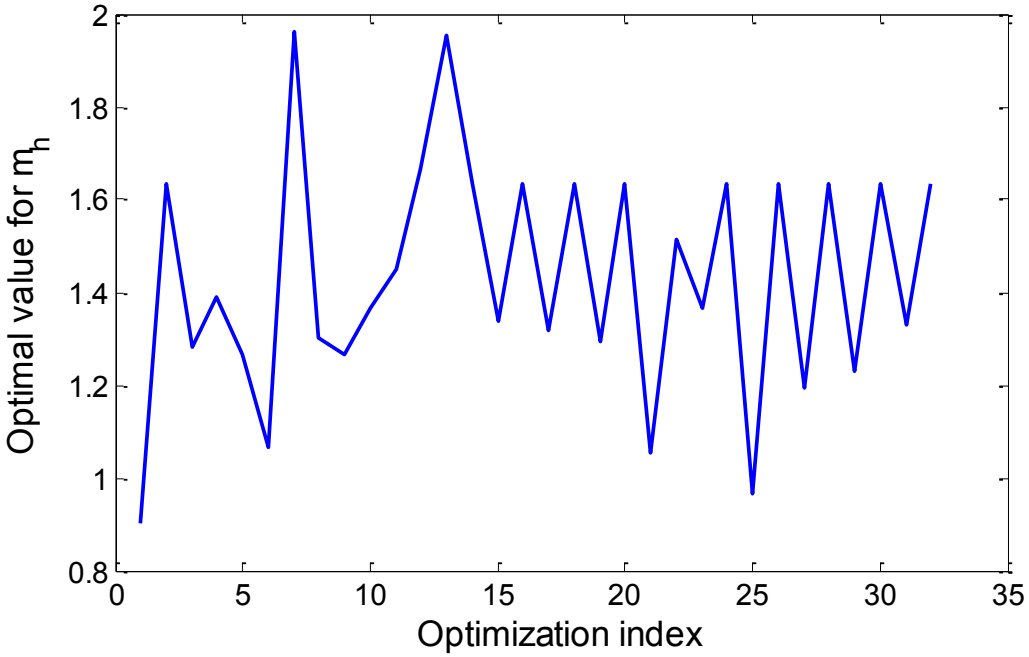

Figure 4.23 Optimal m_h for 32 initial points by combined method

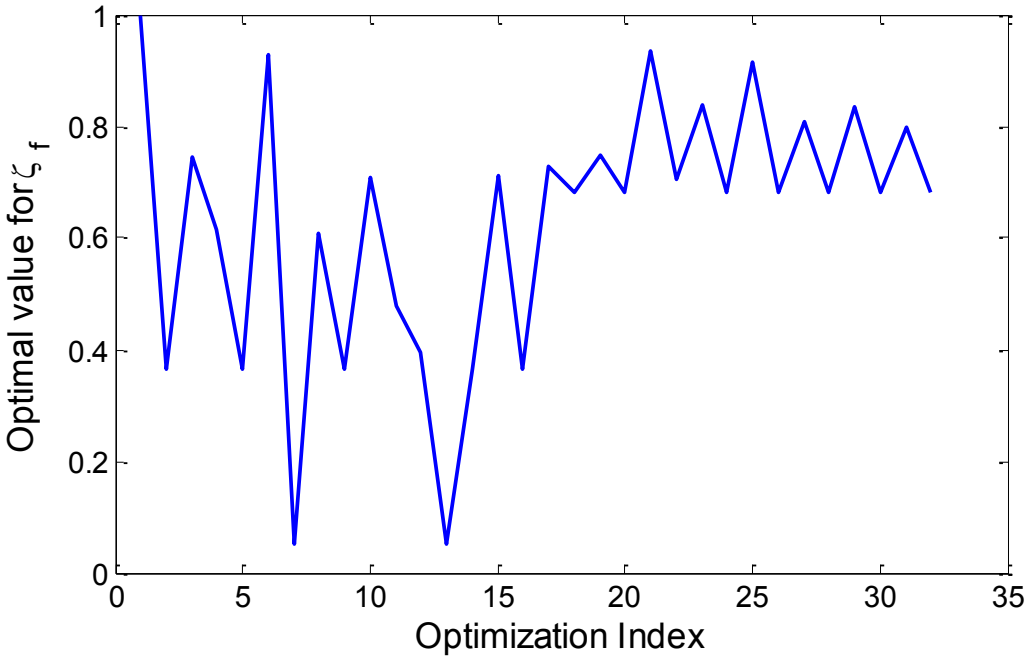

Figure 4.24 Optimal ζ_{t_f} for 32 initial points by combined method

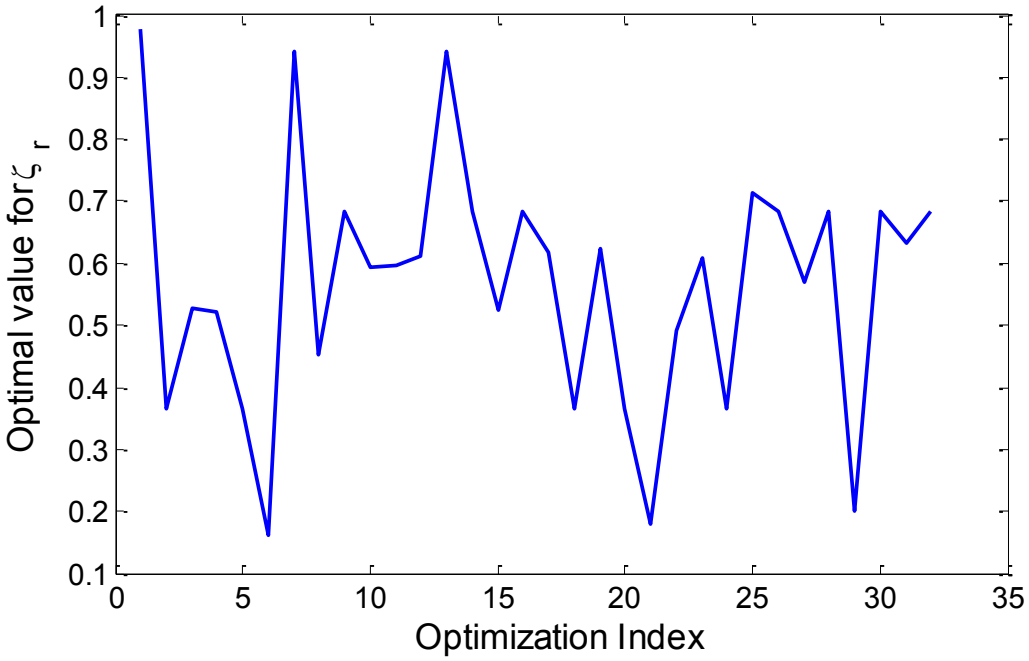

Figure 4.25 Optimal ζ_{t_r} for 32 initial points by combined method

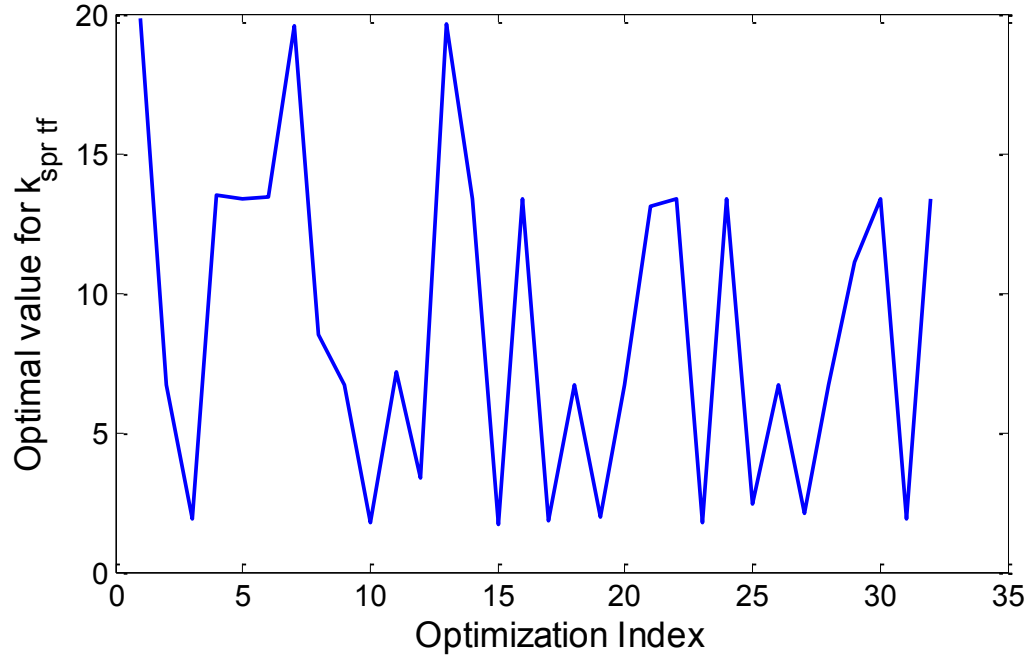

Figure 4.26 Optimal $k_{spr\_t\_f}$ for 32 initial points by combined method

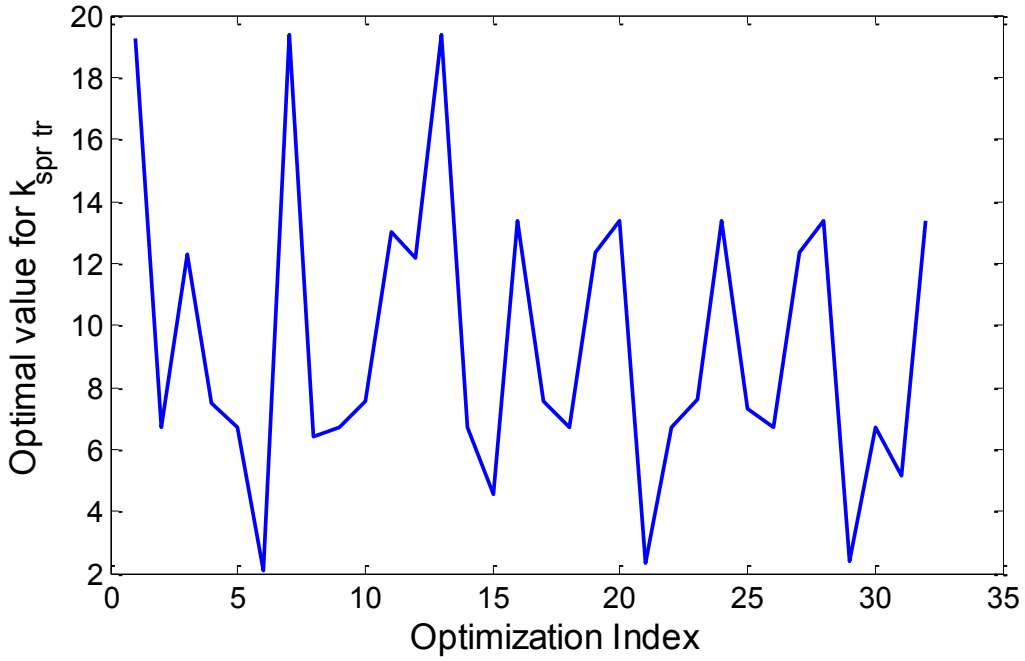

Figure 4.27 Optimal $k_{spr\_t\_r}$ for 32 initial points by combined method

Table 4.5 Parameter design result using combined method

Parameters	Lower bound	Upper bound	Original value	Designed value	Variation (%)
m_h (kg)	4000	10000	5000	6942	38.84
ζ_{t_f}	0.05	1	0.1	0.6139	513.6
ζ_{t_r}	0.05	1	0.1	0.5214	421.4
$k_{spr\_t\_f}$ (N/m)	0.1	20	1	13.53	1253
$k_{spr\_t\_r}$ (N/m)	0.1	20	1	7.46	646

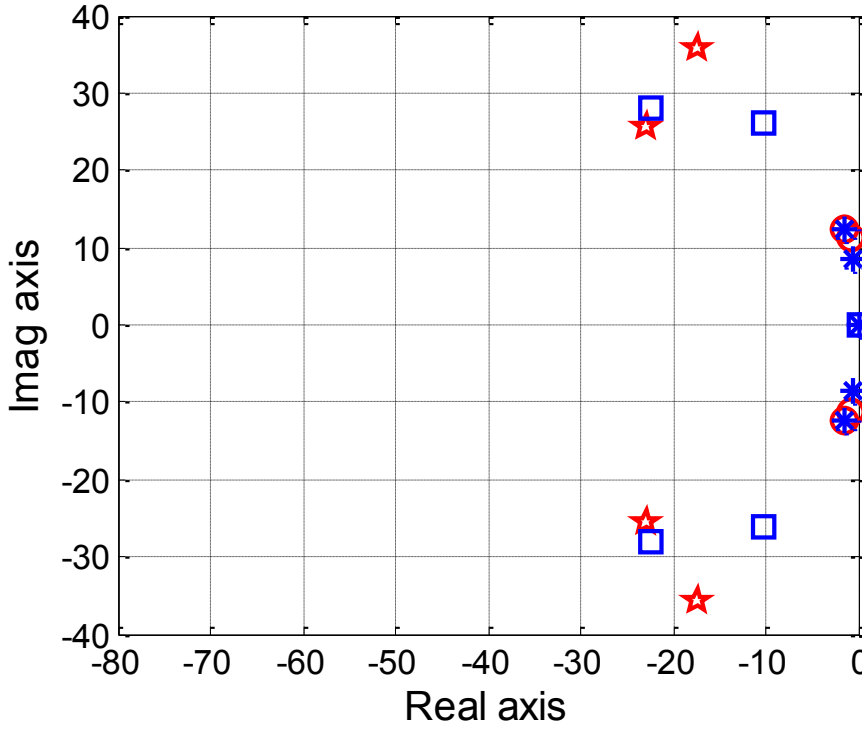

Figure 4.28 Pole and zero position comparison between original and designed systems

Table 4.6 Zero and pole properties for redesigned system using combined method

Zeros/Poles	Undamped natural frequency(Hz)	Damping ratio
$z_1, \bar{z}_1$	6.3177	0.4389
$z_2, \bar{z}_2$	5.4752	0.6647
$p_1, \bar{p}_1$	5.695	0.6249
$p_2, \bar{p}_2$	4.4795	0.3658

4.3.4 Simulated performance comparison

To show how the design of the plant can improve the overall performance of HHC, the simulations of the closed loop system response are shown below in both the frequency domain and the time domain.

With the same specification of the weight functions as shown in Eqs. (4.5) - (4.7), the sensitivity functions of the closed loop system for the original products and their design constraints are illustrated in Figure 4.29. One can see that they all satisfy the design requirements and that the tracking bandwidth is around 1.427Hz. This is the best performance the closed system can achieve with the original location of zeros and poles.

With the optimal controller and plant, the closed loop sensitivity functions by iterative method are shown in Figure 4.30. After design, the system bandwidth is now 2.51 Hz, which is higher than the frequency limitation of the original system.

Similar results for the combined method can be seen in Figure 4.31. After design, the system bandwidth is 2.33 Hz, which achieves approximately the same effect as the iterative method. Therefore, from such frequency domain result, the redesign of the physical system makes the closed loop system able to track faster changing signals and reject disturbances in the broader frequency range. In other words, the combine harvester can drive in the same field with 1.8 times of the original speed, which can improve working efficiency by 80%.

A similar conclusion can be drawn from a time domain performance comparison, as shown in Figure 4.32. The step response of the original system is relatively slow: The rising time is around 0.38 seconds and vibrations last for 2.5 seconds. The performances by both design methods give similar step responses. The rising time is decreased to around 0.15 seconds and the response is very smooth without vibration or overshoot. Such characteristics are desirable since the cutting height of the crops will be smooth and the header error can be largely decreased. As a result, it not only improves the working speed but also helps to decrease food waste and avoid equipment damage.

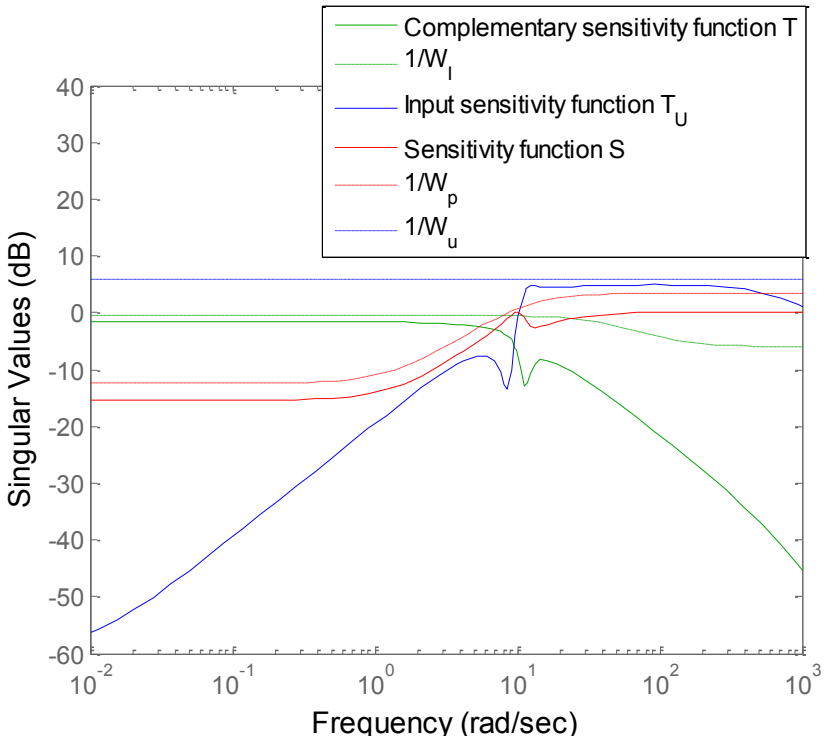

Figure 4.29 Robust control design for original system

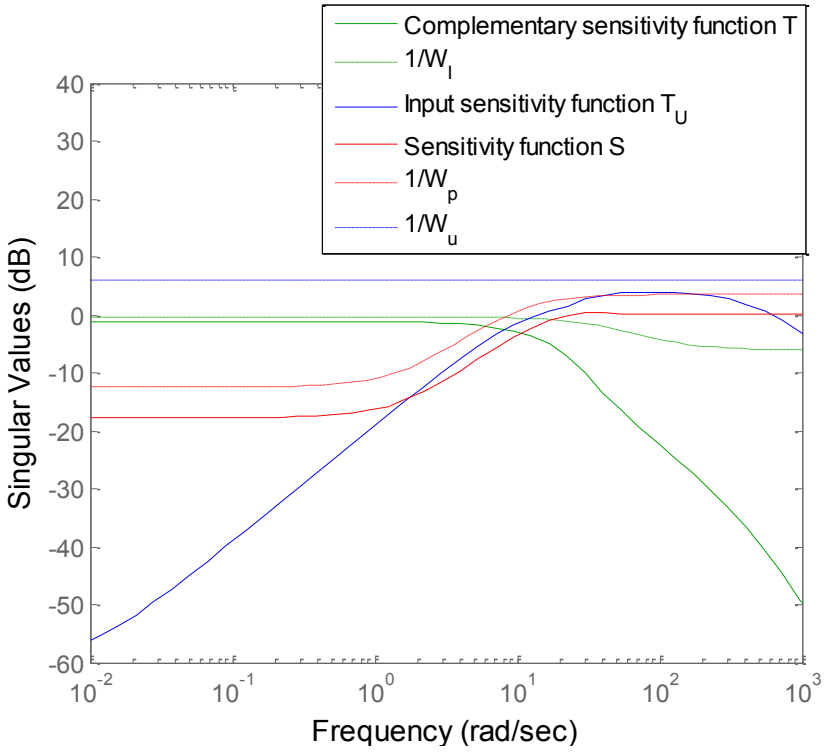

Figure 4.30 Robust control design for $P^*(s)$ by iterative method

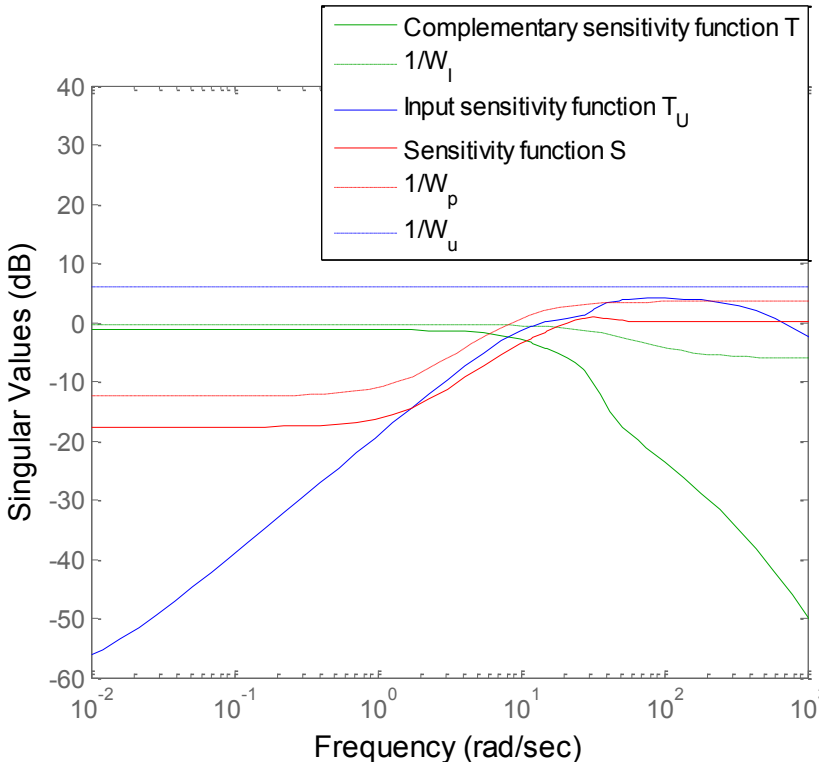

Figure 4.31 Robust control design for $P^*(s)$ by combined method

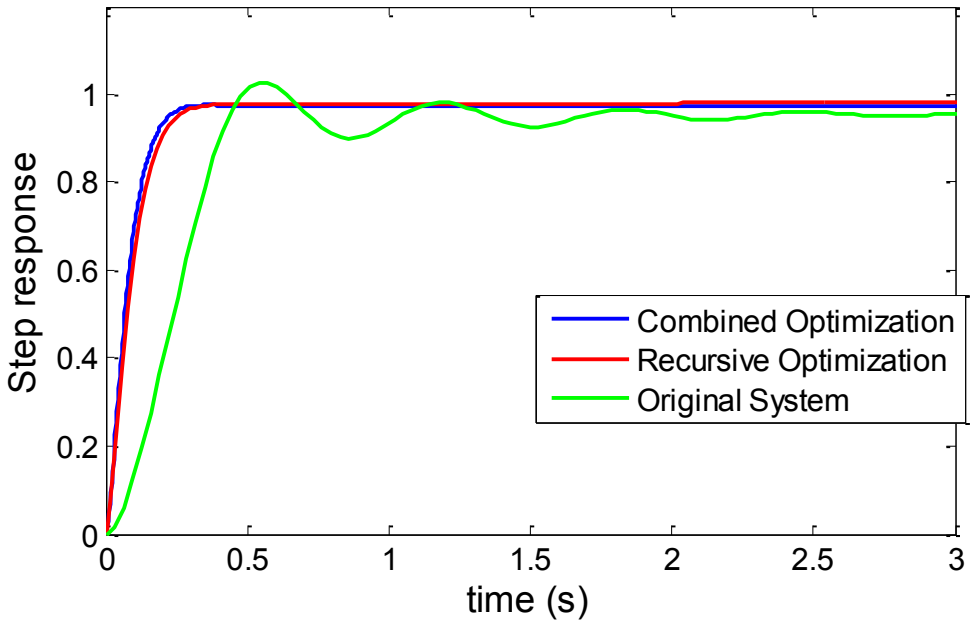

Figure 4.32 Step response comparison between original and designed systems

4.4 Conclusion

In this Chapter, the main limitation from the mechanical dynamics in VEI system is discussed and moderated. In the example of HHC problem, the under-actuation and non-collocation properties of the mechanical system results in lightly damped low frequency the open-loop poles and zeros. The induced bandwidth limitation is around 1.5Hz, which is part of the reasons for the bottleneck in increasing working efficiency.

Clearly, a drastic improvement in the overall system performance cannot be achieved solely by feedback control design. To eliminate or decrease the undesirable mechanical characteristics, the mechanical system needs to be redesigned. We adopt the idea of redesign key parameters in the system to balance the requirements from performance and costs. The parameters are calculated to minimize the H_∞ norm of the closed loop sensitivity functions. Two optimization processes are studied: iterative design and combined design. Both of them improved the physical characteristics of the system: the zeros and poles of the new plant move away from the imaginary axis and obtain much larger damping ratio than the original plant.

The controller is also optimized in the process either iteratively or in one combined step. The tracking performance, disturbance rejection and control effort are balanced to achieve the best performance in frequency domain. The corresponding closed loop system has a bandwidth of 2.51 Hz and 2.33Hz for the two methods respectively, which proves that the potential for automatic control to achieve higher bandwidth is improved by optimizing the parameters of the mechanical system. The increase of the closed loop bandwidth means that the header height control can track faster signals and reject disturbances in higher frequency; as a result, the combine can harvest the crops at a higher speed yet with less grain

loss in the field. Such design method can be expanded to many systems as long as the design is targeting at achieving certain closed loop performance.

Since the design in this chapter focuses on mechanical system, the other limitation of delay is left out. Therefore, the feedback controller obtained in this chapter works for system with only mechanical limitation. When the delay problem exists, more efforts need to be done to get better feedback controller design, which will be shown in Chapter 5.

Chapter 5
Robust Feedback Controller for Time Delayed Systems

Time delays commonly exist in physical systems. For example, the delay in the actuator response can cause an input delay from the control input to the operation of the plant. This is frequently seen in hydraulic actuators with impacts by dead zone in control valves, dry friction, and fluid dynamics [65]. Another kind is the communication delay existing broadly in teleoperation systems [89], communication networks [90, 91], and neural networks [92]. In other cases, it can be caused by the system dynamics, such as the wave propagation in combustion systems [93]. Delay can also appear in the measurement process that induces phase lags in the feedback channel [94].

Particularly in VEI systems, due to the heavy-duty nature of the tasks, delay can appear in the actuation system [95]. Such delay can be much influential to system control: On the one hand, the phase lag caused delay is considerably larger than the one by vehicle dynamics; on the other hand, the delay itself is not consistent all the time. Take the HHC problem for example, the delay in the hydraulic actuator in the experimental system is 0.3s. This delay induces a closed loop bandwidth at 0.5Hz as illustrated in Chapter 3, which is much lower than the natural frequency of the zeros and poles in the plant dynamics.

Therefore, when designing the feedback controller design, delay is an inevitable factor to be considered [64]. In addition, the feedback control also needs to address the model uncertainties caused by the varying delay time and uncertain plant dynamics to ensure robust stability and performance.

In this chapter, an H_∞ controller is introduced targeting the design of a robust controller with consideration of the time delay in the HHC system. As mentioned, there is an upper bound on the achievable bandwidth when time delay exists. The work in this chapter does not try to break such bandwidth limitation, but to seek the best balance among several design requirements when the delay and the physical system limitation are taken into consideration.

5.1 Time Delayed System

5.1.1 System configuration

Due to the various causes in the system, delays can appear in many places within the system model such as at the input, output, feedback channel, states, and even the derivatives of the states. There are no unified control methods to deal with all kinds of delays; therefore, researchers work to develop a case-by-case control algorithm for delayed system [92, 96-99]. In many cases, the general mathematic formulation of the problem is made for the multi-input-multi-output (MIMO) system, but due to the nature of actuator delay in VEI systems discussed in this dissertation, we only focus on loop delay in the SISO system.

A typical SISO unity feedback system with delay is shown in Figure 5.1. Similar to Figure 2.1, r is the reference for the output y to follow. G_{p_r} represents the rational part of

the dynamics of the plant, and e^{-sT} is the delay term with delay time as T; n is the noise, and d is exogenous disturbance with disturbance dynamics G_d.

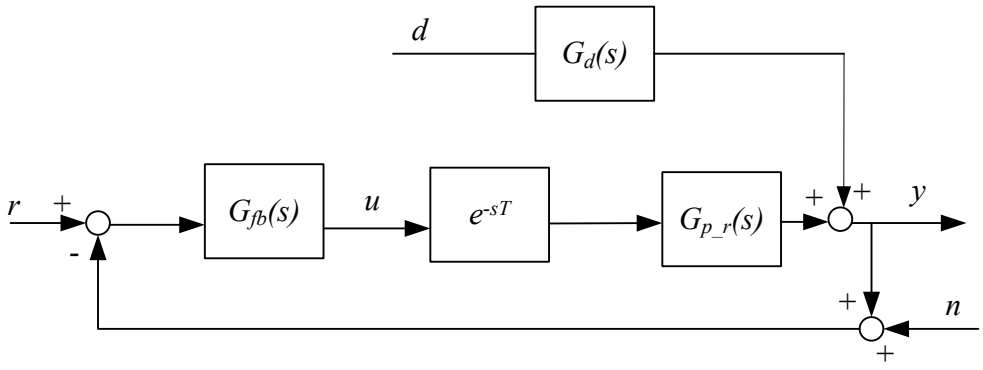

Figure 5.1 Schematic of a delayed system

In many cases, the appearance of the delay will influence the stability of the system. Therefore, it is important to understand such impact to obtain a stable closed loop system and avoid unexpected accidents in practice. Researchers have attempted to identify the stability criteria for both the conservative delay-independent condition [100, 101] and the less conservative delay-dependent condition [100]. In these analyses, the delay is assumed to be a constant.

However, in many real systems, the delay is time varying, which creates uncertainty in the system response. For such time-varying systems, two categories of controllers were studied to solve the problem: One way is to capture the change of the delay online using adaptive algorithms [102, 103]; another is to use a robust controller with specifications on the bound of delay variance [104].

In this dissertation, we adopted the second method to solve the problem. The time-varying delay is treated as a constant delay plus a time-varying uncertainty. Therefore, as only as robust controller can satisfy the stability and performance requirement within the

uncertainty constraints, the feedback control objectives can be achieved. One of the reasons for using robust control is that the delay time changes fast but with small variance in HHC system. This makes robust control a more suitable tool than adaptive control. Another reason is that it can deal not only with time delay uncertainty but also with dynamic uncertainties from other factors such as parameter perturbation [105] or mechanical system inconsistency (e.g., the header is replaced with another header for different tasks in the HHC problem). In Section 5.1.2, further discussion of the control for a time delayed system is presented.

5.1.2 Brief review of control for delayed systems

An obvious control problem arising for the time-delayed system is the infinite dimension from the delay term e^{-sT}. Due to its irrationality, many standard control approaches for linear systems are no longer feasible for direct use in the delayed system.

One way to design the controller for such a time-delayed system is to theoretically solve the infinite-dimensional problem using operator theoretical methods [106, 107]. Such methods usually provide complicated solutions that are not convenient for use in practice. Similarly, the control problem can be formulated to be a numerical optimization problem in the discrete time domain to provide an analytical solution for the controllers [108].

For a simple PID-type controller, the control parameters to be designed are small numbers, usually within 3. Therefore, the stability region of the parameter space can be theoretically calculated for the control of a plant with uncertain parameters [99, 109].

For a higher order, more complicated robust controller, usually a certain kind of transformation is required during the design process to derive a rational optimization problem from the original infinite dimensional system [110]. One common way is to use the state

space system and linear matrix inequality (LMI). The time-delayed systems are expressed in state space form and certain cost function, such as H_∞ performance, is defined within the time domain [111]. By re-defining states in the system, the expression is transformed to be rational and usually a Riccati-type of inequality can be obtained from the new state space model to enable an LMI solvable problem. When considering the time-varying delay case, the range of the time delay is pre-defined and used to obtain a robust H_∞ controller with a similar procedure.

Another way to transform such infinite problem is to use J-spectral factorization and the Smith predictor [112]. The standard H_∞ control problem can be reformulated using equivalent transformation from the original PK block form to be a chain four-block form. The new form simplified the problem to be a one block Smith predictor -type of system, which can be further transformed into a rational optimization problem with J-spectral factorization and solved using rational LMI.

The robust control method we are introducing in this dissertation also uses the Smith predictor. However, instead trying to convert mathematically an irrational LMI problem to a rational problem, the system is transformed equivalently to a delay-free system without changing the nature of the H_∞ norms to be optimized. Therefore, standard synthesis for H_∞ control can be used for the new system to achieve the design requirements of the original system. More details of the design procedure can be found in Section 5.3.

5.2 Smith Predictor

5.2.1 Introduction to Smith predictor

The Smith predictor has been used to control the delayed system for a long time. It was first introduced in the late 1950s [113] and has been considered a very useful tool to obtain a delay-free system from the original delayed system [114, 115]. This is realized by using a local feedback signal from a central controller as its input signal, as shown in Figure 5.2. In the figure, $Z(s)$ is the Smith predictor and $C_0(s)$ is the central controller. A standard Smith predictor has the form shown in Eq. (5.1). Therefore, the feedback controller $G_{fb}(s)$ in Figure (5.2) has a relationship with $Z(s)$ and $C_0(s)$ as in Eq. (5.2).

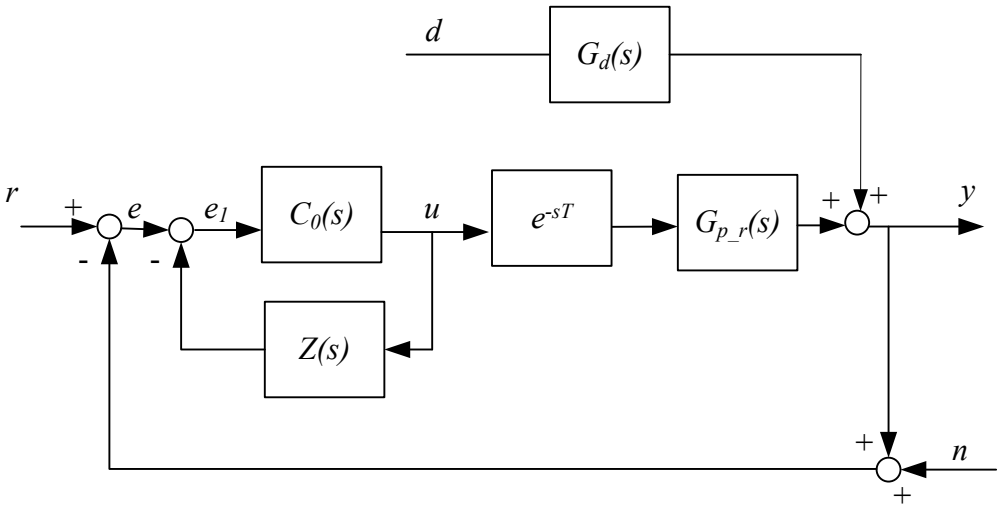

Figure 5.2 Smith predictor in a delayed system

$$Z(s) = G_p(s) - G_p(s)e^{-sT} \tag{5.1}$$

$$G_{fb}(s) = \frac{C_0(s)}{1 + Z(s)C_0(s)} \tag{5.2}$$

The feedback signal from the Smith predictor $Z(s)$ is a predicted version of y. When the noise is not considered, the signal e_1 in Figure 5.2 can be expressed in Eq. (5.3). The signal feedback to the central controller $C_0(s)$ is the error between reference and predicted output. Therefore, the system is equivalent to Figure 5.3, where the delay term is left out of the feedback loop. Note that once the central controller $C_0(s)$ is decided, the original feedback controller $G_{fb}(s)$ is determined. For the reference tracking performance, the sensitivity function from the reference to the tracking error is shown in Eq. (5.4). Also, the complementary sensitivity function becomes Eq. (5.5). Therefore, the original problem of designing $G_{fb}(s)$ for a delayed system is transformed to finding a $C_0(s)$ that stabilizes the delay-free plant $G_{p\_r}(s)$. This transformation provides the advantage of eliminating the original gain constraints for controller design and enabling the classical design methods for normal rational systems.

$$\begin{aligned} e_1 &= r - y - Z(s)u \\ &= r - \left(G_{p\_r}(s)e^{-sT} + Z(s)\right)u \\ &= r - G_{p\_r}(s)u \\ &= r - ye^{sT} \end{aligned} \tag{5.3}$$

$$e = \left(1 - \frac{C_0(s)G_{p\_r}(s)}{1 + C_0(s)G_{p\_r}(s)}e^{-sT}\right)r \tag{5.4}$$

$$T_{Sm} = \frac{C_0(s)G_{p\_r}(s)}{1 + C_0(s)G_{p\_r}(s)}e^{-sT} \tag{5.5}$$

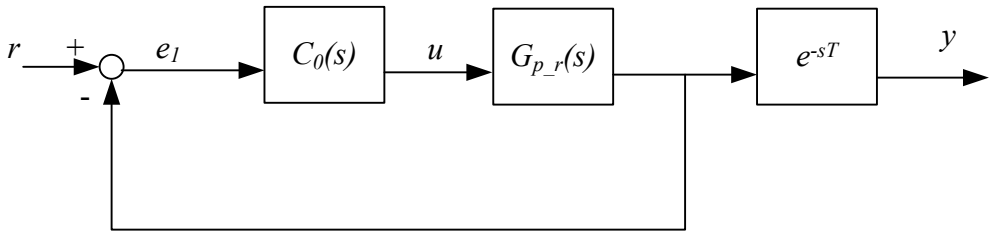

Figure 5.3 Equivalent delay-free system by Smith predictor

5.2.2 Smith predictor in robust control

Although the Smith predictor introduced above is capable of eliminating the infinite-dimensional design for the nominal system, it does not imply unlimited performance when the system is uncertain. The Smith predictor controller requires an accurate model of the plant dynamics and the time delay. When there is inconsistency between the nominal and time-varying delay time, or a mismatch between the model and the process dynamics, it causes poor performance or even instability for the closed loop system. Therefore, research on the implementation of the Smith predictor in robust control has been studied extensively.

The simplest case is to only consider the robust stability of the system. As shown in Eq. (5.5), for a complementary sensitivity function, the delay term is separated. When the true plant dynamics $G_{p0}(s)$ mismatches the plant model $G_{p\_r}(s)$ as shown in Eq. (5.6), the robustness criterion in inequality (5.7) is equivalent to inequality (5.8) [116]. Therefore, the robust control problem is easy to convert to a rational optimization problem and guarantee robust stability.

$$G_{p0}(s) = G_{p\_r}(s)\left(1+\Delta(s)\right) \tag{5.6}$$

$$\left\|\Delta(s)T_{sm}(s)\right\|_{\infty} < 1 \tag{5.7}$$

$$\left\| \Delta(s) \frac{C_0(s) G_{p\_r}(s)}{1 + C_0(s) G_{p\_r}(s)} \right\|_\infty < 1 \tag{5.8}$$

However, in most cases, in addition to robust stability, robust performance is also required when designing the feedback controller. Since the sensitivity function shown in Eq. (5.4) has mixed delay and rational functions, the design of the controller becomes an infinite dimensional problem. One way to avoid this is to approximate the infinite dimensional system with a finite dimensional system using Talyor series approximation [117], Padé approximation [118], or Maclaurin series expansion [119] .

The other way is to keep the original infinite dimensional expression. Such research can be divided into two kinds: One numerically optimizes the controller parameters with the robust performance constraints [120] and the other transform the irrational optimization to an equivalent LMI problem [121]. The latter one will be used in this dissertation.

5.3 Robust Controller Design

5.3.1 Problem formulation for robust control design

A robust controller is used to ensure the robust stability of the system and optimize the robust performance. In Figure 5.4, the uncertain system schematic for the time-delayed system with Smith predictor is shown. When plant G_p has stable poles, $Z(s)$ is stable [121]. The exogenous signals are reformulated as normalized signals as $\begin{pmatrix} r_n & d_n \end{pmatrix}^T$ by Eqs. (5.9) and (5.10) to simplify the later analysis. Weighting functions $W_r(s)$ and $W_d(s)$ describe the frequency content of the reference and disturbance signals respectively. The model uncertainty Δ is weighted by $W(s)$ to specify the upper bound of its frequency

representation. $W_e(s)$ is the weighting function for the error signal. All weights can be constant or dynamic functions of frequency.

$$r_n W_r(s) = r \tag{5.9}$$

$$d_n W_d(s) = d \tag{5.10}$$

The objective for robust controller design is generally achieved by minimizing the norm of particularly structured transfer functions. The well-known H_∞ robust performance problem for the feedback controller can be posed as: *find a stabilizing controller* $C(s)$ *to minimize the structured singular value of* $N(s)$*, which is defined as the transfer function matrix between* $(r_n \quad d_n \quad y_\Delta)^T$ *and* $(z_1 \quad u_\Delta)^T$ *in Figure 5.4.*

$N(s)$ is shown in Eq. (5.11), where H_1 represents the performance of the system, and H_2 represents feedback system robustness. Weight function $W_e(s)$ is used to specify the design emphasis on the robust performance. To clarify the notation used in Eq. (5.11), and in the following content, $T_{A,B}$ and $S_{A,B}$ are defined as the complementary sensitivity function and sensitivity function with plant $A(s)$ and feedback controller $B(s)$, respectively. The objective function is the standard mixed sensitivity problem similar to what is used for the integrated design and control in Chapter 4.

$$N(s) = \begin{bmatrix} H_1 \\ H_2 \end{bmatrix} \tag{5.11}$$

where

$$H_1 = \begin{bmatrix} W_e S_{G_p,G_{fb}} W_r \\ -W_e S_{G_p,G_{fb}} G_d W_d \\ -W_e S_{G_p,G_{fb}} G_{p\_r} e^{-sT} \end{bmatrix}^T, \; H_2 = \begin{bmatrix} W S_{G_p,G_{fb}} G_{fb} W_r \\ -W S_{G_p,G_{fb}} G_{fb} G_d W_d \\ -W S_{G_p,G_{fb}} G_{fb} G_{p\_r} e^{-sT} \end{bmatrix}^T$$

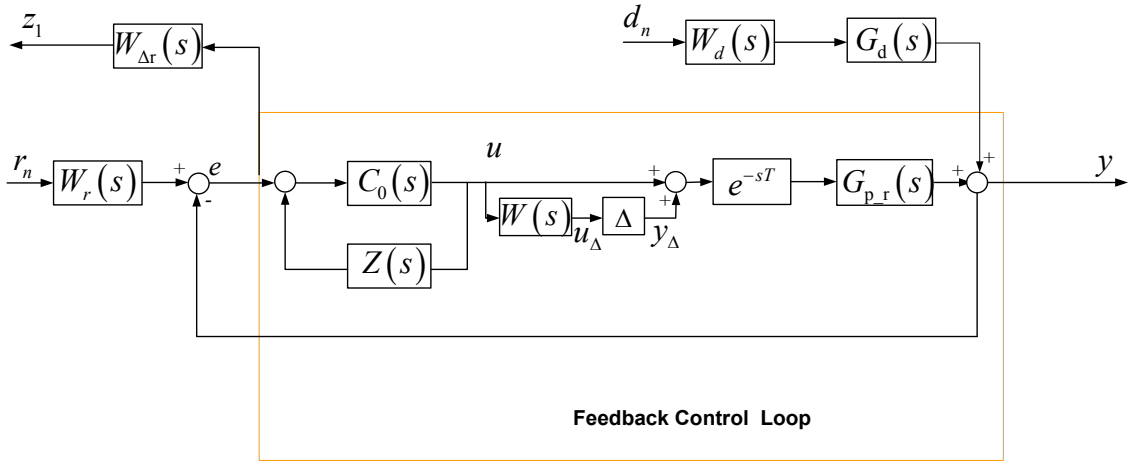

Figure 5.4 Schematic for robust control design

5.3.2 Model referenced performance

Eq. (5.11) provides an optimization problem to find the best H_∞ controller satisfying design requirements. However, to use the standard rational H_∞ controller synthesis, the irrational term from the actuator delay, e^{-sT}, must be addressed.

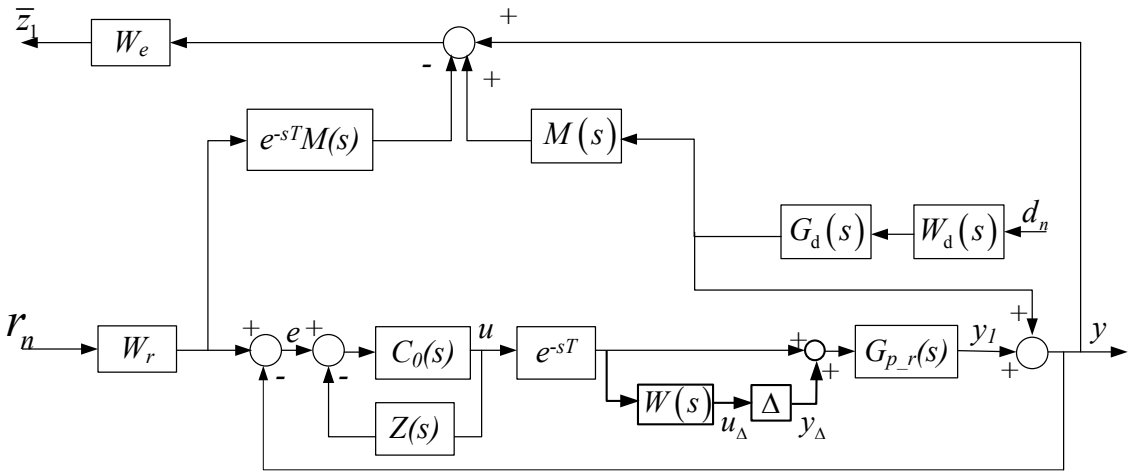

Figure 5.5 Modified feedback loop with model reference

To realize this, a model-matching method similar to [121] is implemented by adding the desired performance functions to construct new sensitivity functions. The structure of the modified feedback loop is shown in Figure 5.5. Ideally, if we do not consider the influence of the disturbances, it is desirable for y_1 to track the reference r_n via some desired linear operator $M(s)$ such that the desired output can be represented as $y_{1,des} = M(s)W_r(s)r_n$. However, due to the delay in the loop, the best tracking performance to expect can only be $e^{-sT}M(s)W_r(s)r_n$. In other words, the feedback control can never compensate for the delay in the loop since it always responds to the feedback signal with a delay T. Similarly, the influence of the delay makes the best expected transfer functions from the two disturbances to y be $e^{-sT}M(s)G_d(s)W_d(s)$. Therefore, the desired output for y can be expressed as y_{des} in Eq. (5.12). The difference between y_{des} and y can be written as Eq. (5.13), which indicates the tracking error between the real output and the desired output. This yields the modified sensitivity function S_{mo} in Eq. (5.14). S_{mo} represents the closeness of the ability of the closed loop system to track the reference and reject the disturbances to what is specified by $e^{-sT}M(s)$.

$$y_{des} = e^{-sT}M(s)\left(W_r(s)r_n - G_d(s)W_d(s)d_n\right) \tag{5.12}$$

$$y_e = S_{mo}\left(W_r(s)r_n - G_d(s)W_d(s)d_n\right) \tag{5.13}$$

$$S_{mo} = e^{-sT}M(s) - T_{G_p,G_{fb}}(s) \tag{5.14}$$

The H_∞ norm is mentioned in Eq. (5.11). Using such modified error signal with a desired performance reference model, the transfer function matrix $N(s)$ shown in Eq. (5.11)

can be changed to $N_{mo}(s)$ in Eq. (5.15) by replacing the original sensitivity function $S_{G_p,G_{fb}}$ with its modified version S_{mo}.

$$N_{mo}(s)=\begin{bmatrix} H_1 \\ H_2 \end{bmatrix} \tag{5.15}$$

where

$$H_1=\begin{bmatrix} W_e S_{mo} W_r \\ -W_e S_{mo} G_d W_d \\ -W_e S_{mo} G_{p\_r} e^{-sT} \end{bmatrix}^T,\ H_2=\begin{bmatrix} W S_{mo} G_{fb} W_r \\ -W S_{mo} G_{fb} G_d W_d \\ -W S_{mo} G_{fb} G_{p\_r} e^{-sT} \end{bmatrix}^T$$

Using such modified error signal with a desired performance reference model, S_{mo} can be further expressed as a delay-free transfer function times the delay term, as shown in Eq. (5.14). The complementary sensitivity function and the modified sensitivity function can be expressed as the multiplication of the delay term and rational functions as shown in Eqs. (5.16) through (5.18). This is the key result for transforming from an irrational optimization problem to a rational one. In this way, the delay term can be "extracted" from the terms in H_1 and H_2 as shown in Eq. (5.19). Since e^{-sT} has the unity magnitude on all frequency ranges, the H_∞ norm of H_1, H_2, and their rational part shown in Eq. (5.20) are the same. Therefore, the original H_∞ problem is equivalent to minimizing the H_∞ norm of N_{eqt}, which can be reformulated as a delay-free system in Figure 5.6.

$$T_{G_p,G_{fb}}(s)=e^{-sT}T_{G_{p\_r},C_0}(s) \tag{5.16}$$

$$S_{mo}(s)=e^{-sT}\left(M(s)-T_{G_{p\_r},C_0}(s)\right) \tag{5.17}$$

$$G_{fb}S_{G_p,G_{fb}}=C_0 S_{G_{p\_r},C_0}(s) \tag{5.18}$$

$$N_{mo}(s)=\begin{bmatrix} H_1 \\ H_2 \end{bmatrix} \tag{5.19}$$

where

$$H_1=\begin{bmatrix} W_e e^{-sT}\left(M(s)-T_{G_{p\_r},C_0}(s)\right)W_r \\ -W_e e^{-sT}\left(M(s)-T_{G_{p\_r},C_0}(s)\right)G_d W_d \\ -W_e e^{-sT}\left(M(s)-T_{G_{p\_r},C_0}(s)\right)G_{p\_r} e^{-sT} \end{bmatrix}^T,$$

$$H_2=\begin{bmatrix} WC_0 S_{G_{p\_r},C_0}(s)W_r \\ -WC_0 S_{G_{p\_r},C_0}(s)G_d W_d \\ -WC_0 S_{G_{p\_r},C_0}(s)G_{p\_r} e^{-sT} \end{bmatrix}^T$$

$$N_{eqt}(s)=\begin{bmatrix} H_1 \\ H_2 \end{bmatrix} \tag{5.20}$$

in which

$$H_1=\begin{bmatrix} W_e\left(M(s)-T_{G_{p\_r},C_0}(s)\right)W_r \\ W_e\left(M(s)-T_{G_{p\_r},C_0}(s)\right)G_d W_d \\ W_e\left(M(s)-T_{G_{p\_r},C_0}(s)\right)G_{p\_r} \end{bmatrix}^T$$

$$H_2=\begin{bmatrix} WC_0 S_{G_{p\_r},C_0}(s)W_r \\ -WC_0 S_{G_{p\_r},C_0}(s)G_d W_d \\ -WC_0 S_{G_{p\_r},C_0}(s)G_{p\_r} \end{bmatrix}^T$$

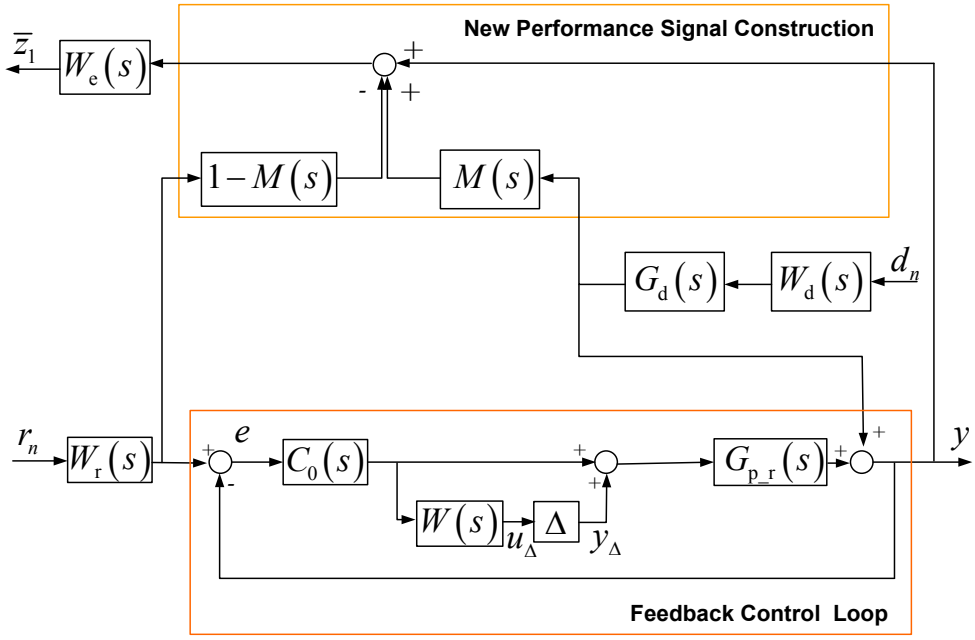

Figure 5.6 Schematic for reformulated robust control design

5.3.3 Rational optimal controller synthesis

The original H_∞ problem discussed in Section 5.3.1 is now reconstructed to find the optimal H_∞ norm of N_{eqt} in Eq. (5.20). This is a standard rational optimization problem.

Using the synthesis technique in [14], it is equivalent to solving the two block problem shown in Figure 5.7. The augmented plant $P(s)$ is given by Eqs. (5.21) and (5.22). The controller $C_0(s)$ can now be calculated by LMI with standard H_∞ optimal control synthesis.

$$\begin{pmatrix} z_{fb} \\ e \end{pmatrix} = P_{fb}(s) \begin{pmatrix} \omega_{fb} \\ u_1 \end{pmatrix} \tag{5.21}$$

$$P_{fb}(s) = \begin{pmatrix} \begin{pmatrix} W_e W_r & -W_e G_d W_d & -W_e G_p \\ 0 & 0 & 0 \end{pmatrix} & \begin{pmatrix} -W_e G_p \\ W(s) \end{pmatrix} \\ \begin{pmatrix} W_r & -G_d W_d & -G_p \end{pmatrix} & -G_p \end{pmatrix} \tag{5.22}$$

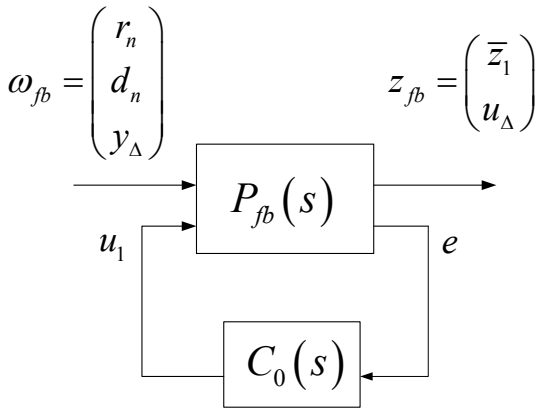

Figure 5.7 Two block construction for standard H_∞ problem

5.4 Controller Design and Simulation Results

5.4.1 Feedback controller design for HHC problem

To parameterize the feedback controller, the performance function and the weighting functions are chosen as in Eqs. (5.23) - (5.26) for the specific system shown in Figure 3.6. The bandwidth limitation caused by the mechanical dynamics is approximately 0.64Hz as described in Section 5.3. Therefore, it is realistic to set the bandwidth of the desired transfer function $M(s)$ to be approximately this value as in Eq. (5.23). $1/W_e(s)$ is an upper bound to the modified sensitivity functions, which has small magnitude at low frequency. W_r can be estimated by using the frequency property curve of the reference, in the HHC case the ground profile. A low order transfer function is used to approximate the frequency distribution of the reference in Figure 5.8 and gives the W_r shown as Eq. (5.25). The disturbance also comes from the ground profile, so the choice of W_d is the same with W_r. W is chosen to be unity.

With the weight functions specified, the augmented plant $P_{fb}(s)$ can be expressed to its state space realization in the form of Eq. 5.27 and the numerical representation of the realization in Appendix D.

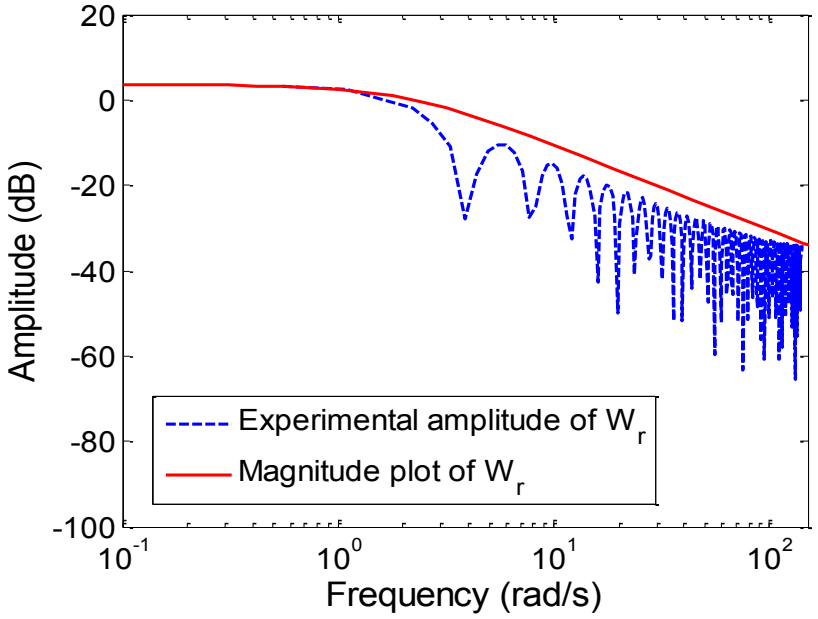

Figure 5.8 Frequency domain properties of the W_r

$$M(s) = \frac{5}{s+5} \tag{5.23}$$

$$W_e(s) = \frac{s+100}{s+3} \tag{5.24}$$

$$W_r(s) = W_d(s) = \frac{1}{s}\frac{0.3}{s+1} \tag{5.25}$$

$$W(s) = 1 \tag{5.26}$$

$$P_{fb}(s) := \left[\begin{array}{c|cc} A & B_1 & B_2 \\ \hline C_1 & D_{11} & D_{12} \\ C_2 & D_{21} & D_{22} \end{array}\right] \tag{5.27}$$

Using the γ-iteration H_∞ optimal control synthesis function 'hinfopt' [122] to calculate the optimal controller results in an 11^{th} order controller $C_0(s)$ .The numerical realization of the controller of Eq. (5.28) (found in Appendix D) satisfies the inequality (5.29). Therefore, robust performance is guaranteed. For the specific model uncertainty shown in Figure 3.11, the requirement for the robust stability in inequality (5.30) is satisfied.

$$C_0(s) := \left[\begin{array}{c|c} A_{C_0} & B_{C_0} \\ \hline C_{C_0} & D_{C_0} \end{array}\right] \tag{5.28}$$

$$\|H\|_\infty = \|H_o\|_\infty < \gamma_h = 0.715 \tag{5.29}$$

$$\Delta_m < \gamma_h \tag{5.30}$$

5.4.2 Simulation results

Frequency domain plots for the sensitivity transfer functions are shown in Figure 5.9. The figure shows the transfer function from the ground profile to the error (which includes the effect by reference and two disturbances), and the magnitude of the function is above 0dB beyond 0.175 Hz. This indicates the feedback control is effective within the frequency range of 0~0.175 Hz.

The system is stable but the feedback controller cannot maintain the desired HHC performance since the bandwidth is very low. With a test ground profile, the time domain HHC response is shown in Figure 5.10 when driving the combine at a speed of 3mph. The controlled system can maintain good HHC performance when the ground profile changes slowly; however, when there are more abrupt ground height changes, the header height has significant vibration and induces considerable header height. Even in some serious conditions, the header hits on the ground.

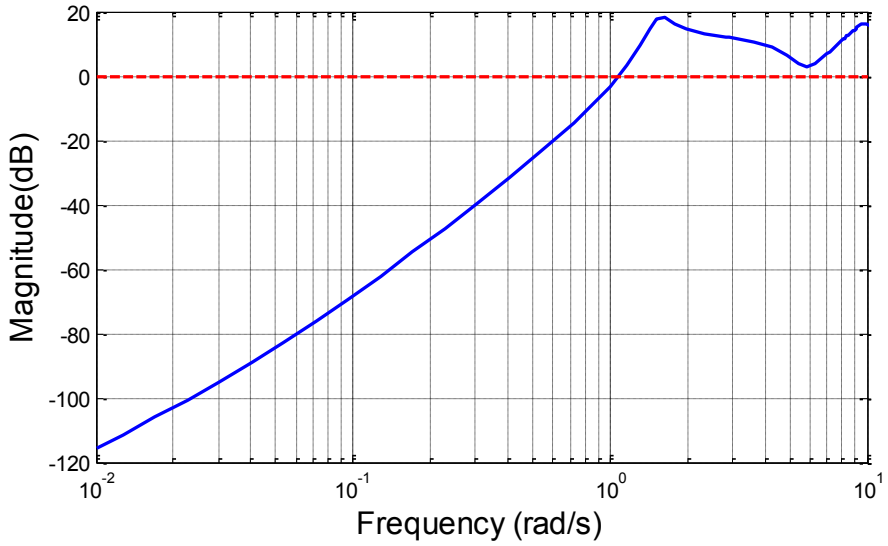

Figure 5.9 Magnitude plots from the ground profile to error with feedback compensator

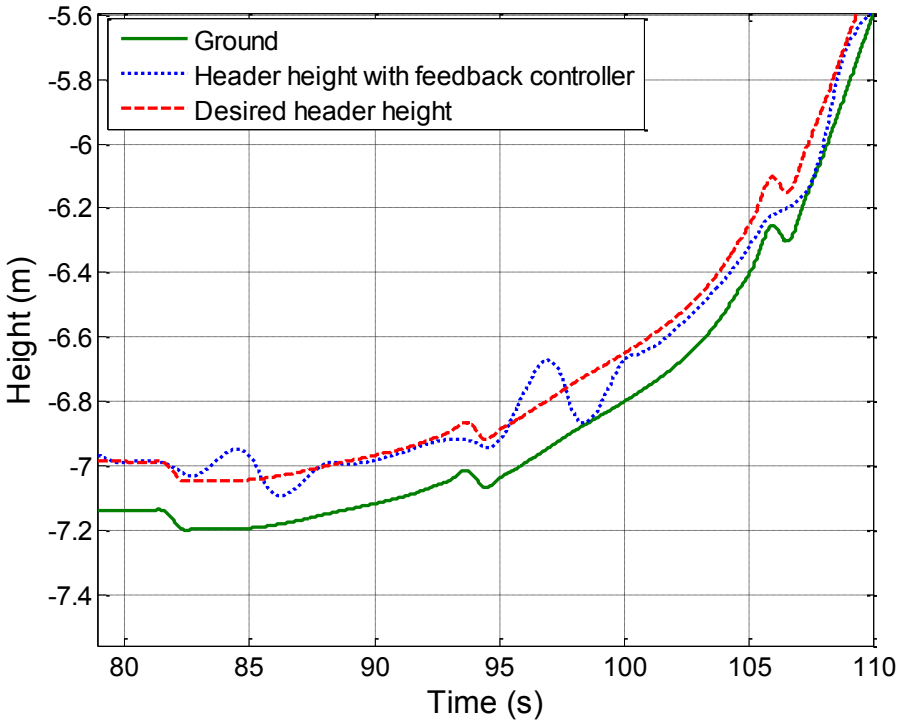

Figure 5.10 Simulation for closed loop HHC control performance

5.4.3 Experimental results

Several tests were performed in August 2012 at the John Deere proving grounds. For the purpose of this paper, two representative test samples were utilized. One test ground was built up by steel ramps, as shown in Figure 3.17. Another was a sandlot test to approximate the natural ground conditions in corn fields, as shown in Figure 5.12. The ground topologies in both cases have a large elevation change within a short distance: 0.18m height change over 1.22m longitudinal distance for the ramp test, and maximum terrain height changes of 0.5m within a longitudinal distance of 5m in the sandlot test. This worst-case terrain disturbance is complemented by other, smaller disturbances in the sandlot test. The test field terrain was chosen to serve as a severe case study for these experiments based on manufacturer experience.

Due to the severe ground profile condition, the maximum speed was limited to 1mph in the ramp test and 0.4mph in the sandlot test with the H_∞ feedback control to avoid equipment damage. The corresponding HHC performance is shown in Figures 5.13 and 5.14, which provide desired and measured header height as a function of longitudinal position.

In both tests, the system was stable all the time, which proves the robustness of the controller. However, due to the slow response speed of the closed loop system, the performance was not as desired. For the ramp test, the most severe situation occurred when the combine drove down from the ramp. The header failed to respond to the induced dramatic header height change and hit on the ground. For the sandlot test, when it was between approximately $25\text{m}<x<35\text{m}$, the feedback HHC could not handle the rapidly changing terrain and the header actually impacts the ground at $x \simeq 34\text{m}$. The results clearly show the limitations discussed in Chapter 3. Although the optimal control input was pursued during

the controller design, the effect of the mechanical limitation and delay prohibited the closed loop system from achieving fast ground profile tracking and ground disturbance rejection.

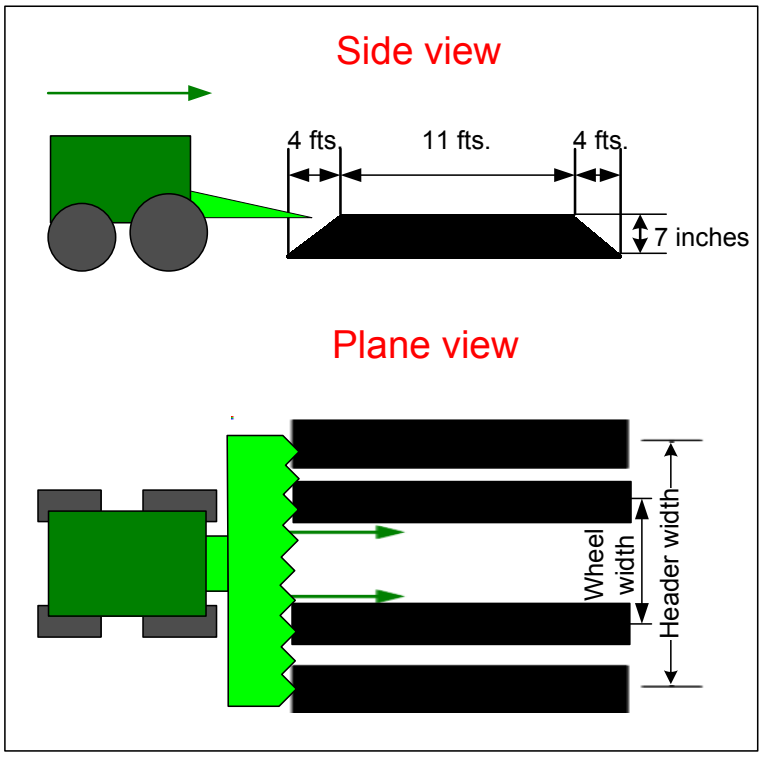

Figure 5.11 Steel ramp ground test

Figure 5.12 Steel ramp ground test

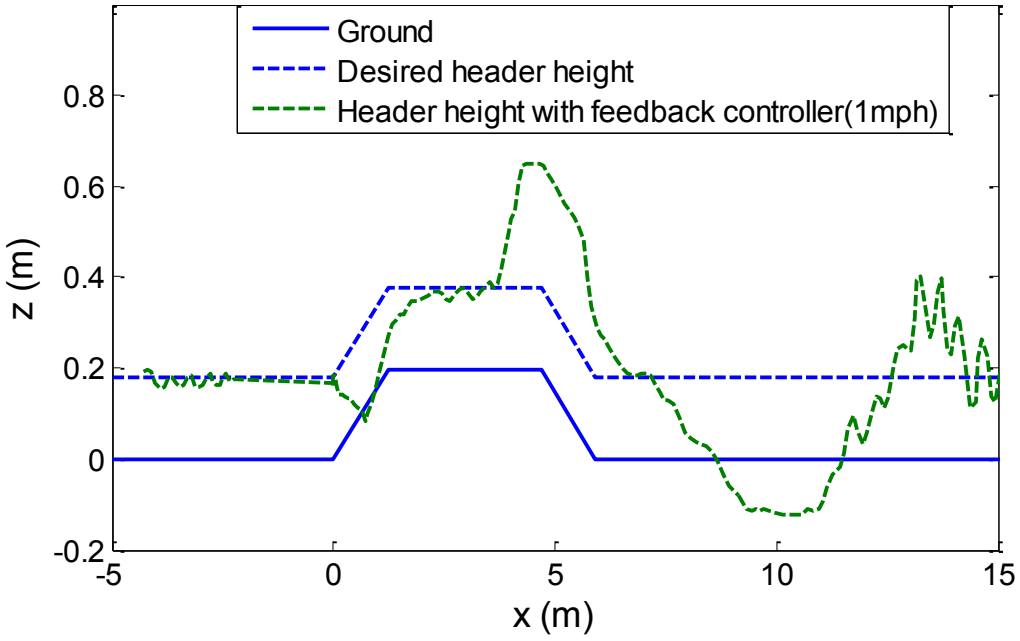

Figure 5.13 HHC performance in the ramp test

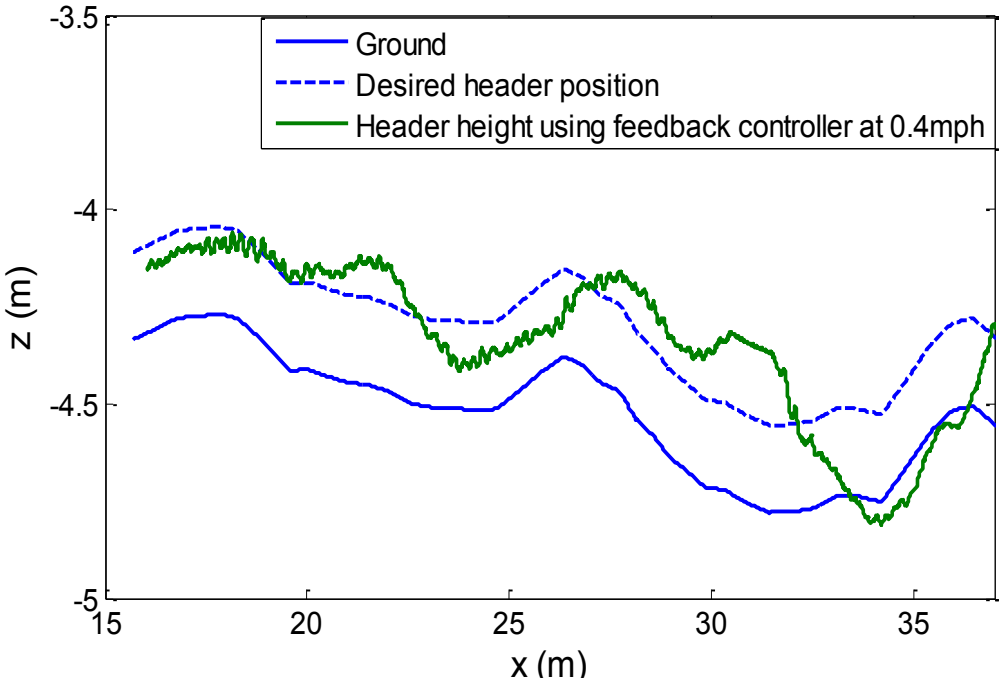

Figure 5.14 HHC performance in the sandlot test

5.5 Conclusion

In this chapter, a method to design an H_∞ robust controller for a time-delayed system is proposed. The design uses mixed sensitivity functions as the design objective; therefore, robust stability, performance, and input gain constraints are all considered in the design procedure. The error signal in the objective function is modified to be the error between a desired output using the reference model and the real output. With use of the Smith predictor, such modification will allow the sensitivity functions to be divided into the delay term and the delay-free part. This helps to eliminate the delay from the H_∞ norm without compromising the performance requirements. As a result, a rational LMI synthesis method can be used to obtain the feedback controller.

As stated at the beginning of this chapter, this feedback controller does not aim to break the limitation imposed by the mechanical system dynamics and delay, but to seek the best balance among performance constraints within the limitations. The estimation of the bandwidth upper bound is given in Section 5.4.1 as 0.25Hz when both of the limitations exist. The design results in a closed loop bandwidth in simulation of 0.178Hz. This is below the upper bound but provides a sufficiently robust stability margin.

Both the simulation and experiment prove the robust stability of the controller although the performance is not exactly desirable under severe ground conditions. In Chapter 6, a feedforward controller will be introduced as a tool to provide better performance by breaking the bandwidth limitation seen in this chapter.

Chapter 6
Feedforward Control with Both Model and Signal Uncertainties

Feedforward control is to compensate for exogenous signals, such as references or disturbances, to achieve better performance. Generally, it is added to a stable, closed-loop system, forming a two DOF control system. The feedback control loop ensures robust stability and performance, as discussed in Chapter 5. However, since feedback control can react only to the output that the system has generated, it lacks the ability to send control signals proactively. As a result, feedback-controlled systems usually cannot respond to exogenous signals instantly, and they cannot compensate for the effect caused by the loop delay mentioned in Section 5.1.

In Chapter 5, a robust feedback controller was designed to achieve balanced consideration of robust stability, performance, and input sensitivity function constraints. Although it has been said to be effective for an uncertain system, it is not sufficient to achieve satisfactory performance. The limitation of the actuator delay in the HHC system and some undesirable features of the mechanical system impose a bandwidth limitation at 0.25Hz, which prevents the HHC from being effective and productive.

Therefore, in this Chapter, a feedforward method, which utilizes the pre-measured information of the exogenous signals, is proposed to compensate for the delay. As described in Chapter 2, the delay effect theoretically can be eliminated by feedforward control under the assumptions of an accurate system model and accurate signal information. However, in reality, such assumptions cannot be satisfied for most physical systems. Thus, feedforward control cannot compensate for the exact exogenous signal or predict the exact response of the system to exogenous signals.

Although it is difficult to achieve ideal output because of the model uncertainty and signal uncertainty, work can be done to determine the optimal balance between good performance with robustness to such uncertainties, which will be the focus of this chapter.

6.1 Two DOF Control Revisited

6.1.1 Two DOF controller structure

Two DOF controllers have various architectures, but they can be transformed mathematically to demonstrate basic equivalence among the various forms, which has been discussed in detail in Section 2.1.3. Figure 6.1 shows the structure of the canonical, two DOF problem. This architecture has been used extensively in many research studies [22, 26, 28]. $G_p(s)$ is the plant model with multiplicative uncertainty, d is the disturbance that generates d_o at the output, $G_d(s)$ is the corresponding disturbance dynamics model, and Δ_d is the uncertainty of the model. The feedforward controller uses the measured reference $\tilde{r}$ and disturbance $\tilde{d}$ to generate a feedforward input.

The plant $G_p(s)$ is assumed to be a minimum phase system; therefore, the feedforward controller can be constructed via a plant inversion approach utilizing pre-filters $Q_1(s)$ and $Q_2(s)$. Note that a similar construction can be used for non-minimum phase systems with minor modifications to the model-inversion process. Popular examples for non-minimum phase systems are the zero phase error tracking control (ZPETC) in [40] and the non-linear model inversion approach in [123]. For the HHC system studied in this dissertation, the plant model includes a time-delay term caused by the actuator delay, and it can be expressed in Eq. (6.1). Therefore, the plant inversion, $G_p^{-1}(s)$, in the feedforward channel contains the non-casual term, e^{sT}. This means that the exogenous signals r, d must be known in advance or measured earlier to enable such preview control.

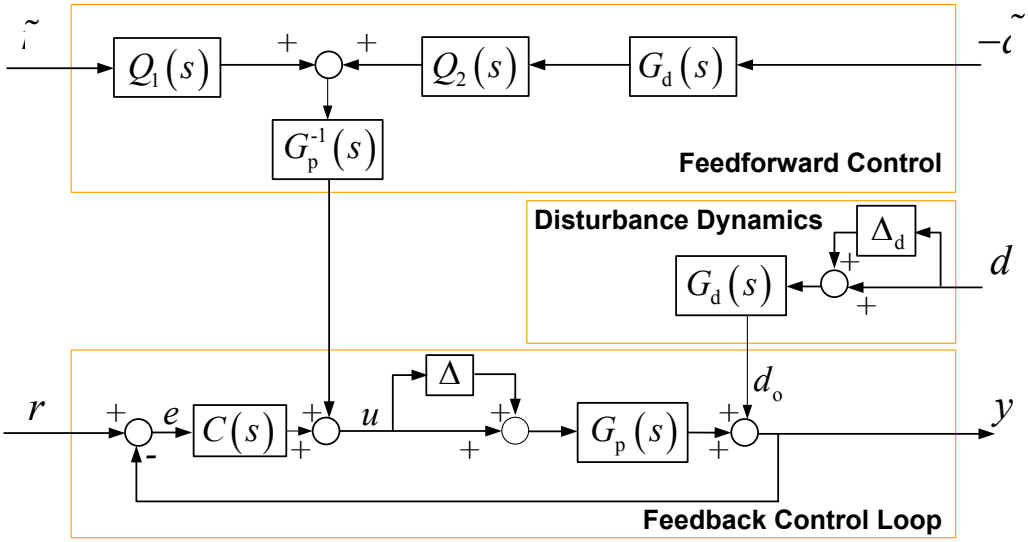

Figure 6.1 Architecture of a two DOF controller

$$G_p(s) = G_{p\_r}(s)e^{-sT} \tag{6.1}$$

When there is neither system uncertainty nor measurement uncertainty, i.e., $\Delta = 0$, $\Delta_d = 0$, $r = \tilde{\imath}$, and $d = \tilde{c}$, it results in a nominal system. In this case, as shown in Section

2.4, the pre-filters in the feedforward controller can be chosen as 1 to achieve perfect nominal performance, i.e., $y = r$. The bandwidth limit on the feedback control performance is removed by introducing the feedforward controller.

In practical applications, the idealized properties above usually cannot be satisfied. Inevitable uncertainties that are present in the plant model will cause a bandwidth limitation for both the feedback and feedforward control, as detailed in Sections 2.3.3 and 2.4.2. At the same time, the feedforward control performance is deteriorated by the uncertainty of signal measurement. In this case, the filters $Q_1(s)$ and $Q_2(s)$ are necessary to mitigate the deterioration of the feedforward performance induced by measurement uncertainty [28].

6.1.2 Literature review of two DOF design methods

In this dissertation, we focus on using the feedforward approach that addresses the pre-known or pre-measured exogenous signals. The approach usually utilizes a model inversion, as shown in Figure 6.1, to generate an additional input, which is injected into the existing feedback loop to compensate for the exogenous signals [124, 125]. In Chapter 2, the variations and equivalence of such two DOF controller structures are addressed in Section 2.1.3.

When the system has neither model uncertainty nor signal measurement uncertainty, the feedforward controller can provide perfect tracking performance without any bandwidth limitation. However, uncertainties are natural occurrences in most control problems and will affect the performance of a given feedforward approach. As stated, the uncertainties fall into two categories, i.e., model uncertainties and signal uncertainties. In Sections 2.4.2 and 2.4.3, the influences of both are studied, respectively. When there are mismatches between the true

plant dynamics $\bar{G}_p$ and G_p or between the true signals $\bar{r}$, $\bar{d}$, and r, d, the compensating input u_1 by the feedforward controller can deviate from its expected value, which results in additional error in the output.

Most of the previous excellent work in the field has focused on the design of feedforward controllers with model uncertainties, as discussed in the following. The conditions required for system model uncertainties for the model inversion feedforward approaches are discussed in [49]. The influences of various model uncertainties on the error signal are shown in [50]. Also, a framework for two DOF controller design using robust control synthesis to improve reference tracking, based on accommodating model frequency domain model uncertainties, was given in [26]. Additional efforts to improve the performance of feedforward control under model uncertainty can be found in [28, 51, 52].

While there have been significant efforts to understand the effects of model uncertainty, the effects of measurement uncertainty have received less research attention for the design of feedforward controllers. This may be due to the fact that the feedforward terms are assumed to be generated by reference commands and not by measureable exogenous signals, with their associated uncertainties. However, in many systems, uncertain measurements can occur due to, e.g., sensor calibrations, sensor bandwidth limitations, sensor saturations, and noise. For example, in the HHC problem, the ground profile works both as the reference for the header to follow and the disturbances to impact the vehicle's dynamics. However, the current digital elevation model (DEM) measurement tools, whether GPS or laser radar (LIDAR), can only provide a rough estimation of the shape of the ground.

Signal uncertainty is inevitable for the HHC system, which motivates the work in this chapter.

The feedforward control error introduced by both model uncertainty and measurement uncertainty is studied in the following sections. The analysis reveals a conflicting relationship between feedforward performance in the ideal case and errors introduced when measurement uncertainties are considered. The measurement uncertainty is characterized in the frequency domain, and an H_∞ control problem is constructed to balance the trade-off between nominal performance and sensitivity to uncertainty. Using some synthesis techniques that will be presented in Section 6.2.4, an optimal feedforward controller is obtained, which results in the highest achievable bandwidth in the presence of combined model and measurement uncertainties.

6.2 Feedforward Filter Design

6.2.1 Formulation of a robust two DOF control system

To better examine the influence of signal measurement uncertainties, the system in Figure 6.1 is reconstructed as Figure 6.2. Here, the measurement uncertainties for the reference and disturbance are expressed as Eqs. (6.2) - (6.5). The exogenous signals are reformulated as normalized signals as $\begin{pmatrix} r_n & d_n & \Delta r_n & \Delta d_n \end{pmatrix}^T$ to simplify the later analysis. The weighting functions, $W_r(s), W_d(s), W_{\Delta r}(s)$,and $W_{\Delta d}(s)$, describe the respective frequency content of these signals. The model uncertainties Δ and Δ_d are weighted by $W(s)$ and $W_d(s)$, respectively, to specify the upper bound of the frequency representation of Δ

and Δ_d. $W_e(s)$ is the weighting function for the error signal. All weights can be constant or dynamic functions of frequency.

$$\Delta r_n W_{\Delta r}(s) = \tilde{r} \tag{6.2}$$

$$\Delta d_n W_{\Delta d}(s) = \tilde{d} \tag{6.3}$$

$$r_n W_r(s) = r \tag{6.4}$$

$$d_n W_d(s) = d \tag{6.5}$$

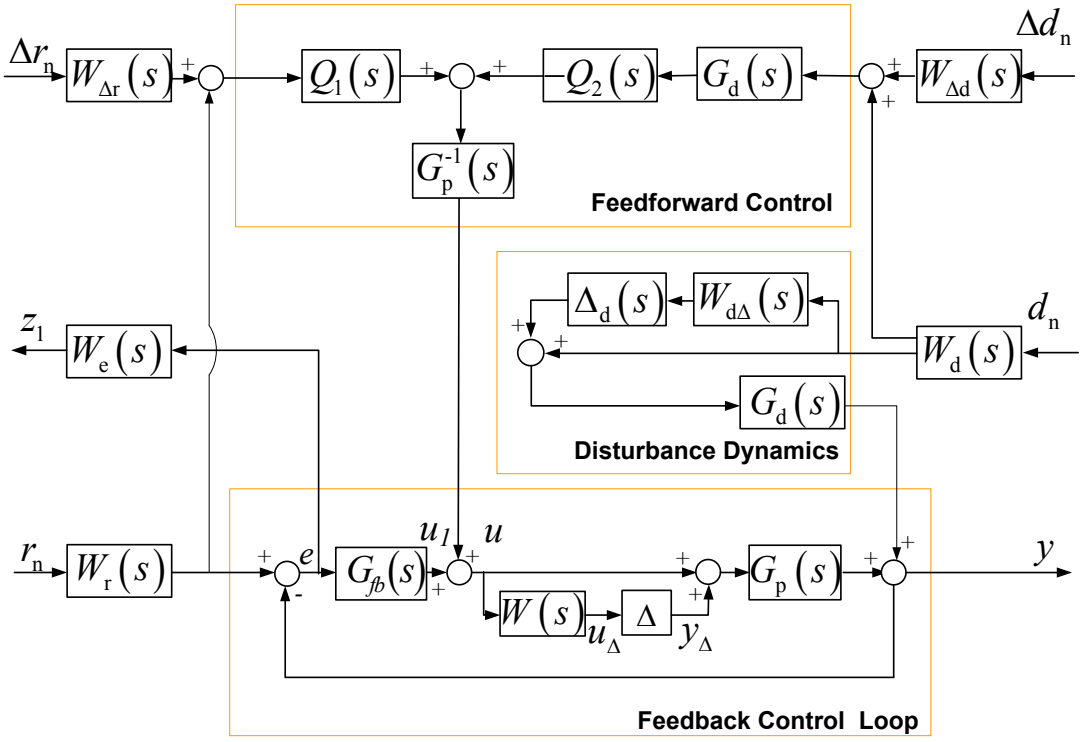

Figure 6.2 Schematic of two DOF control system for robust control design

Compared to the system schematic for the robust feedback controller design in Figure 5.4, the system in Figure 6.2 does not change the feedback loop. Therefore, as long as the feedforward channels themselves are stable, the robust stability guaranteed by the robust feedback controller design in Chapter 5 will not be influenced. Therefore, in the following

analysis, the feedback controller $G_{fb}(s)$ in Chapter 5 is used. The measurements of reference r and disturbance d are used to feed into the feedforward channels and generate the compensating control signal u_1. The signal uncertainties, denoted as Δr_n and Δd_n, are introduced into the feedforward channel, thereby impacting its output.

With such setup, the objective of the feedforward controller design can be specified to be minimizing some objective sensitivity function from $\begin{pmatrix} r_n & d_n & \Delta r_n & \Delta d_n \end{pmatrix}^T$ to the tracking error, e. For the HHC control problem, the feedforward design problem is formulized as Eq. (6.6), where the objective function is chosen as the corresponding H_∞ norm of the sensitivity functions defined in Eq. (6.7). The reference, disturbances, and their uncertainties here are assumed to be signals that are independent of each another. This is a conservative assumption, and correlated signals would still be handled by the analysis presented here.

$$\left(Q_1^*, Q_2^*\right) = \min_{Q_1, Q_2} \left\| \begin{matrix} H_{f1} \\ H_{f2} \\ H_{f3} \\ H_{f4} \end{matrix} \right\|_\infty \tag{6.6}$$

$$e = H_{f1} r_n + H_{f2} d_n + H_{f3} \Delta r_n + H_{f4} \Delta d_n \tag{6.7}$$

6.2.2 Error analysis

The first step to solve the feedforward design problem is to determine the sensitivity functions in Eq. (6.6). With the configuration shown in Figure 6.2, the combined influence of both the model and measurement uncertainties on the error is expressed as Eq. (6.8), where

$S_{fb}(s)$ is the sensitivity function of the feedback loop, and x_{filter} is a signal that is a combination of filtered exogenous signals as expressed in Eq. (6.9).

By observation, the feedback controller $C(s)$ is included only in the sensitivity function $S_{fb}(s)$, while the feedforward filters, $Q_1(s)$ and $Q_2(s)$, show up only in x_{filter} with the filtering transfer function defined in Eqs. (6.10) - (6.13). Therefore, $S_{fb}(s)$ works mathematically as the same weight function in every term of the objective function in Eq. (6.6), which indicates that the design of the feedback loop will not influence the optimal solution for the feedforward control problem established in Section 6.2.1 and can be separated from the feedforward controller design in this chapter. Therefore, the design problem in Eq. (6.6) is changed equivalently to Eq. (6.14).

$$e = S_{fb}(s)\, x_{filter} \tag{6.8}$$

$$x_{filter} = \bar{H}_{f1} r_n + \bar{H}_{f2} d_n + \bar{H}_{f3} \Delta r_n + \bar{H}_{f4} \Delta d_n \tag{6.9}$$

$$\bar{H}_{f1} = W_r(s)\left(1 - \left(1 + W(s)\Delta\right) Q_1(s)\right) \tag{6.10}$$

$$\bar{H}_{f2} = -W_{\Delta d}(s) G_d(s)\left(1 + W(s)\Delta\right) Q_2(s) \tag{6.11}$$

$$\bar{H}_{f3} = -W_{\Delta r}(s)\left(1 + W(s)\Delta\right) Q_1(s) \tag{6.12}$$

$$\bar{H}_{f4} = W_d(s) G_d(s)\left(1 + W_{d\Delta}(s)\Delta_d\right)\left(1 - \left(1 + W(s)\Delta\right) Q_2(s)\right) \tag{6.13}$$

$$\left(Q_1^*, Q_2^*\right) = \min_{Q_1, Q_2} \left\| \begin{matrix} \bar{H}_{f1} \\ \bar{H}_{f2} \\ \bar{H}_{f3} \\ \bar{H}_{f4} \end{matrix} \right\|_\infty \tag{6.14}$$

6.2.3 Feedforward robust performance

With further observation of the filtering transfer functions in Eqs. (6.10) - (6.13), the feedforward filter $Q_1(s)$ only occurs in $\bar{H}_{f1}$ and $\bar{H}_{f3}$, and $Q_2(s)$ occurs only in $\bar{H}_{f2}$ and $\bar{H}_{f3}$. An examination of Figure 6.2 shows that the feedforward paths of $Q_1(s)$ and $Q_2(s)$ are not coupled, so the two filters can be designed separately. Then, the optimization problem becomes a minimization of the H_∞ norms, defined in Eq. (6.15) and Eq. (6.16).

To examine the worst-case scenario, the model uncertainties Δ and Δ_d are replaced by $\bar{\Delta}$ and $\bar{\Delta}_d$, which are the upper bounds of the frequency domains on the plant and the disturbance model uncertainty, respectively. Notice $G_d(s)$ works as the same weight factor in $\bar{H}_{f2}$ and $\bar{H}_{f4}$, it can be ignored in controller optimization algorithms. As a result, the optimization problem for the design of feedforward filters finally is defined as Eq. (6.17) and (6.18).

$$Q_1^* = \min_{Q_1} \left\| \begin{matrix} \bar{H}_{f1} \\ \bar{H}_{f3} \end{matrix} \right\|_\infty \tag{6.15}$$

$$Q_2^* = \min_{Q2} \left\| \begin{matrix} \bar{H}_{f2} \\ \bar{H}_{f4} \end{matrix} \right\|_\infty \tag{6.16}$$

$$Q_1^* = \min_{Q_1} \left\| \begin{matrix} W_r(s)\left(1-\left(1+W(s)\bar{\Delta}\right)Q_1(s)\right) \\ W_{\Delta r}(s)\left(1+W(s)\bar{\Delta}\right)Q_1(s) \end{matrix} \right\|_\infty \tag{6.17}$$

$$Q_2^* = \min_{Q2} \left\| \begin{matrix} W_{\Delta d}(s)\left(1+W(s)\bar{\Delta}\right)Q_2(s) \\ W_d(s)\left(1+W_{d\Delta}(s)\bar{\Delta}_d\right)\left(1-\left(1+W(s)\bar{\Delta}\right)Q_2(s)\right) \end{matrix} \right\|_\infty \tag{6.18}$$

In Eq. (6.17), the first row represents the reference tracking performance, and the second row represents the robustness to the reference signal uncertainty. Similarly, in Eq. (6.18), the first row represents the disturbance rejection performance, and the second row represents the robustness to the disturbance signal uncertainty.

By inspection, there is a trade-off when designing the feedforward filter $Q_1(s)$: a small $Q_1(s)$ can decrease the error induced by Δr_n but will increase the error induced by r_n. In other words, the design of $Q_1(s)$ must determine the balance between the reference tracking performance and the robustness to reference signal uncertainty. Similarly, the design of $Q_2(s)$ must consider the trade-off between the disturbance rejection performance and the robustness to disturbance signal uncertainty. Analogous to feedback control, the balance between performance and robustness needs to be found by optimal design of feedforward control.

6.2.4 Optimization synthesis

In this subsection, a method to solve the optimization problem in Eq. (6.17) and Eq. (6.18) is introduced to obtain optimal feedforward filters, $Q_1^*(s)$ and $Q_2^*(s)$. Note that the first row of Eq. (6.17) contains the term $\left(1+W(s)\bar{\Delta}\right)Q_1(s)$ and the second row contains the term $1-\left(1+W(s)\bar{\Delta}\right)Q_1(s)$. These fit the relationship of the complementary sensitivity function and sensitivity function, respectively, for a unity feedback system. Therefore, an auxiliary feedback system is constructed as shown in Figure 6.3 to reconstruct this optimization problem. The transfer function $G_{a\_Q1}(s)$ is a design degree of freedom

available to the control designer. $W_r(s)$ and $W_{\Delta r}(s)$ are chosen to be the weight functions to construct the performance signals z_{a1_Q1} and z_{a2_Q1}, which makes the weighted sensitivity functions of the auxiliary system have the identical form as Eq. (6.17).

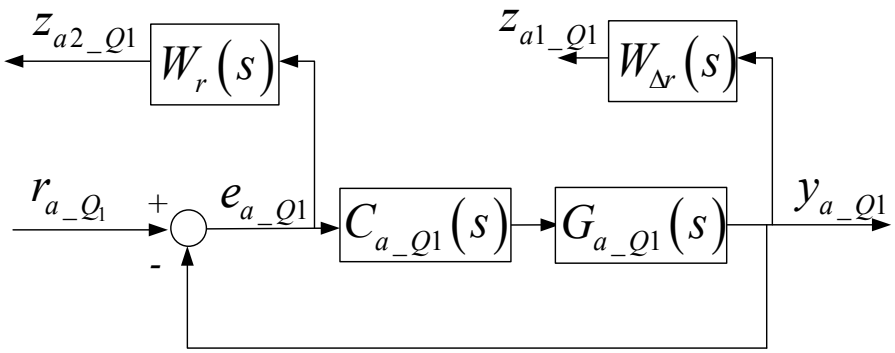

Figure 6.3 Auxiliary system for calculating Q_1

The complementary sensitivity function $T_{G_{a\_Q1},C_{a\_Q1}}$ of the auxiliary system is defined as Eq. (6.19). Since $\left(1+W(s)\bar{\Delta}\right)$ is a pre-defined transfer function, $Q_1(s)$ has a unique and well-defined relationship with $T_{G_{a\_Q1},C_{a\_Q1}}$, as shown in Eq. (6.20). Replacing the term $\left(1+W(s)\bar{\Delta}\right)$ in Eq. (6.17) with $T_{G_{a\_Q1},C_{a\_Q1}}$ and the term $1-\left(1+W(s)\bar{\Delta}\right)Q_1(s)$ with $S_{G_{a\_Q1},C_{a\_Q1}}$, the optimization problem in Eq. (6.17) can be rewritten as Eq. (6.21), which is equivalent to a weighted, mixed-sensitivity problem for feedback controller design of the auxiliary system. As one can see the choice for the design function $G_{a\_Q1}(s)$ determines the order of the optimal controller $C_{a\_Q1}^{*}(s)$ in the auxiliary system; therefore, it also influences the order of $Q_1^{*}(s)$ by the relationship in Eq. (6.20). The frequency property of $G_{a\_Q1}(s)$ does not matter too much because it can always be compensated in the optimization process

for $C_{a\_Q1}{}^{*}(s)$. For simplicity of the design result, it is generally chosen as a low-order low pass filter to reduce the order of $Q_1^*(s)$.

The solution of $C_{a\_Q1}{}^{*}(s)$ for the mixed sensitivity problem can be obtained by standard H_∞ control synthesis tools [30] and solved with LMI. With the relationship between $Q_1(s)$ and $T_{G_{a\_Q_1},C_{a\_Q_1}}$, the optimal $Q_1^*(s)$ can be calculated using Eq. (6.22).

$$T_{G_{a\_Q_1},C_{a\_Q_1}} = \left(1+W(s)\bar{\Delta}\right)Q_1(s) \tag{6.19}$$

$$Q_1(s) = \frac{T_{G_{a\_Q_1},C_{a\_Q_1}}}{\left(1+W(s)\bar{\Delta}\right)} \tag{6.20}$$

$$C_{a\_Q1}^{*}(s) = \min_{C_{a\_Q1}(s)} \left\| \begin{matrix} W_{\Delta r}(s)T_{G_{a\_Q_1},C_{a\_Q_1}}(s) \\ W_r(s)S_{G_{a\_Q_1},C_{a\_Q_1}}(s) \end{matrix} \right\|_\infty \tag{6.21}$$

$$Q_1^*(s) = \frac{T_{G_{a\_Q_1},C_{a}^{*}\_Q_1}}{\left(1+W(s)\bar{\Delta}\right)} \tag{6.22}$$

The procedure for calculating $Q_2^*(s)$ is analogous to $Q_1^*(s)$ by replacing $W_{\Delta r}$ with $W_{\Delta d}$ and W_r with $W_d(s)\left(1+W_{\Delta d}(s)\bar{\Delta}_d\right)$, respectively. Therefore, the auxiliary system for calculating $Q_2^*(s)$ is constructed as Figure 6.4.

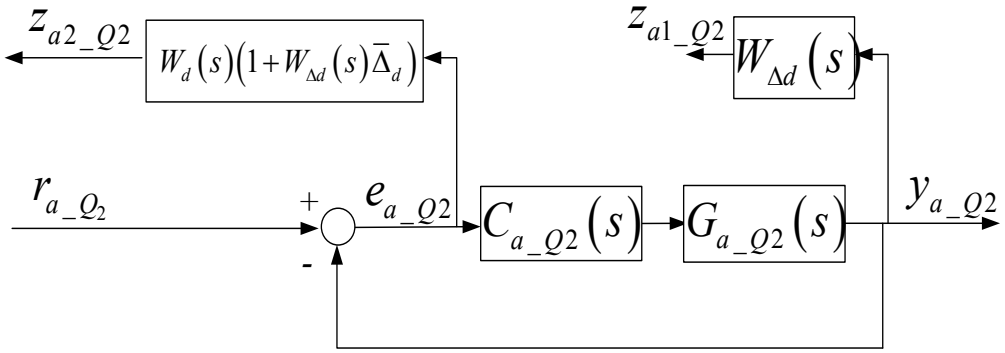

Figure 6.4 Auxiliary system for calculating Q_2

The complementary sensitivity function $T_{G_{a\_Q2},C_{a\_Q2}}$ of the auxiliary system is defined as Eq. (6.23), and has a relationship with $Q_2(s)$ as shown in Eq. (6.24). Replacing the term $\left(1+W(s)\bar{\Delta}\right)$ in Eq. (6.18) with $T_{G_{a\_Q2},C_{a\_Q2}}$ and the term $1-\left(1+W(s)\bar{\Delta}\right)Q_2(s)$ with $S_{G_{a\_Q2},C_{a\_Q2}}$, the optimization problem in Eq. (6.18) can be rewritten as Eq. (6.25), which is equivalent to a weighted, mixed-sensitivity problem for feedback controller design of the auxiliary system. The optimal solution for the feedback controller $C_{a\_Q2}{}^*(s)$ is used to calculate $Q_2^*(s)$ using Eq. (6.26).

$$T_{G_{a\_Q2},C_{a\_Q2}} = \left(1+W(s)\bar{\Delta}\right)Q_2(s) \tag{6.23}$$

$$Q_2(s) = \frac{T_{G_{a\_Q2},C_{a\_Q2}}}{\left(1+W(s)\bar{\Delta}\right)} \tag{6.24}$$

$$C_{a\_Q2}^*(s) = \min_{C_a(s)} \left\| \begin{matrix} W_{\Delta d}(s)T_{G_{a\_Q2},C_{a\_Q2}} \\ W_d(s)\left(1+W_{\Delta d}(s)\bar{\Delta}_d\right)S_{G_{a\_Q2},C_{a\_Q2}} \end{matrix} \right\|_\infty \tag{6.25}$$

$$Q_2^*(s) = \frac{T_{G_{a\_Q2},C_{a\_Q2}^*}}{\left(1+W(s)\bar{\Delta}\right)} \tag{6.26}$$

6.3 A Case Study for Feedforward Controller Design

As the work done in previous chapters, the HHC problem is taken here as an example for applying the feedforward controller design method introduced above. The feedforward controller is added to the existing feedback control loop in Chapter 5. Therefore, all the numerical simulation and experiments in this Section maintain continuity with the work in Section 5.4.

6.3.1 Feedforward filter design for the HHC problem

To specify the design of the feedforward filters for the HHC problem, the physical system is briefly reviewed below. The plant is the mechanical system of the combine-header system with the control input as the cylinder velocity of the hydraulic actuator installed between the two rigid bodies. The system output is the absolute header height. Previous analysis in Section 3.2.3 illustrated that the limitation imposed by the plant dynamics is 1.5 Hz. The hydraulic actuator has a delay that has been estimated for a particular class of production HHC systems to be approximately 0.3 seconds [95]. The delay induces a feedback control bandwidth limitation of $\omega_d = 0.52\ Hz\ \left(3.3\ \text{rad/s}\right)$ as analyzed in Section 3.3.3. The combined effect of the plant dynamics plus delay limits the achievable bandwidth of any feedback control to be only approximately 0.25 Hz, as detailed in Section 3.3.4. Therefore, a feedforward controller is necessary to improve the overall performance, as described in [126].

The plant transfer function $G_{p\_r}(s)$ from hydraulic cylinder velocity to header height, obtained from modeling in chapter 3, is shown in Eq. (6.27). Similarly, the transfer functions from the two disturbances at the front and rear tires to the header height are shown as $G_{df}(s)$

and $G_{dr}(s)$ in Eq. (6.28) and Eq. (6.29). To show their frequency properties, the Bode plots for the three transfer functions are shown in Figures 6.5 - 6.7.

$$G_{p\_r}(s) = \frac{4.8226s^4 + 22.984s^3 + 1371.0s^2 + 3137.1s + 93548.0}{s(s^4 + 4.0927s^3 + 235.89s^2 + 403.23s + 11956.0)} \tag{6.27}$$

$$G_{df}(s) = \frac{2.8129s^3 + 218.71s^2 + 1051.6s + 31161.0}{s^4 + 4.0927s^3 + 235.89s^2 + 403.23s + 11956.0} \tag{6.28}$$

$$G_{dr}(s) = \frac{-\left(1.7036s^3 + 89.718s^2 + 647.18s + 19194.0\right)}{s^4 + 4.0927s^3 + 235.89s^2 + 403.23s + 11956.0} \tag{6.29}$$

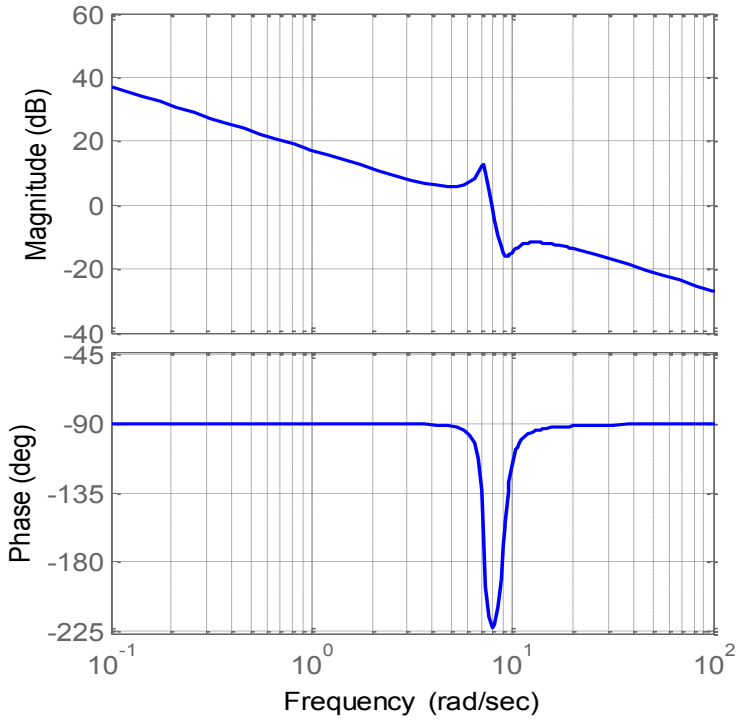

Figure 6.5 Bode Plot of $G_{p\_r}(s)$

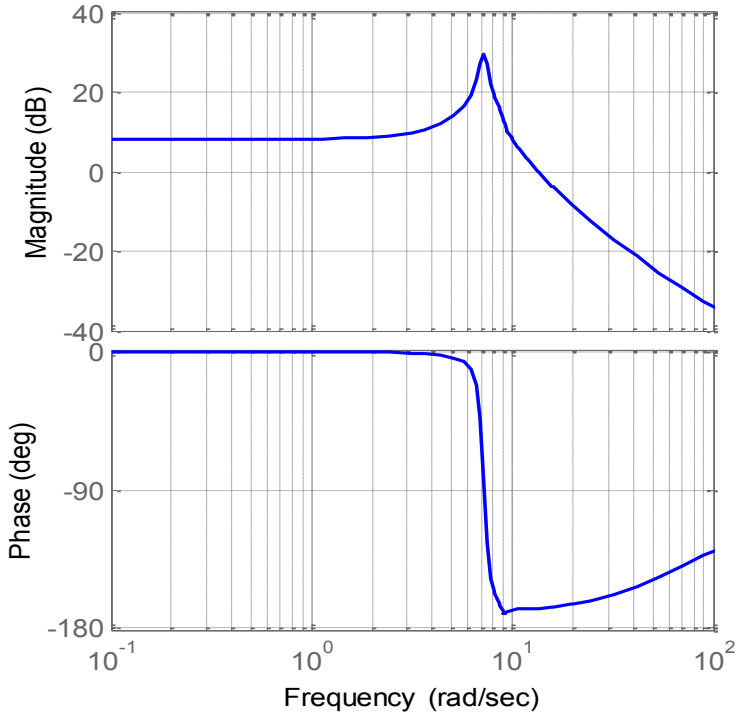

Figure 6.6 Bode Plot of $G_{df}(s)$

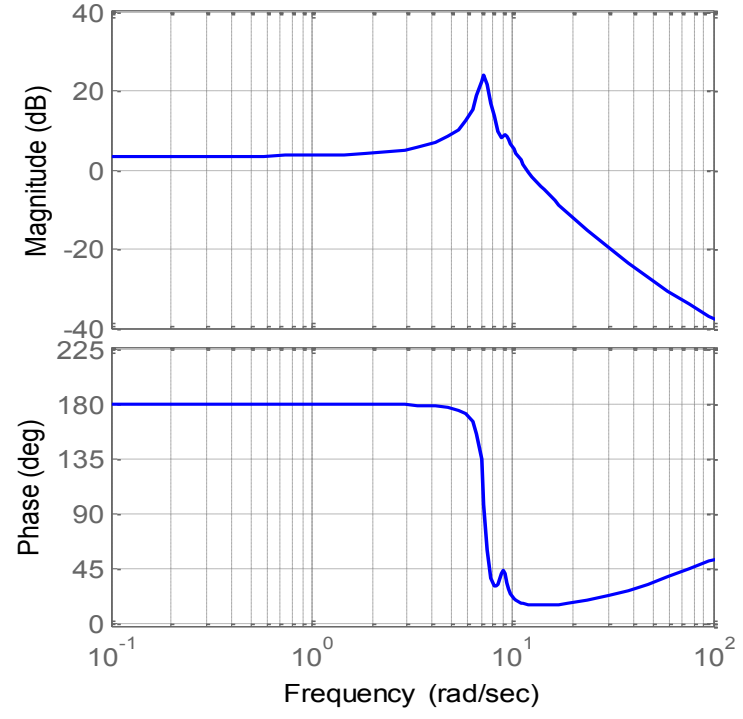

Figure 6.7 Bode Plot of $G_{dr}(s)$

Figure 6.8 shows the structure of two DOF control for the HHC system. While somewhat visually dense, it details the interactions among all the various system signals in graphical form making it useful for system-level understanding. The reference and two disturbances are normalized as r_n, $d_{f,n}, d_{r,n}$ with corresponding measurement uncertainties as Δr_n, $\Delta d_{f,n}, \Delta d_{r,n}$. Their frequency domain properties are described by $W_r(s)$, $W_{\Delta r}(s)$, $W_{df}(s)$, $W_{dr}(s)$, $W_{\Delta df}(s), W_{\Delta dr}(s)$, respectively. The disturbances influence the output of the system through transfer functions $G_{df}(s)$ and $G_{dr}(s)$. These transfer functions introduce two additional plant uncertainties, i.e., Δ_{df}, Δ_{dr}, weighted by $W_{d\Delta f}(s), W_{d\Delta r}(s)$, respectively, in the design. For the HHC system, the feedforward controller must address three exogenous signals: one reference (r_n) and two disturbances ($d_{f,n}$ and $d_{r,n}$). Using a model inversion-based approach, the structure for the feedforward controllers is shown in the feedforward control block in Figure 6.8, where $Q_1(s)$ is the filter designed for reference tracking, and $Q_{2f}(s), Q_{2r}(s)$ are for disturbance rejection.

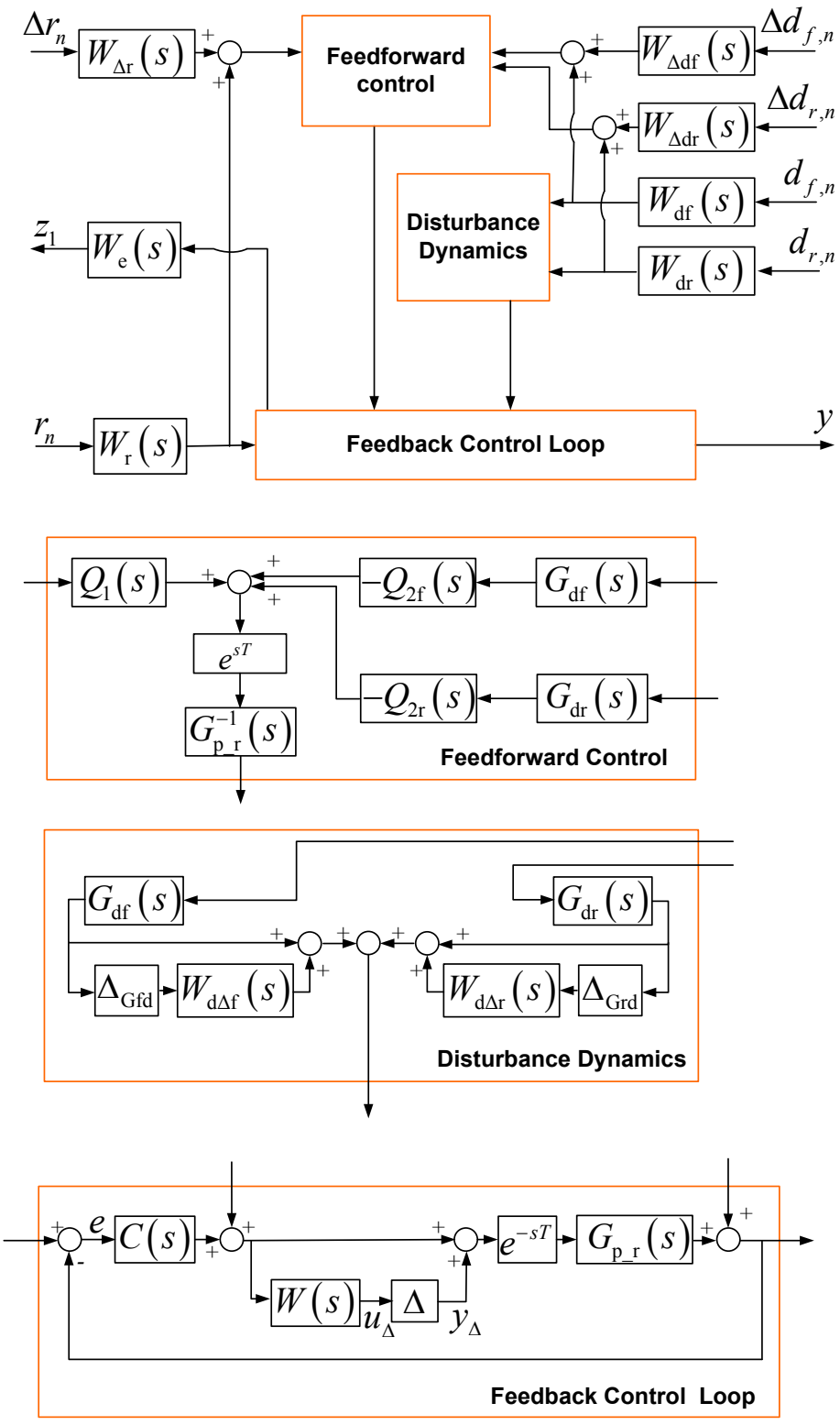

Figure 6.8 Block diagram for two DOF control for the HHC system

6.3.2 Simulation results

In this section, the feedforward controller is designed for a virtual ground profile case to demonstrate its capability in improving the HHC's performance. For the calculation of the feedforward controller $Q_1(s)$, the frequency domain properties of the reference signal and its measurement uncertainty are needed. In the following simulation, we assume the ground profile is a filtered step signal, shown in Eq. (6.30), and the measurement of the ground profile is also a filtered step signal but with an uncertain estimation of the filtered bandwidth, as shown in Figure 6.9. The resulting measurement uncertainty weighting transfer function is given in Eq. (6.31). The corresponding Bode plot is shown in Figure 6.10, from which the specified signal uncertainty has large magnitude in low frequency range.

$$W_r(s) = W_{df}(s) = W_{dr}(s) = \frac{1}{s}\frac{0.3}{s+1} \tag{6.30}$$

$$W_{\Delta r}(s) = W_{\Delta df}(s) = W_{\Delta dr}(s) = \frac{0.3}{s^2+3s+2} \tag{6.31}$$

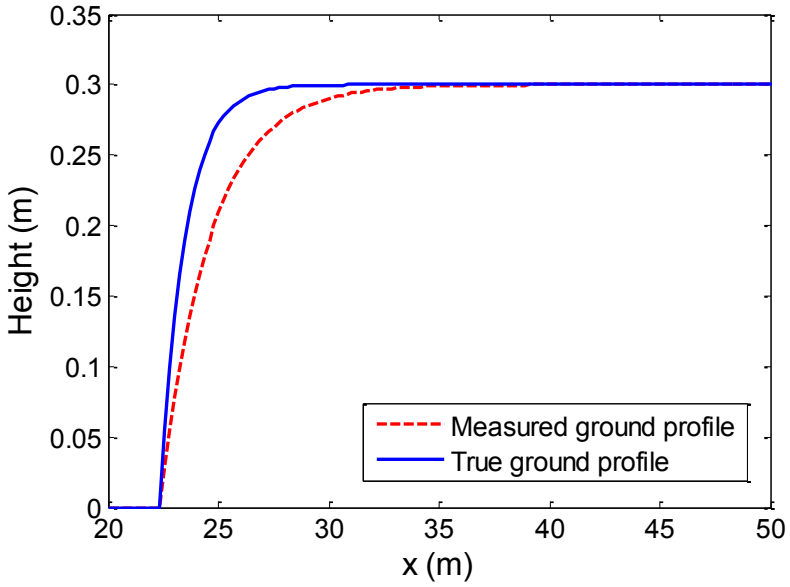

Figure 6.9 Ground profile and its measurement in the simulation case

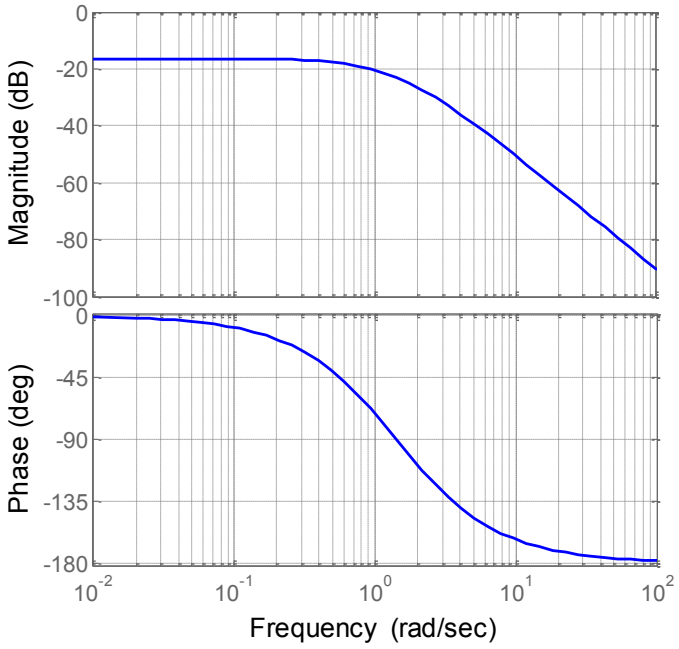

Figure 6.10 Bode plot for the weight function of signal uncertainty

The auxiliary plant $G_a(s)$ is chosen as Eq. (6.32) to give a simple first order transfer function. The upper bound on the multiplicative uncertainties are assumed to be 0.2, i.e., $\|\Delta\|_\infty < 0.2$, $\|\Delta_{Grf}\|_\infty < 0.2$, $\|\Delta_{Gdf}\|_\infty < 0.2$.

$$G_a(s) = \frac{1}{s+1} \tag{6.32}$$

Using the feedforward controller design method introduced in Section 6.2, $Q_1(s)$ is obtained as an 8th order transfer function using function 'hinfopt' in Matlab, which can be reduced to the fourth-order model shown in Eq. (6.33).

$$Q_1(s) = \frac{\left(-2.35\times10^{-4}s^4 + 8.65\times10^{-3}s^3 - 0.17s^2 + 2.224s - 9.233\right)}{s^4 + 10.1s^3 + 67.35s^2 + 132.5s + 73.9} \tag{6.33}$$

The two disturbance channels are assumed to be independent of each other; therefore, the two filters $Q_{2f}(s), Q_{2r}(s)$ can be designed separately. Since the specification for the

weighting functions on model uncertainty and measurement uncertainty are the same for the two disturbance feedforward channels, the two filters are identical, as shown in Eq. (6.34).

$$Q_{2f}(s) = Q_{2r}(s) = \frac{\left(-2.12\times10^{-4}s^4 + 8.05\times10^{-3}s^3 - 0.163s^2 + 2.21s + 10.52\right)}{s^4 + 10.4s^3 + 72.15s^2 + 147.3s + 84.21} \quad (6.34)$$

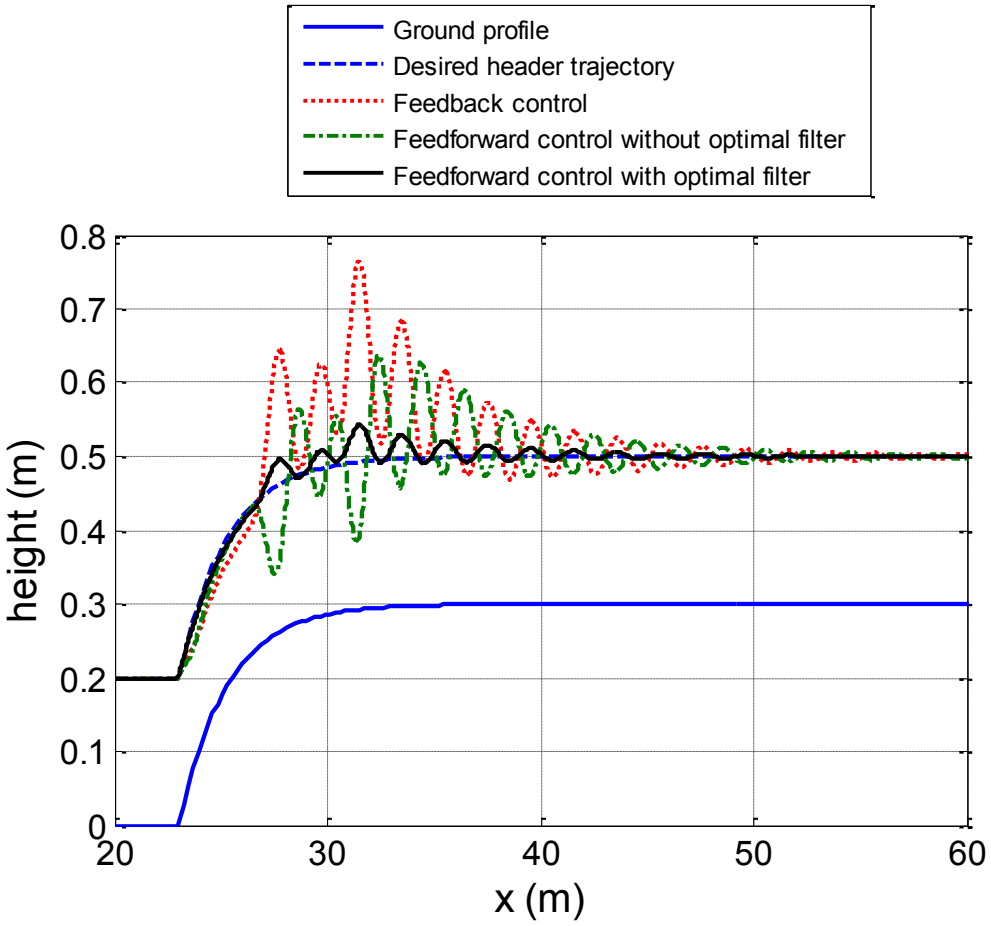

Figure 6.11 Comparison of simulated tracking performances among controllers

The tracking simulation results for the step response are shown in Figure 6.11, where a constant header height is desired over a changing ground profile. For feedback control solely, the header height error is large due to the limited response bandwidth. When the feedforward controller, without the optimal filters, is added, the performance is improved.

However, the improvement is limited since there is considerable measurement uncertainty from the exogenous signals shown in Figure 6.9. When the optimal filters are added into the feedforward channels, the performance is improved significantly by reducing the error caused by the measurement uncertainty.

To analyze the performance of the designed controllers in the frequency domain, the computed magnitudes of the sensitivity functions from $r, \Delta r, d_f, \Delta d_f, d_r$, and Δd_r to the error e are shown in Figures 6.12 - 6.14. The results show that feedforward controllers achieve the purpose of decreasing the error generated from both the reference and the disturbances within the frequency range of interest ($\omega < 1 rad/s$). The comparison between the feedforward controls with and without filters demonstrates that $Q_1(s), Q_{2f}(s)$, and $Q_{2r}(s)$ decrease the error caused by the measurement uncertainty $\Delta r, \Delta d_f$ and Δd_r. The tradeoff is that the robustness to measurement uncertainty is balanced by a reduction in tracking/disturbance rejection performance for r, d_f, and d_r.

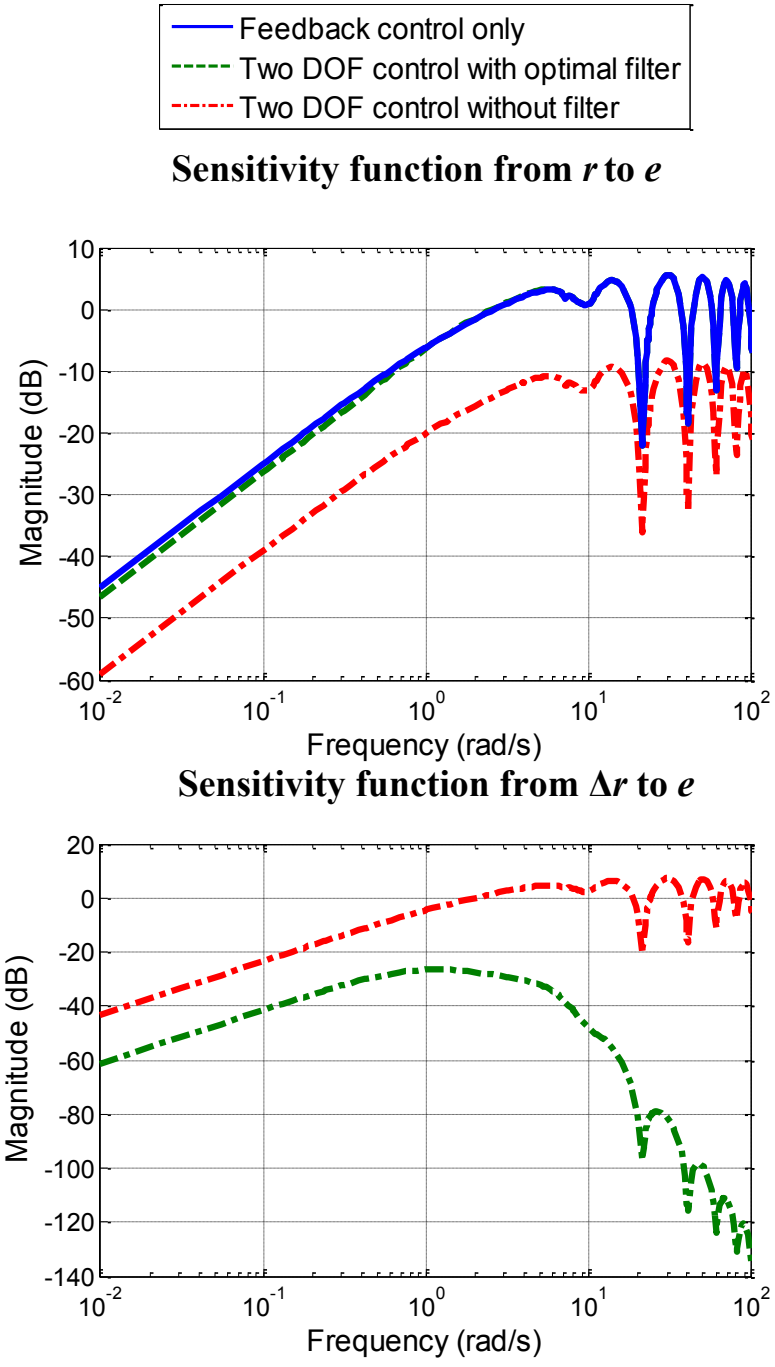

Figure 6.12 Comparison of sensitivity functions from r and Δr to e

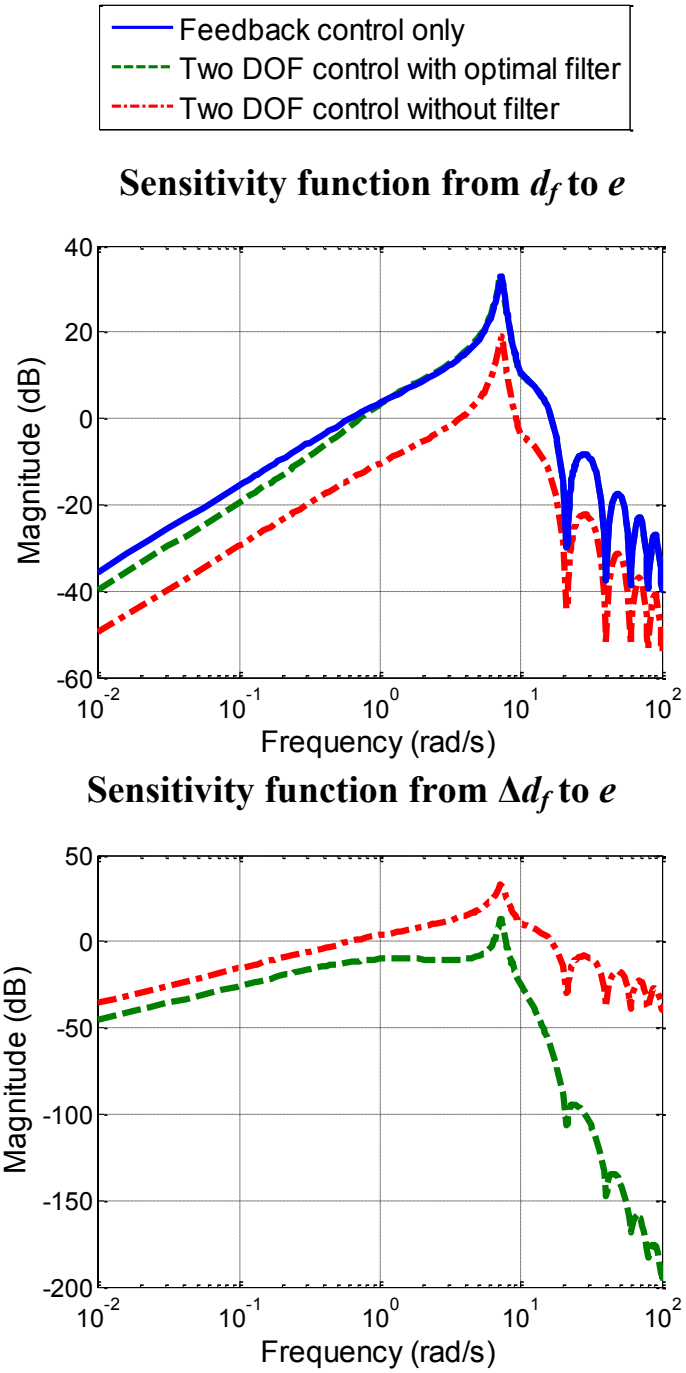

Figure 6.13 Comparison of sensitivity functions from d_f and Δd_f to e

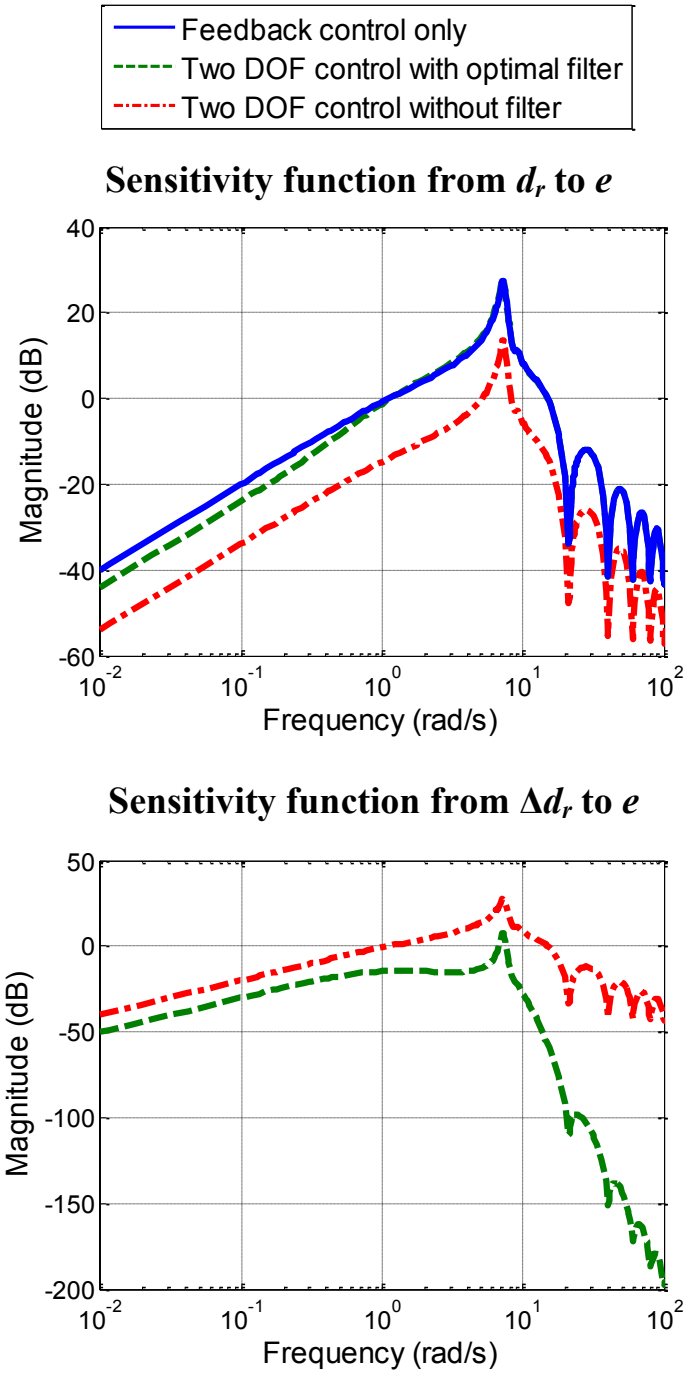

Figure 6.14 Comparison of sensitivity functions from d_r and Δd_r to e

6.3.3 Exogenous signal measurement

The exogenous signals for the HHC problem come from the ground profile that the combine is proceeding on. In practice, the information of the ground profile ahead of the combine is extracted from a pre-measured digital elevation model (DEM). DEM describes the 3D representation of the landscape of a certain area. With a well-established DEM, the shape of the ground's surface is useful information for the purpose of precision farming, such as HHC.

One of the widely-used technologies to pre-measure the DEM is the Global Positioning System (GPS), which provides the widest range measuring result for ground elevation information using remote mapping technologies. In practice, GPS can be implemented with differential corrections data for real-time kinematics (RTK) and reach centimeter-level accuracy, which makes it useful as a tool to generate high resolution DEM [127]. It can be installed on the vehicle to get high-precision, simultaneous measuring of the ground's surface [128]. Another category of DEM is Airborne sensor mapping, such as the Interferometric Synthetic Aperture Radar (InSAR) method and Light Detection and Ranging (LiDAR) method. The basic idea is to install these sensors on aircraft and estimate the shape of the ground's surface by measuring the emitted signal to the objects and the reflected signal from them. The resolution of InSAR is relatively low, horizontally 10 – 20 m [129], and no more than 11 m in depth [130].

In the HHC experimental system, the ground profile is measured by an on-vehicle GPS-RTK system. The current location of the GPS receiver, including the location on the longitude, latitude, and altitude directions, is recorded by the GPS system at a frequency of 5 Hz. When the vehicle is working in some field, the trajectory of the GPS receiver location is

measured and denoted as $\left(x_{GPS}, y_{GPS}, z_{GPS}\right)$ in 3D space. The direction in which the vehicle is proceeding is x, y is perpendicular to x in the horizontal plane, and z is the vertical position. Figure 6.15 shows the geometrical relationship between the GPS receiver and the ground profile in the x-z plane when the combine is driving forward. The pitch angle of the vehicle is θ, which can be measured by a Inertial Navigation System (INS). The terms d_{gfx} and d_{gfz} denote the distance between the GPS receiver and the front tire's lowest point at the x_v-z_v plane of the vehicle coordinate system. Since the lowest point of the front tire always get in touch with the ground's surface, the location of the point in the x-z plane, denoted as x_{ft} and z_{ft}, gives current information about the ground's shape. They can be calculated by the GPS measurement using Eqs. (6.35) and (6.36). When the vehicle is moving, this forms the ground profile trajectory in the direction that the vehicle is driving.

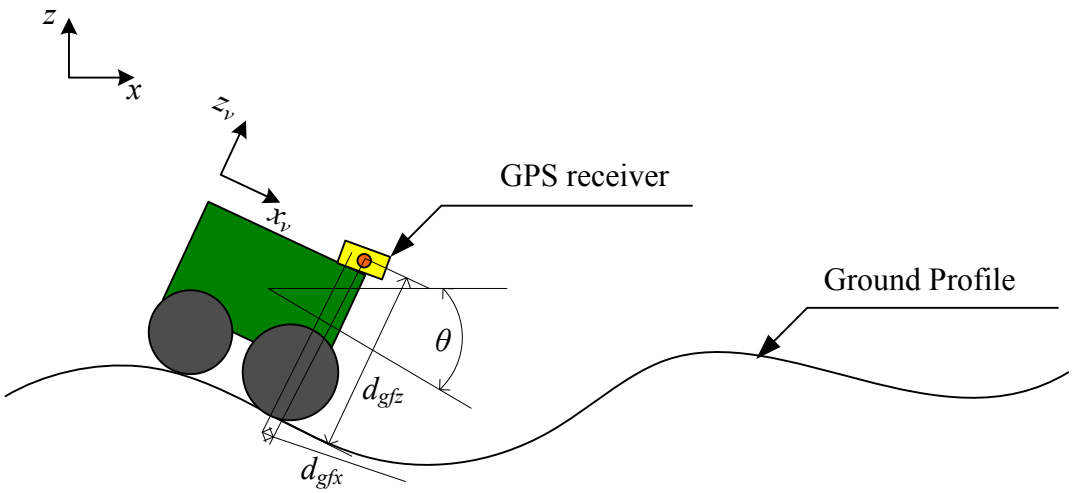

Figure 6.15 GPS-RTK measurement for ground profile

$$x_{ft} = x_{GPS} - \sqrt{d_{gfz}^2 + d_{gfx}^2}\,\sin\left(-\theta + \arctan\frac{d_{gfx}}{d_{gfz}}\right) \tag{6.35}$$

$$z_{ft} = z_{GPS} - \sqrt{d_{gfz}^2 + d_{gfx}^2}\cos\left(-\theta + \arctan\frac{d_{gfx}}{d_{gfz}}\right) \tag{6.36}$$

In the experimental system, to reduce the influence of system uncertainty on the ground profile measurement results, the combine was driven in two directions to give two groups of GPS measurement data, as shown in Figure 6.16. The resulting ground profile curve is shown as the green line.

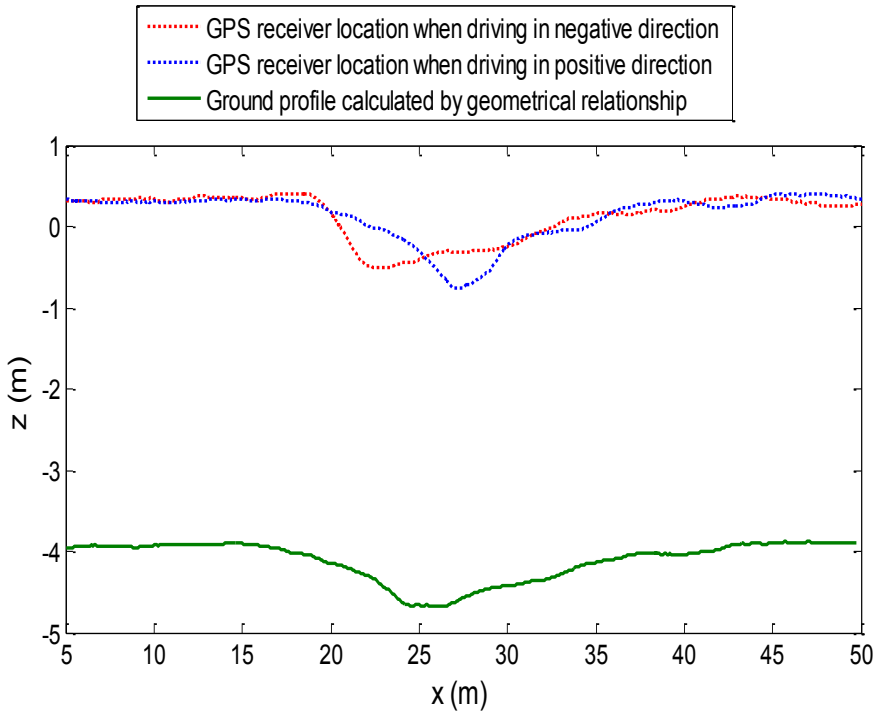

Figure 6.16 GPS-RTK measurements for ground profile

6.3.4 Uncertainty analysis

Although the measurement of the ground profile has been improved by repetitive measurements and adjusted using measurements from different directions, it does not match the ground's profile exactly. Since it is not possible to know exactly what the true ground profile is, the mean value of multiple measurements is taken as the nominal value. Then, the

uncertainty of the signal is defined as the difference between single measurements and the nominal value.

The influential information for designing the feedforward controller is the frequency domain property of such signal uncertainty. Therefore, similar to the work in Figure 5.8 to get the frequency property of the signal itself, the power frequency distribution of the uncertain signal is obtained using Fast Fourier Transform (FFT), as shown in Figure 6.17.

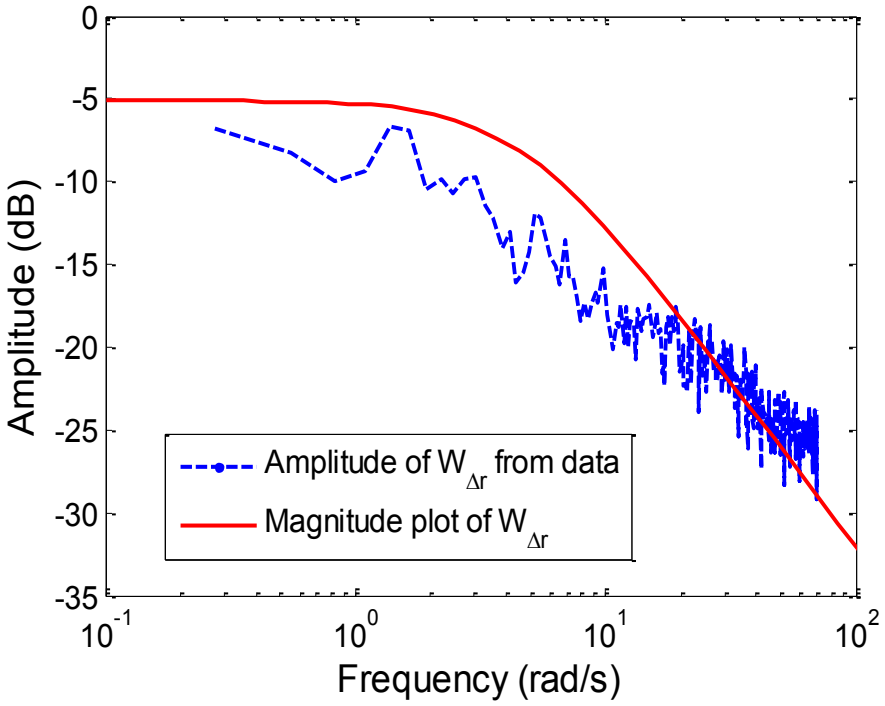

Figure 6.17 Frequency domain properties of the $W_{\Delta r}$

A low-order transfer function is used to indicate the upper bound of the signal uncertainty shown in Figure 6.17 and works as the weight function for the signal uncertainty when designing the feedforward controller. For the HHC system, both the reference and disturbances are from the ground profile; therefore, their weight functions are chosen as the same as shown in Eq. (6.37).

$$W_{\Delta r}(s) = W_{\Delta df}(s) = W_{\Delta dr}(s) = \frac{2.5}{s+4.5} \tag{6.37}$$

6.3.5 Experimental results

Several tests were performed in 2012 at the John Deere proving grounds to experimentally validate the analysis in Section 5.

Following the design procedure in Section 6.2, $W_r(s)$ and $W_{\Delta r}(s)$ were chosen as the weight functions specified in Section 5.4.2, Eq. (5.25) in chapter 5 and Eq. (6.37), because the experiments are conducted repeatedly along the same trajectory in the test field. They are specified to be low-order transfer functions that describe the upper bound of the uncertainty obtained by experimental data. Similarly, the weighting functions $W_{df}(s)$, $W_{dr}(s), W_{\Delta df}(s)$ and $W_{\Delta dr}(s)$ can be specified for the disturbances and their uncertainties. Since the reference and disturbances are all derived from the same ground profile, they have the same frequency domain properties.

With the same system specifications used in Section 6.3.2, the optimal filters can be calculated as Eqs. (6.38) and (6.39).

$$Q_1(s) = \frac{7610s^2 + 4.19\times10^4 s + 3.43\times10^4}{\left(s^5 + 118.1s^4 + 5766s^3 + 4.78\times10^4 s^2 + 1.28\times10^5 s + 8.55\times10^4\right)} \tag{6.38}$$

$$\begin{aligned} Q_{2f}(s) &= Q_{2r}(s) \\ &= \frac{9431s^2 + 5.187\times10^4 s + 4.24\times10^4}{\left(1.2s^5 + 124.9s^4 + 6442s^3 + 5.48\times10^4 s^2 + 1.49\times10^5 s + 1\times10^5\right)} \end{aligned} \tag{6.39}$$

Due to the severe ground-profile condition, the H_∞ feedback controller's maximum speed is limited to 0.4 mph to avoid equipment damage. The corresponding HHC

performance is shown in Figure 6.18, which provides desired and measured header height as a function of longitudinal position. Between approximately 25 m < x < 35 m, the feedback HHC is unable to handle the rapidly changing terrain and the header actually impacts the ground at x = ~34 m. Clearly, this is undesirable. When the feedforward control is added and the delay in the system is compensated, the absolute header height tracks the desired trajectory much better than the feedback controller for the same velocity of0.4 mph. This is analogous to the simulation performance illustrated in Figure 6.9.

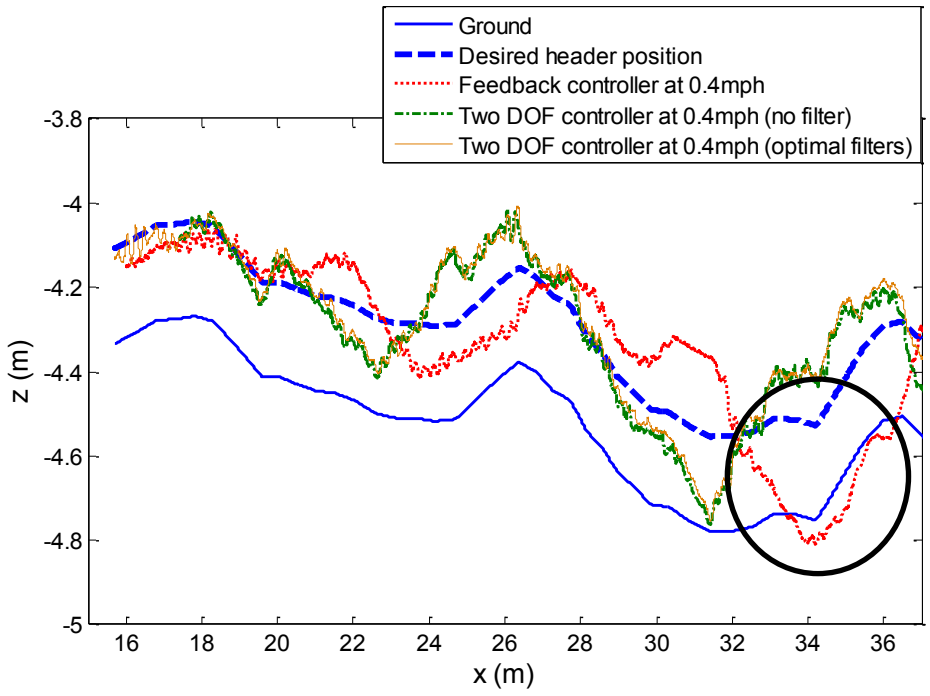

Figure 6.18 Performance comparison between the feedback control and the two DOF control (running at 0.4 mph)

If the combine's speed is increased by a factor of 10, i.e., to4 mph, the HHC performance is still better than the feedback control performance at0.4 mph. However, in this case, the significance of the uncertainty of the measurement of the ground's profile becomes prevalent. The terrain tracking performance is deteriorated significantly at these higher

frequencies, as seen in Figure 6.19. The addition of the optimal feedforward filters greatly reduces the terrain tracking error, and the header is able to follow the ground profile more accurately; the largest improvement can be seen between25 m < x < 35 m.

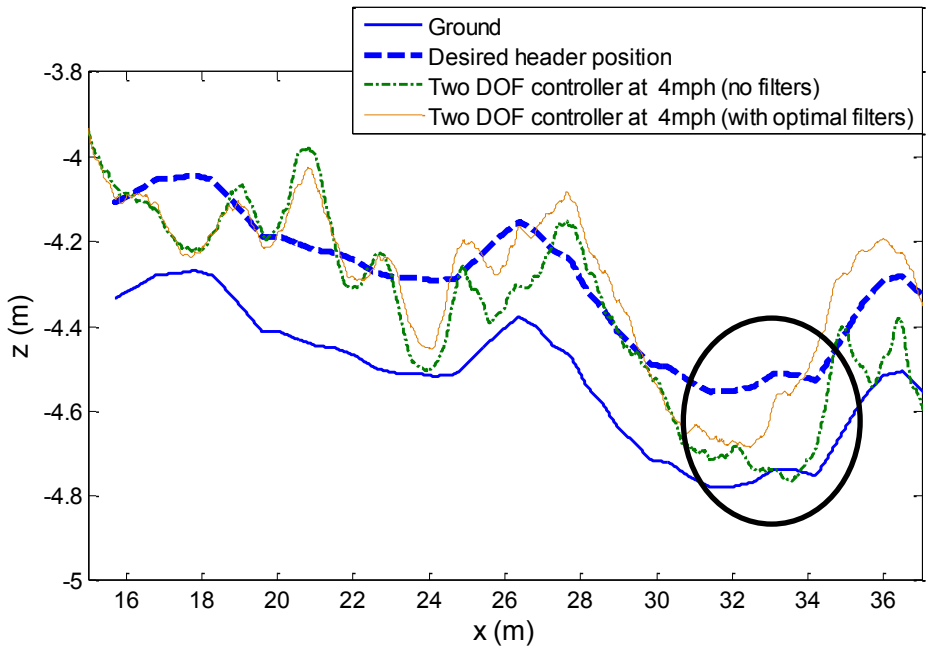

Figure 6.19 Performance comparison of the two DOF controllers (running at 4 mph)

To quantify the performance improvement, the standard deviations of the header height errors are shown in Figure 6.20. This gives the same conclusion as the spatial data shown in Figures 6.18 and 6.19. The standard deviation of the HHC error shows that the two DOF controllers are capable of achieving smaller errors than the one-DOF feedback control; this is true even as the combine's speed is increased by an order of magnitude. When the combine's speed increases, the two DOF controllers with optimal filters decreases the terrain-following error by approximately 20% compared to the controller without filters.

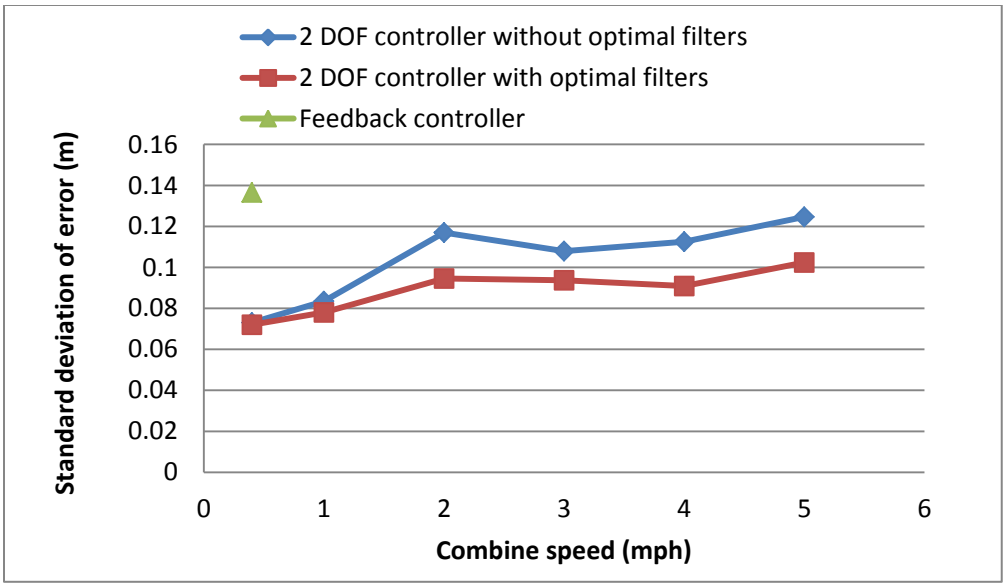

Figure 6.20 Standard deviation of header height error for sandlot test

6.4 Conclusions

Two DOF control is a desirable way to increase system bandwidth if the appropriate exogenous signal information is available. It is particularly effective for systems with delays. However, model uncertainty and signal measurement uncertainty in the system are two main factors that introduce extra error into the output by feedforward control. To address this issue, a method is proposed in this chapter to optimize the feedforward control performance for the time-delayed system.

The error analysis shows the trade-off between performance and robustness to signal uncertainties when designing the feedforward filters. Therefore, the feedforward controller design is formalized as minimizing the H_∞ norm of the corresponding two transfer functions. With estimation of the frequency domain properties of the reference and disturbance and their uncertainties, an optimal solution for feedforward filter design can be developed using some new synthesis technique. The original norms are replaced as weighted

sensitivity functions of an auxiliary system, which provides a mixed sensitivity problem and can be solved by standard H_∞ synthesis.

The application of the method on the HHC for a combine system was studied by both simulation and experiments. From the simulation results, the two DOF controller improved performance over a simple feedback controller. Optimizing the feedforward controller to balance reference tracking or disturbance rejection with reduced sensitivity to measurement uncertainty resulted in a further decrease of the system error when compared to a non-optimal, two DOF control. The experimental results on a production combine showed a significant decrease in error and an increase in speed when an optimally-designed, two DOF controller is used.

The method presented in this chapter can be used in a class of LTI systems that can fit the schematic shown in Figure 6.1. With the information for the model and signal uncertainties, the optimal feedforward controller can be determined with the method in this chapter to give the optimal performance considering both feedforward performance and robustness to the uncertainties.

Chapter 7
Conclusions

In this final chapter, the work presented in this dissertation is summarized. Section 7.1 gives concluding remarks for each chapter. Section 7.2 lists the main results and contributions of the overall dissertation, followed by a discussion in Section 7.3 about the possible future directions of the research work.

7.1 Dissertation Summary

A chapter-wise summary of this dissertation is presented below:

1. Chapter 1 introduces the VEI system and specifically describes the HHC for combine harvesters as the motivation for the research work in the dissertation. The research objectives that are introduced based on this motivation include: the development of theoretical tools for system limitation analysis, integrated design and control, and two DOF controller design for systems with time delays. These objectives form the research flow of this dissertation and are combined through the following chapters to provide a systematic solution for the HHC problem in particular and, more broadly speaking, for an entire class of VEI systems.

2. The fundamental limitations in SISO LTI systems are discussed in Chapter 2. In particular, the most common existing limitations occurring in physical system are presented including: time delays, non-minimum phase zeros, model uncertainty, signal uncertainty and noise. This chapter provides a literature survey and analyses on the bandwidth limitations caused by the physical features mentioned above.

3. Chapter 3 presents the detailed mathematical model for the combine harvester HHC system under study in this dissertation. Based on the modeling work, two major limitations from physical system are observed: These are (i) the undesirable open loop zeros and poles caused by the mechanical structure and (ii) the time delay cause by the actuator behavior. Both the modeling work and the limitation analysis are validated through simulation and experimental results.

4. Targeting improving the mechanical characteristics of the system, an integrated design and control approach is introduced in Chapter 4. Using the H_∞ norm of the closed loop sensitivity functions as the design objective function, the key design parameters of the physical system and controller are optimized with both an iterative and a simultaneous optimization procedure. Both methods provide similar design effects for the physical system dynamics: the open loop zeros and poles obtain larger damping ratios and natural frequencies, which alleviates the limitations caused by the mechanical system design.

5. Chapter 5 introduces a robust H_∞ controller for time-delayed systems with the goal of addressing the actuator behavior. Although this optimal controller is not able to remove the bandwidth limitation from the delay, robust stability is guaranteed and performance maximized by optimizing a mixed sensitivity objective function. A unique method to transform the irrational optimization problem, which is induced by the delay, to its rational counterpart is introduced. Simulation and experimental data are shown to validate the controller design method on the HHC problem.

6. Chapter 6 introduces further improvements to the control performance of Chapter 5 by introducing a feedforward controller into the system. The feedforward control considers both the model uncertainty and signal uncertainty by balancing the trade-off between HHC performance and robustness to the uncertainties. As a result, an optimal controller is calculated and validated in the HHC system. Both simulation and experiments show the significant performance improvement of HHC by using an optimal feedforward control approach.

7.2 Research Contributions

VEI systems studied in this dissertation refer to the vehicle systems that somehow interact with their environment during the operations. This interaction could be the positioning of an end effector or some other working tool as is the case in the current work. The operations of such VEI systems usually involve an unknown reference and disturbance from the changing environment, such as the ground surface shape that the vehicle is proceeding on. To achieve accurate and high speed operation, the controlled system requires

high bandwidth to accommodate the rapidly changing exogenous signals caused by the environment. However, high bandwidth performance is usually difficult to achieve due to the inherent limitations from the physical system. The HHC problem, which is taken as the example system of interest in this dissertation, presents two such limitations: (i) the under-actuated and non-collocated sensing and actuation of the mechanical structure and (ii) significant time delay due to the actuator. These limitations become bottlenecks for greater system productivity, which is a continuous desire by the operators and manufacturers of these machines..

To address the control problems arising from the two limitations, we first provide theoretical analysis to reveal the relationship between the features of the physical system and the resulting bandwidth limitations. The zeros dynamics in an under-actuated and non-collocated system is largely determined by the passive DOFs in the mechanical system. Unfortunately, in the HHC system the passive DOFs, which are the pitch rotation and vertical translation movement of the combine body, have small damping ratios and spring rigidity due to the heavy mass of the combine machine relative to the tire properties. As a result, the zeros and poles in the system are lightly damped at low natural frequencies, which results in a low bandwidth limitation. The understanding of the relationship between the mechanical system structure and its corresponding control limitation is important. We anticipate that a large class of other VEI systems could potentially have the same control problem. With the method introduced in this dissertation, the corresponding bandwidth limitation can be identified and quantified before any controller design approach is applied.

Similarly, results are obtained for addressing the time delay caused by the electro-hydraulic actuation system. The experimental results show the significant influence from the delay in the actuation system on the control performance. The induced bandwidth limitation creates another performance barrier for feedback control design. It motivates the search for a problem solution and there are two options: (i) improving the actuation system to have much less delay, which is not cost-effective, or (ii) using additional information or sensors to develop new control approaches compared with traditional feedback control. The second option is adopted since it is considered as a more realistic solution for eventual transition to practice.

To solve the control problem caused by the mechanical system structure, an integrated design and control method is proposed. By choosing proper adjustable design parameters in the mechanical system, the design problem may be formulated as a non-linear optimization problem. The closed loop control performance is taken as the design objective, which includes both the design parameters from the physical system and the controller as the design variables. As a result, the optimization not only significantly improves the plant dynamics but also provides an optimized controller for the newly-designed system. This integrated design method can be applied to a wide variety of VEI and other systems, above and beyond the HHC system studied in this dissertation. As long as the problem is well defined with properly chosen design parameters, a similar procedure can be used to determine the optimal values of plant parameters, along with optimal controller structure/parameters, for the purpose of achieving better closed loop performance.

For systems with delay, this dissertation provides a two DOF control solution. The feedback controller uses H_∞ synthesis to ensure the stability of the closed loop system influenced by large exogenous signals. For the HHC problem, one example of these large exogenous signals would be a situation where the ground profile has a large height change over a relatively short longitudinal distance. A transformation method is introduced to transform the irrational optimization problem to be a rational one using a modified performance signal and a Smith predictor. This method simplifies the robust controller design procedure for systems with delay compared with complex matrix operations for obtaining rational LMI expressions as solutions to the delay issue. Therefore, we feel our approach provides a practical feedback controller design method that can be widely used in industrial systems.

The feedforward controller that complements the feedback element above needs to use pre-measured signals from the reference and disturbances. In this dissertation, not only the model uncertainty but also the signal uncertainty is studied to design optimal feedforward filters. As a result, the optimal feedforward controller is able to balance the trade-off between performance requirements and robustness to both uncertainties. The commonly existing problem for feedforward controller design – the high sensitivity to both uncertainties – is considered in a formal analysis framework and significantly alleviated.

Combining all of the methods mentioned above, this dissertation provides a systematic way to solve the design and control problem for the HHC, in particular, and VEI systems in general. The simulation results show that the integrated design and control for the system can improve the bandwidth to be 2.51Hz, which is much larger than the theoretical

bandwidth of 1.5 Hz. This is also much higher than the bandwidth estimated by the experimental uncertainty which is limited to 0.64 Hz for the original system. The experimental results for the two DOF controller validate much of this analysis by demonstrating increases in the combine speed on a test field by a factor of 10 X. This is clearly quite promising. Although the simulation and experiments are conducted specifically for HHC system, our experience leads us to believe the approach can be readily extended to the other similar systems to achieve performance improvements.

7.3 Future Extensions

7.3.1 Extension to MIMO systems

The scope of the theoretical tools introduced in this dissertation is limited to SISO LTI systems. However, there are many MIMO systems that can face similar control limitations and could potentially benefit from using similar tools to solve their problems. Therefore, it would be worthwhile to study how the design and control methods mentioned in this dissertation can be modified to be used in MIMO systems. One possible way to do it is to carefully reconstruct the objective functions in Chapters 4, 5 and 6 to make them compatible with the current synthesis methods in the optimization problems.

7.3.2 Extension to other applications

As mentioned above, the current application of the tools in this dissertation is mainly on a HHC system. However, we strongly believe these tools can be of benefit for several other VEI systems without large modifications due to the similarity in system dynamics. Moreover, the theories proposed in this dissertation are not limited in their applications to

only VEI systems. There are a host of other applications that could benefit. As one example, the optimal two DOF controller, with both signal and model uncertainty, can be possibly used for controlling a wind turbine or a wind farm. Laser sensors can provide a prediction of the incoming wind speed and direction, which enables the feedforward control approach in Chapter 6 to optimize the operational effectiveness of the turbine/farm whilst considering both the model and signal measurement uncertainties. We strongly believe several other such opportunities exist.

List of References

[1] J. L. Glancey, "Analysis of header loss from pod stripper combines in green peas," *J. Agr. Eng. Res.,* vol. 68, *(1),* pp. 1-10, 1997.

[2] C. Junsiri and W. Chinsuwan, "Prediction equations for header losses of combine harvesters when harvesting Thai Hom Mali rice," *Songklanakarin J. Sci. Technol.,* vol. 31, *(6),* pp. 613-620, 2009.

[3] G. R. Quick and W. F. Buchele, "The gain harvester," in *ASAE,* St. Joseph, MI, 1978, pp. 269.

[4] G. R. Quick and W. F. Buchele, "Reducing combine gathering losses in soybeans," *T. ASAE,* vol. 72, *(6),* pp. 1123-1129, 1974.

[5] G. T. Lopes, P. S. G. Magalhães and E. G. O. Nóbrega, "Optimal header height control system for combine harvesters," *Biosyst. Eng.,* vol. 81, *(3),* pp. 261-272, 2002.

[6] Y. Xie, A. Alleyne, A. Greer and D. Deneault, "Header height control of a combine harvester system," in *Proceeding of the 2010 ASME Dynamic Systems and Control Conference,* Cambridge, MA, 2010, pp. 7-14.

[7] A. Sharon, N. Hogan and D. E. Hardt, "Controller design in the physical domain," *J. Franklin I.,* vol. 328, *(5-6),* pp. 697-721, 1991.

[8] K. Youcef-Toumi, "Modeling, design, and control integration: a necessary step in mechatronics," *IEEE/ASME Trans. Mechatronics,* vol. 1, *(1),* pp. 29-38, 1996.

[9] P. J. Gawthrop, "Control system configuration: Inversion and bicausal bond graphs," in *Proceedings of the 1997 International Conference on Bond Graph Modeling and Simulation,* Phoenix, AZ, 1997, pp. 97-102.

[10] P. G. Maghami, S. M. Joshi and K. B. Lim, "Integrated controls-structures designs: A practical design tool for modern spacecraft," in *American Control Conference, 1991,* Boston, MA, 1991, pp. 1465-1473.

[11] P. G. Maghami, S. M. Joshi and E. S. Armstrong, "An optimization-based integrated controls-structures design methodology for flexible space structures," NASA Langley Research Center, Tech. Rep. NASA TP-3283, 2003.

[12] S. L. Padula, C. A. Sandridge, J. L. Walsh and R. T. Haftka, "Integrated controls-structures optimization of a large space structure," *Comput. Struct.,* vol. 42, *(5),* pp. 725-732, 1992.

[13] M. D. McLaren and G. L. Slater, "A disturbance model for control/structure optimization with output feedback control," *Struct. Optimization,* vol. 6, *(2),* pp. 123-133, 1993.

[14] G. E. Dullerud and F. G. Paganini, *A Course in Robust Control Theory: A Convex Approach.* Springer, 2000.

[15] F. Lin, *Robust Control Design: An Optimal Control Approach.* Wiley, 2007.

[16] S. Sastry and M. Bodson, *Adaptive Control: Stability, Convergence and Robustness.* Dover Publications, 2011.

[17] K. J. Åström, *Adaptive Control.* Pearson Education, 1995.

[18] L. Grüne and J. Pannek, *Nonlinear Model Predictive Control: Theory and Algorithms.* Springer, 2011.

[19] J. M. Maciejowski, *Predictive Control: With Constraints.* Prentice Hall, 2002.

[20] J. X. Xu, S. K. Panda and T. H. Lee, *Real-Time Iterative Learning Control: Design and Applications.* Springer, 2008.

[21] D. A. Bristow, M. Tharayil and A. G. Alleyne, "A survey of iterative learning control," *IEEE Control Syst. Mag.,* vol. 26, *(3),* pp. 96-114, 2006.

[22] D. R. Lewin and C. Scali, "Feedforward control in the presence of uncertainty," *Ind. Eng. Chem. Res.,* vol. 27, *(12),* pp. 2323-2331, 1988.

[23] G. Pipeleers, B. Demeulenaere, J. De Schutter and J. Swevers, "Design of robust optimal feedforward controllers for periodic disturbances," in *American Control Conference, 2007. ACC '07,* New York, NY, 2007, pp. 5333-5340.

[24] J. Flores, Y. Tang and A. Osorio, "Adaptive feedforward control and disturbance cancellation," in *Decision and Control, 1993., Proceedings of the 32nd IEEE Conference on,* San Antonio, TX, USA, 1993, pp. 2623-2628.

[25] X. Guo and M. Bodson, "Equivalence between adaptive feedforward cancellation and disturbance rejection using the internal model principle," *Int. J. Adapt. Control,* vol. 24, *(3),* pp. 211-218, 2010.

[26] C. Lee and S. M. Salapaka, "Robust broadband nanopositioning: fundamental trade-offs, analysis, and design in a two-degree-of-freedom control framework," *Nanotechnology,* vol. 20, *(3),* 2009.

[27] M. Morari and E. Zafiriou, *Robust Process Control.* Prentice Hall, 1989.

[28] R. Vilanova, O. Arrieta, A. Ibeas, P. Balaguer and C. Pedret, "Disturbance compensation on uncertain systems: Feedforward control design for stable systems," in *Proceedings of the 17th IFAC World Congress,* Seoul, Korea, 2008, pp. 11310-11315.

[29] G. C. Goodwin, S. F. Graebe and M. E. Salgado, *Control System Design.* Prentice Hall, 2001.

[30] S. Skogestad and I. Postlethwaite, *Multivariable Feedback Control: Analysis and Design.* John Wiley, 2005.

[31] Hara, S., Bakhtiar, T., Kanno,M., "The best achievable H_2 tracking performances for SIMO feedback control systems," *Journal of Control Science and Engineering,* vol. 2007, 2007.

[32] Chen, J., Hara, S., Qiu, L., Middleton,R.H., "Best achievable tracking performance in sampled-data systems via LTI controllers," *IEEE Trans. Autom. Control,* vol. 53, *(11),* pp. 2467-2479, 2008.

[33] J. Chen, L. Qiu and O. Toker, "Limitations on maximal tracking accuracy," *IEEE Trans. Autom. Control,* vol. 45, *(2),* pp. 326-331, 2000.

[34] J. B. Hoagg and D. S. Bernstein, "Nonminimum-phase zeros - much to do about nothing - classical control - revisited part II," *IEEE Control Syst. Mag.,* vol. 27, *(3),* pp. 45-57, 2007.

[35] M. Sidi, "On maximization of gain-bandwidth in sampled systems," *Int. J. Control,* vol. 32, *(6),* pp. 1099-1109, 1980.

[36] M. Sidi, "Gain-bandwidth limitations of feedback systems with non-minimum-phase plants," *Int. J. Control,* vol. 67, *(5),* pp. 731-744, 1997.

[37] M. Morari and E. Zafiriou, *Robust Process Control.* Prentice Hall, 1989.

[38] L. Qiu and E. J. Davison, "Performance limitations of non-minimum phase systems in the servomechanism problem," *Automatica,* vol. 29, *(2),* pp. 337-349, 3, 1993.

[39] O. Yaniv and P. -. Gutman, "Crossover frequency limitations in MIMO nonminimum phase feedback systems," *IEEE Trans. Autom. Control,* vol. 47, *(9),* pp. 1560-1564, 2002.

[40] T. C. Tsao and M. Tomizuka, "Adaptive zero phase error tracking algorithm for digital control," *J. Dyn. Syst. -T. ASME,* vol. 190, pp. 349-354, 1987.

[41] B. P. Rigney, L. Y. Pao and D. A. Lawrence, "Nonminimum Phase Dynamic Inversion for Settle Time Applications," *IEEE Trans. Control Syst. Technol.,* vol. 17, *(5),* pp. 989-1005, 2009.

[42] J. A. Butterworth, L. Y. Pao and D. Y. Abramovitch, "The effect of nonminimum-phase zero locations on the performance of feedforward model-inverse control techniques in discrete-time systems," in *American Control Conference, 2008,* Seattle, WA, 2008, pp. 2696-2702.

[43] N. C. Martins and M. A. Dahleh, "Feedback control in the presence of noisy channels: "Bode-like" fundamental limitations of performance," *IEEE Trans. Autom. Control,* vol. 53, *(7),* pp. 1604-1615, 2008.

[44] G. N. Nair, F. Fagnani, S. Zampieri and R. J. Evans, "Feedback control under data rate constraints: An overview," *Proc. IEEE,* vol. 95, *(1),* pp. 108-137, 2007.

[45] A. J. Rojas, "Signal-to-noise ratio fundamental limitations in the discrete-time domain," *Syst. Control Lett.,* vol. 61, *(1),* pp. 55-61, 2012.

[46] A. J. Rojas, "Signal-to-noise ratio fundamental limitations in continuous-time linear output feedback control," *IEEE Trans. Autom. Control,* vol. 54, *(8),* pp. 1902-1907, 2009.

[47] P. B. Goldsmith, "On the equivalence of causal LTI iterative learning control and feedback control," *Automatica,* vol. 38, *(4),* pp. 703-708, 2002.

[48] M. Morari and E. Zafiriou, *Robust Process Control.* Prentice Hall, 1989.

[49] S. Devasia, "Should model-based inverse inputs be used as feedforward under plant uncertainty?" *IEEE Trans. Autom. Control,* vol. 47, *(11),* pp. 1865-1871, 2002.

[50] A. Faanes and S. Skogestad, "Feedforward control under the presence of uncertainty," *Eur. J. Control,* vol. 10, *(1),* pp. 30-46, 2004.

[51] E. J. Adam and J. L. Marchetti, "Designing and tuning robust feedforward controllers," *Comput. Chem. Eng.,* vol. 28, *(9),* pp. 1899-1911, 2004.

[52] Y. Wu and Q. Zou, "Robust-inversion-based 2DOF-control design for output tracking: piezoelectric actuator example," *IEEE Trans. Control Syst. Technol.,* vol. 17, *(5),* pp. 1069-1082, 2009.

[53] J. W. Eaton and J. B. Rawlings, "Model-predictive control of chemical processes," *Chem. Eng. Sci.,* vol. 47, *(4),* pp. 705-720, 1992.

[54] R. H. Middleton, J. Chen and J. S. Freudenberg, "Achievable performance and sensitivity integral constraints in preview control," in *Decision and Control, 2001. Proceedings of the 40th IEEE Conference on,* Orlando, FL, 2001, pp. 3075-3080.

[55] O. Yaniv and M. Nagurka, "Robust performance limitations and design of controlled delayed systems," *J. Dyn. Syst. -T. ASME,* vol. 126, *(4),* pp. 899-904, 2004.

[56] S. O. R. Moheimani, *Perspectives in Robust Control.* Springer, 2001.

[57] Y. Xie and A. G. Alleyne, "A robust two degree-of-freedom controller for system with delay," in *American Control Conference (ACC), 2013,* Washington, DC, 2013, .

[58] D. J. Block and M. W. Spong, "Mechanical design and control of the Pendubot," *SAE Transactions,* vol. 104, *(2),* pp. 36-43, 1995.

[59] M. W. Spong, "Swing up control problem for the acrobot," *IEEE Control Syst. Mag.,* vol. 15, *(1),* pp. 49-55, 1995.

[60] J. Nakanishi, T. Fukuda and D. E. Koditschek, "A brachiating robot controller," *IEEE Trans. Robot. Autom.,* vol. 16, *(2),* pp. 109-123, 2000.

[61] M. W. Spong, "Underactuated mechanical systems," in *Control Problems in Robotics and Automation*, B. Siciliano and K. P. Valavanis, Eds. Springer-Verlag, 1998, pp. 135-150.

[62] H. Arai and S. Tachi, "Position control of manipulator with passive joints using dynamic coupling," *IEEE Trans. Robot. Autom.,* vol. 7, *(4),* pp. 528-534, 1991.

[63] M. W. Spong, S. Hutchinson and M. Vidyasagar, *Robot Modeling and Control.* New York: John Wiley & Sons, Inc., 2006.

[64] B. Magyar, C. Hós and G. Stépán, "Influence of control valve delay and dead zone on the stability of a simple hydraulic positioning system," *Math. Probl. Eng.,* vol. 2010, 2010.

[65] C. L. Lin, C. H. Chen, V. T. Liu and T. S. Hwang, "A new time-delay compensation scheme for hydraulic systems," in *Industrial Electronics, 2004 IEEE International Symposium on,* 2004, pp. 639-644.

[66] Y. Wang, J. Huang, Y. Zhang and F. Zhuang, "Analysis and quenching of limit cycles of electro-hydraulic servovalve control systems with friction and interval transport lag," in *Control Conference, 2008. CCC 2008. 27th Chinese,* Kunming, China, 2008, pp. 212-216.

[67] D. K. Lindner, K. M. Reichard and L. M. Tarkenton, "Zeros of modal models of flexible structures," *IEEE Trans. Autom. Control,* vol. 38, *(9),* pp. 1384-1388, 1993.

[68] K. J. Aström, "Limitaions on Control System Performance," *European Journal of Control,* pp. 2-20, 2000.

[69] G. Stein, "Respect the Unstable," *IEEE Control Syst. Mag.,* vol. 23, *(4),* pp. 12-25, 2003.

[70] G. J. Balas and J. C. Doyle, "Robustness and performance trade-offs in control design for flexible structures," *IEEE Trans. Control Syst. Technol.,* vol. 2, *(4),* pp. 352-361, 1994.

[71] N. M. Thibeault and R. Smith, "Fundamental limits in robustness and performance for unstable, underactuated systems," *IEEE Trans. Autom. Control,* vol. 46, *(8),* pp. 1265-1268, 2001.

[72] H. Olsson, K. J. Aström, C. Canudas de Wit, M. Gäfvert and P. Lischinsky, "Friction models and friction compensation," *Eur. J. Control,* vol. 4, *(3),* pp. 176-195, 1998.

[73] J. G. Ziegler and N. B. Nichols, "Optimal settings for automatic controllers," *ASME Transactions,* vol. 64, pp. 759-768, 1942.

[74] P. S. Buckley, *Techniques of Process Control.* Wiley, 1964.

[75] P. Seferlis and M. C. Georgiadis, *The Integration of Process Design and Control.* Elsevier Science, 2004.

[76] P. J. Gawthrop, "Physical model-based control: a bond graph approach," *J. Franklin I.,* vol. 332, *(3),* pp. 285-305, 1995.

[77] J. B. Layton and L. D. Peterson, "The benefits of integrated control/structure design using covariance control-a comparison of two approaches," in *Collection of Technical Papers - AIAA/ASME Structures, Structural Dynamics and Materials Conference,* La Jolla, CA, 1993, pp. 3126-3136.

[78] H. Asada, J. H. Park and S. Rai, "A control-configured flexible arm: Integrated structure control design," in *Robotics and Automation, 1991. Proceedings., 1991 IEEE International Conference on,* Sacramento, CA, 1991, pp. 2356-2362.

[79] T. N. Madhusudan, "A review of bond-graph representation based design methodologies," Robotics Institute, Carnegie Mellon University, Pittsburgh, PA, Tech. Rep. CMU-RI-TR-95-28, 1995.

[80] Y. Zhang, Z. Fang and G. Wu, "Integrated structure and control parameters optimization for an automotive active suspension system via LMIs," in *Measuring Technology and Mechatronics Automation, 2009. ICMTMA '09. International Conference on,* Zhangjiajie, China, 2009, pp. 804-807.

[81] P. Kiriazov, "Integrated structure-control design of dynamically walking robots," in *Climbing and Walking Robots*, M. O. Tokhi, G. S. Virk and M. A. Hossain, Eds. Springer Berlin Heidelberg, 2006, pp. 295-302.

[82] A. C. Pil and H. H. Asada, "Integrated structure/control design of mechatronic systems using a recursive experimental optimization method," *IEEE/ASME Trans. Mechatronics,* vol. 1, *(3),* pp. 191-203, 1996.

[83] G. L. Slater and M. D. McLaren, "Disturbance model for control/structure optimization with full statefeedback," *J. Guid. Control Dynam.,* vol. 16, *(3),* pp. 523-533, 1993.

[84] J. B. Layton and L. D. Peterson, "Control/structure covariance optimization with a variety of constraints including saturation, stability, and performance robustness," in *Collection of Technical Papers - AIAA/ASME/ASCE/AHS/ASC Structures, Structural Dynamics and Materials Conference,* New Orleans, LA, 1995, pp. 739-748.

[85] S. M. Joshi and P. G. Maghami, "Robust dissipative compensators for flexible spacecraft control," *IEEE Trans. Aerosp. Electron. Syst.,* vol. 28, *(3),* pp. 768-774, 1992.

[86] G. Zames, "On the input-output stability of time-varying nonlinear feedback systems Part one: Conditions derived using concepts of loop gain, conicity, and positivity," *IEEE Trans. Autom. Control,* vol. 11, *(2),* pp. 228-238, 1966.

[87] Y. Xie and A. Alleyne, "Integrated plant and controller design of a combine harvester system," in *Proceeding of ASME DSCC Dynamic Systems and Control Conference,* Arlington, VA, 2011, pp. 819-825.

[88] J. Nocedal and S. Wright, *Numerical Optimization.* Springer, 2006.

[89] H. Du, "H∞ state-feedback control of bilateral teleoperation systems with asymmetric time-varying delays," *IET Control Theory & Applications,* vol. 7, *(4),* pp. 594-605, 2013.

[90] M. J. Khabbaz, H. M. K. Alazemi and C. M. Assi, "Modeling and delay analysis of a retransmission-based bundle delivery scheme for intermittent roadside communication networks," *IEEE Trans. Intell. Transp. Syst.,* vol. 14, *(2),* pp. 700-708, 2013.

[91] C. Peng, Q. -. Han and D. Yue, "Communication-delay-distribution-dependent decentralized control for large-scale systems with IP-based communication networks," *IEEE Trans. Control Syst. Technol.,* vol. 21, *(3),* pp. 820-830, 2013.

[92] V. N. Phat, T. Fernando and H. Trinh, "Observer-based control for time-varying delay neural networks with nonlinear observation," *Neural Comput. Appl.,* pp. 1-7, 2013.

[93] L. Xie, E. Fridman and U. Shaked, "Robust H∞ control of distributed delay systems with application to combustion control," *IEEE Trans. Autom. Control,* vol. 46, *(12),* pp. 1930-1935, 2001.

[94] J. Lei, "Optimal vibration control for uncertain nonlinear sampled-data systems with actuator and sensor delays: Application to a vehicle suspension," *J. Dyn. Syst. -T. ASME,* vol. 135, *(2),* pp. 021021, 2013.

[95] Y. Xie, A. G. Alleyne, A. Greer and D. Deneault, "Fundamental limits in combine harvester header height control," *J. Dyn. Syst. -T. ASME,* vol. 135, *(3),* pp. 034503, 2013.

[96] Y. Li, S. Xu, B. Zhang and Y. Chu, "Robust stabilization and H∞ control for uncertain fuzzy neutral systems with mixed time delays," *Fuzzy Set. Syst.,* vol. 159, *(20),* pp. 2730-2748, 2008.

[97] S. C. Jeong and P. Park, "Constrained MPC algorithm for uncertain time-varying systems with state-delay," *IEEE Trans. Autom. Control,* vol. 50, *(2),* pp. 257-263, 2005.

[98] X. Zhu and J. Zhou, "Infinite horizon optimal control of stochastic delay evolution equations in hilbert spaces," *Abstract and Applied Analysis,* vol. 2013, 2013.

[99] G. H. Yan, S. H. Wang, Z. W. Guan and C. F. Liu, "PID control strategy of vehicle active suspension based on considering time-delay and stability," *Advanced Materials Research,* vol. 706-708, pp. 901-906, 2013.

[100] V. L. Kharitonov and D. Melchor-Aguilar, "On delay-dependent stability conditions," *Syst. Control Lett.,* vol. 40, *(1),* pp. 71-76, 2000.

[101] J. Chen, D. Xu and B. Shafai, "On sufficient conditions for stability independent of delay," *IEEE Trans. Autom. Control,* vol. 40, *(9),* pp. 1675-1680, 1995.

[102] M. T. Nihtilä, "Adaptive control of a continuous-time system with time-varying input delay," *Syst. Control Lett.,* vol. 12, *(4),* pp. 357-364, 1989.

[103] Z. Li, Y. Xia and X. Cao, "Adaptive control of bilateral teleoperation with unsymmetrical time-varying delays," *Int. J. Innov. Comput. I.,* vol. 9, *(2),* pp. 753-767, 2013.

[104] V. L. Kharitonov and A. P. Zhabko, "Lyapunov–Krasovskii approach to the robust stability analysis of time-delay systems," *Automatica,* vol. 39, *(1),* pp. 15-20, 2003.

[105] A. W. Olbrot and C. U. T. Igwe, "Necessary and sufficient conditions for robust stability independent of delays and coefficient perturbations," in *Decision and Control, 1995., Proceedings of the 34th IEEE Conference on,* New Orleans, LA, 1995, pp. 392-394.

[106] H. Dym, T. T. Georgiou and M. C. Smith, "Explicit formulas for optimally robust controllers for delay systems," *IEEE Trans. Autom. Control,* vol. 40, *(4),* pp. 656-669, 1995.

[107] J. R. Partington and K. Glover, "Robust stabilization of delay systems by approximation of coprime factors," *Syst. Control Lett.,* vol. 14, *(4),* pp. 325-331, 1990.

[108] Q. Chai, R. Loxton, K. L. Teo and C. Yang, "A class of optimal state-delay control problems," *Nonlinear Analysis: Real World Applications,* vol. 14, *(3),* pp. 1536-1550, 2013.

[109] R. Farkh, K. Laabidi and M. Ksouri, "Robust design of optimal PID controller for uncertain time delay system," *Mediterranean Journal of Measurement and Control,* vol. 8, *(3),* pp. 447-455, 2012.

[110] G. Tadmor, "Robust control in the gap: a state-space solution in the presence of a single input delay," *IEEE Trans. Autom. Control,* vol. 42, *(9),* pp. 1330-1335, 1997.

[111] E. Tian, D. Yue and C. Peng, "Delay-fractioning-dependent robust H ∞ control for linear systems with delay in state or input and its applications," *Int. J. Syst. Sci.,* vol. 43, *(5),* pp. 820-833, 2012.

[112] L. Mirkin, "On the extraction of dead-time controllers and estimators from delay-free parametrizations," *IEEE Trans. Autom. Control,* vol. 48, *(4),* pp. 543-553, 2003.

[113] O. J. M. Smith, "Closer control of loops with dead time," *Chem. Eng. Progress,* vol. 53, *(5),* pp. 217-219, 1957.

[114] A. T. Bahill, "A simple adaptive Smith-predictor for controlling time-delay systems: a tutorial," *IEEE Control Syst. Mag.,* vol. 3, *(2),* pp. 16-22, 1983.

[115] J. Syder, T. Heeg and A. O'Dwyer, "Dead-time compensators: Performance and robustness issues," in *Proceedings of Process Control and Instrumentation 2000 Conference,* Glasgow, Scotland, 2000, pp. 166-171.

[116] K. S. Hong, D. H. Kang and J. G. Kim, "Robust smith predictor design via uncertainty quantification: Application to a reclaimer," in *IFAC System Identification,* Santa Barbara, CA, 2000, .

[117] H. Ziyuan, Z. Lanlan and F. Minrui, "Robust auto tune smith predictor controller design for plant with large delay," in *Proceedings of the International Conference on Life System Modeling and Simulation,* Shanghai, China, 2007, pp. 666-678.

[118] S. Farhati, S. Bel Hadj Ali Naoui and M. N. Abdelkrim, "H∞ loop shaping control of time delay systems," in *Communications, Computing and Control Applications (CCCA), 2011 International Conference on,* Hammamet, Tunisia, 2011, pp. 1-6.

[119] D. Lee, M. Lee, S. Sung and I. Lee, "Robust PID tuning for Smith predictor in the presence of model uncertainty," *J. Process Contr.,* vol. 9, *(1),* pp. 79-85, 1999.

[120] V. De Oliveira and A. Karimi, "Robust smith predictor design for time-delay systems with H infinity performance," in *Proceddings of the IFAC Joint Conference,* Grenoble, France, 2013, .

[121] G. Meinsma and H. Zwart, "On H∞ control for dead-time systems," *IEEE Trans. Autom. Control,* vol. 45, *(2),* pp. 272-285, 2000.

[122] I. The MathWorks, "Robust Control Toolbox,", 2010.

[123] S. Devasia and B. Paden, "Stable inversion for nonlinear nonminimum-phase time-varying systems," *IEEE Trans. Autom. Control,* vol. 43, *(2),* pp. 283-288, 1998.

[124] G. M. Clayton, S. Tien, K. K. Leang, Q. Zou and S. Devasia, "A review of feedforward control approaches in nanopositioning for high-speed spm," *J. Dyn. Syst. - T. ASME,* vol. 131, *(6),* pp. 061101, 2009.

[125] G. M. Clayton, S. Tien, A. J. Fleming, S. O. R. Moheimani and S. Devasia, "Inverse-feedforward of charge-controlled piezopositioners," *Mechatronics,* vol. 18, *(5-6),* pp. 273-281, 2008.

[126] Y. Xie and A. G. Alleyne, "Two degree of freedom controller on combine harvester header height control," in *Proceeding of 2012 ASME Dynamic Systems and Control Conference,* Fort Lauderdale, FL, 2012, .

[127] J. M. Hedgepeth, "Accuracy potentials for large space antenna structures," *J. Spacecraft Rockets,* vol. 19, *(3),* pp. 211-217, 1982.

[128] S. Abd Aziz, B. L. Steward, L. Tang and M. Karkee, "Utilizing repeated GPS surveys from field operations for development of agricultural field DEMs," *T. ASABE,* vol. 52, *(4),* pp. 1057-1067, 2009.

[129] K. Eldhuset, P. H. Andersen, S. Hauge, E. Isaksson and D. J. Weydahl, "ERS tandem InSAR processing for DEM generation, glacier motion estimation and coherence analysis on Svalbard," *Int. J. Remote Sens.,* vol. 24, *(7),* pp. 1415-1437, 2003.

[130] D. H. Shugar, B. T. Rabus and J. J. Clague, "Elevation changes (19491995) of Black Rapids Glacier, Alaska, derived from a multi-baseline InSAR DEM and historical maps," *J. Glaciol.,* vol. 56, *(198),* pp. 625-634, 2010.

Appendix A Equivalents among Different two DOF Control Architectures

In the following content, the mathematic equivalence among the five two DOF control schemes in Figure 2.5 is shown. The transfer functions from the exogenous signals to the output for different control schemes are shown in Eqs. (A.1) – (A.5).

$$
\begin{aligned}
T_{r\_a} &= \frac{G_{ffr\_a}G_p + G_{fb\_a}G_p}{1+G_pG_{fb\_a}} \\
T_{\Delta r\_a} &= \frac{G_{ffr\_a}G_p}{1+G_pG_{fb\_a}} \\
T_{d\_a} &= \frac{-G_{ffd\_a}G_p + G_d}{1+G_pG_{fb\_a}} \\
T_{\Delta d\_a} &= \frac{-G_{ffd\_a}G_p}{1+G_pG_{fb\_a}} \\
T_{n\_a} &= -\frac{G_{fb\_a}G_p}{1+G_pG_{fb\_a}}
\end{aligned}
\tag{A.1}
$$

$$
\begin{aligned}
T_{r\_b} &= \frac{G_{ffr\_b}G_p}{1+G_pG_{fb\_b}} \\
T_{\Delta r\_b} &= \frac{G_{ffr\_b}G_p}{1+G_pG_{fb\_b}} \\
T_{d\_b} &= \frac{-G_{ffd\_b}G_p + G_d}{1+G_pG_{fb\_b}} \\
T_{\Delta d\_b} &= \frac{-G_{ffd\_b}G_p}{1+G_pG_{fb\_b}} \\
T_{n\_b} &= -\frac{G_{fb\_b}G_p}{1+G_pG_{fb\_b}}
\end{aligned}
\tag{A.2}
$$

$$
\begin{aligned}
T_{r\_c} &= \frac{G_{ffr\_c} G_{fb\_c} G_p}{1 + G_p G_{fb\_c}} \\
T_{d\_c} &= \frac{-G_{ffd\_c} G_p + G_d}{1 + G_p G_{fb\_c}} \\
T_{\Delta d\_c} &= \frac{-G_{ffd\_c} G_p}{1 + G_p G_{fb\_c}} \\
T_{n\_c} &= -\frac{G_{fb\_c} G_p}{1 + G_p G_{fb\_c}}
\end{aligned}
\tag{A.3}
$$

$$
\begin{aligned}
T_{r\_d} &= \frac{\left(G_{ffr\_d} + G_{fb\_d}\right) G_p}{1 + \left(G_p - G_{p0}\right) G_{fb\_d}} \\
T_{\Delta r\_d} &= \frac{G_{ffr\_d} G_p}{1 + \left(G_p - G_{p0}\right) G_{fb\_d}} \\
T_{d\_d} &= \frac{G_d - G_p G_{ffd\_d} + (G_{d0} G_p - G_d G_{p0}) G_{fb\_d}}{1 + \left(G_p - G_{p0}\right) G_{fb\_d}} \\
T_{\Delta d\_d} &= \frac{-G_{ffd\_d} G_p}{1 + \left(G_p - G_{p0}\right) G_{fb\_d}} \\
T_{n\_d} &= -\frac{G_{fb\_d} G_p}{1 + \left(G_p - G_{p0}\right) G_{fb\_d}}
\end{aligned}
\tag{A.4}
$$

$$
\begin{aligned}
T_{r\_e} &= \frac{\left(1 + G_{fb\_e} G_{p0}\right) G_{ffr\_e} G_p + G_{fb\_e} G_p}{1 + G_p G_{fb\_e}} \\
T_{\Delta r\_e} &= \frac{\left(1 + G_{fb\_e} G_{p0}\right) G_{ffr\_e} G_p}{1 + G_p G_{fb\_e}} \\
T_{d\_e} &= \frac{\left(G_d - G_{ffd\_e} G_p\right)\left(1 + G_{fb\_e} G_{p0}\right)}{1 + G_p G_{fb\_e}} \\
T_{\Delta d\_e} &= \frac{-G_{ffd\_e} G_p \left(1 + G_{fb\_e} G_{p0}\right)}{1 + G_p G_{fb\_e}} \\
T_{n\_e} &= -\frac{G_{fb\_e} G_p}{1 + G_p G_{fb\_e}}
\end{aligned}
\tag{A.5}
$$

Mathematically, the transfer functions are equivalent to each other when defining certain relationship among the controllers used in different schemes. Such equivalent transformations from the scheme in Figure 2.5(b) - 2.5(e) to Figure 2.5(a) are shown in Eqs. (A.6) – (A.9), respectively.

$$\begin{aligned} G_{fb\_a} &= G_{fb\_b} \\ G_{ffr\_a} &= G_{ffr\_b} - G_{fb\_b} \\ G_{ffd\_a} &= G_{ffd\_b} \end{aligned} \tag{A.6}$$

$$\begin{aligned} G_{fb\_a} &= G_{fb\_c} \\ G_{ffr\_a} &= (G_{ffr\_c} - 1)G_{fb\_c} \\ G_{ffd\_a} &= G_{ffd\_c} \end{aligned} \tag{A.7}$$

$$\begin{aligned} G_{fb\_a} &= \frac{G_{fb\_d}}{1 - G_{p0}G_{fb\_d}} \\ G_{ffr\_a} &= G_{ffr\_d} + G_{fb\_d}G_{p0}G_p \\ G_{ffd\_a} &= G_{ffd\_d} + \left(G_d G_{p0} - G_{d0}G_p\right)G_{fb\_d}G_p^{-1} \end{aligned} \tag{A.8}$$

$$\begin{aligned} G_{fb\_a} &= G_{fb\_e} \\ G_{ffr\_a} &= G_{ffr\_e}(1 + G_{fb\_e}G_{p0}) \\ G_{ffd\_a} &= G_{ffd\_e} + G_{p0}G_{fb\_e}\left(G_{ffd\_e} - G_d G_p^{-1}\right) \end{aligned} \tag{A.9}$$

Appendix B Nomenclatures in an Experimental Combine System

The following table shows the nomenclatures for an experimental combine system. The symbols used in the table correspond to Figure 3.2 and Figure 3.3. The values of the parameters are also shown but with small variations from their true values due to the manufacturer's confidential policy.

Table B.1 Nomenclatures for the combine system

Symbol	Definition	Value
a, b	the distance in x direction between front/rear wheel axis and gravity center of vehicle body	2m;1.3m
b_f, b_r	the damping constant of front and rear tires	22400kg/s;26300 kg/s
h_o	the original height of the A point	1.2m
α_o	the original value of angle α	0.113m
I_{com}, I_h	the inertias of vehicle body and header with respect to the gravity center and point A separately	66000kg·m²;2200 0kg·m²
l_{t1}, l_{t2}, l_{cgh} l_{ins}, l_h, l_f	structural length	2.9m,3m,2m,0.8 m 4.6m,1.7m

Table B.1 (cont.)

Symbol	Definition	Value
m_{com}, m_h	the masses of the vehicle body and the header	15000kg;5000kg
k_f, k_r	the spring constant of front and rear tires	1303720N/m;1673600N/m
k_{hydr}	coefficient from valve current to the velocity of the cylinder	0.032m/s/A
$\varsigma_h, \varsigma_{cgh}, \varphi_{t1}, \varphi_{t2}$	structural angle	0.3rad, 0.1rad 0.3rad, 0.5rad
F_{Ax}, F_{Az}	the forces at the point A in x and z directions	variable
F_f, F_r	the forces on the vehicle body at the front and rear tires	variable
F_l	the force from the hydraulic cylinder on the header and vehicle body	variable
h	the absolute header height	variable
l_c	the cylinder length	variable
x_A, z_A	the distances between the vehicle body gravity center and the point A in x and z directions	variable
x_{cgh}, z_{cgh}	the distances between the header gravity center and the point A in x and z directions	variable
α, ρ, φ	structural angle variables	variable
β	the header angle with respect to x axis	variable
θ	the pitch displacement of vehicle body	variable
v	the vertical displacement of vehicle body	variable
γ	the angle between header and vehicle body	variable

Appendix C Introduction to the Experimental System

The experimental system is shown in Figure C.2. The experiments are conducted on combine S690 with corn header 612C. Besides the combine system, the experimental system includes a dSPACE box, an integrated Auto tracking system (GPS receiver and displayer) and a computer.

The schematic of the hardware system is shown in Figure C.2. The computer is in charge of controller design and real time experiment monitoring, which are accomplished in Simulink and ControlDesk separately (Figure C.3 and C.4). The programmed control algorithm is downloaded into the dSPACE box and communicates with the sensors in the combine system through CAN bus or analog inputs. On the other hand, control signal is sent to the hydraulic valves by analog outputs from the dSPACE.

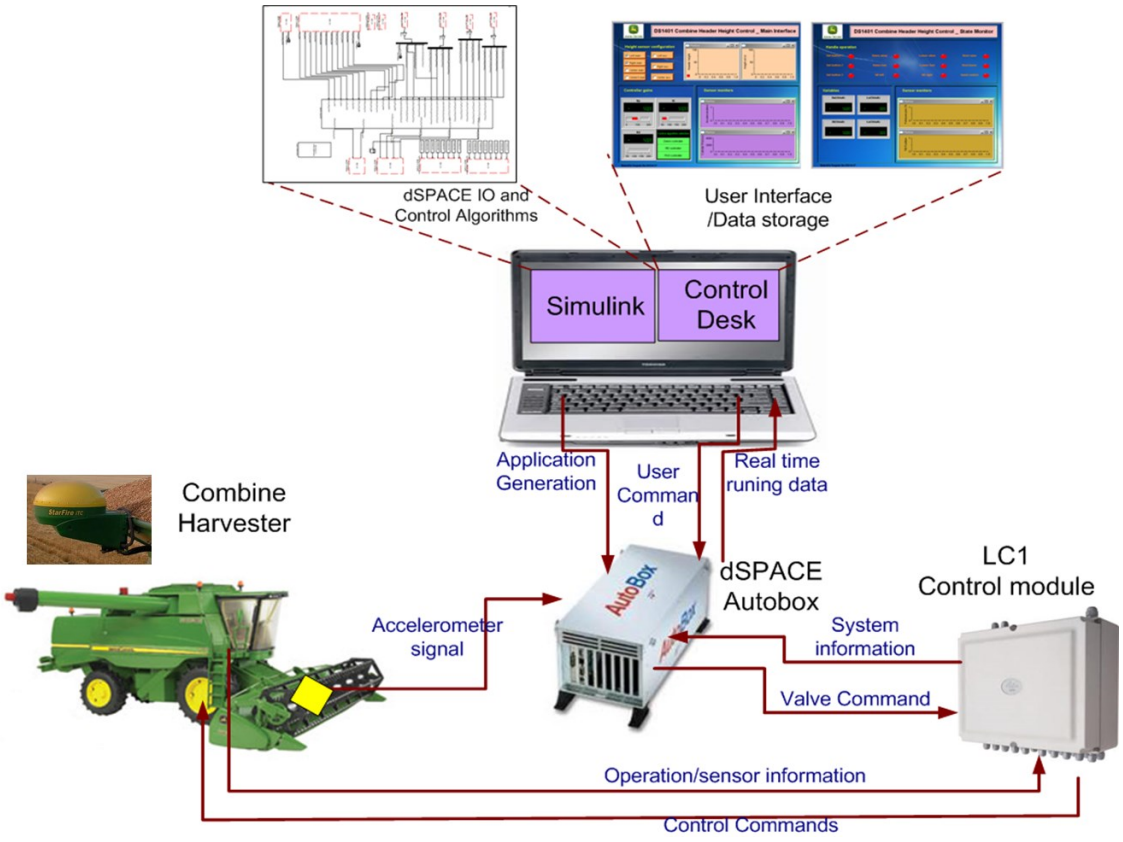

Figure C.1 Experimental system

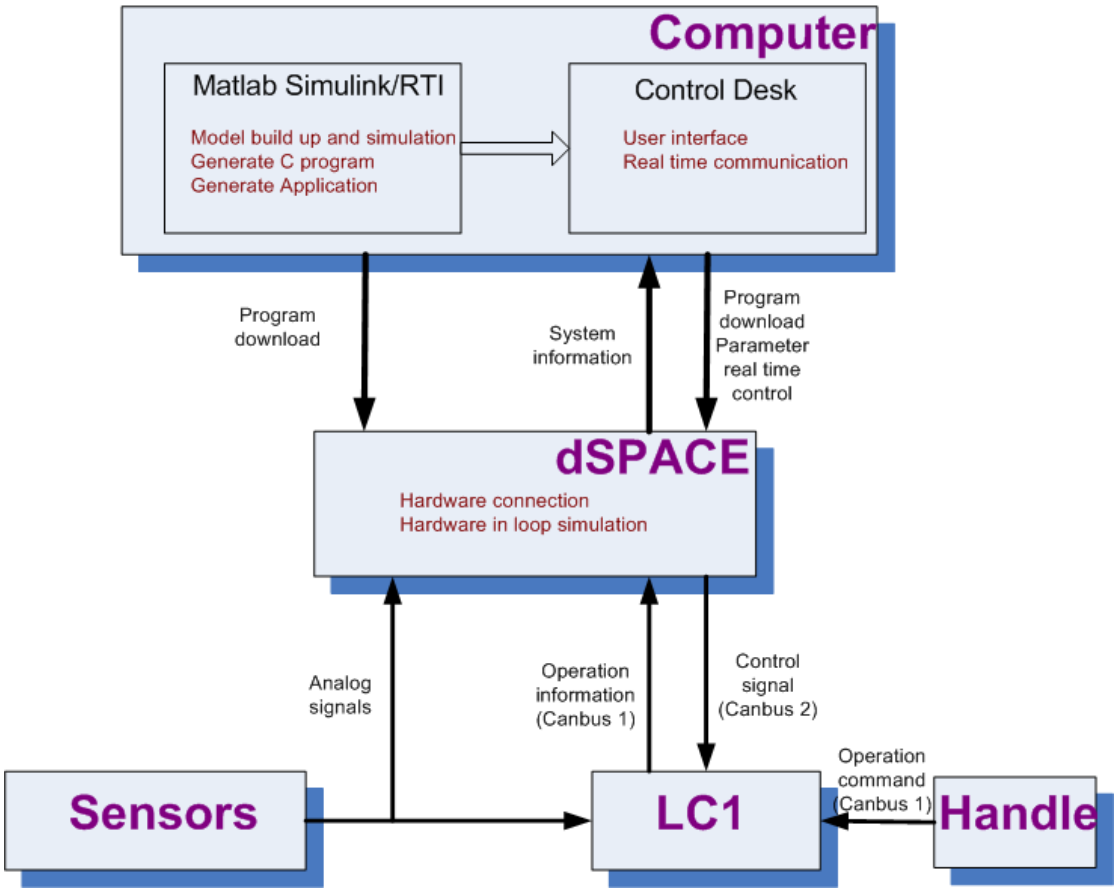

Figure C.2 Schematic of hardware in the experimental system

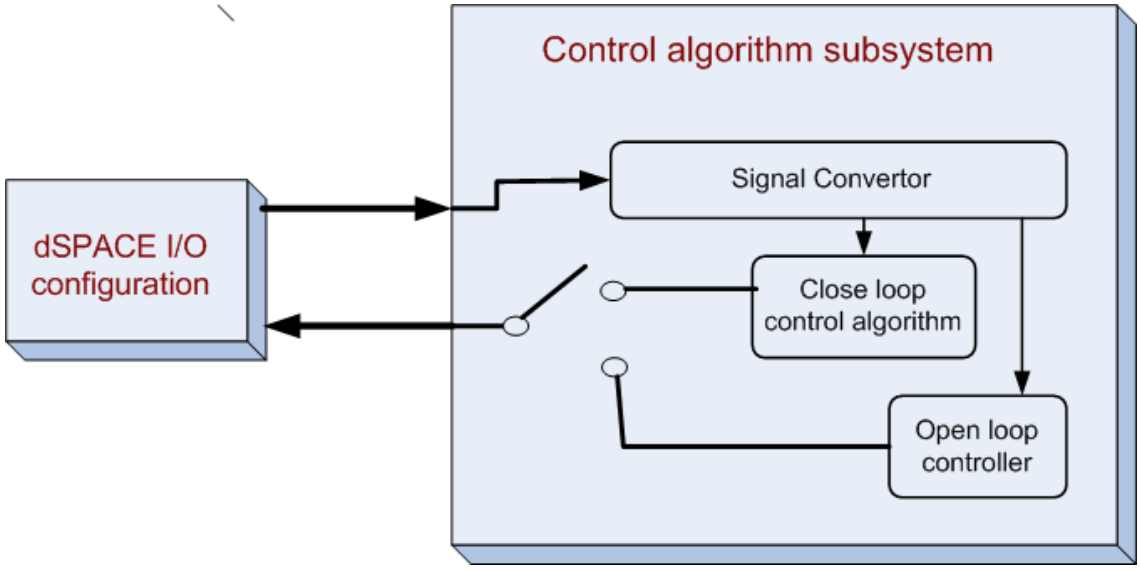

Figure C.3 Schematic of Simulink model

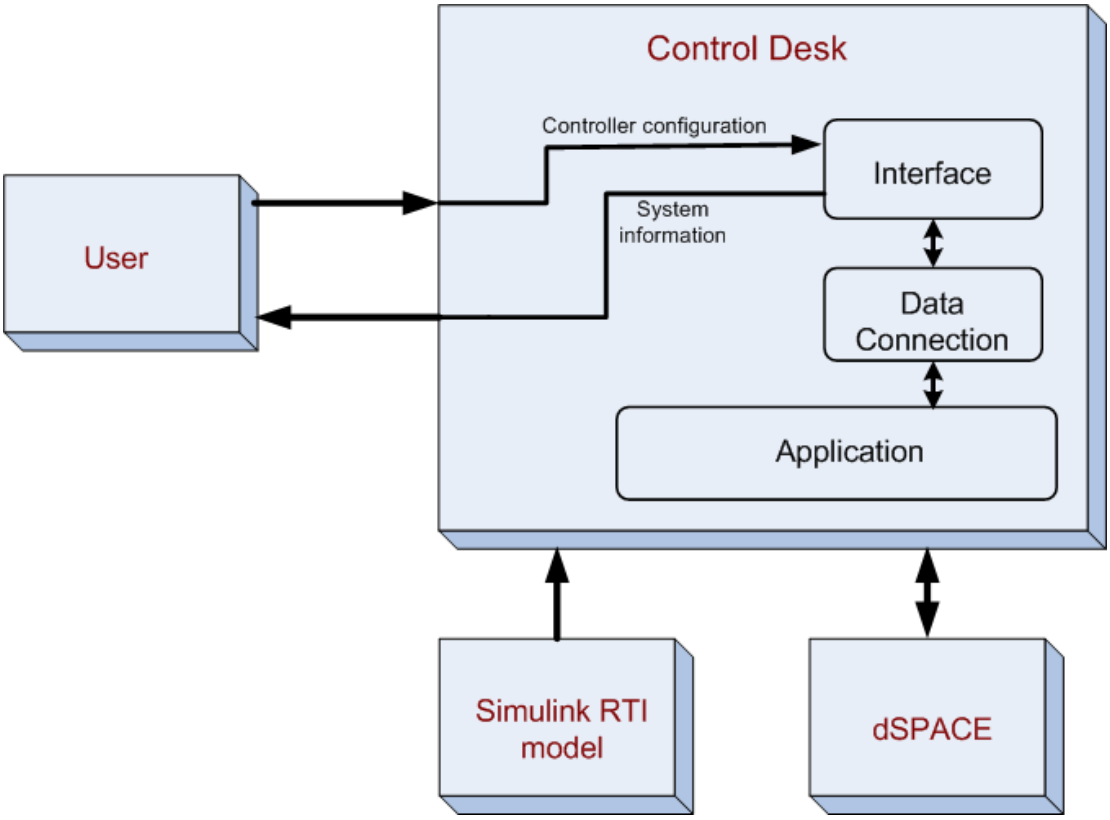

Figure C.4 Schematic of ControlDesk experiment setup

The ground map is pre-measured using the GPS receiver installed on the top of the combine cab. When the combine is driving on the test ground, the 3D coordinate data from the GPS system are recorded. Using coordination transformation, it is stored in local coordinate system. After multiple run of the combine harvester, the data are stored as scatter points and their weighted mean is used to get the final map shown as Figure C.5. The GPS sensor resolution is at 0.1mm level. The standard deviation of the measurement error is about 5cm at the testing field.

When the combine is proceeding with header height control, the current location of the combine is determined by the current GPS measurement. Comparing the current location

with the stored field map and use the information of the current combine speed, the ground profile ahead of the combine can be predicted, which enables feedforward control.

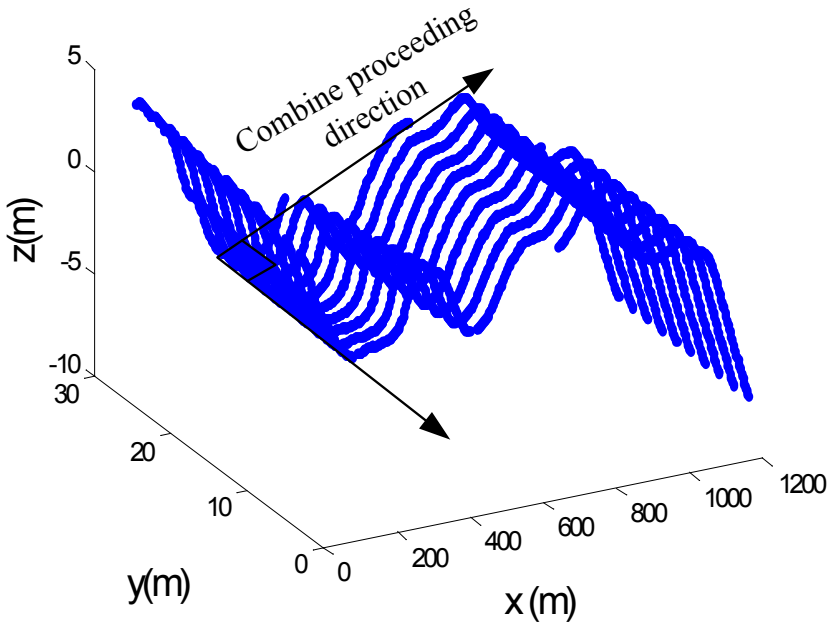

Figure C.5 Exemplary map obtained by GPS measurements

The feedback information of the system comes from the header height sensor installed at the header tip to measure the relative distance between the header tip and the ground. The deviation between the measured data and the desired header height set point is the header height error, which is provided to the feedback controller to generate corresponding feedback control signal. The measurement range of the sensor is 0-46cm with resolution as 0.1mm. It is worth to mention that only planar rotation control of the header is considered in this dissertation for header height control; therefore, the ground profile change perpendicular to the combine proceeding direction is ignored. In real combine system, another actuation system is used to adjust the tilt angle of the header in order to adapt to the

ground slope in this direction. For the purpose of testing the planar rotation actuation for header height control in this dissertation, the testing ground is chosen to have dramatic change in the combine proceeding direction but with relatively minor variation along the perpendicular direction of the combine proceeding trajectory as shown in Figure C.5. To get an averaged measurement of the header height, three sensors are installed at the left side, right side and middle of the header. The feedback signal is calculated by the mean value of the three measured signals.

Appendix D Simulink model used in the experimental system

The implementation of the algorithm on the experimental system is achieved by establishing Simulink model in Matlab. With the support of dSPACE real time control system, the model is able to achieve real time control and data acquisition from the experimental system. Figure D.1 - D.4 show the major function blocks of the Simulink model used for the experimental purpose. Figure D.1 shows the main system, which includes mainly 8 categories of blocks to achieve different functions:

(1) Specify ADC I/O configuration for the dSPACE system.

(2) Setup CAN1 to obtain information from CANBUS 1. CAN 1 is mainly used to exchange the integrated sensor and actuator signals in the combine control system.

(3) Setup CAN2 to obtain information from CANBUS2. CAN2 is mainly used to obtain information from the driver's operation handle.

(4) Setup CAN3 to obtain information from CANBUS3. CAN3 is mainly used to obtain information from the GPS and Auto-tracking system.

(5) Specify control algorithms (with details in Figure D.2).

(6) Specify physical address of the CANBUS system in dSPACE I/O interface

(7) Send out control signal to hydraulic actuators using CANBUS system

(8) Specify model parameters. These parameters are used to define some physical variables that are used in control algorithms, or to define some flag variables for realize user interference during the experiments.

Figure D.2 is to show the function blocks for the control algorithm specification. The labeled blocks have the functions as follows:

(9) Read sensor inputs.

(10) Data processing from original sensor reading to variables that will be used for control signal generation.

(11) Specify various control algorithms.

(12) Open loop control block.

(13) Realize switch function among different controllers.

Figure D.3 corresponds to the implementation of the feedback control algorithm described in Chapter 5, and Figure D.4 corresponds to the implementation of the feedforward control algorithm described in Chapter 6.

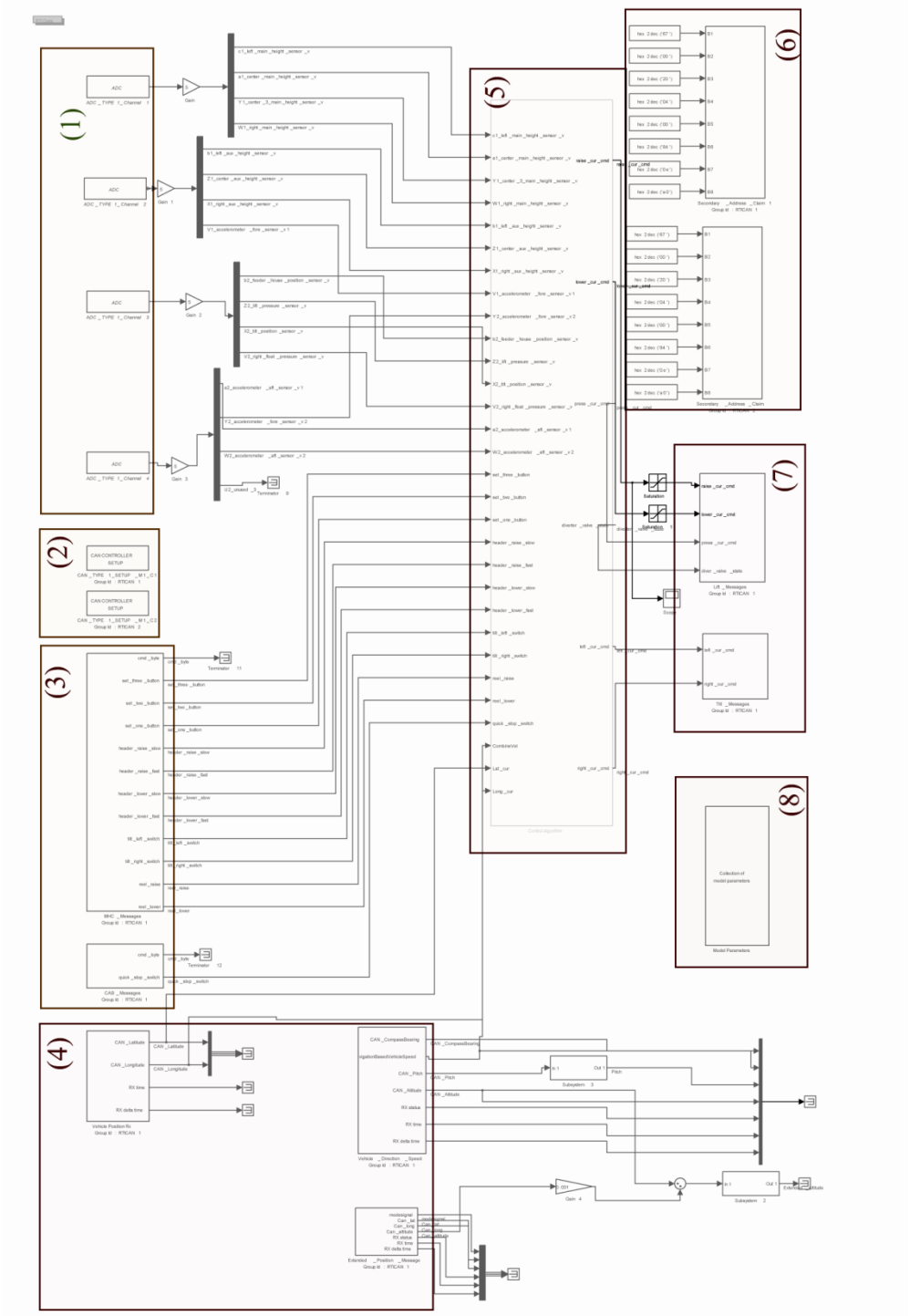

Figure D.1 Main model structure

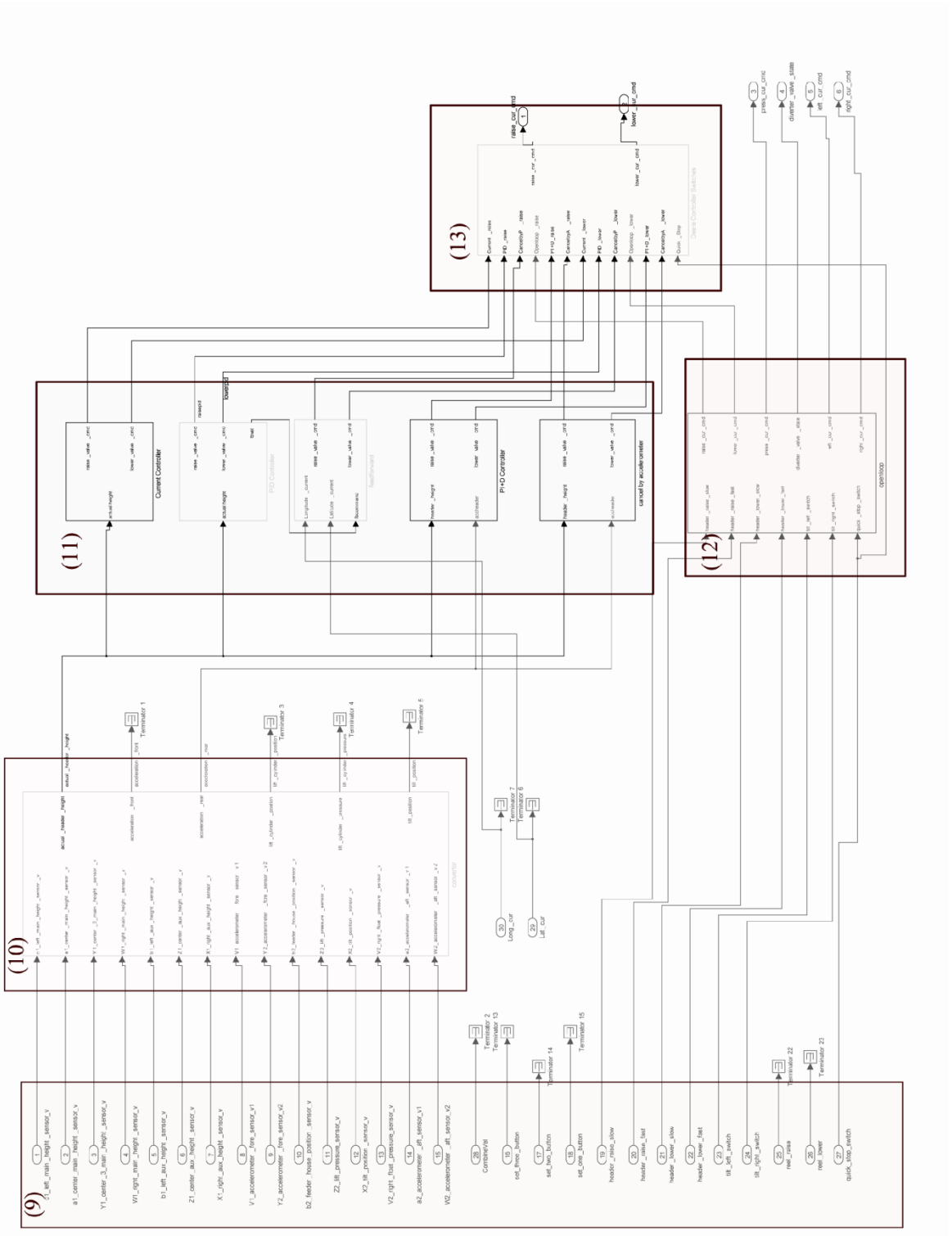

Figure D.2 Control algorithm

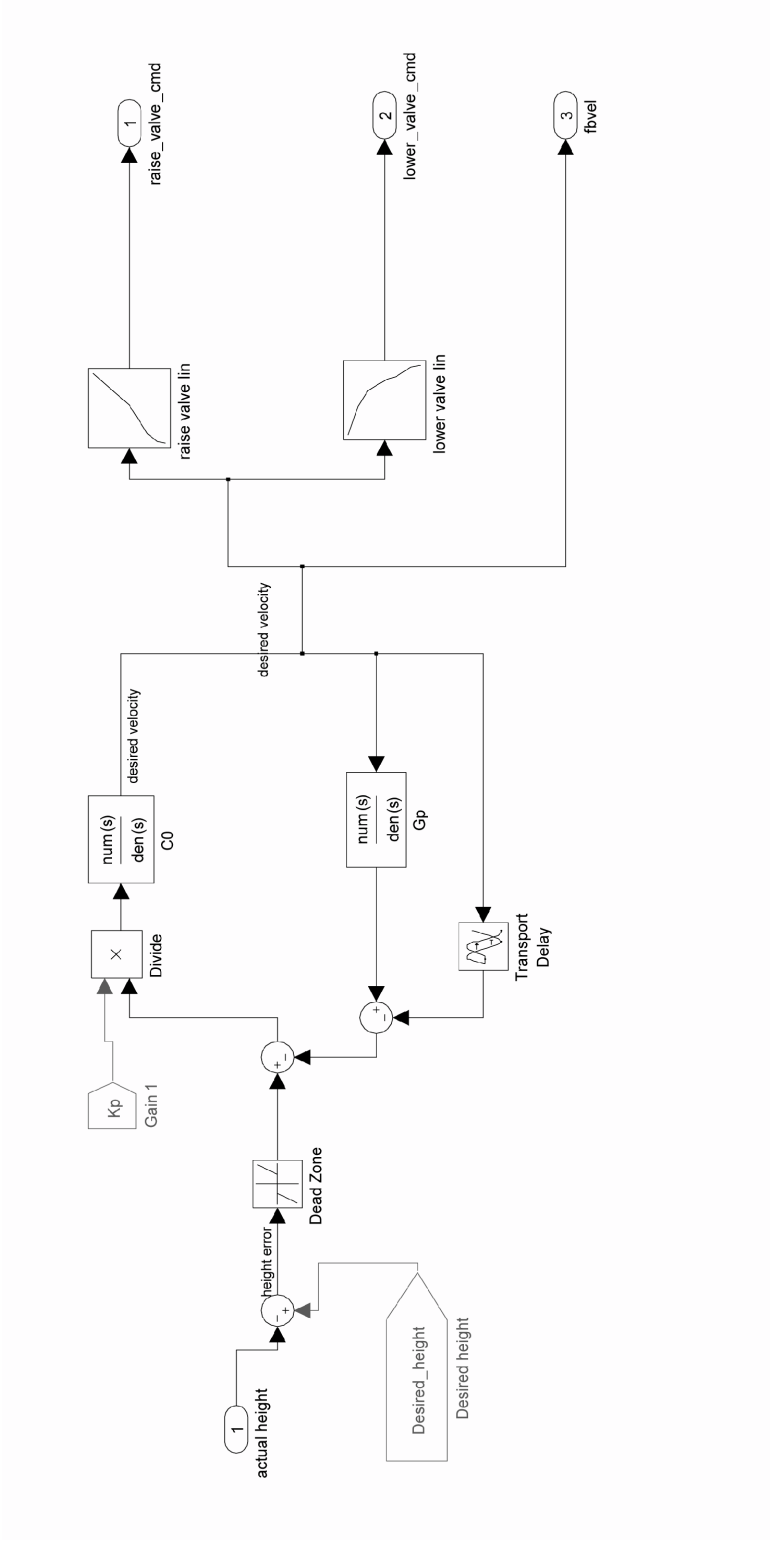

Figure D.3 Implementation of feedback controller

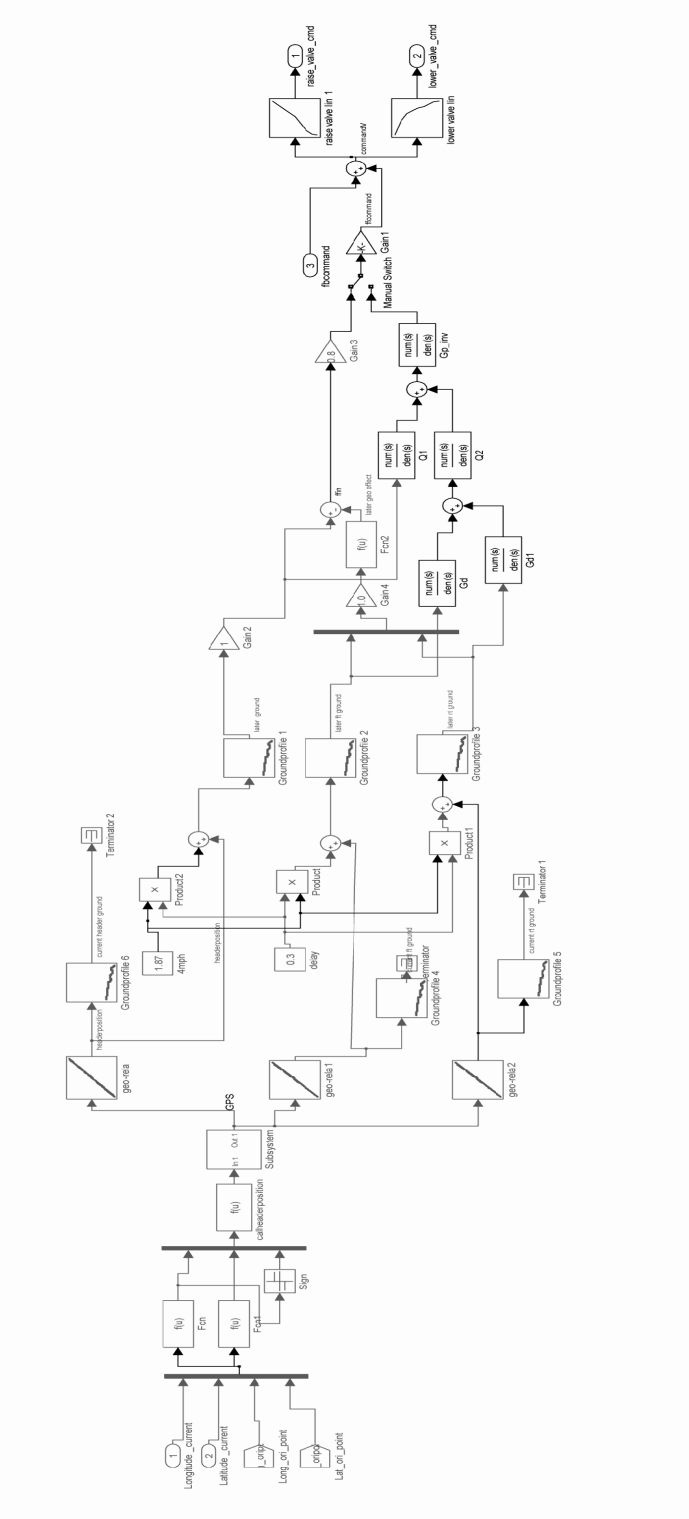

Figure D.4 Implementation of feedforward controller

Appendix E Numerical Realization for Feedback Control

The numerical realizations for designing the robust feedback controller are shown below. The numerical realization for the augmented plant $P_{fb}(s)$ in Eq. 5.27 is shown in Eqs. (D.1) - (D.3). The numerical realization for the central controller $C_0(s)$ in Eq. (5.28) is shown in Eqs. (D.4) - (D.7).

$$A = \begin{bmatrix}
0 & -1 & 0 & 0 & 181.3 & 0 & 0 & 0 & 0 & 28.8 & 179 \\
0 & 0 & -1 & 0 & -1119 & 0 & 0 & 0 & 0 & -177.9 & -1104.9 \\
0 & 0 & 0 & -1 & 9879.7 & 0 & 0 & 0 & 0 & 1571 & 9754 \\
0 & 0 & 0 & 0 & -42271 & 0 & 0 & 0 & 0 & -6719 & -41733 \\
-0.707 & 0 & 0 & 0 & -4.54 & 0 & 0 & 0 & 0 & -0.723 & -4.489 \\
0 & 0 & 0 & 0 & 0 & 0 & -256 & 0 & 0 & 0 & 0 \\
0 & 0 & 0 & 0 & & 1 & -2.92 & -0.012 & 0 & 0 & 0 \\
0 & 0 & 0 & 0 & 0 & 0.0037 & -6026 & -21.93 & 8.52 & 0 & 0 \\
0 & 0 & 0 & 0 & 0.019 & -0.0013 & -14970 & -55.35 & 18.64 & -0.236 & 0.0188 \\
-0.112 & 0 & 0 & 0 & -1.216 & -4.7×10^{-5} & 58500 & 215.88 & -73.9 & -2.85 & 0.227 \\
-0.698 & 0 & 0 & 0 & -4.41 & 0 & -9419.1 & -34.76 & 11.9 & -0.273 & -4.58
\end{bmatrix} \quad \text{(D.1)}$$

$$B_1 = \begin{bmatrix} -20.464 & 14.1 & -8.52 \\ 1179.4 & -1093.6 & 448.59 \\ -2016 & 5258 & -3236 \\ 59780 & -155800 & 95970 \\ 3.54 & 0 & 0 \\ 0 & 232.77 & -98.24 \\ 0 & -5.55 & 2.571 \\ 0 & 13834 & -8306.7 \\ 0 & 39660 & -24500 \\ 0.562 & -152440 & 93897.5 \\ 3.49 & 24544.5 & -15118.6 \end{bmatrix} \quad B_2 = \begin{bmatrix} 47.097 \\ -1485.9 \\ 9992.1 \\ -109233 \\ 467740.6 \\ 47.097 \\ -0.974 \\ 4644.4 \\ 13120 \\ -181784 \\ -444502 \end{bmatrix} \tag{D.2}$$

$$C_1 = \begin{bmatrix} 0 & 0 & 0 & 0 & 0.707 & 0 & 0 & 0 & 0 & 0.1124 & 0.698 \\ 0 & 0 & 0 & 0 & 0 & 0 & 0 & 0 & 0 & 0 & 0 \end{bmatrix}$$

$$C_2 = \begin{bmatrix} 0 & 0 & 0 & 0 & 0 & 0 & -1 & -0.0037 & 0.0013 & 4.75\times10^{-5} & 0 \end{bmatrix} \tag{D.3}$$

$$A_{C0} = \begin{bmatrix} 174 & 618 & 1880 & -325000 & -5850 & -84.8 & 0.0202 & 46800 & 20100 & 13200 & -113000 \\ -141 & -385 & -1130 & 197000 & 3550 & 51.5 & -0.0122 & -28400 & -12200 & -80100 & 68600 \\ 9.09 & 29.2 & 87.7 & -15400 & -276 & -4.01 & 9.57\times10^{-4} & 2210 & 951 & 6240 & -5340 \\ -506 & -1720 & -5220 & 905000 & 16200 & 237 & -0.0561 & 130000 & -55900 & -367000 & 314000 \\ 909 & 3070 & 9290 & -1620000 & -29100 & -420 & 0.1 & 232000 & 99900 & 655000 & -561000 \\ -2000 & -6790 & -20500 & 3560000 & 63900 & 927 & -0.221 & -512000 & -220000 & -1440000 & 1230000 \\ -0.0388 & 0.0228 & 0.124 & -14.7 & -0.274 & -0.00472 & 5.67\times10^{-5} & 1.59 & 14.6 & 6.53 & -6.68 \\ -0.744 & -0.336 & -0.285 & 71.5 & 1.22 & 0.0138 & -7.79\times10^{-5} & -22.1 & -7.86 & -26.8 & 26.40 \\ -0.153 & -0.0563 & -0.0156 & 7.2 & 0.117 & 8.85\times10^{-4} & -3.2\times10^{-5} & -3.54 & -1.15 & -10.1 & -9.56 \\ -0.335 & 0.094 & 0.101 & -2.749 & -0.218 & -0.00196 & -2.53\times10^{-5} & 1.262 & 0.719 & 5.663 & -12.616 \\ 0.256 & 0.108 & 0.0731 & -18.9 & -0.322 & -0.00342 & -1.87\times10^{-5} & 7.03 & 2.48 & 19.7 & -16.8 \end{bmatrix} \tag{D.4}$$

$$B_{C_0} = \begin{bmatrix} 5303.2 & -25547.2 & 15409 & -1173.8 & 68840.4 & -124587.9 & -27.3 & 0.71 & 11.1 & 2.36 & -3.9 \end{bmatrix}^T \tag{D.5}$$

$$C_{C_0} = \begin{bmatrix} 0.0047 & 0.016 & 0.048 & -8.3 & -0.15 & -0.0022 & 5.17 & 1.2 & 0.51 & 3.37 & -2.88 \end{bmatrix} \tag{D.6}$$

$$D_{C_0} = 0 \tag{D.7}$$